PRE-VEGETATION ALLUVIUM: GEOLOGICAL EVIDENCE FOR RIVER BEHAVIOUR IN THE ABSENCE OF LAND PLANTS

by

WILLIAM JOSEPH MCMAHON

This dissertation is submitted

for the degree of

DOCTOR OF PHILOSOPHY

Hughes Hall

Department of Earth Sciences,

University of Cambridge,

February 2018

ABSTRACT

Pre-vegetation alluvium is unique; at the present day, plants affect multiple aspects of river functioning and deposition and so those rivers that operated before the evolution of land plants largely lack modern sedimentological analogue. However, such rivers were the norm for the first 90% of Earth history and so a better understanding of their sedimentary product enables insight into both the fundamental underlying mechanisms of river behaviour and the ways in which fluvial processes operated on ancient Earth and other rocky planets. This study presents five original fieldwork based case studies and an analysis of a holistic database of all of Earth's pre-vegetation alluvium. Together these research strands offer perspectives on the sedimentological characteristics and stratigraphic trends of pre-vegetation alluvium and the behaviour and functioning of pre-vegetation rivers. Results show that, in pre-vegetation alluvial settings: 1) a variety of fluvial styles are represented, but diminished in comparison with syn-vegetation alluvium; 2) 'sheet-braided' architectures are common but may record a variety of fluvial planforms; 3) meandering planforms were less frequent, particularly in small- to moderate-sized river systems; 4) mudrock is on average 1.4 orders of magnitude less common than it is in syn-vegetation alluvium; and 5) microbial matgrounds were present, but had negligible effect on preserved architecture and facies. This thesis demonstrates that whilst the physical laws governing fluvial fluid-sediment interaction have not changed, the theatre in which they operated irrevocably evolved with the greening of the continents.

DECLARATION

This dissertation is the result of my own work and includes nothing which is the outcome of work done in collaboration except as declared in the Preface and specified in the text.

It is not substantially the same as any that I have submitted, or, is being concurrently submitted for a degree or diploma or other qualification at the University of Cambridge or any other University or similar institution except as declared in the Preface and specified in the text. I further state that no substantial part of my dissertation has already been submitted, or, is being concurrently submitted for any such degree, diploma or other qualification at the University of Cambridge or any other University or similar institution except as declared in the Preface and specified in the text

Statement of length

This dissertation is within the prescribed length as defined by the Degree Committee for Earth Sciences and Geography

.

ACKNOWLEDGMENTS

I would like to sincerely thank a number of people for their assistance, knowledge and kindness, which has enabled me to complete this PhD. Firstly, I am deeply indebted to my supervisor Dr Neil Davies, not only for devising this project and providing excellent tuition throughout its duration, but for teaching me a tremendous amount about planet Earth and how to go about its study. I also wish to thank everyone who has taught me geology so far, none more so than Gareth Daniels, without who I surely would not be in this position today.

Thanks are also owed to the great many people whose hard work ensures the Department of Earth Sciences at Cambridge actually functions each day. Most especially, I wish to thank Sarah Humbert, who has put up with my poor jokes on a nearly daily basis and accepted that my office had become an extension of the departmental library for the duration of my occupancy.

A number of people gave their time in productive conversations that greatly improved this thesis. Particular thanks are owed to Prof. Sanjeev Gupta at Imperial College London, who shared his vast expertise on the geology of Mars. Dr David Went is also thanked for sharing his detailed knowledge on the regional geology of Northern Brittany and the UK Channel Islands, which greatly assisted my work on the Series Rouge.

Completing this thesis would have been a more tiresome task had it not been for the superb company provided by my fellow Earth Science postgraduates, most notably, my office mate Anthony Shillito.

Finally, I wish to thank my parents and brother, who have given me excessive amounts of encouragement, support and love long before I embarked on this PhD.

This work was supported by Shell International Exploration and Production B.V. under Research Framework agreement PT38181.

The advent of land vegetation has drastically altered the Earth's surface so that it is difficult to find words to express the geomorphology of the Precambrian Earth

Don Winston

1978

TABLE OF CONTENTS

LIST OF FIGURES

LIST OF TABLES

PREFACE

A vast number of observations have demonstrated that vegetation plays a fundamental role in the operation of modern fluvial systems. This recognition has prompted a large volume of research into fluvial processes and deposits in the absence of vegetation. Whilst much progress has been made, there persist a number of repeated generalizations that can be refined or rejected, and a number of questions regarding the nature of both pre-vegetation rivers and alluvium remain outstanding. Were all pre-vegetation rivers braided? Were channels dominantly broad and shallow? Were high energy-flood events more frequent? The purpose of this thesis is to explore many of the questions frequently asked concerning pre-vegetation rivers, and advance our current knowledge of fluvial processes and deposits in the absence of vegetation. This thesis is divided into nine chapters, each discussing a different aspect of pre-vegetation alluvium.

CHAPTER 1 discusses what is presently known about fluvial processes and deposits in the absence of vegetation, and reviews the history of research into pre-vegetation alluvium.

The methods of study are outlined in **CHAPTER 2**. This includes an introduction to the main field site, the Proterozoic Torridonian Sandstones, and an account of how a database of 704 Archean-Carboniferous aged alluvial deposits was compiled. This compilation is herein referred to as 'the database'.

Part of the discussed methodology has been published in: McMahon, W.J. and Davies, N.S. The evolution of alluvial mudrock forced by land plants. *Science* (2018).

CHAPTER 3 presents the results of an analysis of the sedimentary character of Archean-Carboniferous aged alluvium using the compiled characteristics in the database.

Section 3.1 is based on material published in: McMahon, W.J. and Davies, N.S. The evolution of alluvial mudrock forced by land plants. *Science* (2018).

CHAPTER 4 describes two original case studies of pre-vegetation alluvium interpreted to have been deposited by perennial rivers: 1) The Neoproterozoic Torridon Group; and 2) The Neoproterozoic Jacobsville Formation.

CHAPTER 5 presents a sedimentological analysis of the Mesoproterozoic Meall Dearg Formation (Scotland), and demonstrates that its deposition was typified by supercritical flows during high-energy ephemeral floods, punctuated by prolonged intervals of sedimentary stasis.

This case study is based on material published in: McMahon, W.J. and Davies, N.S. 2018. High-energy flood events recorded in the Mesoproterozoic Meall Dearg Formation, NW Scotland; their recognition and implications for the study of pre-vegetation alluvium. *Journal of the Geological Society*, ***175***, 13-32.

An increasing number of studies have postulated that microbiota may have influenced geomorphic stability and processes in pre-vegetation rivers. **CHAPTER 6** discusses how a microbial influence may have been exerted on pre-vegetation rivers with reference to the Ediacaran-Cambrian Series Rouge, a pre-vegetation succession which contains both well exposed outcrop and multiple lines of evidence for former microbial mat colonies.

This chapter is based on material published in: McMahon, W.J., Davies, N.S. and Went, D.J. 2017. Negligible microbial matground influence on pre-vegetation river functioning: Evidence from the Ediacaran-Lower Cambrian Series Rouge, France. *Precambrian Research*, ***292***, 13-34.

CHAPTER 7 discusses the contentious issue surrounding the abundance of meandering rivers before the evolution of land plants. Evidence based on the alluvial record is reviewed and assessed, and new results from the Allt-na-Béiste Member (Scotland), which to date has provided the most compelling geological evidence for a pre-vegetation meandering river (Santos and Owen, 2016), are presented.

Recent rover missions mean that we now have direct visual access to alluvium that was deposited in (presumably) unvegetated ancient settings on Mars. Pre-vegetation alluvium is increasingly being recommended as a possible Martian analogue. **CHAPTER 8** discusses the merit and limitations of such analogy.

CHAPTER 9 draws together the conclusions from the previous chapters in order to provide a fuller picture of fluvial processes and deposits before the evolution of land plants.

The **APPENDICES** to this thesis contain information on fieldwork localities and the compiled characteristics used in database analyses. References in Table A2 are stored on the enclosed CD-ROM.

Chapter 1

INTRODUCTION

1.1. Fluvial processes and deposits in the absence of land plants: General background

It is now 50 years since Stanley Schumm's (1968) seminal paper in which he described the ways in which rivers that operated before the evolution of land plants would have differed from their more recent counterparts. During the last five decades, a huge number of observations have supported Schumm's (1968) contentions that vegetation plays a fundamental role in the operation of modern fluvial systems, while at the same time there has been increasing recognition that pre-vegetation alluvium consists of anactualistic sedimentary facies; representing the deposits of fluvial systems that largely lack modern analogue, but which were ubiquitous for the majority of Earth history.

Throughout this thesis, 'pre-vegetation' refers to rivers deposited prior to the oldest land plants, whereas 'syn-vegetation' is used to refer to all rivers after this time. 'Syn-vegetation' is preferred to the more commonly used 'post-vegetation' (e.g., Fralick and Zaniewski, 2012; Davies and Gibling, 2013; Santos et al., 2014; Ielpi et al., 2016, 2017; Santos and Owen, 2016; McMahon et al., 2017), as this term implies extinction.

The oldest known plant fossils date from 473 – 471 Ma (Rubinstein et al., 2010) and provide a conservative minimum estimate of the onset of the greening of the continents. Using this early Middle Ordovician age as the hard boundary between 'pre-vegetation' and 'syn-vegetation' rivers, alluvium was deposited in the absence of plants for the first 90% of Earth history. Recently, it has also become more apparent that unvegetated rivers were not just the long-term norm on Earth: rover missions mean that we now have direct visual access to alluvium that was deposited in (presumably) unvegetated ancient settings on Mars.

Rivers operating in the presence of vegetation thus appear to be the exception rather than the rule, yet such rivers are our only frame of reference when we look at modern rivers or post-Ordovician alluvium. A more robust understanding of the properties of pre-vegetation alluvium, and the processes which led to its deposition, promises to reveal details of the abiotic skeleton that underpins the biotic rivers that traverse the Earth's continents at the present day.

1.2. History of research into pre-vegetation alluvium

1.2.1. Foundational ideas

The fundamental differences between Earth surface processes before and after the evolution of land plants have long been commented upon. As early as the 1930's, Kaiser (1931) discussed the ways in which the hydrological cycle should be expected to have been different, and raised the crucial issue of a lack of modern analogue; noting the complete absence of present-day 'plantless' environments in humid climates. Vogt (1941) appears to be the first to specifically consider the effects of a lack of vegetation on ancient river systems, noting that the Middle Devonian strata in Svalbard consist of much more weathered mineral grains than strata of Lower Devonian age. He ascribed this fact to more rapid transportation and sedimentation in the Lower Devonian due to the existence of only sparse vegetation, leaving atmospheric factors a shorter duration to act on the mineral grains. Later, Russell (1956) suggested that ancient Earth surface processes could only be understood with reference to the character of vegetation at the time, splitting geological history into: 1) pre-vegetation time; 2) time during colonization of alluvial areas by primitive vegetation; 3) time during colonization by flowering plants; and 4) time following the appearance of grasses.

1.2.2. Setting the stage for modern analysis of pre-vegetation alluvial systems (1960-1979)

The rise of the facies model paradigm in the 1960's and 70's (e.g., Allen, 1964; Walker, 1976), saw an increasing attempt to categorise the sedimentary facies of pre-vegetation rivers, within the context of early work that had discussed their uniqueness. Principal amongst such studies, Schumm (1968) used data from modern, sparsely vegetated alluvial catchments to suggest that pre-vegetation rivers would have operated under far greater rates of denudation and surface runoff. He suggested that large floods would have resulted in the deposition of sheets of (predominantly coarse) sediment, decreasing the likelihood of the development of meandering channel patterns. Cotter (1978) expanded on these ideas, using sedimentary geological data from Ordovician-Carboniferous alluvial formations in the Appalachian Basin to demonstrate a paucity of clearly channelized architectural units within pre-vegetation alluvium. Emphasizing this difference, he introduced the term 'sheet-braided' to refer to a distinct fluvial style (discussed in Section 7.2.2). At the same time, Long (1978) noted the scarcity of fine-grained clastic material within Proterozoic alluvium, which he explained by: 1) a dominance of bedload type streams; 2) high vulnerability of overbank deposits to subsequent reworking; 3) the removal of fines from fluvial systems as wash load; and 4) lower rates of mud production (through chemical weathering) in the absence of land plants. He also recognised the problem of determining a marine or fluvial origin for thick sandstone-dominated successions that lack palaeontological indicators (see Section 2.3) and noted that any previous interpretations of meandering rivers from pre-vegetation alluvium had been based solely on unreliable criteria (fining-up profiles and palaeocurrent variation).

1.2.3. Pre-vegetation facies models (1980-2009)

Following on from the work of Schumm, Cotter and Long, a large number of studies into pre-vegetation alluvium were undertaken during the last two decades of the twentieth century. Among the key generalizations made during this interval, Fuller (1985) suggested that pre-vegetation rivers would have had width:depth ratios in excess of 1000:1, due to the absence of bank-stabilizing vegetation. Other researchers also noted the size discrepancy between ancient and modern rivers, proposing that pre-vegetation braidplains were often enormous due to the frequent switching of unstable channels (e.g., Rainbird, 1992; MacNaughton et al., 1997). In terms of planform, a consensus developed that most pre-vegetation rivers were braided from source to sink, and terminated in braid-deltas at the shoreline (McPherson et al., 1987; Els, 1998; Sønderholm and Tirsgaard, 1998; Hadlari, 2006) regardless of gradient. High run-off rates were also inferred, leading to the conclusion that pre-vegetation rivers were more sensitive to climate change; explaining rapid stratigraphic transitions between perennial and ephemeral characteristics within their alluvial deposits (Tirsgaard and Øxnevad, 1998). The influence of land plants on aeolian processes within the alluvial realm was also subject to scrutiny, leading to the conclusion that, in pre-vegetation settings the absence of plant related baffling and binding meant greater wind-reworking of non-marine deposits (Dalrymple et al., 1985; Fuller, 1985; Eriksson and Simpson, 1998; Tirsgaard and Øxnevad, 1998). The knock-on effect that an absence of land plants had on marine environments was also considered, as common thick, offshore siliciclastic successions were attributed to the inferred greater rates of fluvial and aeolian sediment supply (Dott and Byers, 1981; Dalrymple et al., 1985; Lindsey and Gaylord, 1992; Dott, 2003).

1.2.4. Recent studies of pre-vegetation alluvium (2010-2018)

While much work was being focussed on fully pre-vegetation alluvium, Davies and Gibling (2010a) updated Cotter's (1978) study into alluvium from the interval of geological history when vegetation evolved and expanded. Through an extensive analysis of reported Cambrian to Devonian alluvial formations, they confirmed that syn-vegetation alluvium has a far greater abundance of mudrock and architectural elements such as laterally-accreting inclined heterolithic stratification, most frequently interpreted as the sedimentary expression of point bar migration within a sinuous channel. In contrast, pre-vegetation alluvium was almost uniformly comprised of 'sheet-braided' sandstones (using Cotter's (1978) definition of the term) (discussed in Section 7.2.2).

Utilizing architectural element analysis (Miall, 1985) (described in Section 2.1.2), Long (2011) updated his 1978 review of pre-vegetation alluvium. He considered sandy braided systems, dominated by sandy-bedforms and downstream-accretion elements, to be the most abundant fluvial style; though noted that ephemeral channelized and unconfined deposits filled with upper flow regime elements were also particularly common. Long (2011) suggested that sandy meandering systems could be identified within pre-vegetation alluvium by measuring the directional relationships between foresets and their underlying bounding surfaces, and suggested conceptual models based on modern distributive systems should be more frequently considered when studying pre-vegetation alluvium.

A variety of low-sinuosity pre-vegetation fluvial styles have been recognised in recent studies, with multiple authors demonstrating that the predominant ‘sheet-braided’ architectural style actually encompasses a number of fluvial channel-patterns (Santos et al., 2014; McMahon and Davies, 2018). It has been shown that, whilst alluvial successions may appear monotonous at outcrop, satellite images may reveal larger scale architectural complexity (Ielpi and Rainbird, 2016a). Using a dataset of Proterozoic to modern alluvial channel dimensions, it has recently been suggested that the aspect-ratios of deep channels have not varied significantly over time (Ielpi et al., 2017). The variously proposed impact of vegetation on deposited alluvium emphasize that further investigation of these anactualistic sedimentary systems is required, especially in order to assess their proposed suitability as Martian analogues (Owen and Santos, 2014; Ielpi and Rainbird, 2016a; Santos and Owen, 2016; Ielpi et al., 2017) (Chapter 8).

Chapter 2

METHODS, TERMINOLOGY AND CHALLENGES

2.1. Fieldwork

Fieldwork was undertaken at a number of locations over the course of this study. The primary field site was the NW Scottish Highlands and Islands, where the later Proterozoic Torridonian Sandstones were studied over a total duration of 107 days (Section 2.1.1). Additionally, Ediacaran-Lower Cambrian alluvium was studied across NW France and the UK Channel Islands (29 days) (Chapter 6). Proterozoic alluvium was studied in Michigan, Minnesota and Wisconsin over the course of 14 days, with the findings of an analysis of the Jacobsville Sandstone, Michigan, presented in Chapter 4. The Archean Jackson Lake Formation, which crops out in the NW Territories of Canada, was studied for three days and is incorporated into Chapter 7. Specific locations of all field sites are presented in Table A1.

In order to ensure that all claims of the unique character of pre-vegetation alluvium are genuine, control sites were studied in both: 1) pre-vegetation marine strata (Neoproterozoic Jura Quartzite, Scotland, 2 days; Cambrian Cap de la Chèvre Formation, France, 2 days; Cambrian Eriboll Formation, Scotland, 2 days; Cambrian Gog Group, Canada, 3 days; Cambrian Wrekin Quartzite, England, 2 days); and 2) syn-vegetation alluvium (Silurian Milford Haven Group, Wales, 3 days; Devonian Brownstones Formation, England, 1 day; Carboniferous Alston Formation, England, 3 days; Carboniferous Millstone Grit, England, 3 days; Jurassic Scalby Formation, England, 2 days; Cretaceous Horseshoe Canyon Formation, Alberta, 1 day). 13 days were also spent studying the predominantly marine Silurian Tumblagooda Sandstone, Australia. The locations of all the control sites visited are also listed in Table A1, but are only incorporated in the main body of the thesis when relevant.

Data was collected in the form of maps of field relationships, sedimentary logs and architectural panels. Most studied sites have exposures suited to facies and palaeocurrent analysis. Palaeocurrents were obtained whenever reliable surfaces were available. Foreset planes were re-oriented on a stereonet to remove bedding dip whenever dip amount exceeded 10°. Techniques used to present palaeocurrent measurements are described in Section 2.1.3. Detailed architectural element analysis (discussed in Section 2.1.2) requires exposures of substantial size, which were available on most occasions in Scotland and France and on rare occasions in Michigan. The exposure quality of the Archean Jackson Lake Formation, NW Territories of Canada, was restricted to small, low relief patchy glacially scoured bedrock, thus was unsuitable for detailed architectural element analysis. Observations of sedimentary structures, erosional and depositional surfaces, grain-size trends and palaeoflow dispersal directions (in sections both parallel and perpendicular to regional palaeoflow) were plotted on architectural panels in order to assess depositional architecture.

Terms used in this thesis that are either new (*) or have been used in conflicting ways in exisiting literature (**) are presented in Table 2.1.

Table 2.1. Glossary of terms.

TERM	DEFINITION
'Sheet-braided'**	Bed with aspect ratio exceeding 20:1 (discussed in Section 7.2.2)
Fluvial style**	A character of an alluvial rock sequence, opposed to an interpretation of fluvial processes
Architectural element**	A package of strata formed by a distinct fluvial process (List of architectural elements in Table 2.2)
Architectural unit*	Genetically related package of strata which comprises multiple architectural elements
Mudrock**	Umbrella grouping of multiple distinct types of fine-grained sediment (< 62.5 μm grains: mudstone, siltstone, claystone, shale)

2.1.1. Main field location: The Torridonian Sandstones

The 'Torridonian Sandstones' (or simply 'the Torridonian') is the informal stratigraphic name for a >10 km thick succession of Proterozoic siliciclastic strata, overlying the Archaean Lewisian gneiss complex, in the Highland region of NW Scotland. It comprises, from oldest to youngest, the Stoer, Sleat and Torridon groups. The Torridonian has been a well-studied unit of British regional stratigraphy for almost 200 years (e.g., MacCulloch, 1819; Sedgwick and Murchison, 1829; Peach et al., 1907). Its historical renown arises from both its wide geographical outcrop extent (200 km north to south, even greater at subcrop (Blundell et al., 1985; Stein, 1988, 1992; Williams and Foden, 2011)), and its status as the oldest unmetamorphosed sedimentary rock in the British Isles.

During the last 50 years, numerous studies have concerned themselves with the sedimentary history of the Torridonian (e.g., Selley, 1965; Williams, 1966, 2001; Gracie and Stewart, 1967; Stewart, 1969, 1982; Nicholson, 1993; McManus and Bajabaa, 1998), its provenance and geochemistry (e.g., Stewart, 1991; Stewart and Donnellan, 1992; Van de Kamp and Leake, 1997; Young, 1999; Williams and Foden 2011), and its palaeomagnetic (e.g., Stewart and Irving, 1974; Smith et al., 1983; Williams and Schmidt, 1997) and tectonostratigraphic (Kinnaird et al., 2007) characteristics. Recently, the succession has seen a revival of interest because: 1) microfossils extracted from Torridonian mudstones, first described by Teall (1907), have been deemed to be the Earth's oldest non-marine eukaryotes (Strother et al., 2011; Battison and Brasier, 2012; Brasier et al., 2016); 2) indirect evidence for early microbial life on land has been described (Prave, 2002; Callow et al., 2011; Strother and Wellman, 2016); and 3) the

Torridonian contains some of the most extensive and easily accessible successions of pre-vegetation alluvial strata worldwide (Owen and Santos, 2014; Ielpi and Ghinassi, 2015; Ielpi et al., 2016; Santos and Owen, 2016; Lebeau and Ielpi, 2017; Ghinassi and Ielpi, 2018; McMahon and Davies, 2018).

The last comprehensive sedimentological study of the Torridonian's entire 200 km x 30 km wide outcrop belt was published in a Geological Society Memoir authored by Sandy Stewart (2002), a culmination of over 40 years of research (e.g., Stewart, 1962, 1963, 1966a,b, 1969, 1972, 1982, 1991, 1995; Stewart and Irving, 1974; Stewart and Parker, 1979). Whilst this work provided abundant information on the lithofacies assemblages of multiple outcrop locations, little to no attention was given to variations in depositional architecture, or the fact that the sedimentary system was operating in the complete absence of vegetation. Over the course of this project, the entire Torridonian outcrop belt was revisited (Fig. 2.1). The findings of this field study are presented in Chapter 4 (Applecross and Aultbea formations), Chapter 5 (Meall Dearg Formation) and Chapter 7 (the Allt-na-Béiste Member of the Diabaig Formation). Specific details regarding the stratigraphic setting of each of the discussed units are presented within their constituent chapters.

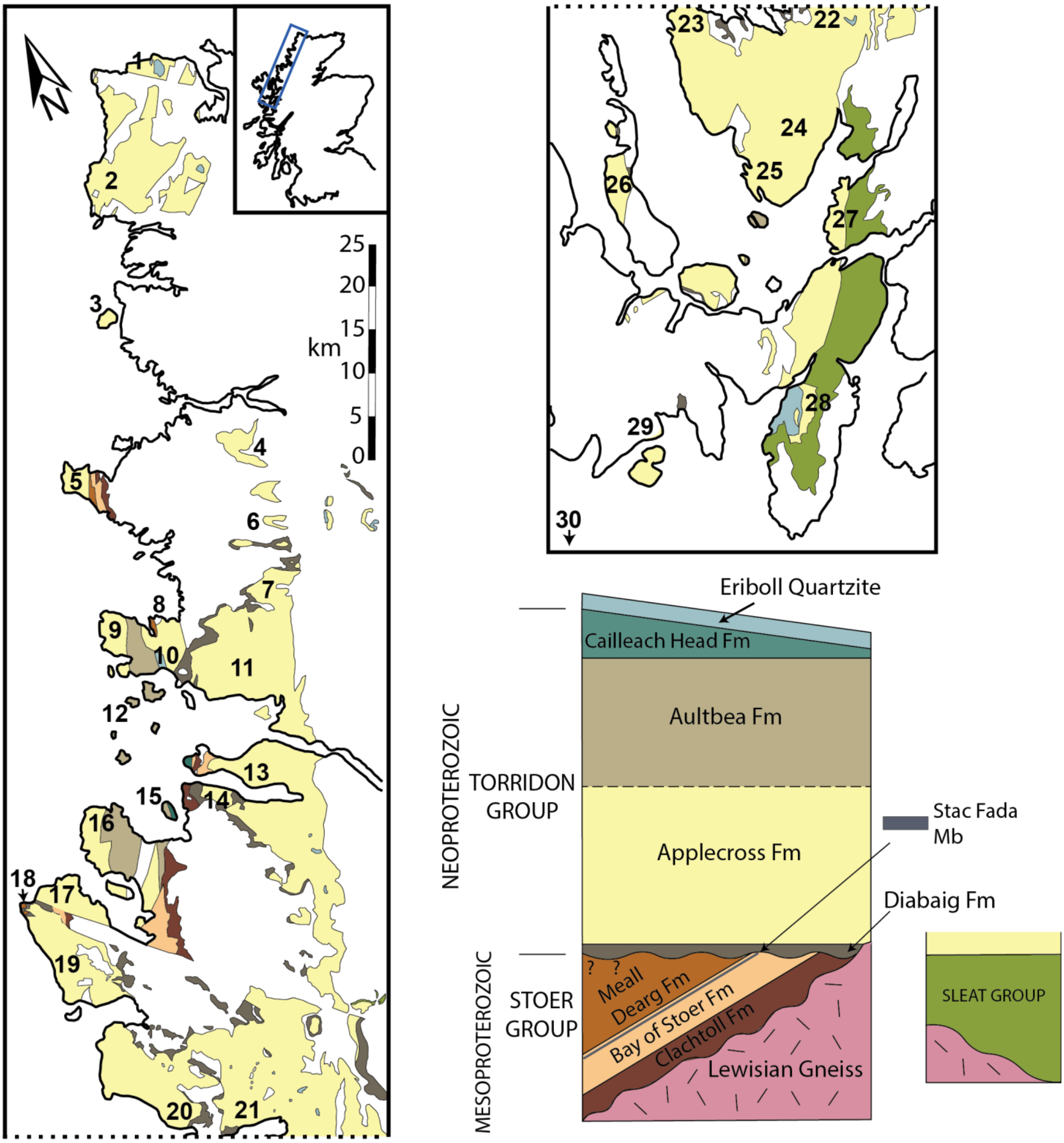

Figure 2.1. Geographic and stratigraphic setting. Left and top right: Geological map of the Torridonian outcrop belt (modified after Stewart, 2002). Numbers mark the studied areas. 1) Cape Wrath; 2) Sandwood Bay; 3) Handa Island; 4) Quinag-Assynt; 5) Stoer peninsular; 6) Suilven; 7) Inverpolly; 8) Enard Bay; 9) Reiff; 10) Achiltibuie; 11) Stac Pollaidh; 12) Tanera Beg; 13) Badrallach; 14) Stattic Point; 15) Gruinard Island; 16) Aultbea-Rubha Mor; 17) Bac an Leth-choin; 18) Rubha Réidh; 19) Big Sand-North Erradale; 20) Diabaig; 21) Alligin-Liathach-Glac Dhorch; 22) Upper Loch Torridon; 23) Fearnmore; 24) Bealach na Ba; 25) Toscaig; 26) Raasay; 27) Kyle of Lochalsh – Kyleakin; 28) Ord; 29) Camasunary; 30) Rùm. Grid references for each of these locations are provided in Table A1. Bottom right: Stratigraphic column of the Torridonian Sandstones.

2.1.2. Architectural element analysis

Alluvial architecture was originally defined by J.R.L., Allen (at the First International Symposium on Fluvial Sedimentology in his keynote address) (Allen, 1978) to describe the geometry and internal arrangement of channel and overbank deposits preserved within alluvium. It is the stratigraphic geometric product of the scale and behaviour of a fluvial system over time, and the orientation relative to palaeoflow which the alluvial outcrop is ultimately exposed. Significant progress has been made in the evaluation of alluvium due to the appreciation that strata can be subdivided into genetically related packages (e.g., Allen, 1983; Friend, 1983; Miall, 1985). The most widely used approach is architectural element analysis (Miall, 1985, 1988, 1996; Fielding, 2006; Long, 2011). This technique attempts to bridge the gap between fluvial sedimentology and modern geomorphology by organising alluvium into basic 'architectural elements' which together have been suggested to comprise all components of a modern fluvial system (Miall, 1985) (Table 2.2; Fig. 2.2).

Table 2.2. List of architectural elements referred to in this study. After Miall (1985, 1996), Fielding (2006) and Long (2011)

Element	Acronym	Description
Channels	CH	Channel margins are present/bedforms have underlying erosional concave-up geometry
Gravel bars and bedforms	GB	Any lithofacies comprising gravel-grade sediment
Sediment-gravity-flow deposits	SG	Narrow, elongate lobes or sheets which can be confidentially related to debris flow or related formation mechanisms. Typically interbedded with GB or SB elements.
Sandy bedforms	SB	Sand-grade elements not genetically related to their underlying surface.
Downstream-accretion element	DA	Bedform migration ±30° down-slope of a genetically related underlying surface
Downstream-lateral-accretion element	DLA	Bedform migration 30°-60° down-slope of a genetically related underlying surface
Lateral-accretion-element	LA	Bedform migration 60°-120° of the underlying surface
Upstream-accretion element	UA	Bedform migration ±30° up-slope of a genetically related underlying surface
Upstream-lateral-accretion element	ULA	Bedform migration 30°-60° up-slope of a genetically related underlying surface
Upper-flow-regime element	UFR	Any element comprising bedforms which developed under upper-flow regime conditions.
Hollow	HO	Elements bounded at the base by curved, concave-up surfaces. They are not cylindrical in shape (as are channels), but are scoop-shaped.
Levee deposit	LV	Wedge shaped element which can be confidently linked to overbank flooding. LV deposits must taper away from an identified CH element.
Crevasse-channel deposit	CR	Element which can be confidently linked to a break in the main channel margin
Crevasse-splay deposit	CS	Element which can be confidently linked to progradation from a crevasse channel into the floodplain
Floodplain fines	FF	Deposits of overbank sheetflow, floodplain ponds and swamps
Abandoned channel fills	FF(CH)	Like CH elements, FF(CH) elements have an underlying erosional concave-up geometry, but channel fill is typically mud-silt grade.

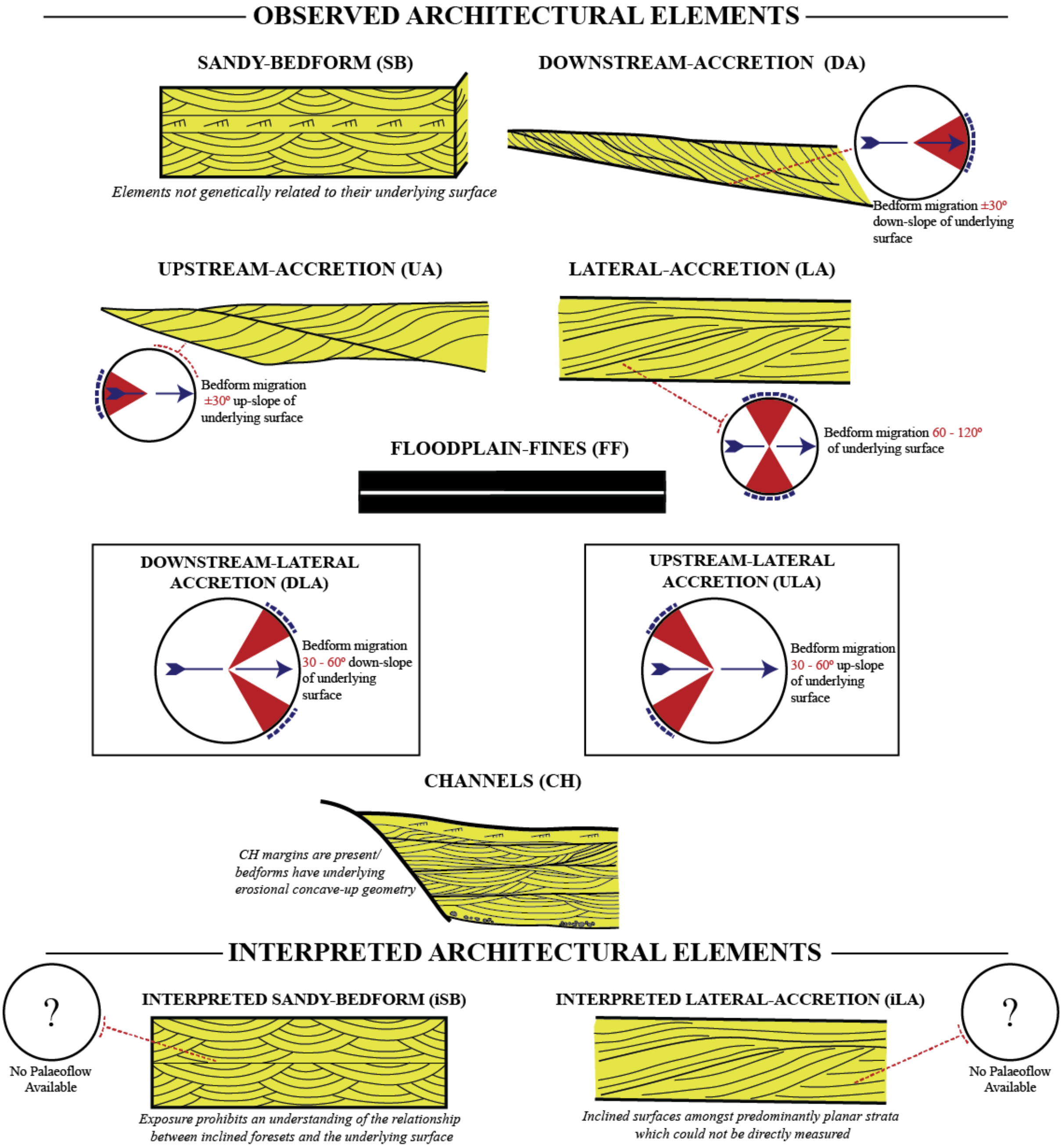

Figure 2.2. Examples of observed and interpreted architectural elements used in this thesis (after Miall (1985, 1996) and Long (2011)). Blue arrows denote direction of dip of underlying surface. *Architectural elements listed not exhaustive*.

While successful application of architectural element analysis has been proven to permit interpretation of past fluvial processes (e.g., Long, 2006; McLaurin and Steel, 2007; Ghazi and Mountney, 2009), its practical application in natural rock outcrops has limitations because confident differentiation often requires large, clearly-weathered three-dimensional exposures that are not always available. Additionally, depending on the balance of depositional-dip/-strike exposures in an outcrop belt, exposure orientation can impose an observation bias on any census of architectural elements within a succession.

A further discordance between theoretical and practical architectural element analysis is that, in the field, many natural exposures do not contain sufficient evidence to conclusively prove whether or not an element is accretionary. Accretionary elements are those which contain internal growth increments defined by multiple set/coset boundaries each terminating against a common underlying surface. The dip and strike of the common underlying surface, relative to the dip directions of inclined foresets (palaeoflow), reveal the orientation of accretion (e.g., DA, LA, UA (Fig. 2.2)). Conversely, elements may be genuinely genetically unrelated to their underlying surfaces. For example, 'sandy-bedform' elements (SB) develop when fields of ripples and dunes accumulated predominantly by vertical aggradation (Fig. 2.2). On occasions where the vagaries of outcrop exposure prohibit an accurate understanding of the relationship between inclined sets/cosets and their underlying surface, conclusively discriminating between these element types is not possible.

In order to mitigate any inherent uncertainty involved in applying architectural element analysis in the study of natural rock outcrops, in this thesis, architectural elements that can be classified definitively are differentiated from those which can only be identified with a degree of interpretation. To avoid conflation of observation and interpretation, if an architectural element was interpreted only, because bounding surfaces were not directly measurable, it was given the prefix 'i' (e.g., iDA, iLA) (Fig. 2.2). This prefix was also assigned to 'sandy-bedforms', which are here distinguished into two categories: (1) those unambiguously unrelated to their underlying surface (SB); and (2) those which may or may not be genetically related, but where exposure prohibits an understanding of the relationship between inclined foresets and the underlying surface (iSB).

During the application of architectural element analysis, it is important also to appreciate that no single architectural element relates to only one geomorphic unit (defined as the building blocks of a modern river (Brierley and Hickin, 1991)) (Fig. 2.3). Therefore, in order to interpret preserved geomorphic units in ancient alluvium, configurations of multiple architectural elements must be recognised at outcrop. This is reflected in the fact that whilst there are only 14 architectural elements in common usage (Miall, 1985, 1988, 1996; Fielding, 2006; Long, 2011), fluvial geomorphologists have identified 68 geomorphic units when describing modern riverscapes (Wheaton et al., 2015). Of these, 37 are depositional, such that they may feasibly be preserved in the rock record. However, 10 of these require vegetation (e.g., island, backswamp) or other lifeforms (e.g., beavers; beaver meadow) in order to develop. In total, 27 of the depositional geomorphic units identified by Wheaton et al. (2015) require no biological input such that they may feasibly be preserved within pre-vegetation alluvium (Fig. 2.3, Table 2.3).

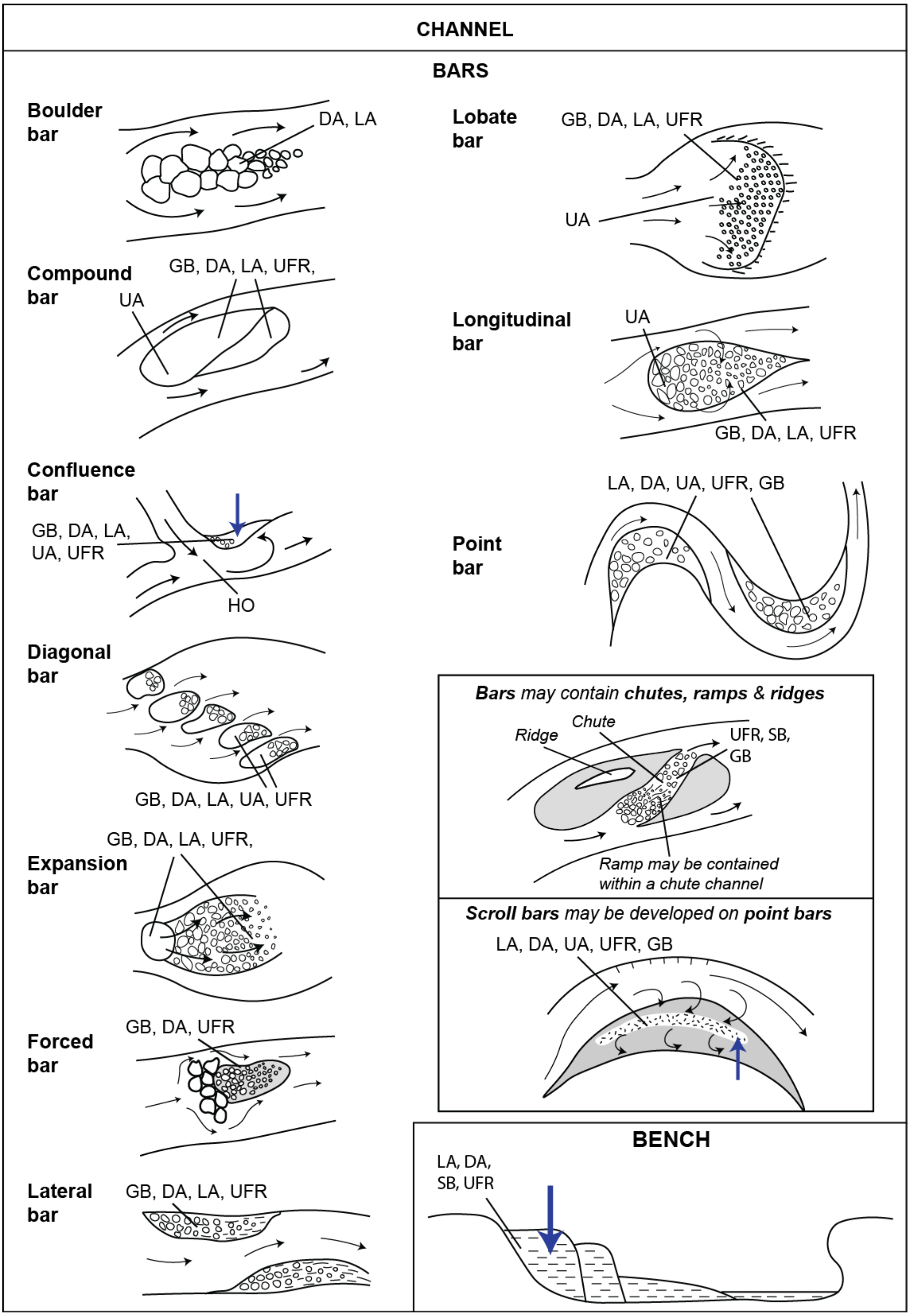

Figure 2.3. Relationship between architectural elements and geomorphic units that may feasibly be preserved in pre-vegetation alluvium. Architectural elements after Miall (1985, 1988, 1996), Fielding (2006) and Long (2011). Geomorphic units after Wheaton et al. (2015). Blue arrow (when used) highlights geomorphic unit. Diagrams of geomorphic units modified from Fryirs and Brierley (2012). *Continued overleaf*

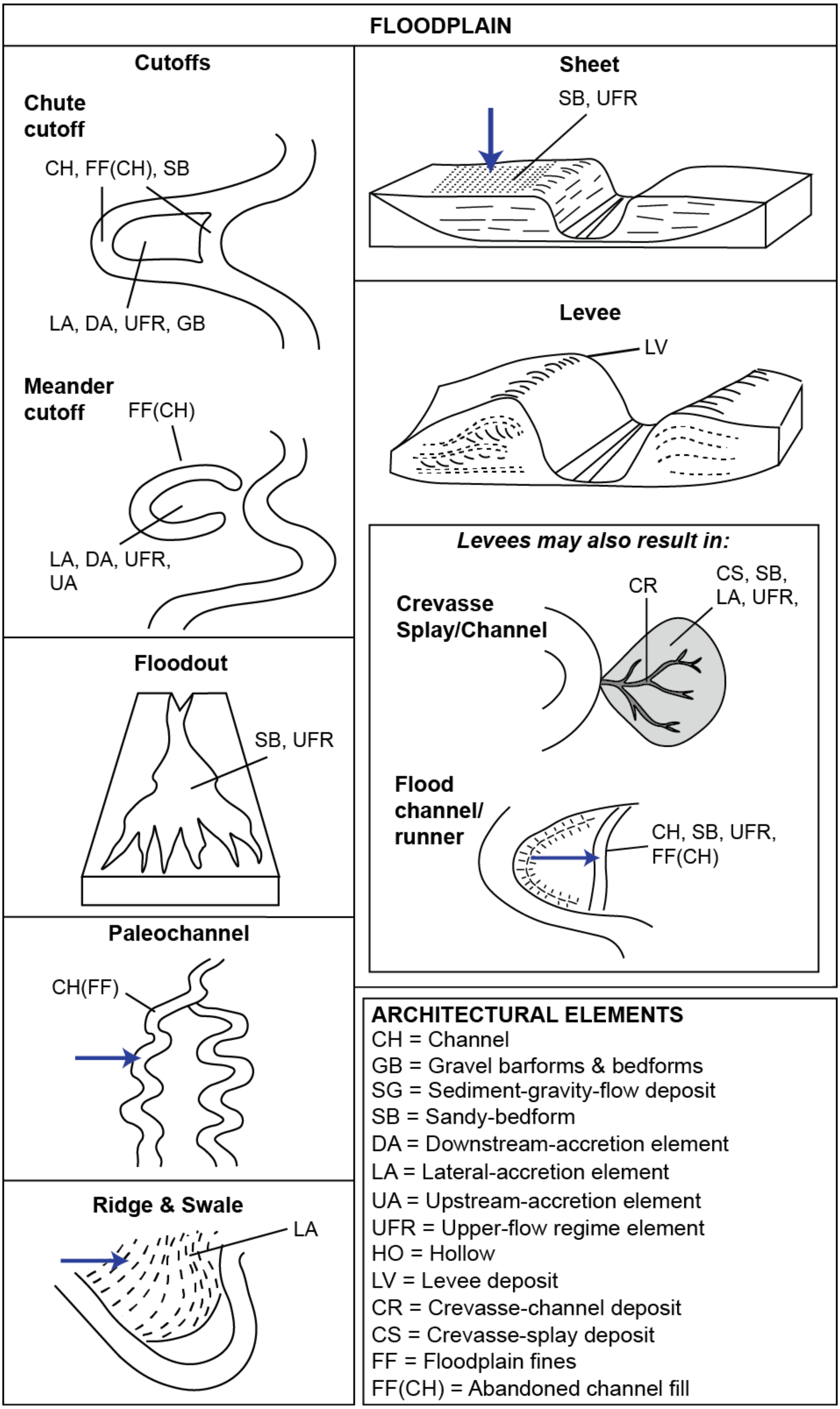

Figure 2.3. *(Continued)*

Table 2.3. Descriptions of geomorphic units which may feasibly be preserved within pre-vegetation alluvium. Definitions from Fryirs and Brierley (2012)

Geomorphic Unit	Description
1. Bench	Stepped, elongate feature that is inset along a bank. These in-channel sediment storage units are often situated atop bar deposits
2. Boulder bar	Linguoid-shaped boulder feature. Comprise a cluster of boulders, fining in a downstream direction
3. Chute	Elongate, relatively straight channel that dissects a bar surface
4. Chute cutoff	Straight/gently curved channel that dissects the convex bend of the primary channel, short-circuiting the bend
5. Compound bar	Bar that comprises an array of smaller scale geomorphic units
6. Confluence bar	Formed at, and immediately downstream of, the mouth of tributaries. They represent a form of slackwater deposit that is not elevated above the channel and is prone to reworking
7. Crevasse splay	A sediment tongue fed by a crevasse channel that breaches the levee
8. Diagonal bar	Mid-channel bar, oriented diagonally to banks
9. Expansion bar	Mid-channel bar with a fan-shaped planform. Often occur downstream of a bedrock constriction that hosts a forced pool
10. Flood channel	Low-sinuosity subsidiary channel with a defined bed and banks
11. Flood runner	Relatively straight depression that occasionally conveys floodwaters
12. Floodout	Lobate/fan-shaped body that radiates downstream from an intersection point of a discontinuous channel
13. Floodplain	Lies adjacent to or between active or abandoned channels and the valley margin
14. Forced bar	Barform that is induced by a flow obstruction (e.g., bedrock outcrop, boulders)
15. Lateral bar	Bank-attached bar developed along low-sinuosity reaches of a channel. These bars occur on alternating sides of the channel
16. Levee	Raised elongate asymmetrical ridge that borders the channel
17. Lobate bar	Mid-channel bar, oriented perpendicular to flow, generally found at points of abrupt channel and flow expansion points
18. Longitudinal bar	Mid-channel, elongate bar, aligned with flow direction
19. Meander cutoff	A meander bend that has been cut through the neck, leaving an abandoned meander loop on the floodplain
20. Paleochannel	Inactive channel on the floodplain
21. Point bar	Bank-attached arcuate-shaped bar developed along the convex banks of meander bends
22. Ramp	Ramp-like feature that partially infills a chute channel
23. Ridge	Linear, elongate deposit formed atop a bar platform on a mid-channel or bank-attached bar
24 & 25. Ridge & Swale	Ridges are scroll bars that have been incorporated into the floodplain. Swales are the intervening low-flow channels
26. Scroll bar	Elongate ridge form developed along the convex bank of a bend. Commonly develop on point bars with an arcuate morphology
27. Sheet	Flat, tabular laterally extensive sheets in non-levee settings. Differentiated from splays by their shape, extensive area, and lack of distal thinning

2.1.3. Graphical presentation of palaeocurrent directions

Outcrop photographs which show two-dimensional representations of three dimensionally dipping surfaces (e.g., cross-bed foresets) are commonly used throughout this thesis. In many instances, accurate depiction of the dip direction of such features is challenging as an outcrop photograph often presents information on a vertical plane and directional data refers to a horizontal plane. In these instances, the graphic method for depicting horizontal data on vertical outcrop photographs recently described by Davies et al. (2018) is used (Fig. 2.4).

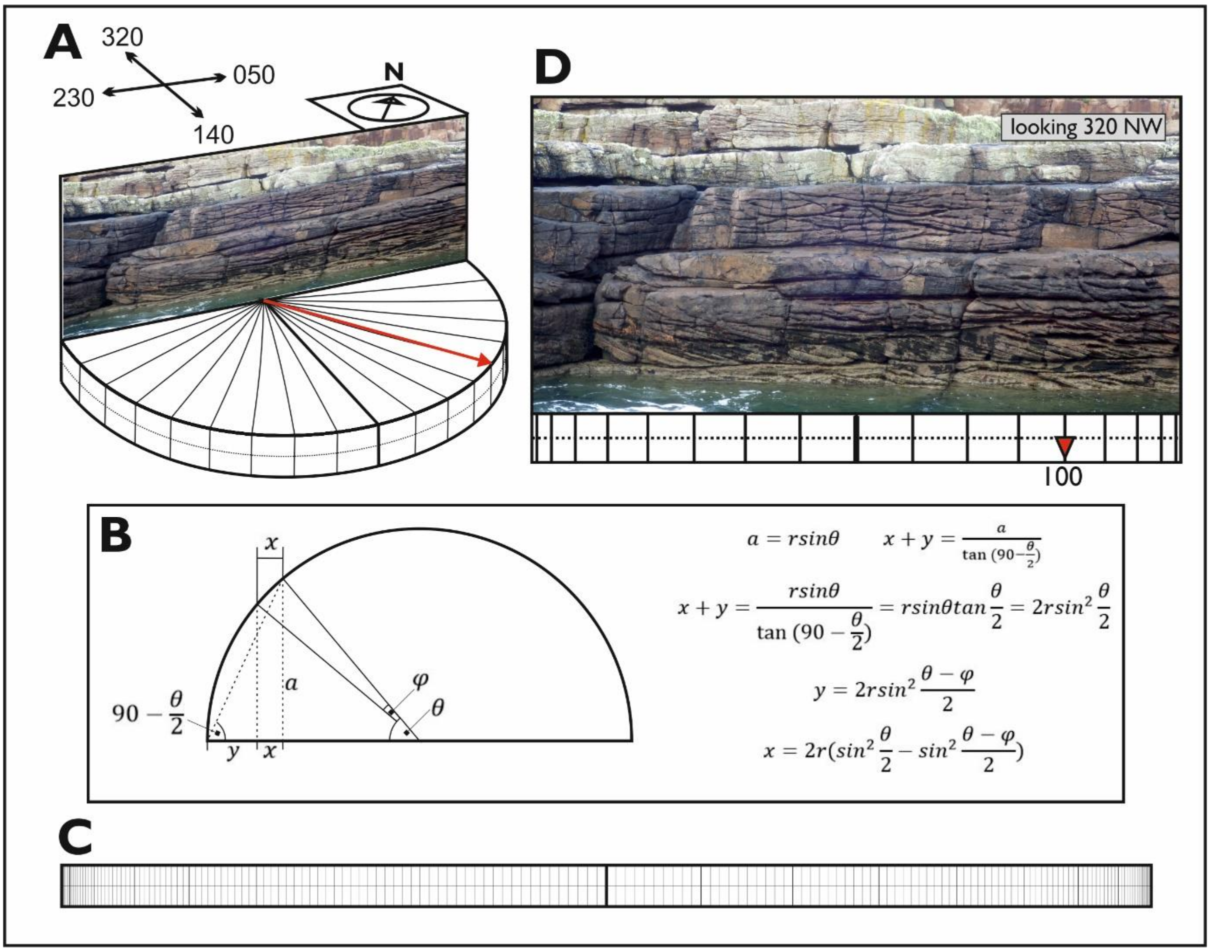

Figure 2.4. From Davies, McMahon and Shillito (2018) (their Figure 2): A) Visualization of an outcrop face (at Handa Island) relative to a semi-circle (showing palaeoflow) and compass points; B) Calculations used to determine degree spacing on the 2D bar in (C): derivation of the length of the projection of an arc onto a line parallel to the diameter of a semicircle (x) for any given θ, φ and r. Where θ is the central angle of a sector from the diameter encompassing the projected arc, φ is the central angle of a sector only encompassing the projected arc, and r is the radius of the semicircle; C) Rectangular bar, subdivided into 180 degree increments, with upper bar indicating flow into outcrop and lower bar indicating flow out of outcrop; to be used as a template for reporting paleoflow relative to outcrop; D) Worked example of use of paleocurrent bar using image from (A): note that this image shows only mean palaeoflow direction, and that the palaeoflow of individual beds could be illustrated. Further details of the methodology can be found in Davies et al. (2018).

2.2. Database of Archean-Carboniferous alluvium

The oldest preserved alluvium worldwide is found within the 3.6 Ga Serra do Córrego Formation, Brazil (Teles et al., 2015), and younger alluvium is known from every subsequent interval of geological history. The alluvial stratigraphic record thus represents periods before, during and after the evolution of vegetation. As such, it is our primary means of studying the effect vegetation evolution had on ancient landforms and Earth sedimentary processes. In order to observe and quantify shifts in the frequency of sedimentary facies, structures, architectures and lithologies, coeval with the evolution of land plants, a database of Archean-Carboniferous alluvium was constructed (herein referred to as 'the database') (Table A2, Table A3). Results from database analyses are incorporated throughout this thesis.

2.2.1. Database construction

The database covers formations from every present-day continent thus permitting as global view as possible of the variety of pre-vegetation and syn-vegetation alluvial characteristics. Data was collated from a survey of Earth's 704 globally-distributed Archean-Carboniferous alluvial stratigraphic units, reduced and analysed from 1196 published reports (Table A2, Table A3). This is an exhaustive list of all published records searchable when applying the methodology detailed below. A variety of characteristics were recorded for Archean-Cambrian alluvium (listed in Table 2.4 and Table A3). Additionally, mudrock abundance was quantified in all compiled Ordovician-Carboniferous alluvial units which had this information available/obtainable (Table A2, Section 2.2.3).

The compilation was initiated using the internet search engines ISI Web of Science (http://wok.mimas.ac.uk), GeoRef (https://www.americangeosciences.org/georef/georef-information-services), and Google Scholar (https://scholar.google.com/), using the search terms "fluvial" and "alluvial" in conjunction with both extant and outdated, global and regional stratigraphic terms in both American and British English (e.g., "Paleoproterozoic", "Palaeoproterozoic"). The dataset was further expanded utilizing references cited within these results, and by incorporating conference abstracts, regional guidebooks, geological survey reports, and PhD and Masters theses where these could be identified or were already known. The method has ensured that any unit in the database has previously been interpreted, from its sedimentary character, to represent an alluvial sedimentary deposit. Where any given stratigraphic formation was composed of the facies of multiple environments, only the alluvial facies of that unit are referred to. Note that the search was not undertaken on lithological grounds and terms such as 'Sandstone' or 'Quartzite' are only listed in the database where these are local names for lithostratigraphic units (i.e., metasedimentary units were also included in the database, but only if their depositional environment had previously been interpreted; e.g., "60. Baraboo Quartzite" (Table A2)).

Each publication of relevance was individually data-mined for relevant information applying the methods set out in Table 2.4. The formations cited in these were grouped or subdivided into the most recently used or formal stratigraphic nomenclature, where known, with particular use made of the online stratigraphic lexicons of the UK (http://www.bgs.ac.uk/lexicon/), USA (http://ngmdb.usgs.gov/Geolex/geolex_home.html), Canada (http://weblex.nrcan.gc.ca/weblexnet4/weblex_e.aspx) and Australia (http://dbforms.ga.gov.au/www/geodx.strat_units.int). After the data was collected, some limitations became apparent. For example, insufficient data existed to enable a statistical analysis of the various architectural elements preserved in pre-vegetation alluvium, or the various palaeolatitudes at which alluvium was deposited.

Table 2.4. Compiled characteristics of Archean-Cambrian alluvium (data presented in Table A3). Mudrock abundance was additionally calculated for all compiled Ordovician-Carboniferous units (data presented in Table A2).

Sedimentary feature	Comments
1) Age	Used when explicitly recorded in original studies or online stratigraphic lexicons. Where a range of ages was given, the mean value was used in analyses
2) Rock Unit	Rock unit name as described by original authors (e.g., group, formation or member)
3) Location	Present-day geographic location of rock unit
4) Interpreted fluvial style	Recorded only when explicitly interpreted by original authors
5) % Mudrock in the succession	Recorded from text or assessed from sedimentary logs following the methodology described in Section 2.2.3
6) Succession thickness	Recorded for reference purposes when explicitly stated in original publications
7) Sandstone petrology	Original authors recorded sandstone petrology using various sandstone classification schemes. Petrology was translated to the scheme devised by Folk (1980) whenever possible. In instances where this was not possible (e.g., arkosic arenite), terminology used by the original authors was retained
8) Sedimentary structures	Sedimentary structures were recorded if original authors stated they were present, either in the text or using sedimentary logs. Numerical values were only recorded when stated by original authors in the text
9) Cross-stratification thickness	Minimum, average and maximum cross-stratification height recorded when explicitly stated by original authors
10) Architectural elements	Architectural elements recorded when explicitly stated by original authors
11) Presence of soft-sediment deformation	Recorded when explicitly stated by original authors
12) Palaeolatitude	Recorded when explicitly stated by original authors
13) Basin type/Tectonic setting	Recorded when explicitly stated by original authors
14) Palaeoclimate	Recorded when explicitly stated by original authors
15) Additional information	Any other pertinent information about the alluvial succession. For example: 1) presence of intraformational mud clasts (Section 3.2); 2) presence of microbially induced sedimentary structures (MISS)

2.2.2. Geographic bias

Geographic bias could skew observed trends if particular palaeo-tectonic or -climatic settings were over-represented. However, this is not considered a problem within the dataset. Although North American and European case studies dominate the (predominantly English-language) survey, the survey has global coverage (Fig. 2.5, Fig. 2.6) and data from every modern continent are represented in the study; North America (n = 262, 37.3%); Europe (n = 195, 27.7%); Asia (n = 65, 9.2%); Africa (n = 80, 11.3%); Australia (n = 56, 8.0%); South America (n = 41, 5.8%); Antarctica (n = 5, 0.7%).

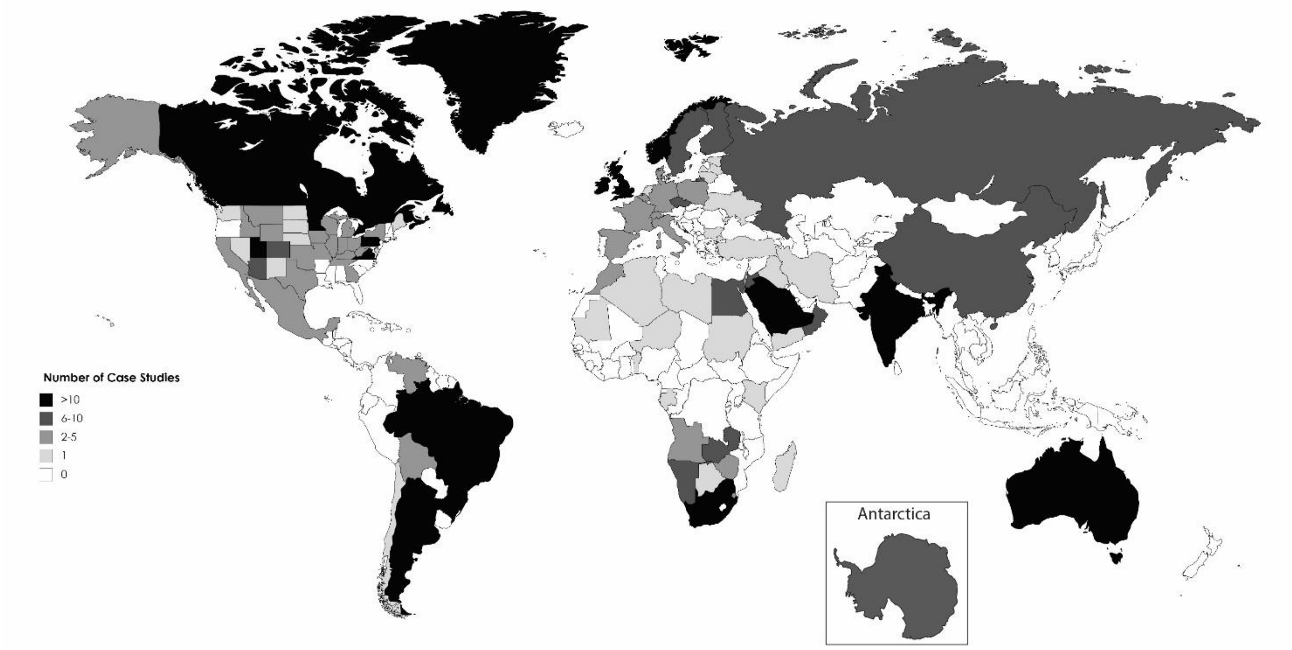

Figure 2.5. Geographic distribution of Archean-Carboniferous case studies (Table A2).

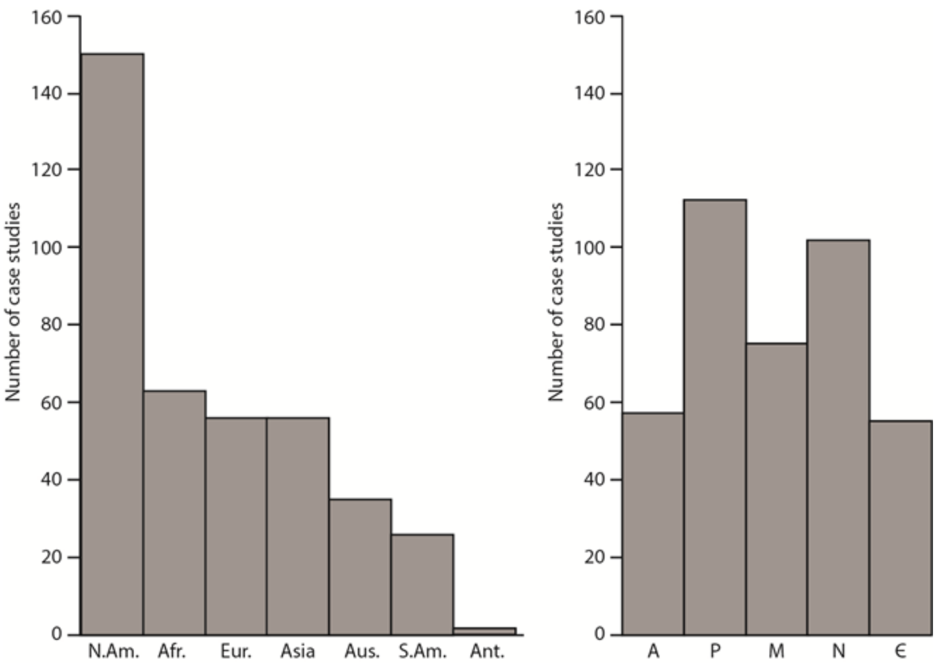

Figure 2.6. Distribution of Archean-Cambrian case studies in the database, showing number of case studies from each age/locality (Table A3). Left: Geographic distribution (present-day continents). Right: Stratigraphic distribution. A=Archean, P=Palaeoproterozoic, M=Mesoproterozoic, N=Neoproterozoic, C=Cambrian

A lack of studies or published data for certain regions (e.g., central Africa) is a natural limitation of the project, but near-global coverage of the existing data mitigates against the likelihood that these regions contain any unique signatures that would skew observed trends if they were available for inclusion. Further, plate tectonic realignment of the continents since the deposition of the different formations means that the palaeogeographic spread of datapoints is substantially more global for any given interval than is apparent from the modern geographic spread.

2.2.3. Assessing mudrock abundance

An analysis of preserved mudrock in Archean-Carboniferous alluvium is presented in Section 3.1, with the information collected from a survey of 704 globally-distributed Archean-Carboniferous alluvial stratigraphic units (Section 2.2.1). The abundance of mudrock was assessed by measuring the stratigraphic thickness of the lithology, relative to coarser sediment fractions within each alluvial formation. For published data, where the proportional thickness was explicitly recorded by the original authors this information was used. If the original authors gave a range of mudrock values, the average value was used. In other instances, such data was not noted, but the presentation of stratigraphic logs enabled the proportion to be calculated by my own direct measurement of the thicknesses of different strata. For 110 of the 704 total formations, retrieving any value of mudrock percentage was not possible.

The abundance estimates are made using stratigraphic thickness because such information is readily retrievable from published data and in the field. The stratigraphic thickness of mudrock refers to the relative proportion of mudrock at a point locality (e.g., as exposed in outcrop or core). It differs from volumetric data, but is more accurate for the present study for the following reasons: 1) while volume is ultimately the desired value, it cannot be directly measured in the same way as stratigraphic thickness. Volumetric data is estimated, primarily calculated using outcrop data (e.g., the areal extent of a mapped lithologic unit, combined with tectonic dip (Ronov, 1994; Peters and Husson, 2017)). Subsurface variation in mudrock content cannot be addressed using either volume estimates or thickness measurements; however, the latter provides true data in the form of random sampling of points within a volumetric succession (i.e., those parts of the succession which happen to be exposed); 2) thickness can be directly corrected for tectonic tilt; 3) it is important to note that the values presented are cumulative: that is, without exception in all 704 formations, there was no direct segregation of mudrock and coarser sedimentary lithologies. For example, a 100 metre thick succession with 50% mudrock would never be 50 metres of sandstone followed by 50 metres of mudrock, but rather alternating and repeating sandstone and mudrock layers on a cm- to m-scale. Resolving such fine detail is only possible through measurement from stratigraphic sections and cannot be achieved using coarser datasets such as geologic maps. The alternating nature of such heterolithic strata also mitigates against issues of suspected preferential erosion of mudrock strata in that lithified mudrock cannot be surgically extracted from between sandstone layers whilst retaining the integrity of a stratigraphic exposure; and 4) mudrock strata undergo greater post-depositional compaction than coarser sedimentary rocks. However, it is inconsequential that thicknesses of mudrock strata do not reflect original thicknesses of mud accumulation. Strata of Archean to Carboniferous age are all fully lithified and comparison of the proportion of mudrock strata relative to coarser sediment is an accurate proxy for understanding relative mudrock abundance.

In the studies used to compile the database, the classification of mudrock type was made to widely different levels of accuracy, depending on the individual scientific remit of any one original publication. As such, mudrock terminology (mudrock, mudstone, siltstone, claystone, shale) is reported in accordance with the usage of the original authors, and no interpretive grouping of terms was undertaken, in order to mitigate misinterpretation. For this reason, the trends in mudrock proportion as a whole are likely to be more accurate than for individual mudrock types (which may originally have been diagnosed with varying degrees of certainty).

2.3. Distinguishing marine vs non-marine strata

Pre-vegetation clastic successions are dominantly tabular and cross-bedded regardless of marine or continental influence (e.g., Dott et al., 1986; Runkel et al., 2007; Davies and Gibling, 2010a; Davies et al., 2011) meaning that there is a heightened risk of misidentifying depositional setting. Examples of pre-vegetation formations that have been interpreted as both marine and non-marine by different authors include (but are not limited to): 1) Mississagi; 2) Serpent; 3) Lorrain; 4) Bradore; 5) Adams Sound; and 6) Daspoort (see references in Table A2).

Very few sedimentological criteria are diagnostic of a particular environment, such that it has been proposed that in many instances individual outcrops will present little conclusive evidence in favour of either a marine or non-marine origin (Long, 1978). Considerable overlap of the grain size, petrology, scale and abundance of sedimentary structures exists between the two settings. For example, whilst desiccation cracks and rain drop impressions provide evidence of temporary emergence, these structures occur in any emergent environment where muddy substrates develop. Even stromatolites, where present, may have developed within entirely non-marine settings (Fedorchuk et al., 2016) (Fig. 2.7).

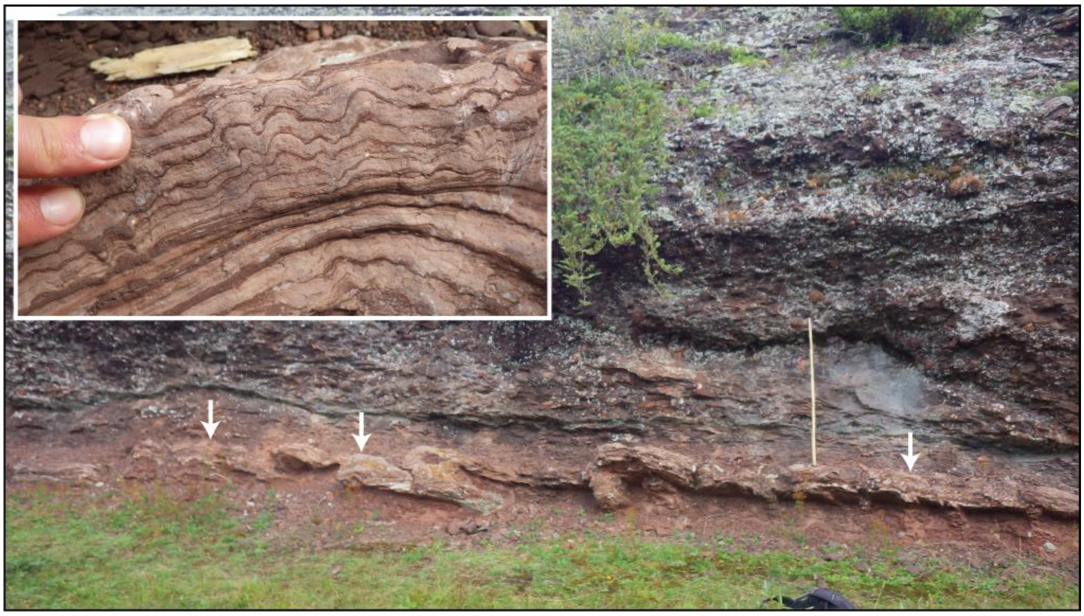

Figure 2.7. Stromatolites in the Mesoproterozoic Copper Harbour Formation, Michigan. Stromatolite layer (marked by white arrows and base of metre rule) situated in siltstone facies directly beneath alluvial fan conglomerates. Inset. Detail of stromatolite.

Analysis of palaeocurrent dispersal is a widely used approach towards distinguishing marine and non-marine. Most fluvial environments are characterised by a low degree (e.g., Rainbird, 1992), or radial dispersal (e.g., Weissmann et al., 2010), whereas marine and marginal-marine settings often show diffuse (e.g., Wermund, 1965) or bimodal patterns (e.g., Hofmann, 1966). An architectural element approach (Section 2.1.1) may also aid in determining depositional origin, as this provides an objective method for identifying the three-dimensional geometry of sedimentary packages (Allen, 1983; Miall, 1985, 1996; Long, 2011). Alluvium may contain particular architectural elements which strongly suggest deposition by fluvial processes. For example, stacked downstream-accretion elements imply deposition by periodically migrating barforms during peak-floods within a perennial river (e.g., Long, 2006). Lateral-accretion elements may develop on the sinuous bends of fluvial systems (Miall, 1985), or by accretion on side- or in-channel-bars (Bristow, 1987). However, even in these instances, interpretations based on the local occurrence of architectural elements are often insufficient as such elements are not necessarily unique to fluvial environments. For example, periodically accreting barforms also develop within frequently emerged intertidal settings, within which tidal bars migrate when fully submerged (Legler et al., 2013). Lateral accretion also occurs in tidal flat and tidal channel environments (Mowbray, 1983); although in these environments they are more frequently heterolithic (Thomas et al., 1987).

In order to minimise uncertainty, the configuration of architectural elements must be studied across as large as area as possible, such that the regional relationships between elements and lithofacies can be identified and basin-wide transitions analysed. Only by assessing the balance and combination of sedimentary characteristics, including architectural elements, palaeocurrent dispersal and lithofacies, can an authoritative interpretation of marine or non-marine be made.

While the problem of distinguishing marine and non-marine is particularly acute for Precambrian strata, in Cambrian and younger pre-vegetation strata, confidently differentiating certain clastic successions as marine is increasingly made possible by palaeontological evidence (e.g., shelly fossils, bioturbation).

Chapter 3

SEDIMENTOLOGICAL CHARACTER OF PRE-VEGETATION ALLUVIUM

3.1. Mudrock

In terms of bulk lithology, it is a long-held anecdotal contention that mudrock is rare in alluvium that was deposited prior to the evolution of land plants, but common thereafter (Long, 1978; McCormick and Grotzinger, 1993; Grotzinger et al., 2014). This contention is quantitatively tested here and found to be true (Fig. 3.1).

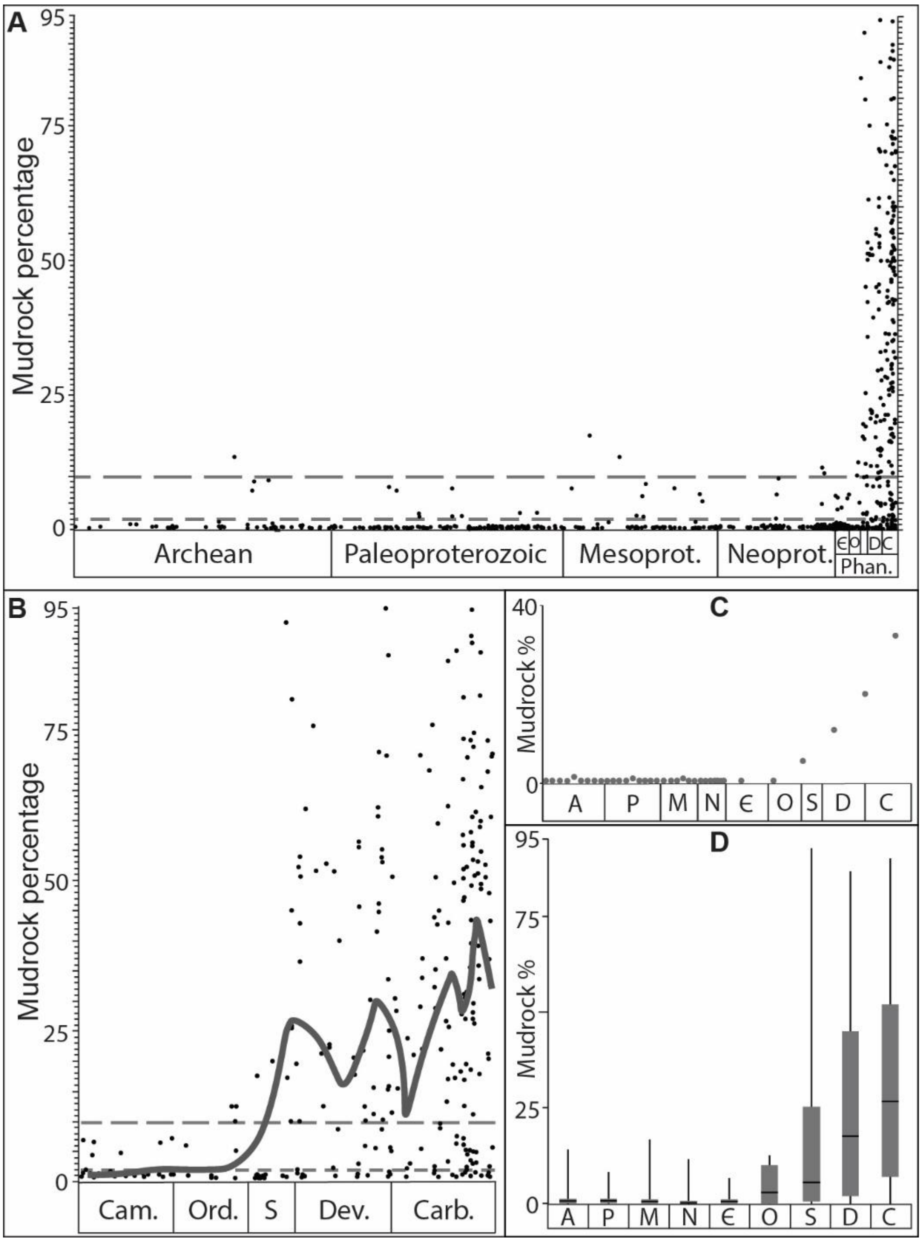

Figure 3.1. Range and maximum proportion of mudrock in alluvial successions increases dramatically after the evolution of vegetation. Proportion of mudrock within alluvial successions (% of vertical stratigraphic thickness) plotted against geologic age (x-axis scaled to numerical ages – start of intervals based on the GTS2012: Archean [4000 Ma], Paleoproterozoic [2500 Ma], Mesoproterozoic [1600 Ma], Neoproterozoic [1000 Ma], Cambrian [541.0 Ma], Ordovician [485.4 Ma], Silurian [443.8 Ma], Devonian [419.2 Ma], Carboniferous [358.9 Ma], Permian [298.9 Ma]): A) Each individual plot records one of the known 594 alluvial stratigraphic units deposited during this interval. Long-dashed line = 10%; Short-dashed line = 2%; B) Enlarged plot for the Phanerozoic with LOESS regression line (solid grey line). LOESS was conducted with a smoothing parameter of 0.9; C) Proportion of mudrock corrected for variation in sampling intensity by subsampling. Each individual plot represents the median value seen across 100 individual subsampling trials (see Section 3.1.3.3); D) Median, range, upper quartile and lower quartile of mudrock proportion for each interval.

Figure 3.1 demonstrates that mudrock is a negligible component of alluvial strata deposited during the first c. 3.0 Ga of Earth's sedimentary rock record, but common or dominant after the middle Palaeozoic (mudrock defined lithologically; all rocks dominantly composed of detrital and weathered sedimentary grains, <= 0.063 mm (siltstone) (Ilgen et al., 2017)). In Archean (4000-2500 Ma) strata, the cumulative stratigraphic proportion of mudrock within alluvial strata ranges between 0-14% (median: 1.0%), whereas in Carboniferous (358.9-298.9 Ma) strata the range is 0-90% (median: 26.2%) (Fig. 3.1D). LOESS regression analysis of the data constrains the onset of the upsurge to between the Late Ordovician and Silurian (458-419 Ma) (Fig. 3.1B), after which interval the range and average proportion of mudrock in alluvium never reverted to the same low values that characterised the first 3 Ga of Earth's stratigraphic record. Subsampling of the data shows that, relative to Archean to Middle Ordovician (3500-458 Ma) values, the percentage of mudrock was 1.1 orders of magnitude greater in the Late Ordovician to Silurian (458-419 Ma), 1.3 orders of magnitude greater in the Early to Middle Devonian (418-379 Ma), 1.45 orders of magnitude greater in the Late Devonian to early Carboniferous (378-339 Ma), and 1.75 orders of magnitude greater in the middle to late Carboniferous (338-299 Ma) (Fig. 3.1C) (subsampling methodology is discussed in Section 3.1.1.3).

This stratigraphically unidirectional upsurge in alluvial mudrock likely rules out a cause due to episodic or cyclic geological phenomena (such as tectonic or climatic controls) that persisted on the Earth throughout the Archean to Carboniferous (Davies et al., 2017a) (Fig. 3.2). The first 3 Ga of the studied interval witnessed multiple alternations between icehouse and greenhouse conditions (Hoffman, 2009), the assembly of at least two supercontinents (Bradley, 2011) and 16 known regional orogenies (Torsvik and Cocks, 2016). None of these events seem to have had any apparent influence on the near-uniform global scarcity of preserved alluvial mudrock. Similarly, the Late Ordovician onset of the trend does not correlate with other prominent potential triggers in the geological record. For example, it post-dates Paleoproterozoic oxygenation by at least 1640 Ma (Lyons et al., 2014), Neoproterozoic oxygenation by 142 Ma (Lyons et al., 2014*)* and the inferred advent of microbial life on land by 2540 Ma (Lenton and Daines, 2017), and pre-dates the increased preservation of non-marine strata by roughly 60 Ma (Peters and Husson, 2017). Testing the data against various alternative hypotheses (Section 3.1.1), the most plausible explanation is that pre-Ordovician Earth had unique syn-depositional controls on sedimentation, which discouraged the production or accumulation of alluvial mudrock. The trend mirrors the fossil plant record (Rubinstein et al., 2010; Matsunaga and Tomescu, 2016; Boyce and Lee, 2017) and the appearance of primitive plants would have introduced three mechanisms important for producing mudrock-rich alluvial strata. Plants lead to an increased production of the directly-weathered fraction of fines (clays) (Nesbitt et al., 1997; Quirk et al., 2012; Hazen et al., 2013; Edwards et al., 2015; Morris et al., 2015; Mitchell et al., 2016; Xue et al., 2016; Boyce and Lee, 2017). They also increase retention of all (weathered and detrital) fines in continental deposystems, through binding (i.e., the fastening of masses of grains by plant parts such as roots) (Mitchell et al., 2016; Xue et al., 2016). Finally, the process of baffling (i.e., the capture and forced deposition of grains from within a moving fluid passing over and around plant parts) also increases retention of all (weathered and detrital) fines in continental deposystems (Gurnell, 2014; Moor et al., 2017).

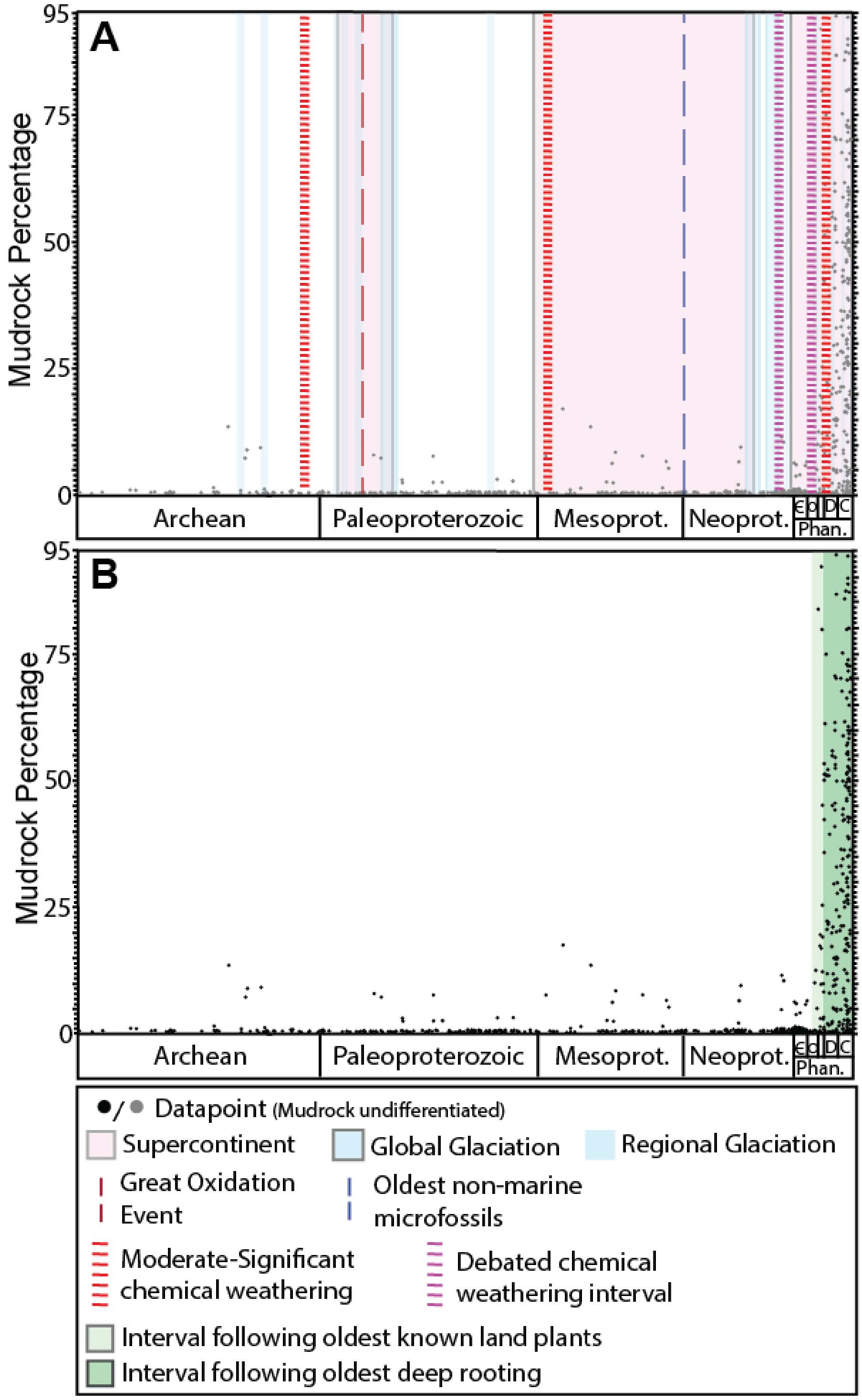

Figure 3.2. Proportion of mudrock within alluvial successions of different ages with major episodic, cyclic and unidirectional changes in the Earth system shown: A) Tectonic, climatic and atmospheric changes; B) Palaeobotanic changes. References: Supercontinent-Bradley (2011); Global Glaciation-Hoffman (2009); Regional Glaciation-Torsvik and Cocks (2016); Great Oxidation Event-Lyons et al. (2014); Oldest non-marine microfossils-Lenton and Daines (2017); Moderate-Significant chemical weathering-1) Boyce and Lee (2017); 2) Mitchell et al. (2016); 3) Corcoran and Mueller (2002); Debated chemical weathering interval-1) Nesbitt et al. (1997); 2) Quirk et al. (2012); 3) Edwards et al. (2015); 4) Tosca et al. (2010); Interval following oldest known land plants-Rubinstein et al. (2010); Interval following oldest deep rooting-Matsunaga and Tomescu (2016).

Terrigenous fines are sourced into sedimentary systems through the mechanical mass wasting of chemical weathering profiles, supplying both weathered and detrital silt, mud and clay particles (Nesbitt et al., 1997). Land plants are not a necessary pre-requisite for the mechanical production of fines, and abiotic, microbial and fungal processes could all promote the silicate weathering of clays on pre-vegetation Earth (Nesbitt et al., 1997; Kennedy et al., 2006; Tosca et al., 2010; Boyce and Lee, 2017; Lenton and Daines, 2017). The presence of minor mudrock in alluvium of all ages demonstrates these alternative pathways (Fig. 3.1A, Table A2), in addition to known terrigenous mudrocks from pre-vegetation lacustrine and marine facies. However, land plants do promote the production of clay minerals and the depth of chemical weathering profiles by increasing atmosphere-substrate connectivity through rooting, the direct secretion of organic acids and chelates, and by developing symbiotic relationships which increase the capacity of Cyanobacteria and Fungi to dissolve soil grains (Nesbitt et al., 1997; Quirk et al., 2012; Hazen et al., 2013; Edwards et al., 2015; Morris et al., 2015; Mitchell et al., 2016; Xue et al., 2016; Boyce and Lee, 2017). The degree to which the earliest bryophyte-grade plants could have boosted silicate weathering (Quirk et al., 2012, 2015; Edwards et al., 2015; Porada et al., 2016; Lenton and Daines, 2017) remains a point of debate, but a clear global intensification followed the evolution of a deeper-rooted Devonian flora (Quirk et al., 2012; Morris et al., 2015; Xue et al., 2016; Boyce and Lee, 2017). The initial range expansion of mudrock proportions in the Ordovician-Silurian (Fig. 3.1B) suggests that even the earliest plants played some role in promoting mudrock in alluvium (Mitchell et al., 2016), before the dramatic rise seen after the Devonian evolution of rooting. However, even if the earliest bryophytes increased weathering, net production alone may not account for the trend. In limited instances where mudrock type has previously been distinguished, siltstone abundance exhibits the same unidirectional trend as mudstone, claystone and shale abundance (Fig. 3.3), suggesting that even fines with a greater (though not exclusive) propensity to have been abiotically/mechanically-generated (i.e., siltstones) (Nesbitt et al., 1997) are diminished in pre-vegetation alluvium.

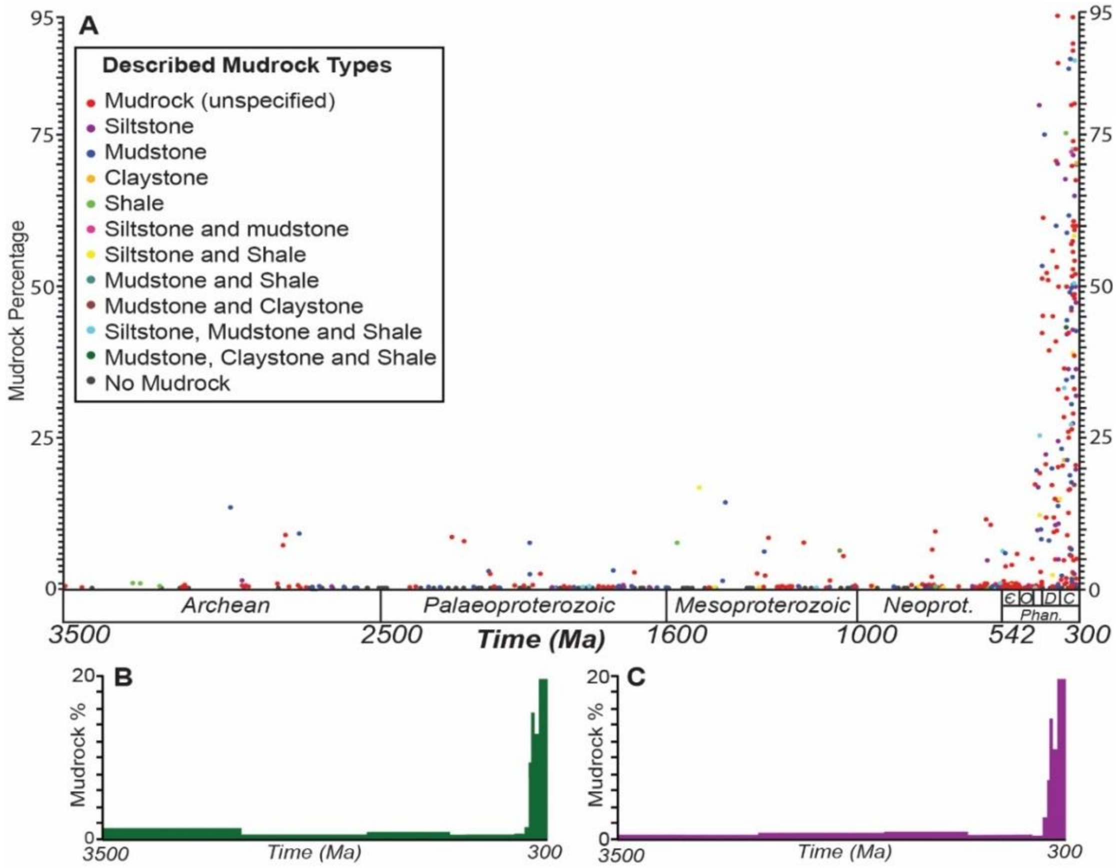

Figure 3.3. A) Proportion of mudrock (differentiated by type) within alluvial successions of Archean to Carboniferous age. Each individual plot records one of the known 594 alluvial stratigraphic units deposited during this interval; B) Average plot of mudstone, claystone and shale calculated for each geological Eon (Archean), Era (Paleoproterozoic to Neoproterozoic) and vegetation stage (Davies and Gibling, 2010a) (Cambrian to Carboniferous); C) Average plot of siltstone calculated for each geological Eon (Archean), Era (Paleoproterozoic to Neoproterozoic) and vegetation stage (Davies and Gibling, 2010a) (Cambrian to Carboniferous).

Prior to vegetation, continents were colonized by microbial mats (Lenton and Daines, 2017) but the lack of below-ground structure to these communities meant that they were prone to undercutting and reworking by fluvial channels, so had a negligible effect on the retention of sediment (Chapter 6). In contrast, the establishment of root systems offered novel mechanical protection against the erosion of sediment in alluvial settings (Edwards et al., 2015; Xue et al., 2016) and would thus have promoted the physical retention of clay, mud and silt. This importance of below-ground stabilization would clearly have played some role in the major Devonian upsurge in mudrock, but the root systems of earlier land plants were limited (Edwards et al., 2015; Boyce and Lee, 2017), so this is an unlikely explanation for the Late Ordovician onset.

The above-ground structures of even shallow-rooted and small-stature vegetation today can reduce near-surface flow of water and wind below a critical velocity that promotes sediment deposition (Gurnell, 2014; Moor et al., 2017). Observations of mosses and liverworts show effective trapping of individual fine grains between their stems, leaves and thalli, incorporating sediment into cryptogamic ground covers (Mitchell et al., 2016). Even though direct physiological analogy between modern and early land plants may be inappropriate (Boyce and Lee, 2017) the earliest above-ground plant structures must have introduced a wholly unprecedented biological component of roughness to the Earth's surface. This suggests a large role for baffling by even primitive above-ground plant constructions, promoting the recurrence frequency of deposition of fines in the alluvial realm, and driving the initial Late Ordovician mudrock increase.

The Palaeozoic increase in alluvial mudrock is an important characteristic of the global sedimentary geological record. The timing with the appearance of plants is unlikely to be a coincidence as plants can greatly contribute to the development and retention of alluvial mudrocks. The source-to-sink deposition of pre-vegetation mud was thus profoundly different to that seen at the present day (Leithold et al., 2016). On pre-vegetation Earth, all fines had limited potential for final (preserved) deposition within continental conduits, regardless of any non-vegetation related variations in chemical weathering intensity (Corcoran and Mueller, 2002; Kennedy et al., 2006; Tosca et al., 2010) or sediment flux (Peters and Gaines, 2012). Archean to Middle Ordovician marine settings would have received a generally greater flux of whatever terrigenous fines were being produced in continental source areas. After the Late Ordovician, and accentuated after the Devonian, an increasing proportion of terrigenous fines were both 1) produced and/or 2) retained on the continents: thus the marine realm may have received diminished fraction of total continentally-weathered fines. Yet this need not necessarily have equated to a progressively diminished volume because net production at source would have been greater. A fuller understanding of mudrock in the absence of vegetation is a prerequisite for any study that invokes ancient terrestrial mudrock strata as a primary archive of geochemical or petrological data, and will have implications for the context and nature of mudrocks increasingly known from non-vegetated planets such as Mars (Grotzinger et al., 2014; Schieber et al., 2017).

3.1.1. Elimination of hypothesized non-vegetation causes for the trend

The observed trend, of increasing alluvial mudrock proportion within younger strata, could abductively be explained by: (1) syn-depositional basin space controls on mudrock accumulation; (2) post-depositional attrition and erosion of older mudrock; (3) misidentification of mudrock-rich alluvial successions in older strata; or (4) tectonic or climatic controls. These four hypotheses have been tested and rejected, for the reasons outlined in the following sections.

3.1.1.1. Rejection of basinal causes for the trend

There is a superficial similarity between the observed decrease in mudrock as a *fraction* of total alluvial sedimentary rock volume, and the recently quantified decline in *total* non-marine sedimentary rock volume with time (Peters and Husson, 2017). The superficiality of this trend becomes immediately apparent when Figure 3.1A plot is inverted to show the proportion of non-mudrock sedimentary strata in alluvium, and thus shows no positive correlation with total non-marine sedimentary rock volume (Fig. 3.4).

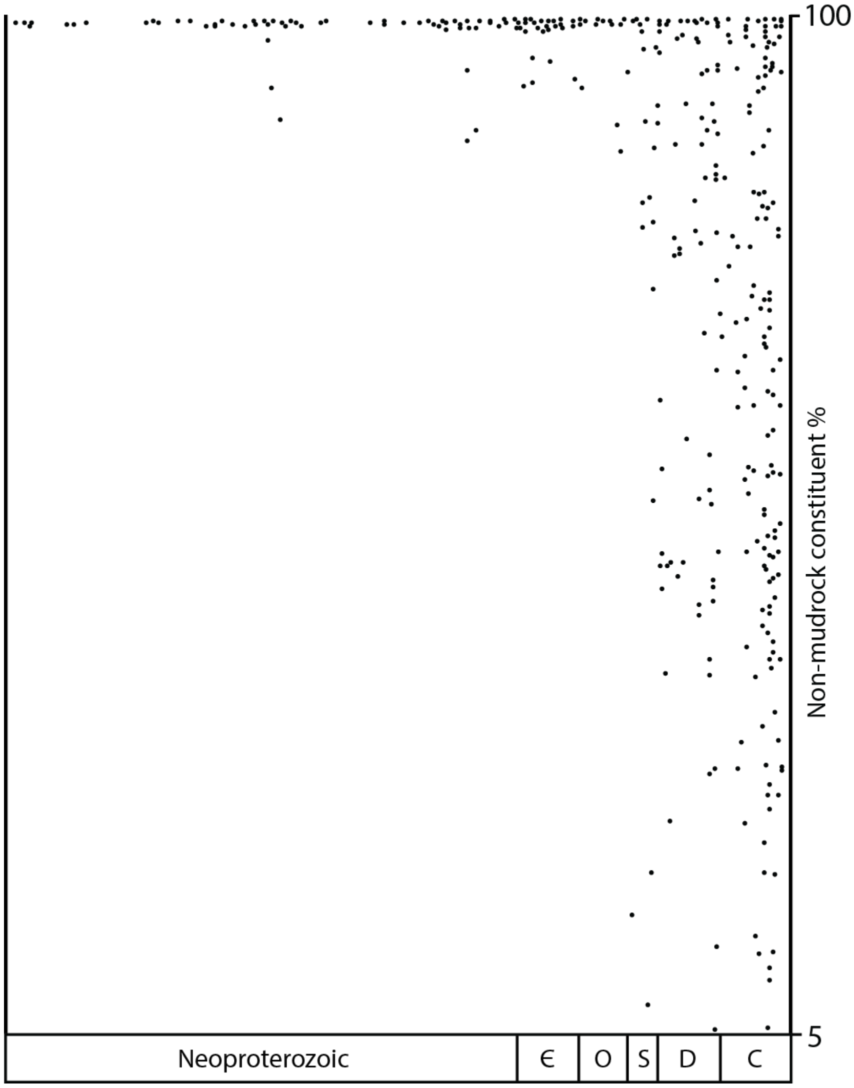

Figure 3.4. Proportion of non-mudrock sedimentary strata within alluvial successions of Neoproterozoic to Carboniferous age. Each individual plot records one of the known 367 alluvial stratigraphic units deposited during this interval.

As a quantification of vertical stratigraphic proportions, rather than bulk volume, the plot is thus wholly different in nature to plots that consider the aerial coverage of sedimentary strata (i.e., as determined from geological maps) as a proxy for the amount of sedimentary rock for a given interval (Peters and Husson, 2017). While intensive (proportion) and extensive (volume) properties of the geological record are not directly comparable, there is a chance that they share a common cause. Studies of non-marine sedimentary rock volume have ascribed an early Palaeozoic increase to major changes in accommodation space on the continents (Peters and Husson, 2017). If the proportion of mudrock had the same underlying cause, then it should be expected to mirror the trends seen in total sedimentary rock volume: however, Figure 3.5 shows that it does not. The proportion of mudrock remains minimal throughout the Precambrian, even during intervals where total rock volume spikes to levels analogous to post-vegetation intervals (e.g., intervals of the late Neoproterozoic have amounts of rock volume comparable to or greater than at the Silurian-Devonian transition, yet mudrock is significantly more abundant during the latter interval). Furthermore, the onset of increasing sedimentary rock volume is considerably delayed from the Late Ordovician onset of the mudrock rise (Fig. 3.5). The amount of mudrock as a proportion exhibits a reduction in the latest Carboniferous (Fig. 3.5C), which partly mirrors the rock volume trend. This observation suggests that accommodation space could potentially play a role in mudrock content during this interval, but that it is clearly subservient to the role of evolving land plants (Fig. 3.5B).

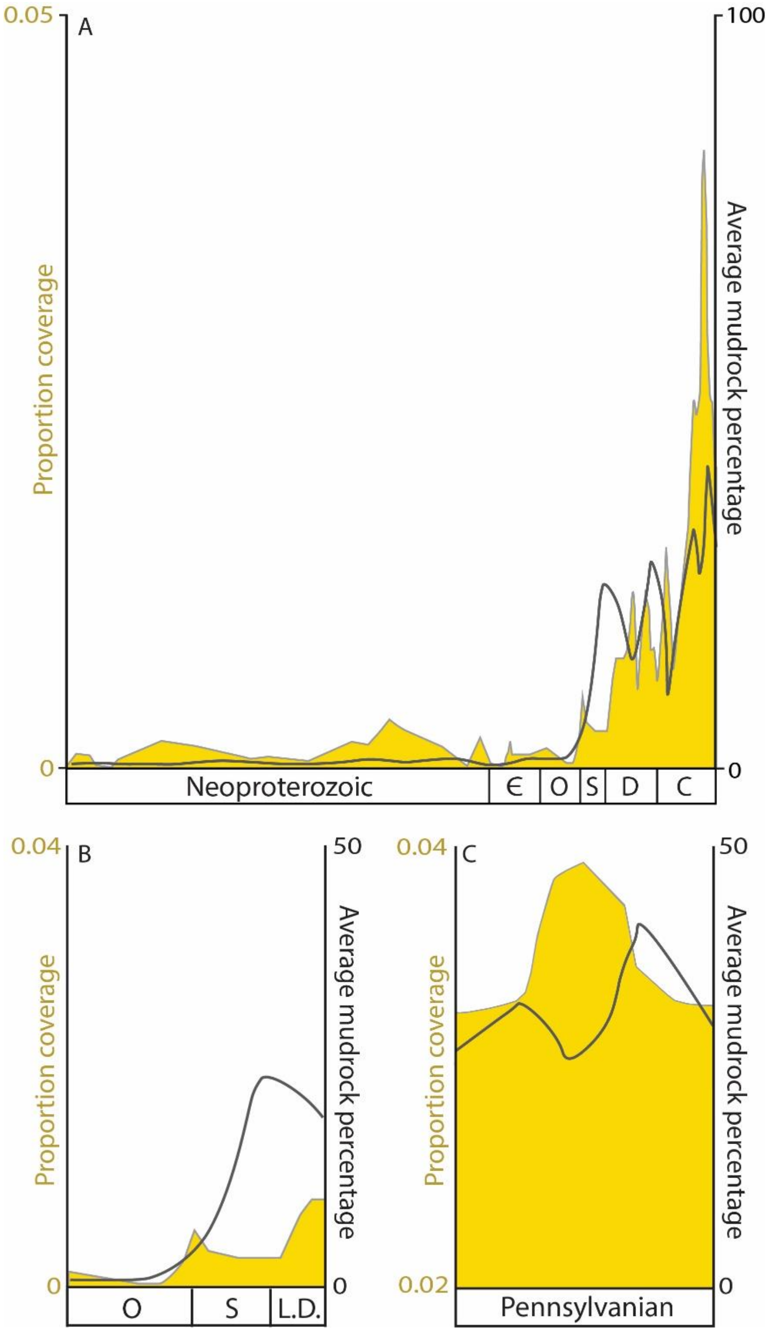

Figure 3.5. LOESS regression of proportion of mudrock within alluvial successions (solid grey line) plotted against non-marine sedimentary rock volume (yellow shading) (Peters and Husson, 2017). LOESS was conducted with a smoothing parameter of 0.9.

3.1.1.2. Rejection of attrition and erosion as a cause for the trend

The amount of preserved non-marine sedimentary rock generally diminishes further back in geological time (Sadler, 1981; Peters and Husson, 2017), but such preservation reduction cannot explain the observed trends in mudrock distribution through time. There is no logical reason why bulk post-depositional attrition would preferentially affect mudrock strata, especially within heterolithic successions, because controls such as out-of-basin erosion and tectonic recycling should affect all lithologies with an equal likelihood. There is no logical reason why bulk post-depositional attrition would preferentially affect mudrock strata, especially within heterolithic successions, because controls such as out-of-basin erosion and tectonic recycling should affect all lithologies with an equal likelihood. In respect to such attrition, while the deep time mudrock record is indisputedly incomplete, the record of coarser-grained sedimentary rocks should be equally incomplete; rendering a null effect on the inclusive values discussed here. It is therefore highly unlikely that random attrition led to the observed trend (i.e., no units between 3500-411 Ma containing >15% mudrock).

This likelihood is formally evaluated here using cumulative frequency plots. Cumulative frequency vs. time plots have been constructed by cumulatively summing the mudrock fraction of each sample and dividing by the total mudrock fraction (Fig. 3.6); in this way, the cumulative frequency is 0 before the first sample at 3.5 Ga and is 1 by the end of the Carboniferous, with the structure both reflecting how samples are distributed in time and their mudrock content. By then constructing synthetic cumulative frequency plots, based on the random sampling of the 400-300 Ma sample population (the most well represented 100 Myr interval), the observed data distribution can be tested against null hypotheses. Two null hypotheses were compared with the actual distribution of data, with synthetic data calculated 100 times for each, following the Monte Carlo Method (Rubinstein and Kroese, 2016): 1) A scenario where mudrock percentage follows a normal distribution, using mean and standard deviation values calculated from the entire dataset (Precambrian and Phanerozoic) (Fig. 3.6A); and 2) A scenario where mudrock percentage follows a normal distribution, using mean and standard deviation values calculated from Phanerozoic values only (Fig. 3.6B). The first test illustrates the likelihood of the actual distribution of data arising by chance. By being restricted to the well-populated key interval of change, the second test assesses the likelihood of progressively decreased sampling deeper into geological time having affected the observed mudrock distribution. Neither of the synthetic profiles presented in Figure 3.6 demonstrate either: 1) very small cumulative mudrock values (<0.075) between 3500 Ma – 500 Ma; or 2) a sharp increase in cumulative mudrock values timed approximately with the first appearance of land plants. This demonstrates that the sharp increase in post-Devonian mudrock fraction is not an attrition artefact, as no synthetic distributions reproduce the trend.

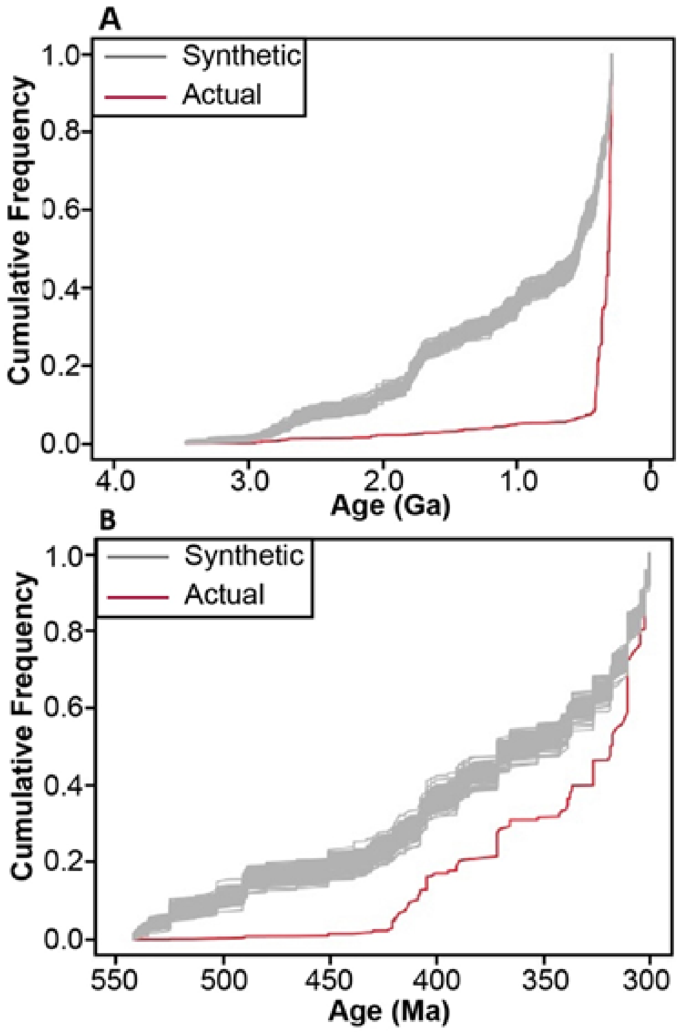

Figure 3.6. Cumulative frequency plots comparing the actual distribution of data (red line), with synthetic data (n = 100) (grey lines) assuming the null hypothesis that mudrock distribution follows a normal distribution. A) Using the mean and standard deviation values of the entire database (Precambrian and Phanerozoic); B) Using the mean and standard deviation values of the Phanerozoic only.

To quantitatively test similarity of the synthetic and real cumulative frequency distributions the Kolmogorov-Smirnov test was used. The Kolmogorov–Smirnov statistic, d(K–S) (the maximum in separation between cumulative frequency curves), assesses cumulative distributions for similarity (Press et al., 1992), with smaller d(K–S) values indicating more similar distributions. Both scenarios returned large d(k-s) values (scenario 1 = 0.541933 (Fig. 3.6A), scenario 2 = 0.540084 (Fig. 3.6B)), thus emphasizing the dissimilarity between the actual and synthetic distributions. Furthermore, d(k-s) is far greater than the critical value in both instances (dcrit = 0.068514, $\alpha = 0.01$), indicating that the null hypotheses can be rejected with a confidence level significantly greater than 99.9%.

The erodibility of mudrock is also ruled out as an explanation. Mudrocks may be more susceptible to modern erosion and weathering from outcrop than coarser-grained sedimentary rocks, due to internal fissility and mechanical weaknesses. However, this study compares rock with rock: post-lithification, there is no reason why a Precambrian mudrock should be any more or less susceptible to modern erosion than a Phanerozoic mudrock and each dataset should be equally prone to this depleting effect. Precambrian mudrocks, being older and therefore subject to a potentially greater array of burial/heating events, may in fact be suspected to be less prone to erosion as metasedimentary mudrocks are often mechanically stronger than 'fresh' mudrock. Additionally, the heterolithic and interbedded nature of mudrock and sandstone means that it is not possible to surgically remove only mudrock, despite its greater erodibility, even during those syn-depositional erosion events that excise large parts of the stratigraphic record (Sadler, 1981).

Where exposed on Earth's surface today, sandstone-dominated successions tend to form cliffs (more amenable to geological investigation), whereas erodible mud-rich successions are more likely to be hidden by soil and talus. Thus, there is an inherent observation bias in favour of sandstone-dominated strata in outcrop investigation. However, this observation bias is again uniform across the entire geological record (certainly so for fully lithified ancient strata of Precambrian through Carboniferous age) and so cannot detract from the validity of the mudrock upsurge presented in Figure 3.1.

3.1.1.3. Rejection of observer bias as a cause for the trend

The holistic approach that has been employed negates, to the maximum extent possible, issues of sampling bias. As it encompasses all possible datapoints, the trend accurately represents what is preserved in the global rock record, as is currently known. Subsampling of the data was used to remove any concern that uneven sampling for different time intervals may have biased the data (Fig. 3.1C). A random subset of the available dataset was drawn until each interval, called a sampling bin, includes the same estimated number of datapoints (Alroy et al., 2008). The dataset was split into 30 sampling bins separated at 100 million year intervals from 3500-700 Ma, and then at 40 million year intervals from 699-299 Ma. These intervals were chosen as they provide great enough temporal resolution to ensure each key interval in the Phanerozoic is represented, whilst ensuring each sampling bin contains enough original data on mudrock proportion to randomly draw from. 125 datapoints were randomly drawn from the original data for each sampling bin. This process was repeated 100 times to obtain averages. In Figure 3.1C, each datapoint represents the median value seen across the 100 individual subsampling trials. In addition to correcting for variation in sampling intensity, subsampling enables the order of magnitude increase in mudrock proportion for each key interval to be calculated (see Section 3.1).

The misidentification of mudrock-rich alluvial strata as being of a marine origin in older units may reasonably be expected to have biased the observed trend. There are instances in which it may be problematic to conclusively distinguish alluvial strata from marine strata, particularly in the Precambrian (see Section 2.3). Instances where previous authors have misinterpreted strata based on limited and non-diagnostic criteria (e.g., using an abundance of cross-bedded sandstones to declare a unit ‘fluvial’) cannot be accounted for. The strength of the observed trend would require that the misidentification of alluvial strata was an endemic problem to a significant fraction of the studies of 383 pre-Ordovician units, carried out over the last c.70 years, as cited in the database, but could be a source of uncontrolled bias. However, there are four reasons why the effects of any such bias may be minimal: 1) the Ordovician-Devonian upsurge in preserved mudrock post-dates the evolution of abundant marine shelly fossils and bioturbation in the Cambrian. For this latter interval, palaeontological and ichnological data reduce the risk of inaccurately discerning marine and alluvial strata and yet alluvial mudrock remains minimal and analogous to the preceding Precambrian Eras (Fig. 3.1B); 2) 52% of the formations in the database are known from multiple papers by different authors: the likelihood of multiple sets of authors making the same erroneous conclusion is more limited than for those studies that involve only one previous study; 3) the majority of studies were undertaken specifically as sedimentary geology studies, with the express intent of understanding palaeoenvironment. Researchers within this field of expertise are less likely to have made simplistic assumptions (e.g., trough cross-bedding = fluvial) than non-specialist researchers, as multiple lines of sedimentological evidence exist to identify marine strata, with or without the presence of palaeontological information (i.e., through an assessment of the balance and combination of sedimentary characteristics including palaeocurrent variance and sedimentary architecture (e.g., Miall, 1996, 2014; Davies et al., 2010; Davies and Gibling, 2012) (Fig. 3.7)) (Section 2.3); and 4) the issue of misidentification would only negate the observed trend if certain (mud-rich) pre-vegetation fluvial strata have been misidentified as marine and therefore missed during the data collection: if the converse is true, whereby some marine strata have been interpreted as fluvial, this makes no material difference to the dataset - it might contain some ‘false’ datapoints (most likely in older strata lacking fossil evidence), but does not affect the trend.

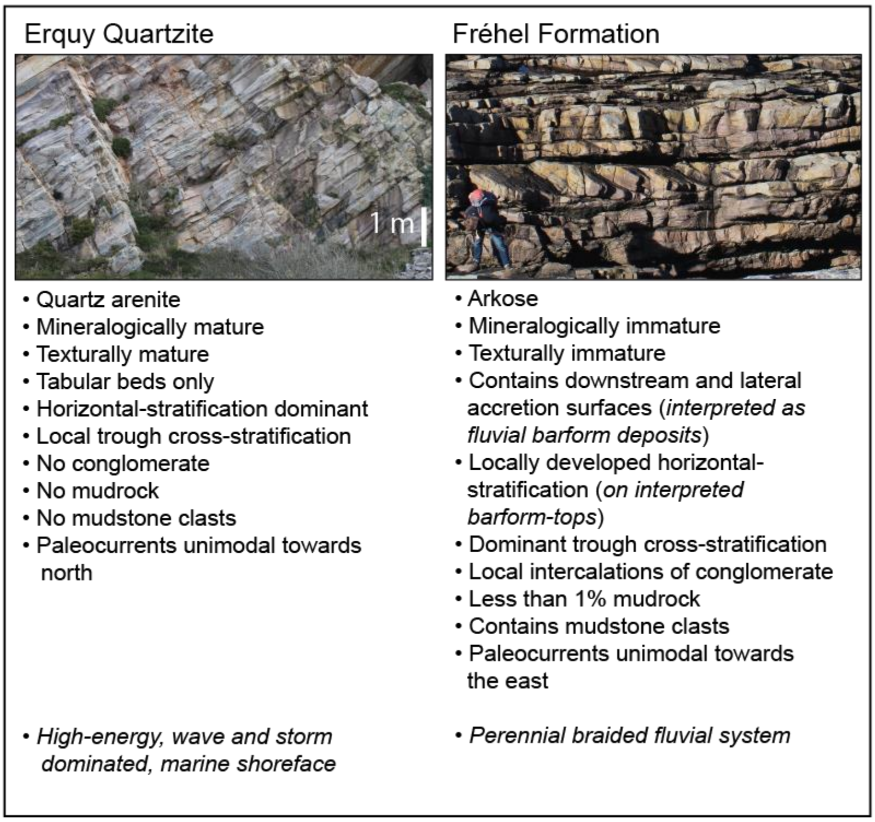

Figure 3.7. Example case study where marine and non-marine depositional environments could be interpreted through an assessment of the balance and combination of the sedimentary characteristics of the two formations. Geologist in B is 187 cm tall.

3.1.1.4. Rejection of cyclic allogenic forces as a cause for the trend

The statistical tests used to mitigate against attrition as a cause for the trend (Section 3.1.1.2 and Section 3.1.1.3) suggest that the trend marks a stratigraphically unidirectional shift of increasing alluvial mudrock, which is thus not readily explainable as having been forced by those cyclic geological phenomena that were continually in operation prior to the onset of the trend (Fig. 3.2A).

Modern-style plate tectonics are known to have been continuously active since at least 1830 Ma (Weller and St-Onge, 2017), and sea-level and climate fluctuations were continually operational across the entire 3200 Myr study interval. None of these can account for the stratigraphically unidirectional nature of the onset of the observed trend. Even accounting for the high sea-levels and orogenic basins in the Devonian (which may have been more amenable to mudrock accumulation), the absence of earlier mudrock spikes suggest that a unidirectional change to the Earth system is required in addition to any tectonic/climate/sea-level controls (Hoffman, 2009). Numerous Precambrian supercontinents are known (Bradley, 2013), as well as at least 16 pre-Ordovician orogenies (Torsvik and Cocks, 2016), which should be expected to have contributed to earlier spikes, yet the directly observed data and statistical tests demonstrate that it is highly unlikely that such spikes previously existed but were later eroded.

Whilst cyclical phenomena undoubtedly have an effect on the preserved global alluvial record, the variation in mudrock abundance that these induce can only be directly compared in similarly aged intervals (i.e., not between pre- and syn-vegetation evolution intervals). For example, in rocks of a common age, before and after the Ordovician, alluvial mudrock is, as expected, more abundant in strata deposited adjacent to active orogenic belts than in strata deposited away from active orogenies. However, mudrock deposited adjacent to active orogenic belts prior to the evolution of land plants is significantly less abundant than mudrock deposited away from orogenies after the evolution of land plants (Fig. 3.8). Climatically, there is little discernible correlation between global alluvial mudrock proportion and the presence or absence of polar glaciations (Fig. 3.9), yet both glacial and non-glacial intervals are markedly more mud-rich during syn-vegetation icehouse conditions (e.g., the late Carboniferous) than they are during pre-vegetation icehouse conditions (e.g., the Cryogenian).

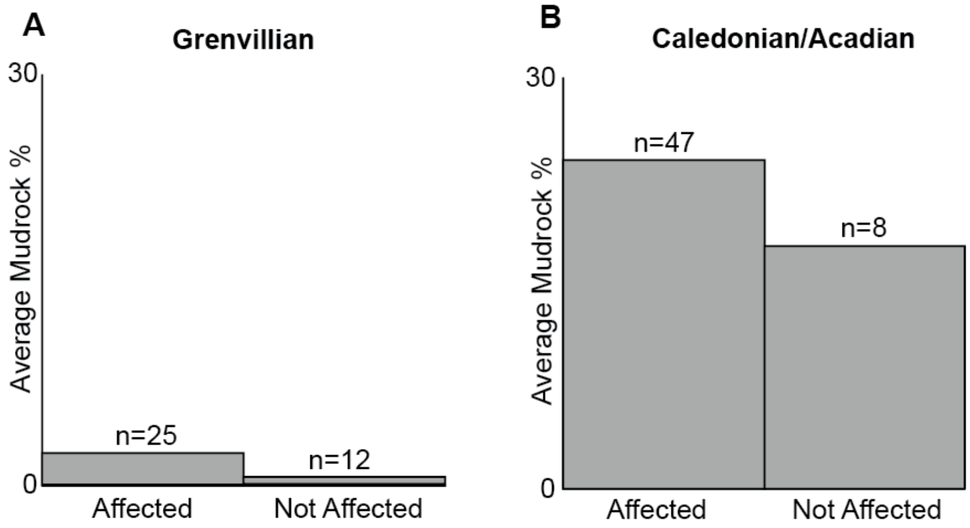

Figure 3.8. Histograms comparing mudrock percentage in worldwide alluvium deposited during intervals of orogenic events: A) Affected (deposited neighbouring orogeny) and not affected (deposited away from orogeny) by the Grenvillian Orogeny (1100-900 Ma); B) Affected and not affected by the Caledonian/Acadian Orogeny (440-390 Ma).

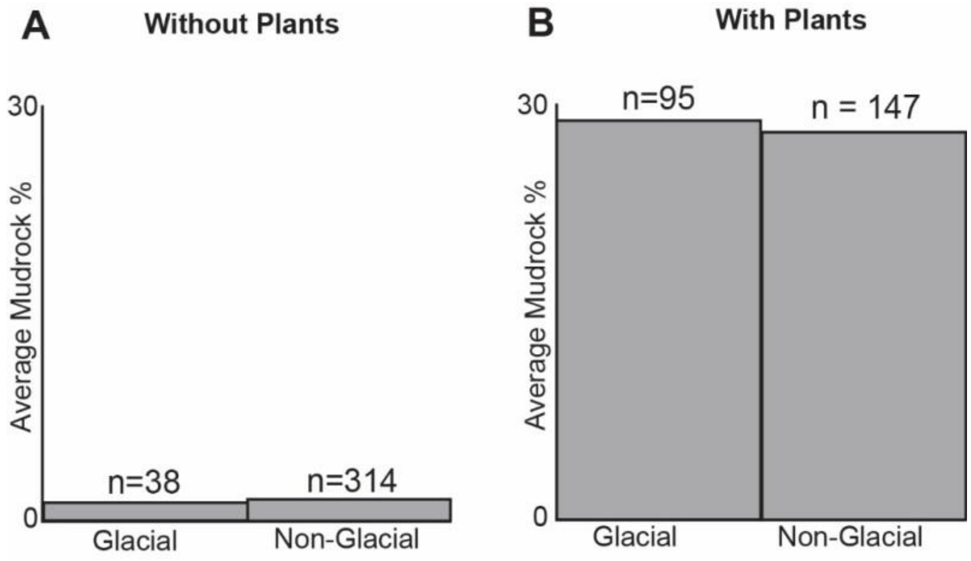

Figure 3.9. Histogram plots comparing average mudrock percentage in worldwide alluvium: A) Deposited during glacial intervals versus non-glacial intervals in the absence of land plants; B) Deposited during glacial intervals versus non-glacial intervals in the presence of land plants.

3.1.1.5. The timing of the greening of the continents and the onset of increased alluvial mudrock abundance

The unidirectional onset, and progressive nature, of the increase in mudrock abundance does show strong correlation with the fossil plant record (Rubinstein et al., 2010; Matsunaga and Tomescu, 2016; Boyce and Lee, 2017) (Fig. 3.2B). The studied interval can be divided into three parts: 1) Pre-vegetation. The average proportion of mudrock in alluvial successions is 1.3% across all Archean to Early Ordovician formations (n=348), and only 11.2% of the formations contain greater than 2% mudrock strata; 2) Primitive vegetation. The average proportion of mudrock in alluvial successions is 15.4% for Middle Ordovician to Silurian formations (n=30), post-dating the evolution of the earliest land plants (Rubinstein et al., 2010), and 53.0% of these formations contain greater than 2% mudrock; and 3) Post-rooting. The average proportion of mudrock in alluvial successions is 29.9% for formations deposited after the Early Devonian evolution of rooting (Matsunaga and Tomescu, 2016) (n=216), where 78.6% of units contain greater than 2% mudrock, and 27.9% of alluvial units are dominated by mudrock (50-95% proportion) over coarser-grained sedimentary strata. With current knowledge, the only primary unidirectional global change associated with the two accelerations of alluvial mudrock abundance (Late Ordovician and Devonian) is vegetation evolution (the first land plants and rooting, respectively). It is emphasised that this correlation is made with the tangible plant fossil record. As noted by other researchers (Boyce and Lee, 2017), there presently exist a multitude of hypotheses regarding the timing of land plant colonization of the continents, made using secondary or derived datasets. For example: palaeoweathering surfaces have been used to suggest limited greening of the continents in the Ordovician and Silurian (Jones et al., 2015); clay minerals have been used to suggest a late Precambrian greening of the continents (Kennedy et al., 2006); weathering models based on modern plant weathering suggest major Devonian greening (Berner, 2004) (enigmatically preceding the Carboniferous expansion of forests (Boyce and Lee, 2017)); and molecular clock data postulate a minimum Cambrian origin for land plants (Clarke et al., 2011). Clearly, all of these hypotheses are mutually-exclusive and a fuller understanding of the timing of the greening of the continents requires more than one derived source of interpreted data.

It is noted that: (1) the observations of mudrock increase presented here are closely linked to the undisputed land plant fossil record; (2) cannot be reasonably explained by the most likely alternative hypotheses considered (Section 3.1.1); and (3) that multiple mechanisms, as seen in modern vegetation, are known to promote mud production and deposition, and that these were absent from the Earth surface prior to Palaeozoic evolutionary innovations. In light of these factors, it is reasonable to abductively infer plant-related causes as the best explanation for the outcome preserved in the global rock record (i.e., a shift in mudrock abundance throughout the Palaeozoic) (see Section 3.1). The tangible shift in the character of the alluvial mudrock record may thus be of potential use in the calibration of other derived estimates of the greening of the continents.

Cumulative mudrock proportions binned into 100 Myr intervals visually demonstrate how the increase in mudrock proportion on land is broadly coeval with the palaeobotanic record of land plant evolution, with intervals post-dating the first plant fossils showing overall trends closer to a normal distribution than those pre-dating the first plant fossils (Fig. 3.10). Similarly, Figure 3.11 illustrates the abrupt increase in the frequency of alluvial formations containing >2% mudrock percentage after the evolution of land plants, as evidenced in the fossil record.

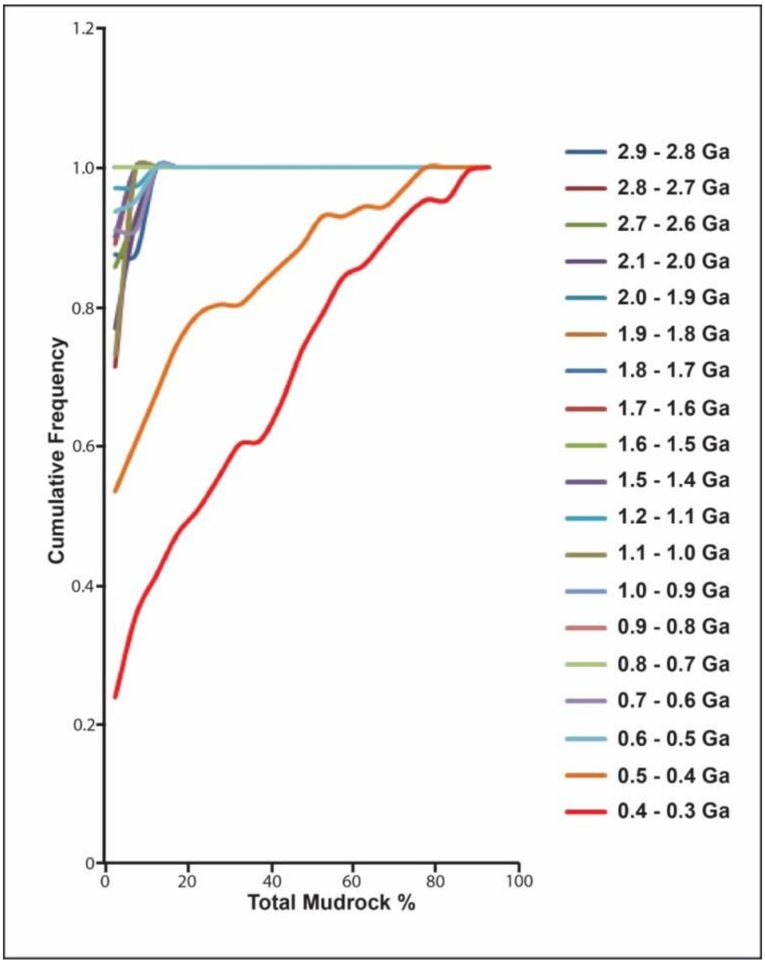

Figure 3.10. Line graphs showing cumulative frequency and total mudrock percentage for each 100 million year interval where there are 7 or more case studies. Two lines recording intervals after plant evolution (0.5-0.4 Ga and 0.4-0.3 Ga) distanced from earlier lines.

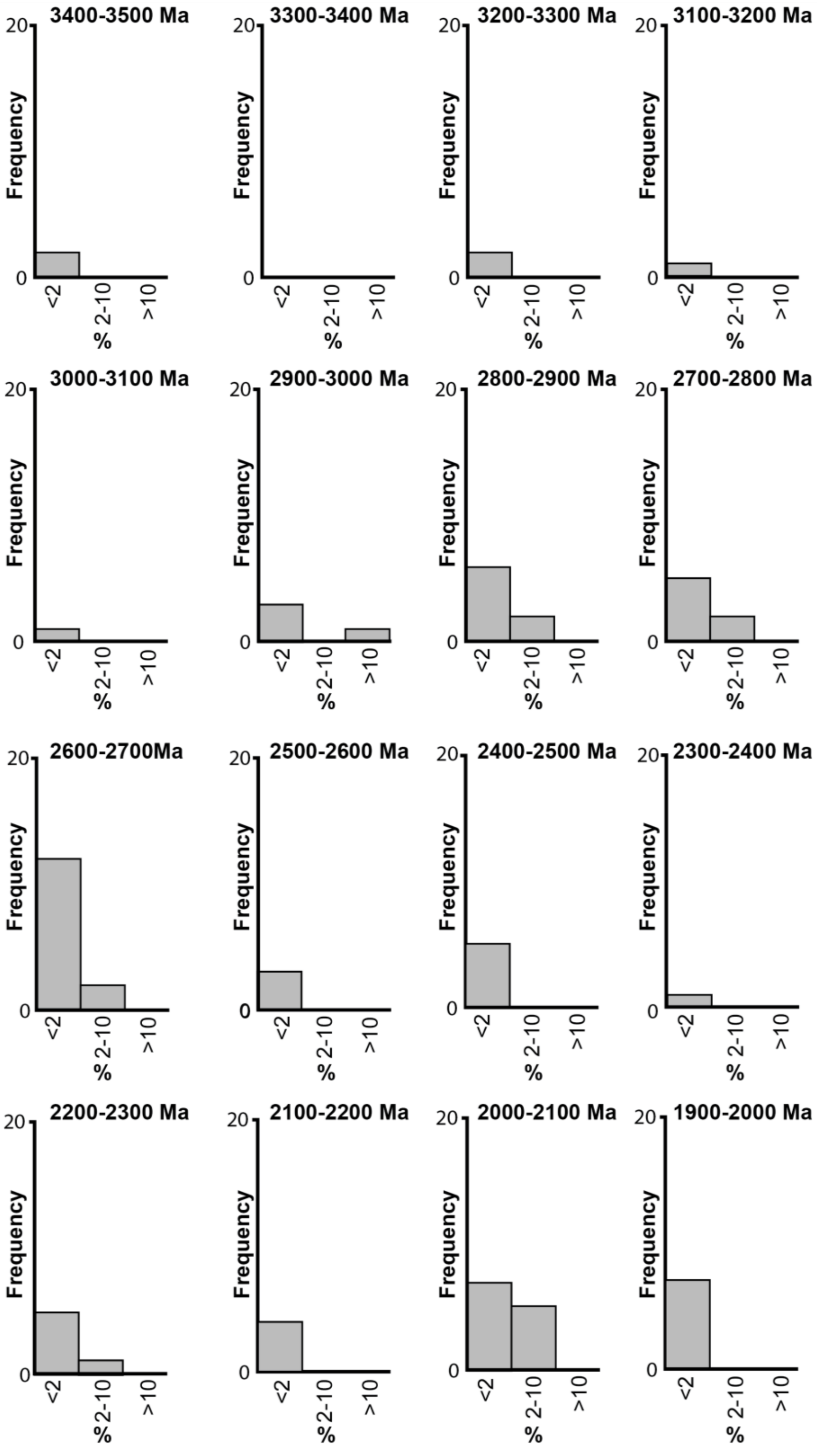

Figure 3.11. Histograms showing the frequency of mudrock distributions of each 100 million year interval in the database. Note increase in mudrock content during bin encompassing Middle Ordovician (400-500 Ma).

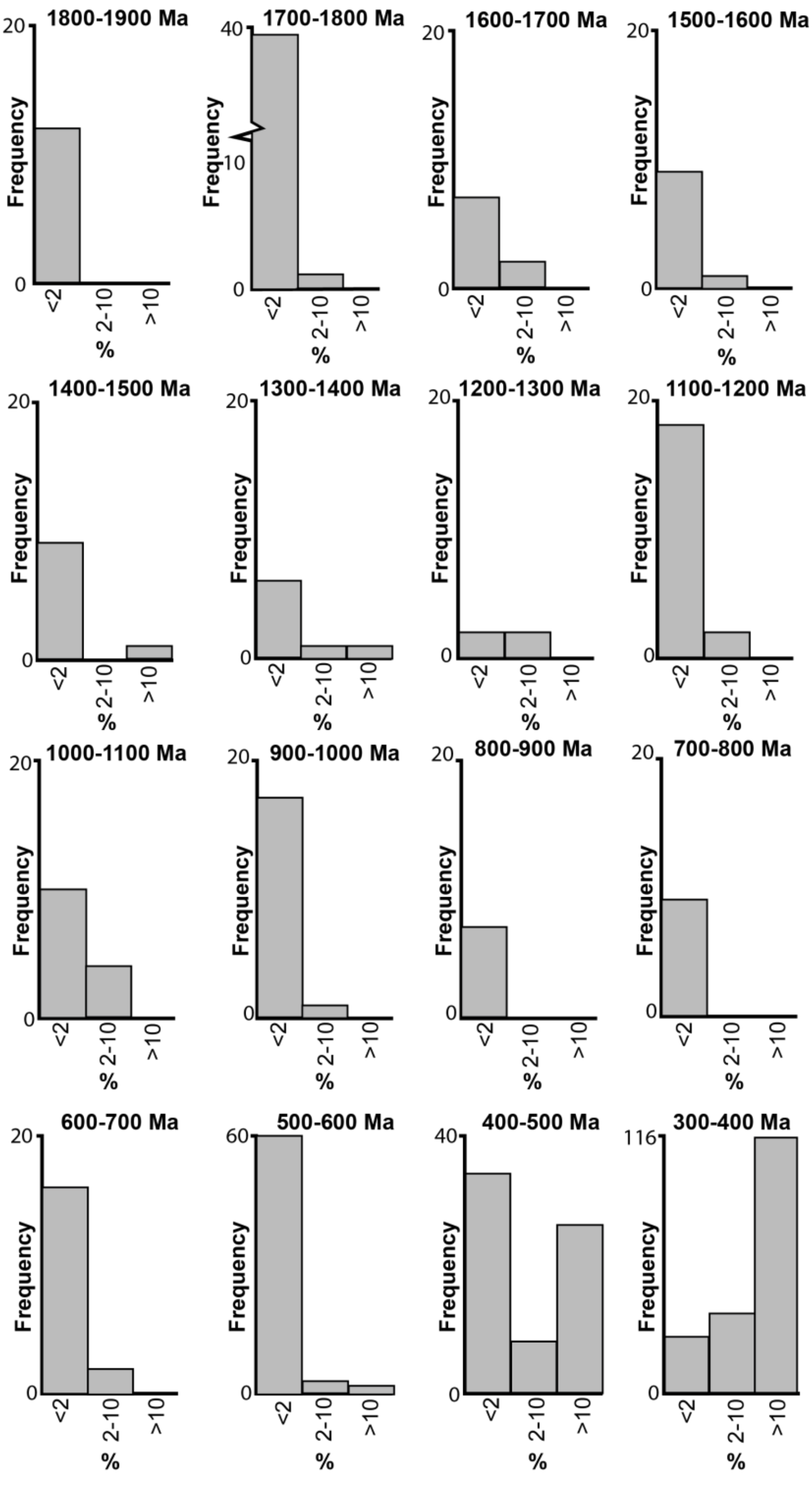

Figure 3.11. *Continued*

3.2. Intraformational mudstone clasts

Fluvial intraformational mudstone clasts represent consolidated aggregates of fine-grained sediment that enter river systems by bank collapse or the rip-up of floodplain and in-channel muds (Tunbridge, 1981). The percentage of Archean-Cambrian case studies which contain mudstone clasts is consistently low and shows no discernible trend (Fig. 3.12A). In their database study of the characteristics of Cambrian-Devonian alluvium, Davies and Gibling (2010a) demonstrated that the proportion of case studies which contain mudstone clasts increases between the Cambrian and Devonian (Fig. 3.12B). The number of successions containing mudstone clasts between the Archean and Devonian therefore displays a similar increase in abundance than that shown for the increase proportion of total mudrock (Fig. 3.1), suggesting the two characteristics of alluvium are connected.

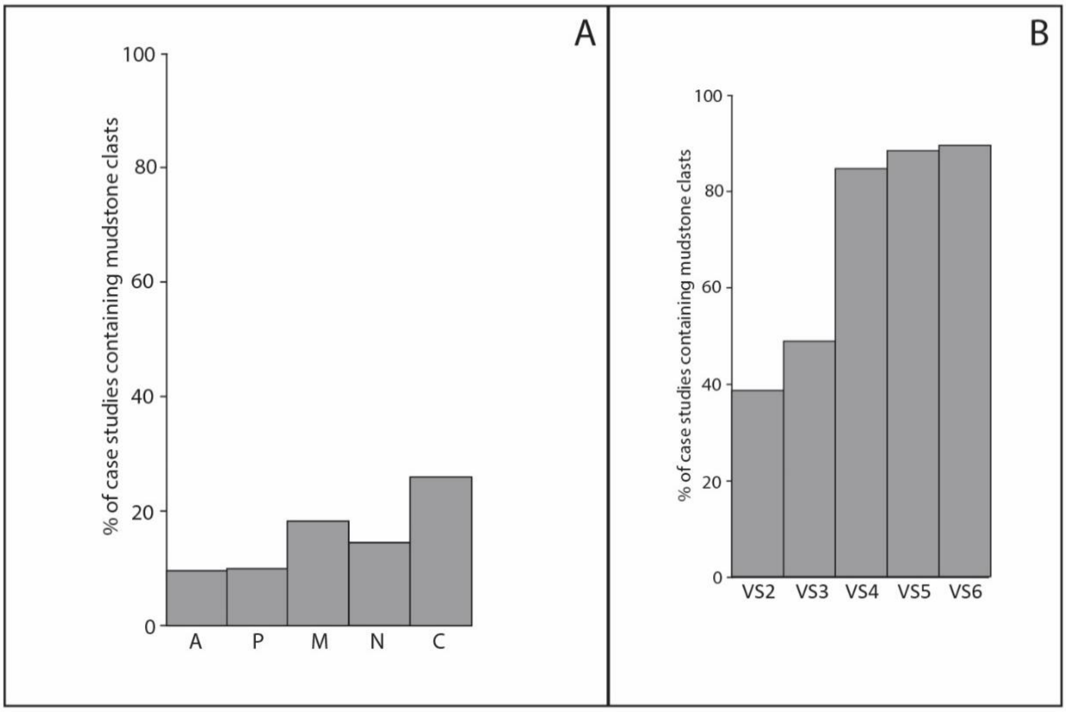

Figure 3.12. A) Percentage of case studies for each Era/Period that contain intraformational mudstone clasts. (n=52 [Archean], n=109 [Paleoproterozoic], n=69 [Mesoproterozoic], n=98 [Neoproterozoic], n=57 [Cambrian]): B) From Davies and Gibling (2010a). Percentage of case studies for each vegetation stage. (n=29 [VS2], 10 [VS3], 13 [VS4], 16 [VS5], 29 [VS6]). See Davies and Gibling (2010a) for definitions of vegetation stages.

3.3. Arkose

In this review, studies of 271 alluvial formations recorded the petrographic classification of fluvial sandstones (Table A3). The proportion of pre-vegetation successions containing arkosic and subarkosic sandstones is 58.6% (Fig. 3.13A). Consistently high proportions of arkosic and subarkosic sandstones throughout the Precambrian and Cambrian support earlier contentions, made by Davies and Gibling (2010a), that the evolution of land plants resulted in a significant decrease in the proportion of alluvial K-feldspar rich sandstones (Davies and Gibling, 2010a) (Fig. 3.13B). Davies and Gibling (2010a) hypothesised that this decrease after land plant evolution was due to: 1) increased potassium chelation, resulting in the breakdown of detrital K-feldspar components (Basu, 1981); and 2) decreased transportation rates of unweathered terrestrial K-feldspar (Hiscott et al., 1984; Fedo and Cooper, 1990).

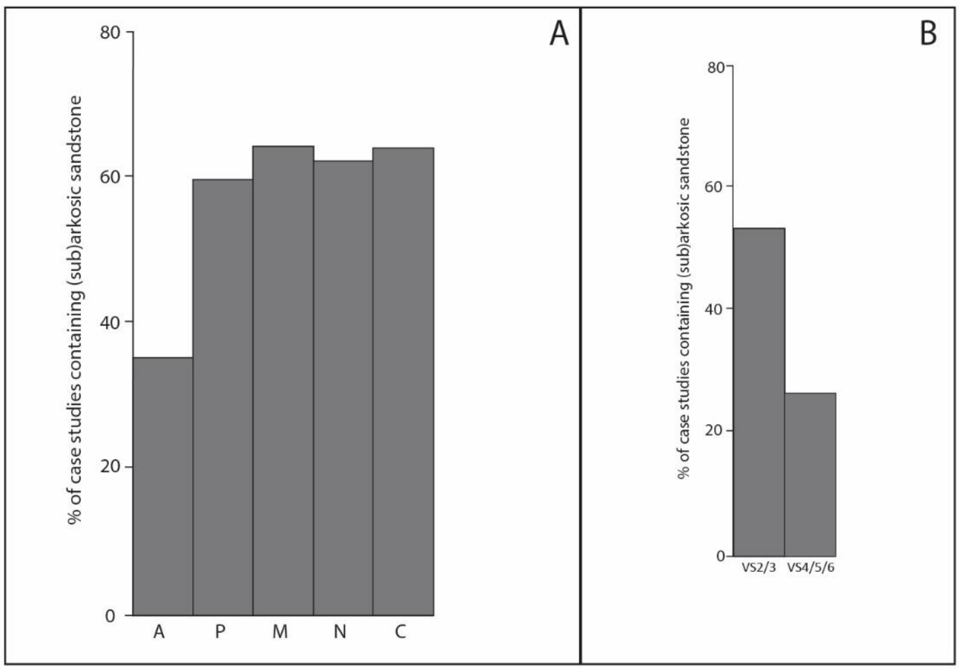

Figure 3.13. A) Graph showing percentage of case studies for each Era/Period that contain arkosic or subarkosic sandstones. (n=31 [Archean], n=81 [Paleoproterozoic], n=54 [Mesoproterozoic], n=72 [Neoproterozoic], n=33 [Cambrian]); B) From Davies and Gibling (2010a). Graph showing percentage of case studies for each vegetation stage that contain arkosic or subarkosic sandstones. (n=30 [VS2/3], 32 [VS4/5/6]).

Whilst conclusively identifying trends in sandstone petrology from database analysis is problematic, primarily because formations were deposited in a variety of tectonic and climatic settings that would have produced sands with varied petrographic signatures (Dickinson and Suczek, 1979; Suttner et al., 1981), the marked drop in K-feldspar rich sandstones after plant evolution supports the notion that the evolution of vegetation enhanced chemical weathering in uplands and lowland sites of alluvial storage.

3.4. Chapter summary

The global record of alluvial mudrock provides clear evidence for how the evolution of land plants fundamentally altered sedimentary processes and environments at Earth's terrestrial surface. Mudrocks (mudstones, siltstones, claystones and shales) are rare in alluvium deposited by Precambrian and early Palaeozoic rivers, before becoming increasingly dominant between the Ordovician and Carboniferous (Fig. 3.1). This increase in alluvial mudrock in tandem with the Palaeozoic rise of plants reflects changes in sediment transport and deposition by rivers forced by novel plant-induced mechanisms. Although the mudrock upsurge has been known anecdotally for numerous decades, the timing and magnitude of the transition has never been quantified. Section 3.1 presents collated data from every known Archean to Carboniferous aged alluvial formation on Earth, thus covering intervals before, during and after plant evolution. For each of stratigraphic section, mudrock percentage was extracted, enabling it to be presented as a function of time. The onset of the mudrock transition can be constrained to the Late Ordovician to Silurian: a timing which suggests that Earth's most primitive plants were capable of substantial bioengineering. Two mechanisms may explain how such rootless vegetation may have triggered the Palaeozoic alluvial facies shift: 1) by facilitating an increase in the production of cohesive mud through chemical weathering; and 2) by altering floodplain construction owing to the introduction of novel above-ground baffling effects (the trapping and forced deposition of sediment from within a moving fluid passing through above-ground plant structures). Increased above-ground topography likely facilitated mud accumulation in proximity to active channels. Greater cohesion due to mud trapping would have caused reduced floodplain erodibility thus increased preservation potential. Figure 3.1 demonstrates that alluvial mudrock percentage continued to increase through the Devonian and Carboniferous, following the increased diversification of embryophytes and the evolution of deeply rooted tracheophytes. Root structures facilitate channel bank armouring, thus restrict channel migration and consequently further assist the preservation of mud-rich floodplains. In total, mudrock is shown to be on average 1.4 orders of magniture more common in syn-vegetation alluvium than in pre-vegetation. The unidirectional onset, and progressive nature, of the increase in mudrock abundance rules out alternative episodic or cyclic geological explanations (discussed in Section 3.1.1). Additional contrasts between the character of pre- and syn-vegetation alluvium (Section 3.2, Section 3.3.) further demonstrates the significant sedimentological impact of the evolution of land plants.

Chapter 4

PRE-VEGETATION ALLUVIUM DEPOSITED BY PERENNIAL RIVERS

The following chapter consists of two original case studies of pre-vegetation alluvium: 1) The Neoproterozoic Torridon Group, Scotland; and 2) The Neoproterozoic Jacobsville Formation, Michigan, USA. Both formations are considered the deposits of perennially flowing fluvial systems, although the depositing rivers were of vastly different scale.

4.1. The Neoproterozoic Torridon Group

4.1.1. Stratigraphic and palaeogeographic setting

The Torridon Group is the topmost group of the Torridonian Sandstones (introduced in Section 2.1.1). It is approximately 6 km thick and crops out in the NW Highlands of Scotland (Fig. 2.1). The group is divided into four formations, in order:

1) The Diabaig Formation infills palaeotopographic depressions in the Lewisian Gneiss basement (Rodd and Stewart, 1992). Alluvial fan breccias and sandstones transition vertically and laterally into lacustrine siltstones.

2) The Applecross Formation, up to 3000 metres thick, is the predominant component of Torridon Group stratigraphy (Fig. 2.1, Fig. 4.1). Whilst still considered as part of the same group, multiple lines of evidence suggest a significant stratigraphic break between the Diabaig and Applecross Formations (e.g., erosional discordance, sedimentary facies, minerology, diagenesis and organic carbon character) (Prave, 2002; Kinnaird et al., 2007; Muirhead et al., 2017; Chapter 7). The Applecross Formation consists of amalgamated, tabular coarse- to pebbly-sandstone units widely interpreted to have been deposited by low-sinuosity, braided rivers (e.g., Nicholson, 1993; Stewart, 2002; Ielpi and Ghinassi, 2015; Ghinassi and Ielpi, 2018).

3) The Aultbea Formation, approximately 1500 metres thick, consists dominantly of medium-grained sandstones without pebbles and occurs gradationally above the Applecross Formation. The Applecross-Aultbea succession represents one continuous phases of deposition, with the Aultbea Formation reflecting a facies transition (Nicholson, 1993; Rainbird et al., 2001; Stewart, 2002; Kinnaird et al., 2007). The Applecross Formation and Aultbea Formation are here collectively referred to as 'Torridon alluvium'.

4) The Cailleach Head Formation, 800 metres thick, has so far been interpreted as freshwater deltaic deposits (Stewart, 1988).

The Torridon Group unconformably overlies the Mesoproterozoic Stoer Group and is unconformably overlain by the Lower Cambrian Eriboll Formation (Stewart, 2002). Detrital zircon population provenance and ages (1070-990 Ma) (Rainbird et al., 1992, 2017; Krabbendam et al., 2017), and regional palaeoflow (Nicholson, 1993) (Section 4.1.5) suggest that Torridon alluvium may be the product of weathering and erosion of the syndepositional orogenic Grenvillian Mountain Belt.

Figure 4.1. Examples of extensive exposures of Torridon alluvium: A) Liathach SSE facing flank (depositional-strike to oblique section); B) Liathach SW facing flank (depositional-dip section). Circled area presented in Figure 4.4D.

4.1.2. Methods

Methods for fieldwork are detailed in Section 2.1. Architectural units were described in terms of their sedimentary facies, geometry and internal accretion surfaces. In total, 2333 palaeoflow indicators were collected from dipping cross-stratification foresets, and 270 accretion directions were collected from set and coset boundaries genetically related to a common underlying surface.

4.1.3. Architectural units: description and interpretation

Three architectural units were recognised over the course of this study: 1) Erosionally based cross-stratified sheets (c. 80%); 2) Inclined accretionary strata (c. 20%); and 3) Discontinuous mudstone to very-fine grained sandstone units (<<1%).

4.1.3.1. Erosionally based cross-stratified sheets

4.1.3.1a. Description

Erosionally-based cross-stratified sheets account for a far greater proportion of total alluvium volume than the other two architectural units combined. They range in thickness from 0.4 – 4.75 metres (mean 1.96 m) (n = 145, S = 101.8) (S = Standard Deviation) (Fig. 4.2). No trends in thickness variation were documented across the outcrop belt. They overlie basal erosional surfaces that lack significant relief (Fig. 4.2A). Dominant grain-size decreases up-section from pebbly-sandstones (and rare pebble conglomerates) (Fig. 4.3A) to medium-grained sandstones (Fig. 4.3B). Granule and pebble lags (Fig. 4.3C) and mudstone rip-up clasts (Fig. 4.3D) regularly occur along the bases of thicker units. Units are composed dominantly of trough cross-stratified sets (Fig. 4.3E), with subordinate planar-tabular cross-stratified sets (Fig. 4.3F). Maximum trough set thickness is 105 cm (average 27 cm) and maximum planar-tabular set thickness is 80 cm (average 28 cm). Cross-set height shows no dimensional trend up-section. Coset boundaries are planar and trend parallel to underlying erosional surfaces, distinguishing them from inclined accretionary units which consist of multiple inclined cosets each truncating a common underlying surface (Section 4.1.3.2).

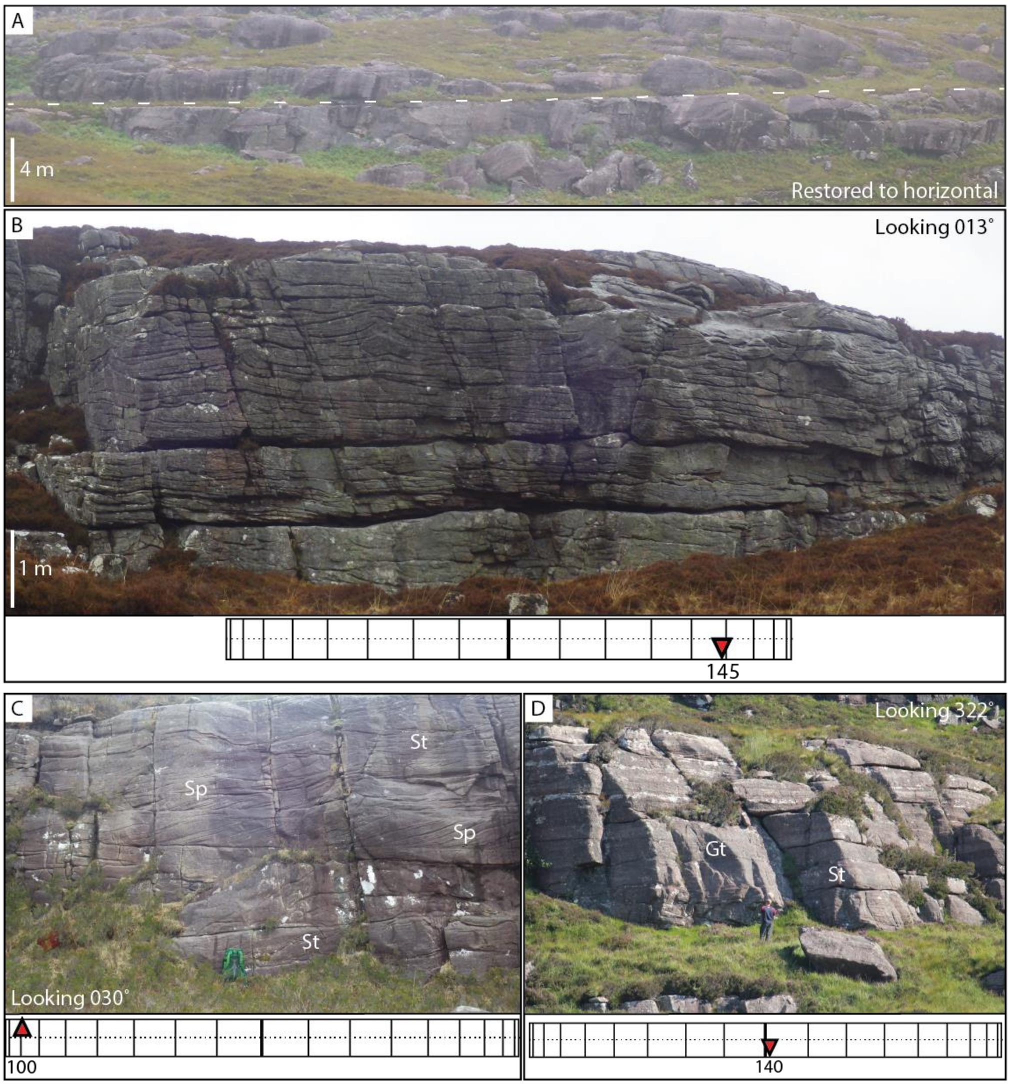

Figure 4.2. Examples of erosionally based cross-stratified sheet units: A) Prominent basal erosional surface (Liathach); B) Multiple, stacked sheet units exposed in three-dimensions (Liathach); C) Sandstone dominated unit (Stac Pollaidh). Bag is 37 centimetres high; D) Gravel dominated unit (Assynt). Person is 187 centimetres tall. St/Gt = Trough cross-stratified sandstone/granular sandstone; Sp = Planar cross-stratified sandstone. Red arrowheads indicate average palaeocurrent direction

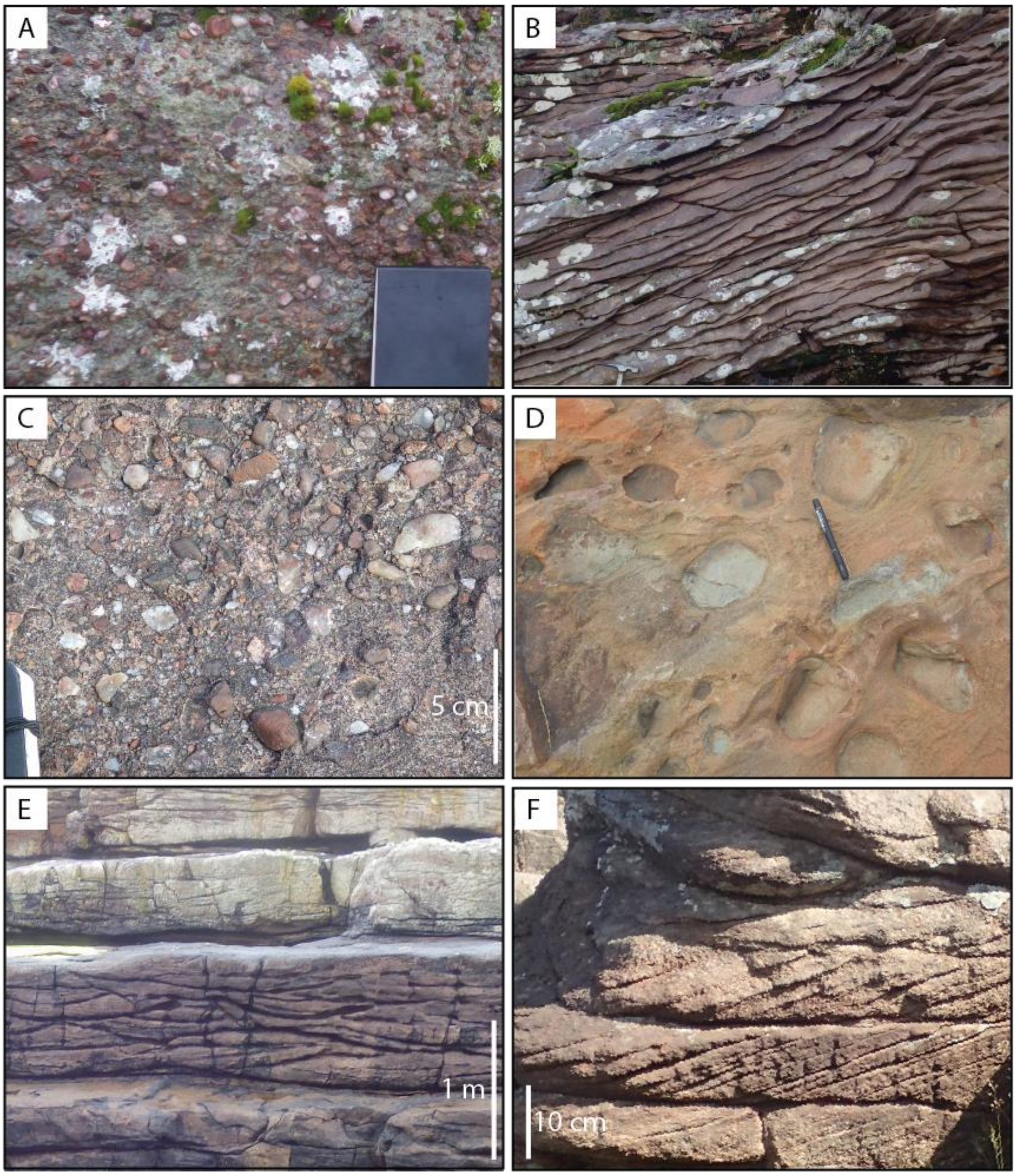

Figure 4.3. Sedimentological features of erosionally based cross-stratified sheet units: A) Pebbly sandstone (Handa Island). Notebook is 13 cm wide; B) Trough cross-stratified medium-grained sandstone (Toscaig). Hammer head is 18 cm wide; C) Granule to pebble lag flooring a lower erosional boundary (Stoer); D) Intraformational mud clasts flooring a lower erosional boundary (Liathach). Pen is 14 cm long; E) Trough cross-stratification (Handa Island); F) Planar cross-stratification (Handa Island).

Thicker units show significant soft-sediment deformation, from mildly deformed cross-beds with oversteepened foresets and small-scale contortions (Fig. 4.4A-C), through to laterally-extensive chaotically folded and disturbed stratification (Fig. 4.4D-G) that is often truncated by the overlying beds (Fig. 4.4H). Soft-sediment deformation is more abundant within erosionally-based sheets than it is in either of the other two architectural units: affecting approximately 55% of sand-bodies and becoming increasingly abundant up-section (possibly due to the modal medium-sand grain-size, optimal for sediment liquefaction (Owen, 1987)).

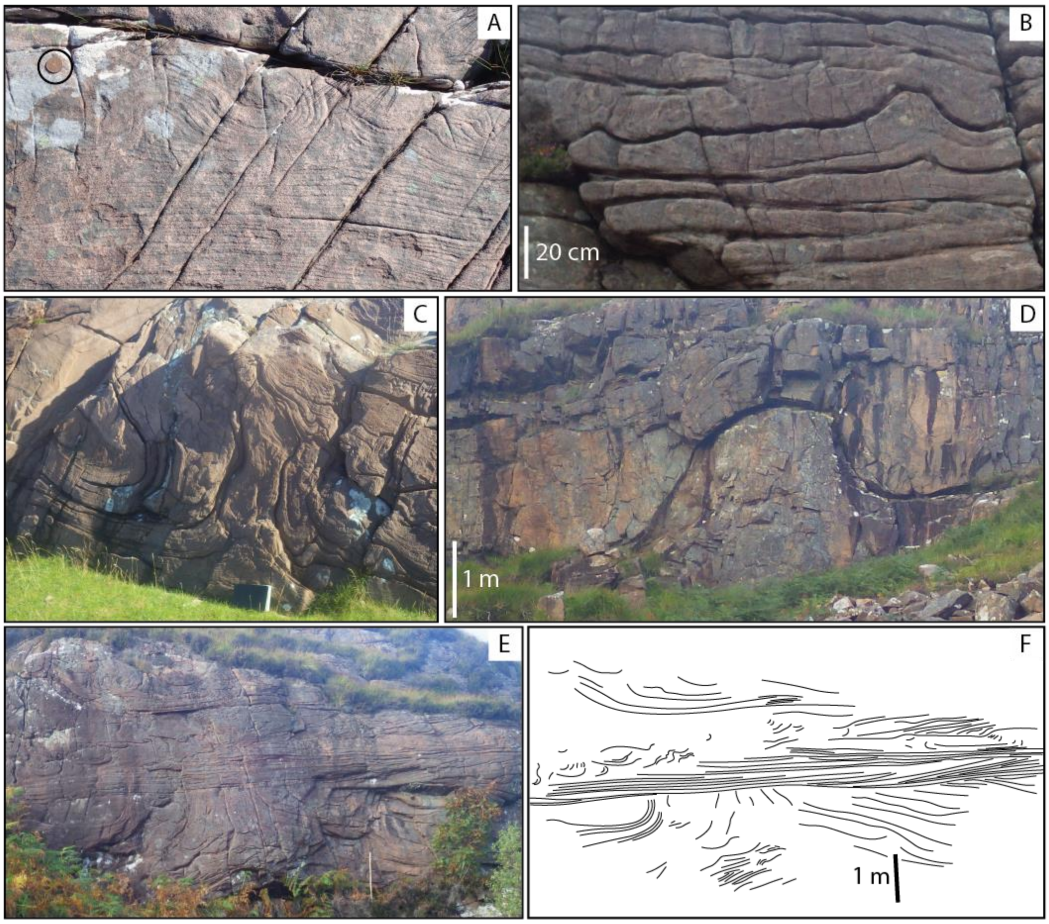

Figure 4.4. Examples of soft-sediment deformation in Torridon alluvium. A) Small-scale contortions within a single bedded unit (Toscaig). Coin (circled) is 2 cm wide; B) Soft-sediment deformed horizons displaying predominant vertical shear (Liathach); C) Chaotically disturbed stratification (Aultbea). Notebook is 21 cm long; D) Laterally persistent soft-sediment deformed horizon displaying significant vertical shear (Liathach). Circled in Figure 4.2B; E) Laterally persistent, top-truncated soft-sediment deformed horizon (Toscaig). Metre rule for scale; F) Line drawing of E.

Units are near-ubiquitously tabular, extending along depositional-strike sections for up to 350 metres regardless of thickness (Fig. 4.1B). Units are therefore categorised as 'sheet-braided' (beds have width-thickness ratios greater than 20:1). Channel-margins cannot be identified at outcrop, and the full lateral-extent of bounding surfaces in depositional-strike sections is limited by available exposure.

These architectural units most frequently occur within thick (up to 17 m) multistorey sandstone sequences (Section 4.1.4.1). Less frequently there is an upwards transition from erosionally-based cross-stratified sheets to inclined accretion strata (Section 4.1.3B). Where units are not erosionally-truncated, original dune topography is sometimes preserved. Planform exposures of dune topography are exposed at a number of locations (Fig. 4.5).

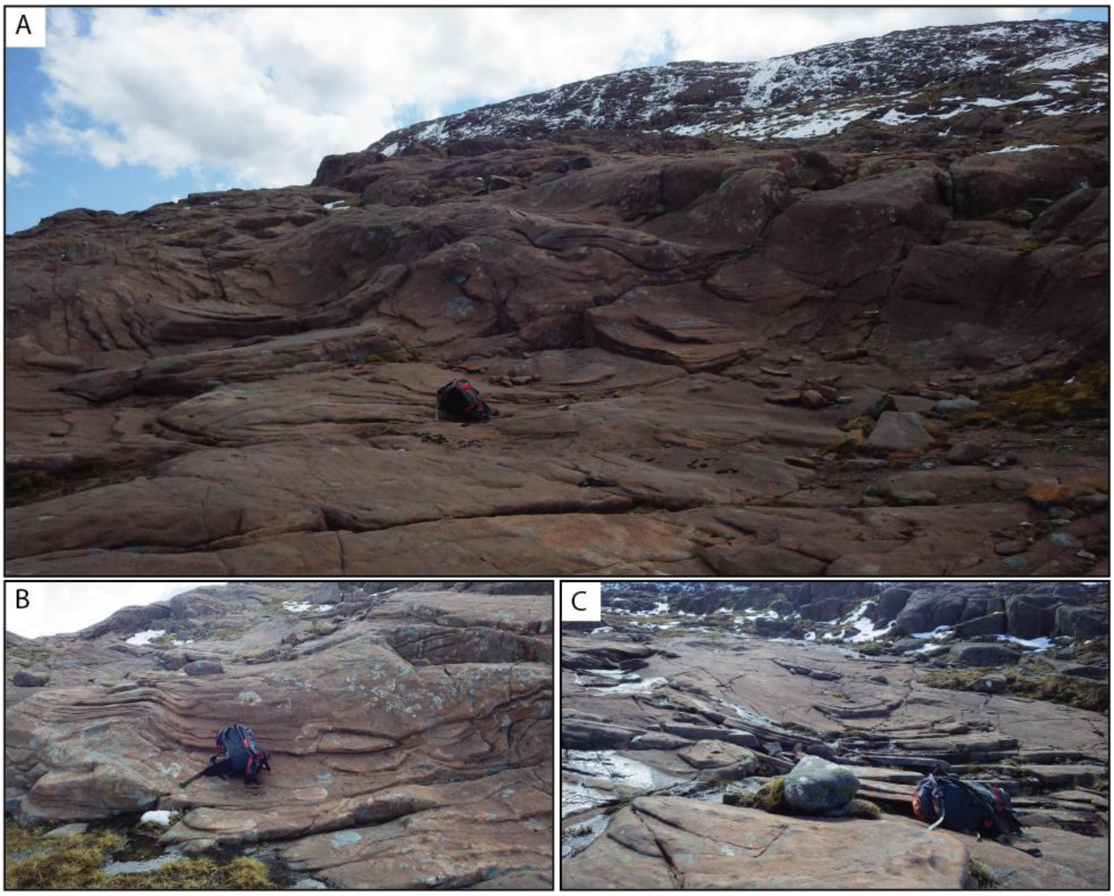

Figure 4.5. Preserved depositional topography. A) Wide trough cross-stratified sets and soft-sediment deformation; B) Soft-sediment deformed trough-cross stratification; C) 2 metre wide trough-cross stratified set. All Bealach na Ba. Bag is 35 cm high.

4.1.3.1b. Interpretation

Coarse-grained sandstones, with planar basal erosion surfaces that are lined with coarser-lags and mudstone rip-up clasts, are analogous to modern sediments deposited in the deeper portion of channels during active flow (Cant and Walker, 1976; Miall, 1996; Carling et al., 2000). The cross-bedding records deposition from sinuous- and straight-crested dunes that migrated in response to unidirectional flow under lower-flow regime conditions. The absence of identifiable accretion surfaces, despite extensive exposures, suggests that these architectural units do not record in-channel barform migration, but rather the migration of bedforms which accumulated predominantly by vertical aggradation (i.e., sandy-bedforms) (Miall, 1985, 1996). Thick successions of cross-bedded deposits are known to accumulate in the deeper parts of modern fluvial channels, and this is a likely origin for such facies as seen in the Torridon Group.

These architectural units are herein referred to as ‘channel-fill units’. Successive channel-fill units each separated by a planar erosion surface are referred to as ‘multistorey channel-fill sequences’ (Section 4.1.4.1). Laterally persistent erosional surfaces are most commonly associated with systems with large channel bodies (Hajek and Heller, 2012). Channel-margins become gentler in slope (and therefore less recognisable at outcrop) with increasing channel width (Miall, 1996). Additionally, laterally mobile channels may rework pre-existing channel margins producing tabular sandstone bodies far greater in width than the original channel morphology (Friend, 1983; Hajek and Straub, 2017).

4.1.3.2. Inclined accretionary strata

4.1.3.2a. Description

This architectural unit most frequently occurs above coarser, underlying channel-fill units (Fig. 4.6). It consists of inclined sets and cosets of cross-stratified sandstone all genetically related to a common underlying bounding surface (Fig. 4.6, Fig. 4.7). Maximum coset thickness is 510 cm (mean 184 cm) ($n = 52$, $S = 107$). Individual inclined sets are predominantly planar or planar-tangential (Fig. 4.6), though sigmoidal geometries also occur (Fig. 4.7A-B, Fig 4.7D). Maximum planar set thickness is 160 cm (average 97 cm) ($n = 36$, $S = 33.6$) and maximum sigmoidal set thickness is 200 cm (mean 132 cm) ($n = 16$, $S = 32.0$). Occasional low-angle cross-stratification and horizontal-laminae occur towards the top of individual units (Fig. 4.7C, Fig. 4.7F). Some stratification show oversteepening by soft-sediment deformation (Fig. 4.7D-E). Accretion directions are varied, dipping downstream and normal to local palaeoflow (Fig. 4.6, Fig. 4.7A). Units are never heterolithic, though display subtle fining- and coarsening-up profiles. Rare reactivation surfaces are predominantly marked by gravel lags.

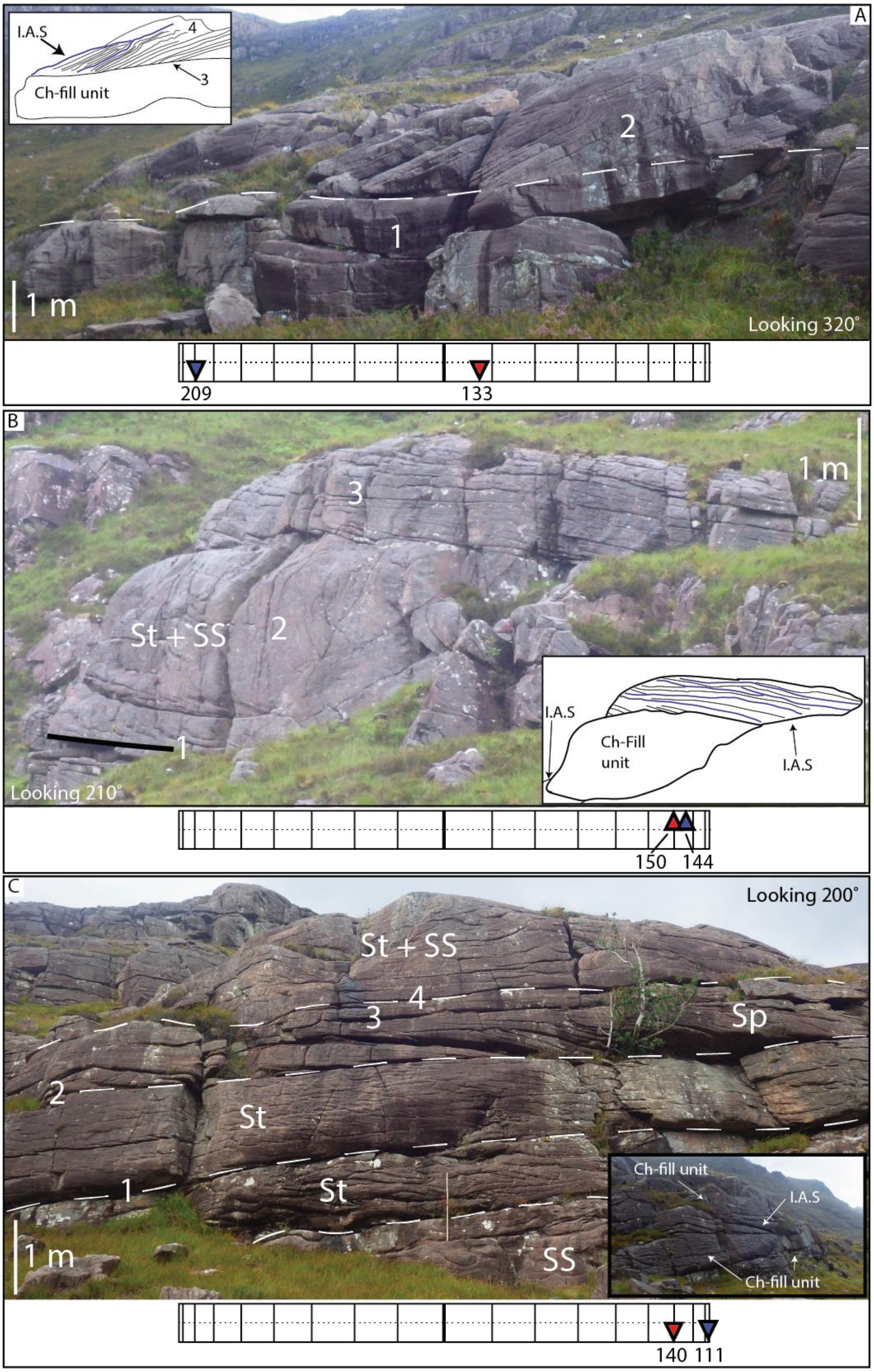
A
I.A.S
4
3
Ch-fill unit
2
1
1 m
Looking 320°
209
133
B
1 m
3
St + SS
2
1
Looking 210°
I.A.S
Ch-Fill unit
I.A.S
150
144
C
Looking 200°
St + SS
4
3
Sp
2
St
1
St
1 m
SS
Ch-fill unit
I.A.S
Ch-fill unit
140
111

Figure 4.6. Stratigraphic relationships between inclined accretionary strata and channel-fill units: A) A channel-fill unit (1) is overlain by multiple large sets of inclined planar accretionary strata (2) accreting at a high angle to local palaeoflow. Each inclined set abuts against a common underlying surface (3). Soft-sediment deformation is observed in inclined accretionary strata (4) (Liathach); B) An erosion surface (1) marks the base of the channel-fill unit (2). Overlying inclined accretionary strata (3) are accreting into the outcrop at a high angle to local palaeoflow (Glac Dhorch); C) A multistorey channel-fill sequence (1) is overlain by inclined planar accretionary strata (2). Inclined accretionary strata accrete in approximately the same orientation as local palaeoflow (3). An erosion surface marks the base of an overlying channel-fill unit (4) (Liathach). Blue lines in schematic sketches mark accretion surfaces. I.A.S = Inclined accretionary strata. St = Trough cross-stratified sandstone; Sp = Planar cross-stratified sandstone; SS = Soft-sediment deformation. Red arrowheads indicate average palaeoflow direction. Blue arrowheads indicate average accretion orientation.

Figure 4.7. Sedimentological characteristics of inclined accretionary strata. 1) Channel-fill unit (1) overlain by sigmoidal inclined accretionary strata (2) accreting nearly perpendicular to local palaeoflow (Upper Loch Torridon). Red arrowhead indicates average palaeoflow. Blue arrowhead indicates average accretion orientation. Bag is 35 centimetres high; 2) Large sigmoidal inclined accretionary strata. Metre rule for scale (Liathach); C) Low-angle accretionary strata (2) overlying trough cross-stratified channel-fill unit (2) (Glac Dhorch). Bag is 35 centimetres high; D) Oversteepened sigmoidal inclined accretionary strata (Liathach); E) Large-scale sigmoidal and low-angle accretionary strata showing significant soft-sediment deformation (Diabaig); F) Horizontal-stratification occurring in outcrop directly above large-scale inclined planar accretionary strata (not shown in figure) (Liathach). Bag is 35 centimetres high. St = Trough cross-stratified sandstone; Sl = Low-angle cross-stratified sandstone; Sh = Horizontally-stratified sandstone.

Units are up to 70 m wide in depositional-strike sections (constrained by available exposure), and can be traced down depositional-dip for more than 100 metres (constrained by available exposure). Rarely, units are overlain by fine-grained material (Section 4.1.3.3), or stack to form multistorey composite bodies (Section 4.1.4.3). However, they are most commonly erosively overlain by a succeeding channel-fill unit (Fig. 4.8).

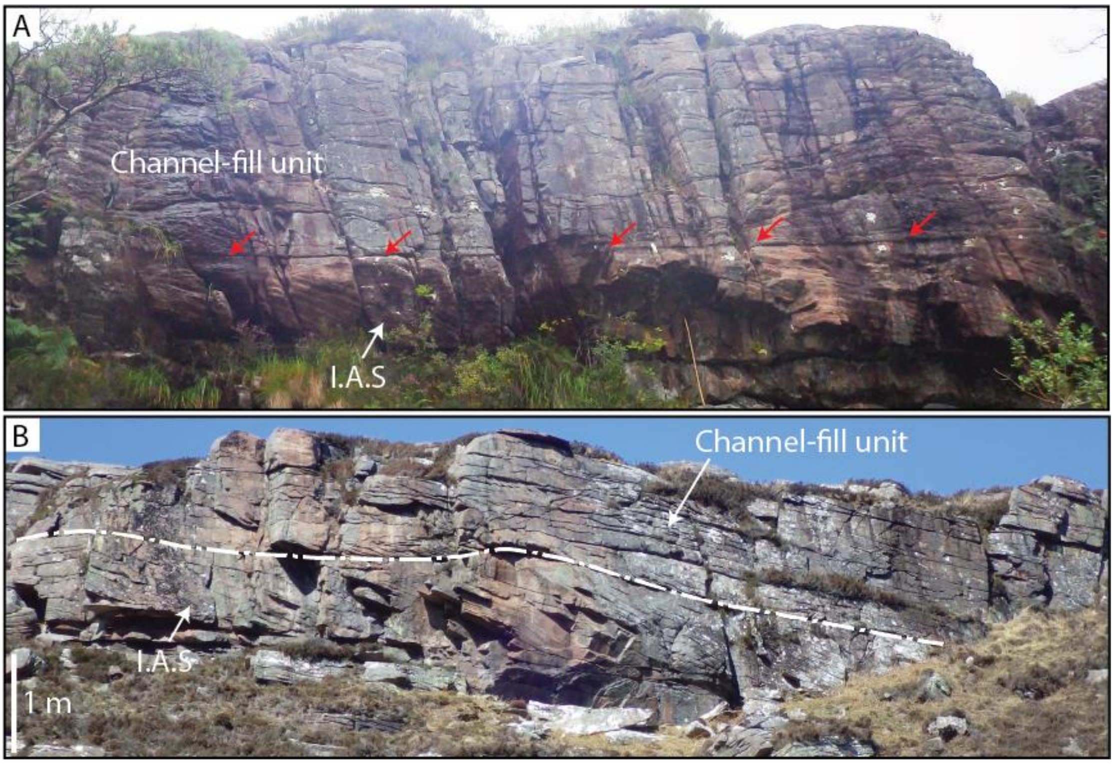

Figure 4.8. Examples of inclined accretionary strata erosively overlain by channel-fill units. A) Alligin. Metre rule for scale. Red arrows highlight boundary between inclined accretionary strata and channel-fill unit; B) Roadside outcrop near Ullapool. Sigmoidal sets accreting near perpendicular to local flow direction (125°).

4.1.3.2b. Interpretation

Inclined accretionary units are interpreted as barform units, where the inclination of coset surfaces reflects barform migration (Miall, 1985; Long, 2011). The palaeoflow orientations of cross-stratification within each coset represent the migration of bedforms along the bar. Of the 262 units where accretion and palaeocurrent directions were available, 56% showed downstream accretion (n=147) and 33% showed lateral accretion (n=85). Downstream- and lateral-accretion elements are the principal products of accretion within barforms of major sand-bed channels (Miall, 1996). The incremental character of inclined accretionary elements suggests periodic migration of barforms during peak flood, separated by periods of low flow (e.g., Bristow, 1987; Best et al., 2003; Long, 2006).

Rare barform reactivation surfaces may represent falling stage modifications to the bed surface (Collinson, 1970). Upstream-accretion elements (Table 2.2) were recognised in association with these surfaces (n=30, 11%). In modern rivers, upstream accretion surfaces are observed at the upstream end of large mid-channel barforms, with accretion predominantly occurring during falling flood stages (Bristow, 1987, 1993; Best et al., 2003). Such a refined assessment was not possible for Torridon alluvium as the original barforms are never preserved in their entirety.

More sigmoidal accretionary surfaces displayed lateral accretion than inclined planar accretionary surfaces, as is reflected in their mean accretion directions of 76° and 113° respectively (mean palaeoflow 126°) (Section 4.1.5). Due to the range of possible accretion directions, barform units in modern alluvial systems dispay greater flow dispersal than channel-fill units (Fig. 4.14, Section 4.1.5). It is important to note that there were many instances where accretion directions could not be obtained at all from suspected barform units. Internal three-dimensional geometric complexity mean three-dimensional exposures are often required to determine directions of accretion.

No channel-fill units were witnessed passing laterally into barform units (i.e., bank-attached bars). The only occasions where bank-attached bars could be interpreted were in instances where inclined accretion surfaces were observed to dip towards, and be truncated by, fine-grained deposits interpreted to have filled abandoned channels (n=2) (Ielpi and Ghinassi, 2015, their Figure 8).

4.1.3.3. Discontinuous mudstone to very fine-grained sandstone units

4.1.3.3a. Description

Discontinuous mudstone to very fine-grained sandstone units form by far the least abundant of the three recognised architectural units, with only 14 observed examples across the entire 200 x 30 km wide outcrop belt and throughout alluivum's entire 4.5 km thickness. Note this figure does not include examples in the Allt-na-Béiste Member, which is better considered as the topmost member of the underlying Diabaig Formation (discussed in Chapter 7).

Units are up to 30 m wide (Fig. 4.9A) and 240 cm thick (Fig. 4.9C) (mean 0.25 cm (S = 0.6)). They most often succeed barform units, although on three occasions erosively overlie channel-fill units (Fig. 4.9A). Mudstones and siltstones are either distinctively oxidised (Fig. 4.9A) or grey in colour (Fig. 4.9B-C). Horizontal laminae and ripple cross-lamination are common in coarse-grained siltstones and very fine-grained sandstones (Fig. 4.9D-E). Some ripple cross-laminated sandstones show soft-sediment deformation (Fig. 4.9E) and contain small intraformational mud clasts (Fig. 4.9F).

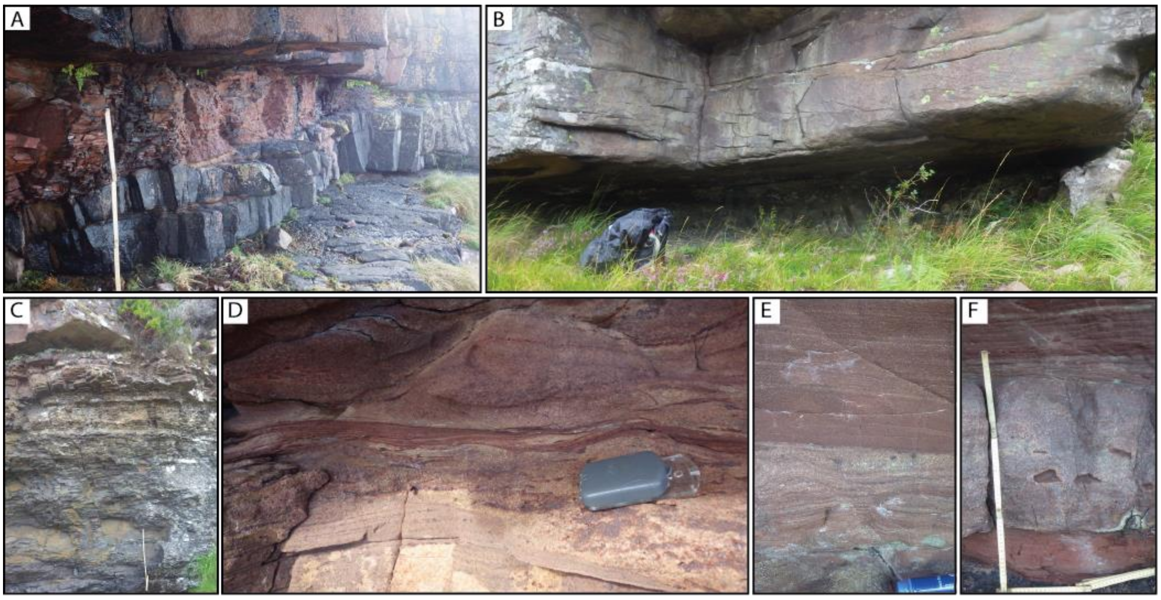

Figure 4.9. Discontinuous mudstone to very fine-grained sandstone units: A) Channel abandonment deposits, composed of plane-parallel laminated mudstone and siltstone (Stoer). Metre rule for scale; B) Discontinuous siltstone bed erosively overlain by a channel-fill unit (Liathach). Bag is 35 cm high; C) Thick mudstone unit erosively overlain by a channel-fill unit (Tanera Beg). Metre rule for scale; D) Ripple cross-laminated very fine sandstone unit (Stac Pollaidh). Compass for scale is 11 cm long; E) Ripple cross- and plane parallel-laminated (Sr, Sh) deposits showing incipient soft-sediment deformation (Big Sand, North Erradale). Pen for scale is 2 cm long; F) Preserved intraformational mud clasts (Achiltibuie). Metre rule for scale.

4.1.4. Architectural unit stacking patterns

The observed architectural units stack to form a hierarchy of well-defined sequences (Fig. 4.10).

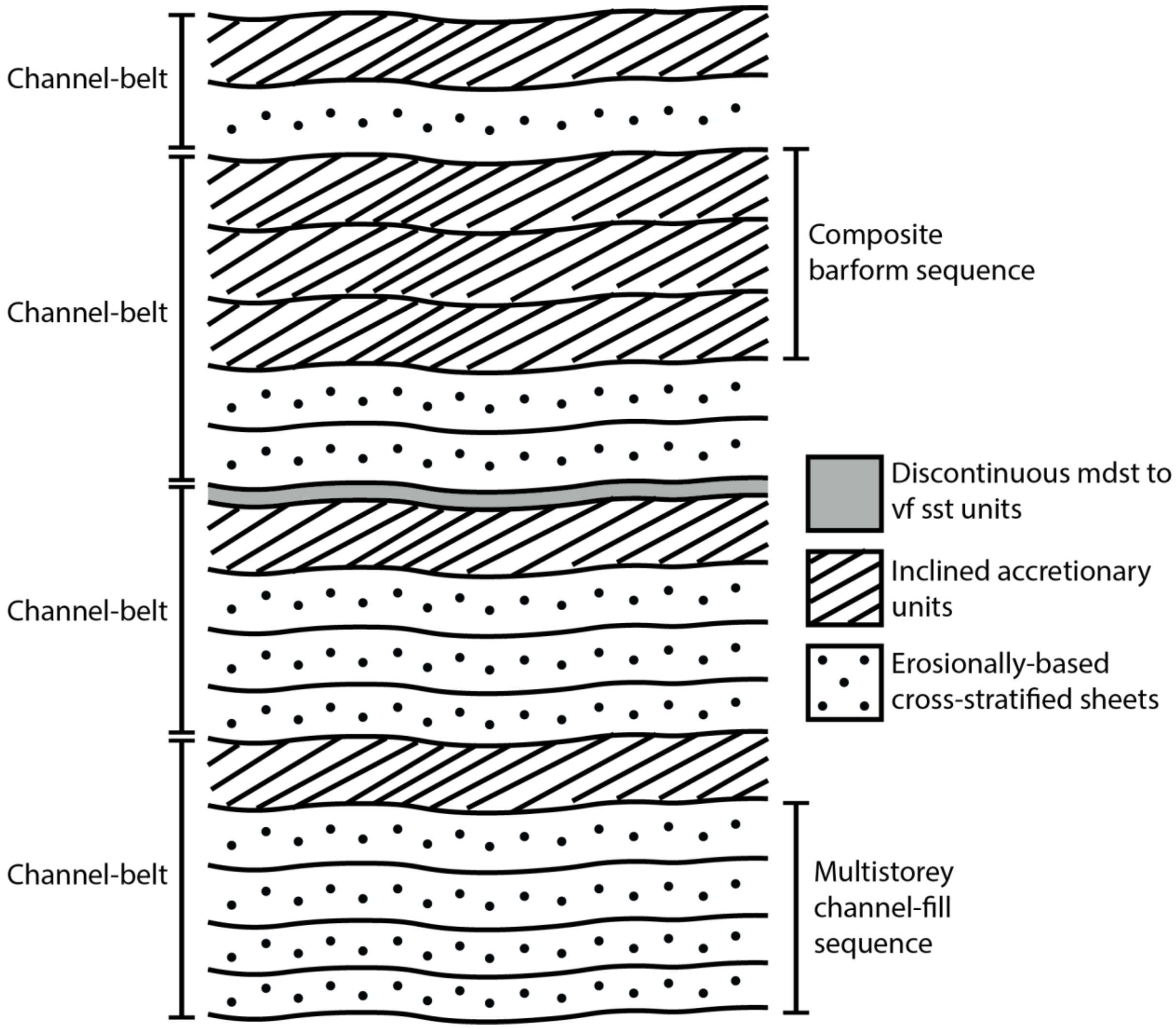

Figure 4.10. Schematic diagram illustrating the relationship between the defined architectural units. No scale intended.

4.1.4.1. Multistorey channel-fill sequences

In an ideal case, the architectural units defined in Section 4.1.3 should stack into one cycle (ascending: channel-fill unit, barform unit, out-of-channel material), representing the migration and infilling of a channel, succeeded by abandonment and the establishment of floodplain deposition (Allen, 1965). However, autogenic reorganisation of any fluvial system inevitably leads to partial shredding of its sedimentary record, so it is unsurprising that such ideal sequences are only very rarely observed in the Torridon Group. Most commonly, multiple channel-fill units stack vertically without preserving any associated barform or out-of-channel units (Fig. 4.2B). These successions are termed 'multistorey channel-fill sequences'.

Multistorey channel-fill sequences are biased (through shredding) to the sedimentary record of the topographically lowest portions of the fluvial system (e.g., Godin, 1991; Todd and Went, 1991; McLaurin and Steel, 2007; Went and McMahon, 2018). Preservation of only the deepest parts of a river system is regarded as the product of aggradation co-occurring with lateral channel-migration (Bluck, 1971; Miall, 1980; Todd and Went, 1991; Lewin and Macklin, 2003). Lateral channel migration or combing reworks barforms and out-of-channel material and enables the longer-term aggradation of several generations of channel-fill units.

4.1.4.2. Channel-belts

Channel-fill units or multistorey channel-fill sequences which are succeeded by a barform unit (and rarely in turn by out-of-channel material) are described here as ‘channel-belt’ sequences (Fig. 4.10, Fig. 4.11). In instances where barform units (and rarely in turn out-of-channel material) do succeed channel-fill sequences, these units must have escaped reworking by subsequent channel migration because the active channel-belt is located elsewhere. Preservation of barform units directly above channel-fill units is therefore suggestive of a shift in the location of the main trunk channel of the fluvial system, or possibly avulsion of the entire braidplain (e.g., Bristow, 1996; Heller and Paola, 1996; McLaurin and Steel, 2007; Hajek and Heller, 2012). Sequences of channel-fill units or multistorey channel-fill sequences capped by a barform unit were deposited between avulsion events and can therefore be defined as ‘channel-belt’ sequences (Fisk, 1944).

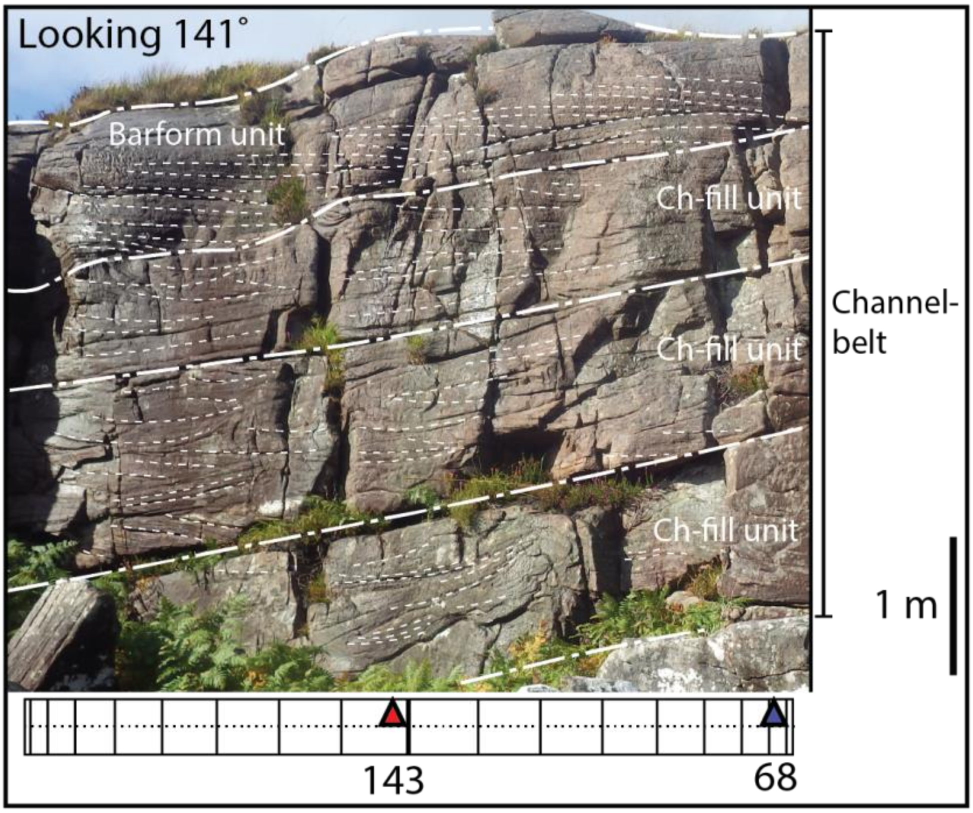

Figure 4.11. Example channel-belt sequence (Glac Dhorch). A multistorey channel-fill sequence is overlain by a barform unit. Palaeoflow in channel-fill units is approximately towards observer. Accretion in barform unit is approximately from the left to the right of the image. Red arrowhead indicates average palaeocurrent direction of three figured channel-fill units. Blue arrowhead indicates accretion direction of figured barform unit.

Constraints on maximum channel-belt thickness are restricted in some instances by the inaccessibility of some large vertical successions (e.g., sea cliffs). However, Torridon alluvium also flanks a number of accessible mountains. Alluvium was studied at Liathach (Fig. 4.1), Beinn Eighe, Ben Alligin, Slioch, An Teallach, Glac Dhorm; Stac Pollaidh, Suilven and Quinag (Fig. 2.1), enabling multiple channel-belt sequences to be detailed through their entire stratigraphic thickness. In these instances, the thicknesses of channel-belt sequences demonstrate no trend across the outcrop belt, ranging from 2.8 – 18.4 metres (mean = 8.8 metres (n = 42; S = 5.3).

4.1.4.3. Composite barform sequences

In certain areas, multiple stacked barform units crop out forming sequences up to 9 metres thick. These intervals are termed 'composite barform sequences' (Fig. 4.10, Fig. 4.12).

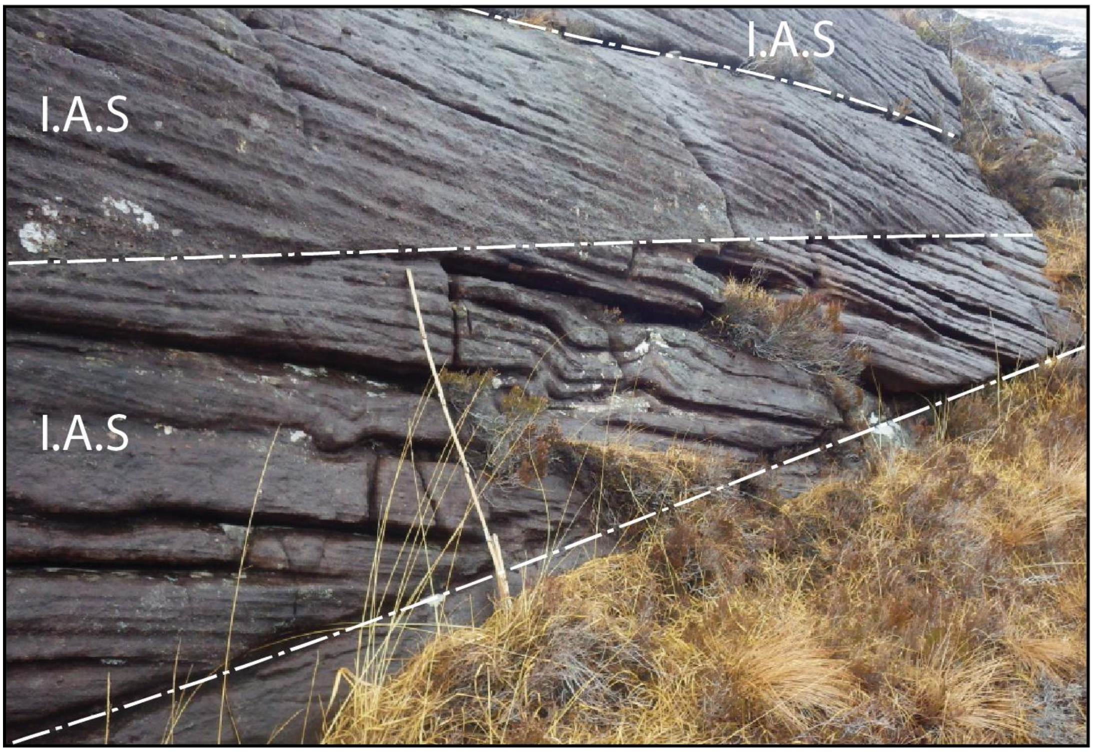

Figure 4.12. Example composite barform sequence (Liathach). Succession consists of three stacked barform units each separated by a planar erosional surface. Metre rule for scale.

The process responsible for barform unit stacking is uncertain. Preservation of fluvial deposits is known to be affected by the relative balance between aggradation rate and available accommodation space (Bristow and Best, 1993). One suggestion is that episodes of bar-build up may relate to phases of high-aggradation (possibly during early waning-flood stages) (Ielpi and Ghinassi, 2015) as such conditions would allow less time for barform reworking by channel-migration. Their apparent stochastic distribution across the outcrop belt implies that cyclical changes to base level were unlikely to be the cause for these shifts in preserved style.

4.1.5. Palaeocurrent analysis

Palaeocurrent directional data may provide an indication of channel sinuosity. A low dispersion is consistent with a low-sinuosity system (Bridge, 1985) whereas a higher dispersion may indicate meandering (Bluck, 1971) (Chapter 7). Palaeocurrent directions were obtained from the foreset planes of cross-stratified surfaces and were plotted geographically to assess regional transport patterns. Across the entire outcrop belt, mean transport direction was towards 127^0 (n = 2333, S = 45.7). This is similar to the result of Nicholson (1993) who calculated a mean flow towards 123^0 (n = 2802). There is also little variance in palaeocurrent direction between locations, with low palaeoflow dispersal across the entire outcrop belt (Fig. 4.14). However, there is a far lower dispersal for channel-fill units than there is for accretion of barform units (Fig. 4.14) ($n = 270$, $S = 83.6$), a result which reflects the variety of modes of barform accretion directions recorded (i.e., lateral and downstream). Channel-fill units with and without directly overlying barform units exhibit similar palaeoflow orientations (128° vs 127°).

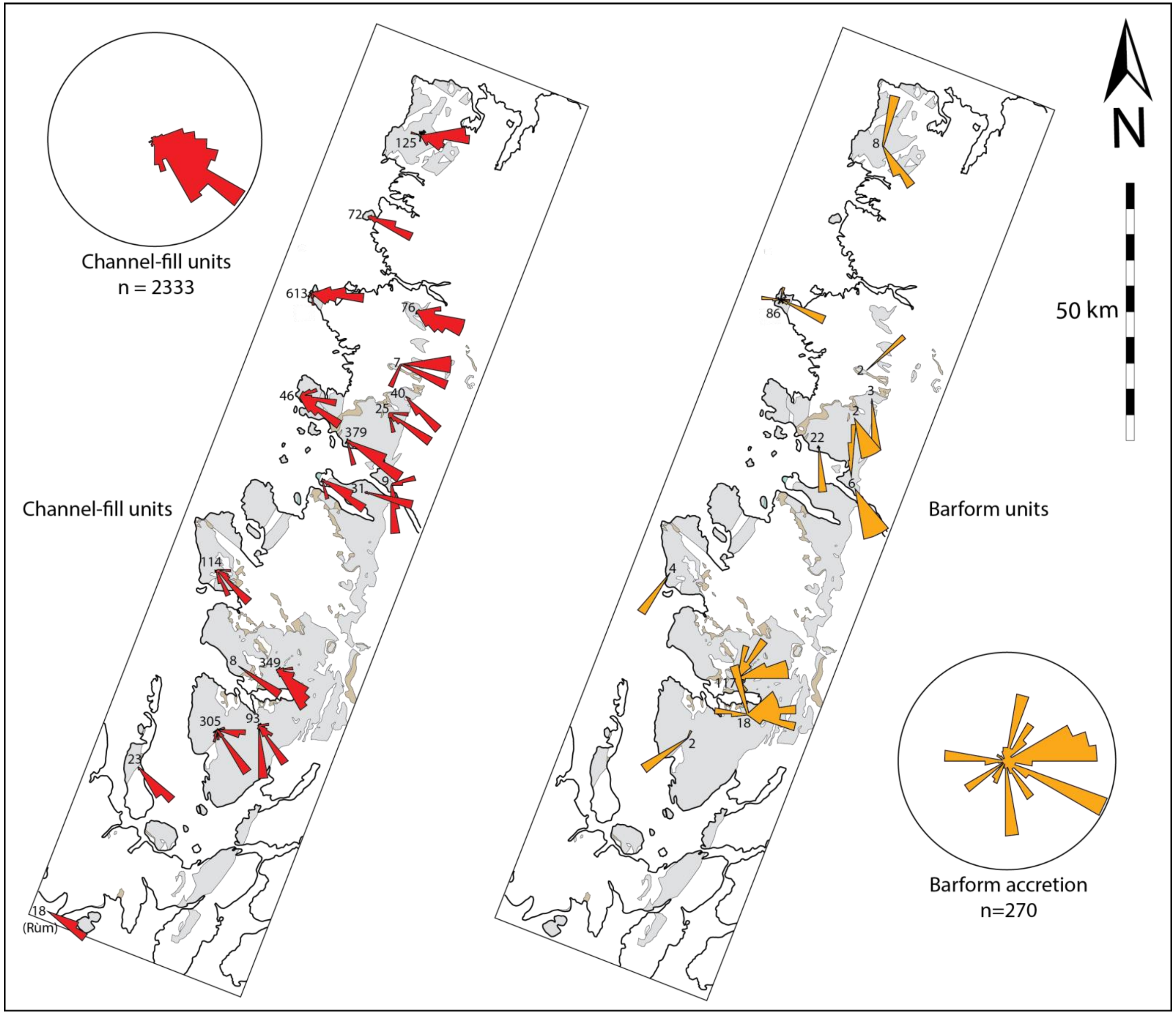
Channel-fill units
n = 2333
Channel-fill units
125
72
613
76
7
46
40
25
379
9
31
114
8
349
305
93
23
18
(Rùm)
N
50 km
8
86
2
3
2
22
6
Barform units
4
117
18
2
Barform accretion
n=270

Figure 4.13. Map of palaeoflow and barform accretion directions measured across the Torridon outcrop belt. Torridon alluvium highlighted in grey. Values attached to each rose diagram represent the total number of readings.

Owen and Santos (2014) suggested that a large proportion of preserved soft-sediment deformation structures formed in inactive but water-saturated areas of the fluvial system, and considered this more consistent with a fluvially-dominated alluvial fan or distributive fluvial system (DFS) depositional model, than the previously suggested alluvial braidplain model (Nicholson, 1993). The palaeocurrent measurements do not support such an interpretation at the scale shown by Owen and Santos (2014) in their depositional model (Fig 4.14). Whereas conclusive identification of such a DFS in the rock record would necessitate the identification of a radial distribution of palaeocurrent directions (e.g., Hartley et al., 2010), the collected palaeocurrent directions show similar modal orientations across the entire 30 km x 200 km wide outcrop belt (Fig. 4.13, Fig. 4.14). Equally however, this palaeocurrent arrangement does not permit the interpretation of a tributive fluvial pattern either, and only demonstrates that: 1) there is little change in channel orientation across the outcrop belt; and 2) there are few vertical changes in flow direction throughout the stratigraphic succession, indicating minimal vertical changes in fluvial style as the depositional system evolved.

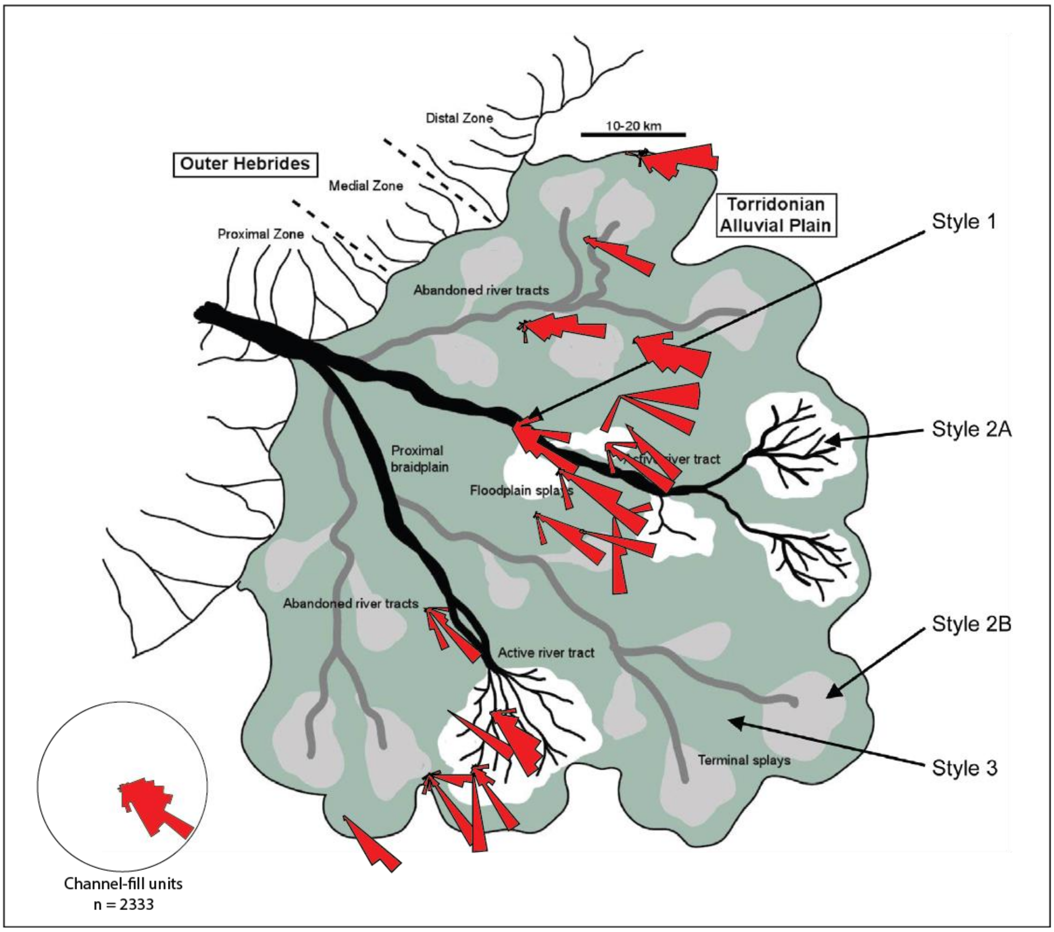

Figure 4.14. Palaeoflow data collected in this study (Figure 4.13) aligned with previously suggested depositional model for Torridon alluvium (represented as a distributive fluvial system) (from Owen and Santos (2014), their Figure 14).

4.1.6. Depositional model

Torridon alluvium is here interpreted as the deposit of a low-sinuosity, braided river system. Evidence for this includes: 1) the coarse nature of the bedload; 2) lack of preserved out-of-channel material; 3) low palaeocurrent variance; 4) lack of observable channel-margins; and 5) evidence for predominantly downstream accreting in-channel barforms.

Extensive erosionally based sheets (channel-fill units), and a paucity of channel margins despite evidence of considerable water depths (barforms units up to 510 cm thick), suggests channels were laterally mobile. Numerical models of laterally mobile channel networks have produced stratigraphic stacking patterns dominated by units with similar tabular geometries (Wang et al., 2011; Straub and Wang, 2013). Inclined accretionary strata (barform units), when recognised, demonstrate varied components of bar growth, although downstream accretion is most dominant. The incremental character of barform deposits demonstrates that not all sand-bodies were deposited in single episodes of flooding such that flow may have been perennial (Long, 2006). Additionally, Torridon alluvium is dominated by stacked, lower flow regime, 3D sedimentary structures, typical of perennial fluvial flow (e.g., Bristow, 1987; Best et al., 2003).

Soft-sediment deformation localised within individual cross-stratified sets (Fig. 4.4A-B) may have formed by flow-induced shear during deposition. Laterally extensive soft-sediment deformed horizons (Fig. 4.4C-F) are frequently top-truncated (Fig. 4.4E-F), indicating that deformation did not occur through compaction after deposition. No evidence was uncovered in this study to determine the exact trigger of this liquefaction. Previous studies have variously hypothesized: 1) groundwater movements (Owen and Santos, 2014); 2) flow-related turbulence (Owen, 1996); or 3) seismic activity (Owen and Santos, 2014). It may be possible to rule out the role of groundwater in most instances, as in a perennially flowing river system, the sediments would be permanently wet. In Davies et al. (2005), seismites were conclusively proven in the Late Silurian Stubdal Formation, Norway, because it was demonstrated that the same stratigraphic horizon saw different expressions of soft-sediment deformation depending on lithology. Within Torridon alluvium, lithological monotony makes confident stratigraphic correlation between outcrops, separated by non-exposure and drift cover, impossible. Thus there was no conclusive way of determining whether the same horizons show soft-sediment deformation across their entire lateral extent. Consequently, a seismic origin can neither be confidently determined nor conclusively ruled out.

Channel-fill, multistorey channel-fill and channel-belt dimensions appear stochastically distributed throughout the succession. The lack of systematic trends suggests cyclical controls in accommodation space were not the dominant control on preserved sedimentary architecture. Minor areas of barform build-up may relate to high aggradation after flood events (Ielpi and Ghinassi, 2015). Fluvial style demonstrates little variation throughout the sedimentary succession implying sedimentation was largely undisturbed throughout Torridon alluvium's entire depositional history. Few, if any, reliable criteria exist with which to interpret regional channel patterns (distributive or tributive).

4.2. The Neoproterozoic Jacobsville Sandstone

A small case study of the Neoproterozoic Jacobsville Sandstone is presented in this section to illustrate a fuller spectrum of the potential range of river scales which may be preserved within pre-vegetation alluvium. Palaeogeographic reconstructions (Rainbird et al., 2017) and preserved sedimentary character imply that the Torridon Group was predominantly deposited by large-scale, deep (possible pan-continental) rivers. In contrast to this, the Jacobsville sandstone nearly entirely consists of thin, low-relief sedimentary packages best interpreted as the deposits of small in-channel barforms. Paleohydraulic reconstructions (Section 4.2.3) suggest bankfull water depths significantly less than 1 metre. The rivers which deposited the Jacobsville sandstone would have therefore been wholly different in character to the previously discussed Torridon Group, justifying additional discussion here.

4.2.1. Introduction

The Neoproterozoic Jacobsville Sandstone, Michigan, is known largely through core data, only rarely cropping out at the surface. It is a sandstone dominated succession approximately 900 m thick overlain unconformably by the late Cambrian Munising Sandstone (Hamblin, 1958). The succession consists predominantly of fluvial facies, with palaeoflow orientations displaying considerable variation (Malone et al., 2016). Sandstone petrology varies from subarkosic to quartz arenitic (Kalliokoski, 1982). A 250 metre wide roadcut near L'Anse offers a rare opportunity to study the fluvial architecture of the succession (Fig. 4.15). The outcrop is orientated almost exactly parallel to local palaeoflow which is directed towards the southwest. Photomosaics were constructed and bedding contacts, lithological information, details of internal structure and palaeocurrent data (lower beds only) were recorded in the field. Internal stratification in places is obscure. In these instances, no attempt is made to trace lines on the presented photomosaics.

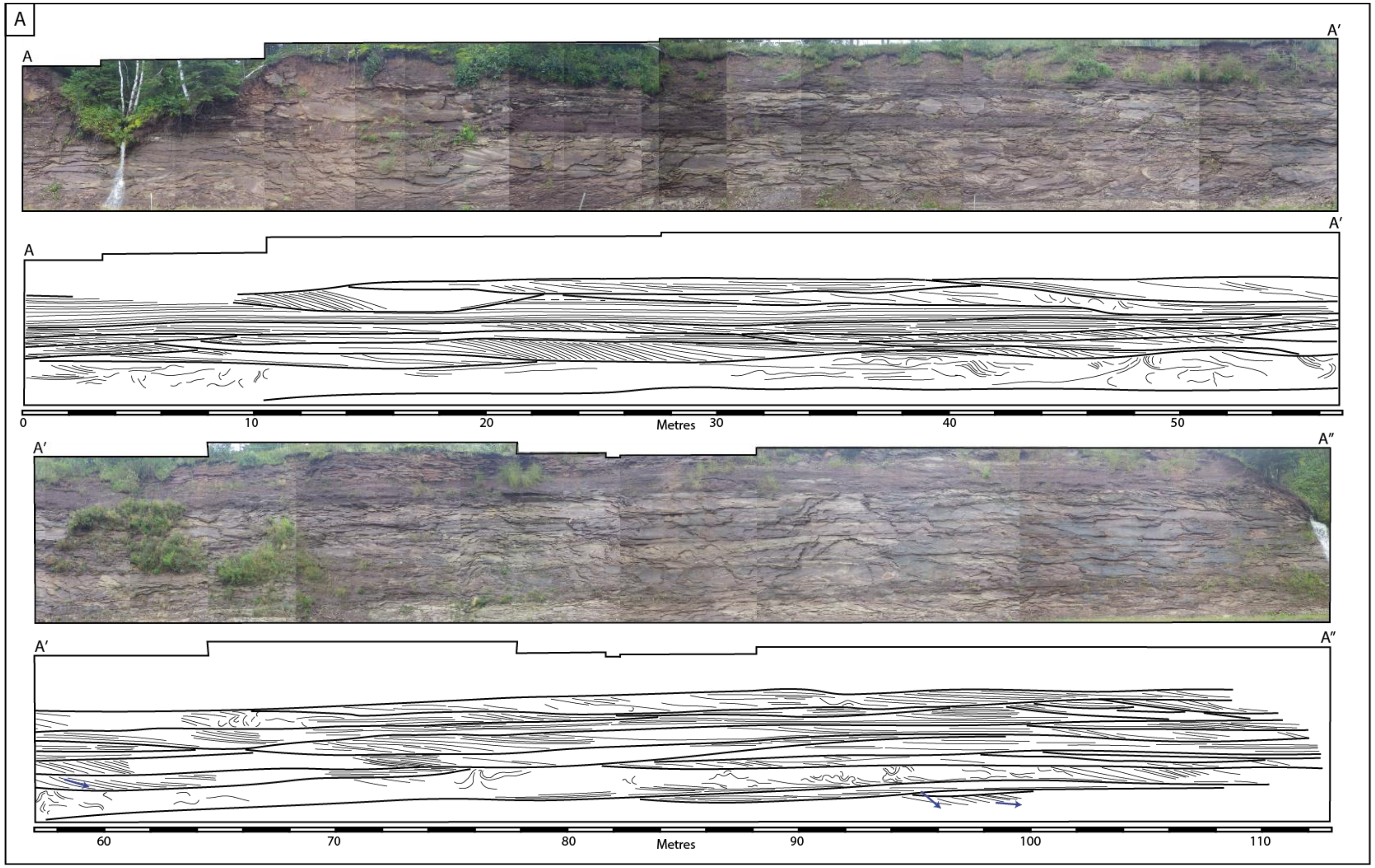

Figure 4.15. Architectural panel of Jacobsville alluvium at L'Anse. The directions indicated by the arrows are organized with respect to the architectural panel so that arrows pointing up indicate dip directions away from the observer, and those pointing down indicate dip directions towards the observer. Procedure after Long (2006).

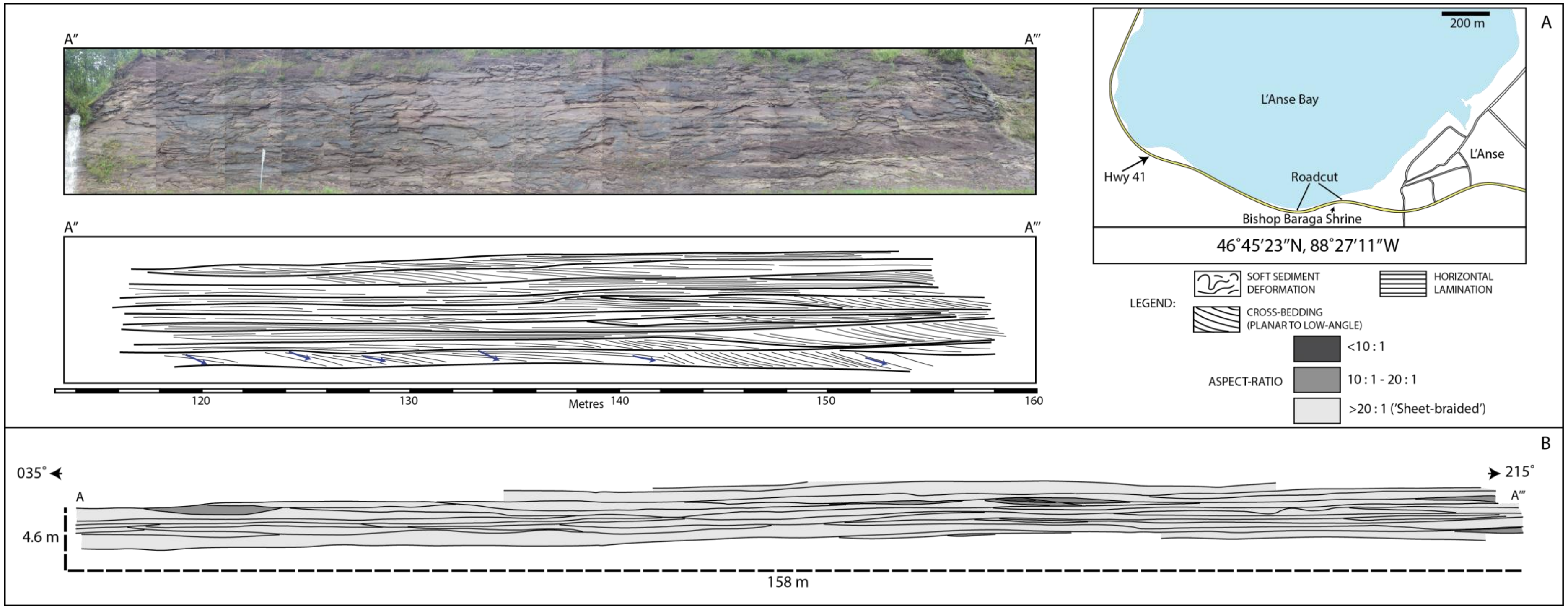

Figure 4.15 *(continued).*

4.2.2. Sedimentology

Many laminae and strata in the Jacobsville have an appreciable original depositional dip. Bedding contacts are either planar or concave-up. As individual packages are never greater than 1.6 m, the sandstone bodies are predominantly categorised as 'sheet-braided' as defined by Cotter (1978) (Fig. 4.15B). This is despite the clear intersecting erosional surfaces spread across the outcrop. These largely erosional bedding contacts divide the beds into structured packages. Internally, sedimentary packages contain two sedimentary facies: 1) Horizontally-stratified sandstones; and 2) Cross-bedded sandstones.

1) Horizontally-stratified medium-grained sandstones are most abundant. The facies is represented by medium- to coarse-grained sandstones developed into laterally extensive (up to 52 metres wide) parallel laminae. Laminae are typically several millimetres thick, with individual packages up to 95 centimetres thick. Occasionally laminae show gently concave- or convex-up geometries, mimicking the underlying topography.

2) Cross-bedded facies consist of medium- to very coarse-grained sandstones with very rare granules. Each bed represents a single, solitary cross-bedded set. Beds range in thickness from 0.3 to 1.6 metres and contain both high- and low-angle planar foresets. Thicker beds contain extensive soft-sediment deformation, consisting of laterally extensive tabular horizons of chaotically disturbed stratification. Lower contacts are predominantly erosional, though often partially preserve the underlying depositional topography. Upper contacts may be erosional or transitional. If transitional, foresets flatten out into horizontally-stratified sandstones. Cross-bedded facies may also pass down depositional-dip into low-angle cross- and horizontal-stratification.

Packages which consist of planar cross-bedded and horizontally-stratified sediments are consistent with deposition by small channel-barforms. Whilst some barform deposits consist solely of a solitary cross-bedded set with an erosional upper and lower contact, most comprise both cross-bedded and horizontally-stratified facies. Bases are predominantly smooth, but can display both concave- and convex-up forms. The internal geometry of the barform deposits is consistent with downstream-accretion in all instances, probably occurring within a low-sinuosity channel. Erosional truncation usually means that only what would have originally been the lower part of the barform structure can be observed. However, instances where cross-bedded facies transition upwards into horizontal- or low-angle cross-stratification can be interpreted as transitions to bar-top facies. Since bars grow near the free water surface, topsets of horizontal stratification suggest near full preservation. In these instances, units range in thickness from 0.3 – 0.9 metres and measure 25 – >250 metres long. Horizontally-stratified facies are predominantly erosively overlain by succeeding sedimentary packages, indicating that even in these examples, barforms are not completely preserved. Cross-bedded sets which pass down depositional-dip into horizontal-stratification demonstrate either a decrease in water depth or increase in flow strength. Erosively-bounded packages which only comprise horizontal-stratification are interpreted to have developed on smooth to gently sloping surfaces in very shallow water and/or high-energy flows.

4.2.3. Discussion of palaeohydraulics and preserved sedimentary architecture

Proxy estimates of palaeoflow depth from stacked-barform deposits can be obtained directly from measurements of preserved barform deposits (Hajek and Heller, 2012). While compaction can decrease scale, these effects are generally small in sandy terrestrial environments (Nadon and Issler, 1997). The average of preserved barform deposit therefore approximates the average bankfull water depth. The average barform package thickness in the Jacobsville Sandstone at L'Anse (as measured through the thickest part of the preserved barform deposit) is 71 cm (n=25, S = 21.8). In most of these instances sets are erosively overlain, but values still provide an estimate of minimum water depth. Nearly fully preserved barform deposits (those which transition vertically-upwards into horizontal-stratified bar-top facies) range in height from 0.3 to 0.9 metres. Maximum recorded barform thickness is 1.6 metres. These measurements generally suggest that water depth was rarely greater than a metre, thus the succession can be considered the product of a relatively shallow river.

4.3. Alluvial signatures of perennial pre-vegetation rivers - Summary

The case studies presented in this section each contain accretion elements, interpreted as barform deposits, whose incremental character demonstrates that not all sand-bodies were deposited in single episodes of flooding such that flow may have been perennial (Long, 2006). Additionally, Torridon alluvium is dominated by stacked, lower flow regime, 3D sedimentary structures, typical of perennial fluvial flow (e.g., Bristow, 1987; Best et al., 2003). An increasing number of authors have recognised large barform deposits preserved in pre-vegetation alluvium and used this observation to interpret perennial flow (e.g., Long, 2006, 2011; Ielpi and Rainbird, 2016a; Lowe and Arnott, 2016; McMahon et al., 2017; Ghinassi and Ielpi, 2018). Such interpretations are contrary to claims that, without vegetation to act as a baffle between rainfall, runoff and evaporation, all pre-vegetation rivers would have been effectively ephemeral (Trewin, 1993; Love and Williams, 2000; Gouramanis et al., 2003; Bose et al., 2012; Mukhopadhay et al., 2014).

Recognition of large barform deposits with similar dimensions to those of modern, deep perennial rivers are also starting to dispel notions that pre-vegetation rivers were uniformly characterized by broad, shallow channels (e.g., Fuller, 1985, Eriksson et al., 1998, Bose et al., 2012). This hypothesis initially arose from two key modern and ancient observations: 1) in active channels that have weak banks (such as those lacking the fortifying effects of plants), widening, rather than incision, is the primary sedimentary response to fluctuating flow conditions (Wolman and Brush, 1961; Xu, 2002); and 2) the majority of pre-vegetation alluvial sandstones have very high aspect ratios and lack distinct channel margins (e.g., Fedo and Cooper, 1990; Nicholson, 1993; Hjellbakk, 1997; Els, 1998; Mueller and

Corcoran, 1998; Long, 2004). The latter of these observations does not imply that all pre-vegetation rivers were broad and shallow. In the absence of vegetation, there were fewer mechanisms which may have provided sufficient bank stability to restrict lateral channel migration. Consequently, mobile channel networks with noncohesive sediment likely produced tabular sandstone units far wider than their original channel dimensions (Gibling, 2006; Wang et al., 2011). Any inferences of channel geometry based on successions dominantly comprising 'sheet-braided' architectures should therefore be made with great caution.

4.4. Chapter summary

Chapter 4 presents the findings of fieldwork-based analyses of two pre-vegetation alluvial formations interpreted as having been deposited by perennially flowing rivers: 1) the Neoproterozoic Torridon Group, Scotland (the main field site of the thesis (Section 2.1.1)); and 2) the Neoproterozoic Jacobsville Sandstone, Michigan, USA.

With a total stratigraphic thickness in excess of 4500 km, alluvium comprises the vast majority of preserved Torridon Group Stratigraphy. Combined facies, architectural and palaeocurrent analysis strongly suggest deposition by a large, low-sinuosity braided river system. Three architectural units are defined and interpreted: 1) Erosionally based cross-stratified sheets (c. 80%); 2) Inclined accretionary strata (c. 20%); and 3) Discontinuous mudstone to very-fine grained sandstone units (<<1%). Erosionally-based cross-stratified sheets regularly contain coarser-grained lags and mudstone rip-up clasts. Trough-cross stratification dominates, with dipping foresets displaying a consistent south-east directed transport direction. Soft-sediment deformation affects slightly over half of the sand-bodies, and becomes increasingly abundant up-section in tandem with a gradual decrease in modal grain size (pebbly-sandstone to medium-grained sandstone). These sedimentary bodies are analogous to modern sediments deposited in channel thalwegs during active flow, and are hence interpreted as channel-fill units. Inclined accretionary strata, distinguished from channel-fill units by the presence of multiple cosets of cross-stratification each genetically related to a common underlying bounding surface (i.e., an accretion surface), can be compared to modern barform units. Such barform units overly channel-fill units whenever identified. Their scarce preservation, in comparison to channel-fill units, reflects autogenic reorganisation of the Torridon fluvial system. Frequent lateral channel migration (and/or channel combing) results in barform (and out-of-channel material) reworking, resulting in the longer-term aggradation of several generations of channel-fill units. In the instances where barform units do succeed channel-fill sequences, these units likely escaped reworking due to a shift in the location of the main trunk channel, or possibly avulsion of the entire braidplain. The lack of systematic trends throughout the succession suggests cycles in accommodation space were not the dominant control on preserved sedimentary architecture. Instead, autogenic dynamics and self-organization appear to have determined preservation. Low palaeocurrent dispersion (mean = 127º, n = 2333, S = 45.7) is consistent with a low-sinuosity system. Combined with observations of: 1) coarse bedload material; 2) predominantly downstream accreting in-channel barforms; 3) a lack of preserved out-of-channel material; and 4) a lack of identifiable channel-margins, a braided river system depositional model is preferred. The incremental character of barform deposits (when preserved) suggests flow was perennial.

In addition to the detailed analysis of the Torridon Group, a short case study of the Neoproterozoic Jacobsville Sandstone is presented to illustrate the potential range of river scales which may become interred into the pre-vegetation alluvial record. Fully preserved (downstream-dipping) barform units imply modal water depths of less than 1 metre. Despite depositing rivers wholly different in character, a common characteristic of both Torridon Group alluvium and the Jacobsville Sandstone is that their constituent sand-bodies are predominantly "sheet-braided" (see Section 7.2.2).

Chapter 5

PRE-VEGETATION ALLUVIUM DEPOSITED BY EPHEMERAL RIVERS

This chapter presents a sedimentological analysis of the Torridonian's constituent Meall Dearg Formation (late Mesoproterozoic), recognizing a dominance of alluvial facies, with subordinate aeolian facies. Alluvial strata within the Meall Dearg Formation contain direct evidence for event deposition by high-energy ephemeral floods, including the following: (1) widespread upper and transitional upper flow regime elements; (2) frequent stacking of successively lower flow regime elements; (3) common subcritical subaqueous dune fields with superimposed ripple marks; (4) occasional thin, desiccated mudstones; and (5) evidence that microbial mats colonized substrates during intervals of sedimentary stasis. Together these strands of primary sedimentary geological evidence indicate that the alluvial deposition of the Meall Dearg Formation was typified by supercritical flows during high-energy ephemeral floods, punctuated by prolonged intervals of sedimentary stasis. The preservation potential of all of the features was boosted by highly aggradational sedimentary conditions.

5.1. Introduction – The Mesoproterozoic Meall Dearg Formation

This chapter contributes new data to the global pool of studies concerning ephemeral pre-vegetation rivers, through an original sedimentological analysis of the least-studied constituent unit of the Torridonian Sandstone: the Mesoproterozoic Meall Dearg Formation (MDF) (Section 2.1.1, Fig. 2.1, Fig. 5.1). Considering the long history of geological investigations into the region, and the number of studies that have focused on the more well-known alluvial formations of the Torridonian (e.g., the Applecross (Selley, 1965; Nicholson, 1993; Owen, 1995; Stewart, 2002; Owen and Santos, 2014; Ielpi and Ghinassi, 2015; Santos and Owen, 2016) and Bay of Stoer (Stewart, 1990, 2002; Ielpi et al., 2016) formations)), the MDF has remained largely overlooked.

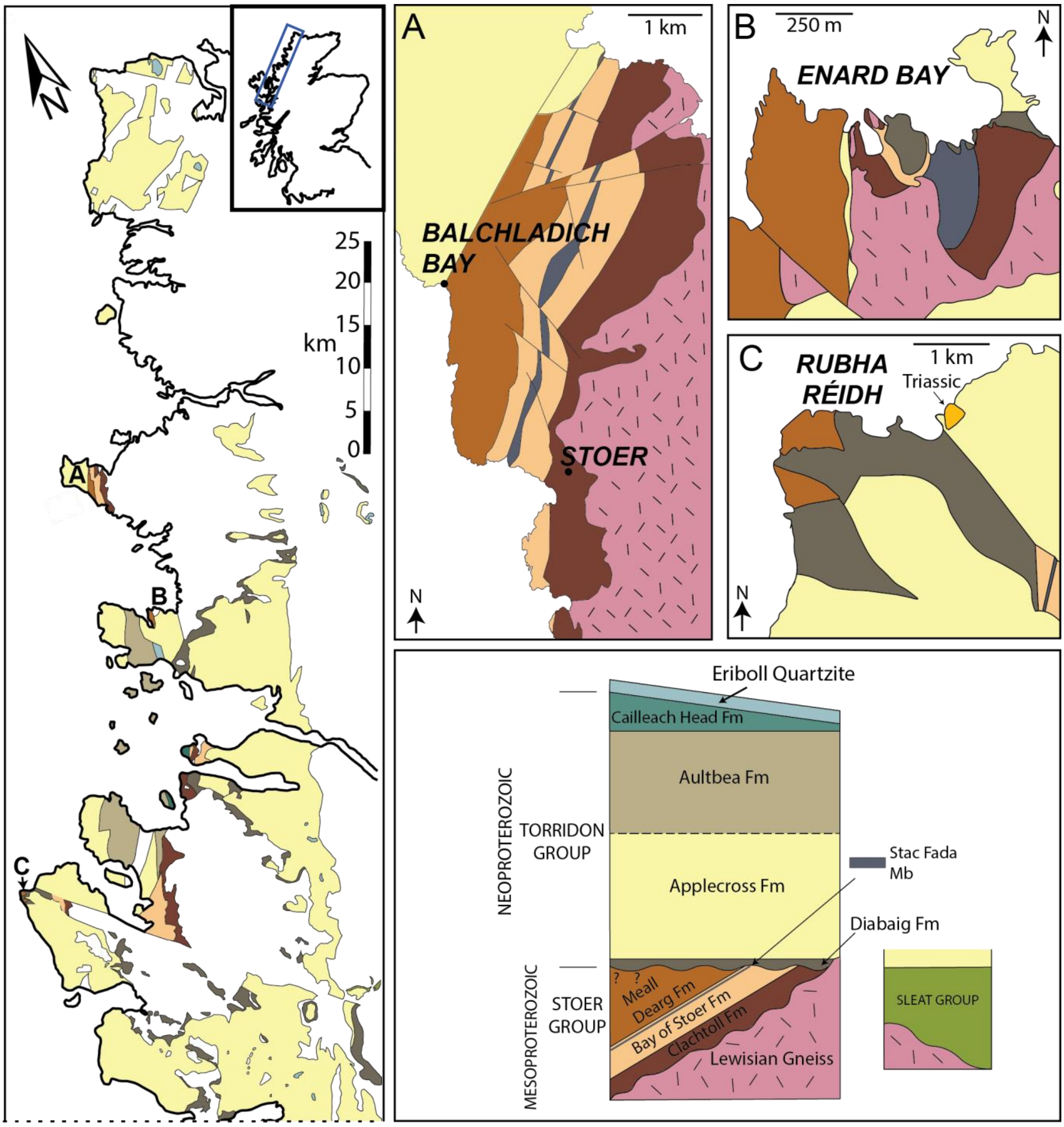

Figure 5.1. Left: Geological map of the Torridonian outcrop belt (modified after Stewart, 2002). Letters mark the studied areas of the Meall Dearg Formation. Right top: Higher resolution maps of Meall Dearg Formation locations of study. Letters in top left corner of each map refer to the regional geological map. Bottom right: Key of geological units.

This chapter discusses: (1) the architectural characteristics of the constituent sand-bodies of the MDF; (2) the spatial distribution of stratification types in accordance with established flow regime models; (3) the variety of preserved bedding plane features within the MDF; and (4) recurring facies that record prevailing sedimentary processes. These observations permit the interpretation of the MDF as recording distinct signatures of dominant high-energy alluvial event (and subordinate aeolian) sedimentation, owing to exceptional aggradational conditions.

5.2. Stratigraphic and geological context

The Torridonian Sandstones comprise, from oldest to youngest, the Stoer, Sleat and Torridon groups (Fig. 2.1), of which the MDF is the youngest constituent formation of the >2000 m thick Stoer Group. The MDF succeeds the Bay of Stoer Formation and is unconformably overlain by the lacustrine Diabaig Formation of the Torridon Group. The Bay of Stoer Formation consists of dominantly fluvial, and subordinate interpreted aeolian (Park et al., 2002; Ielpi et al., 2016) sandstones. Specifically, the MDF succeeds the shallow lacustrine/tidally influenced Poll a'Mhuilt Member of the Bay of Stoer Formation, apparently conformably (Stewart, 2002; Stueeken et al., 2017). Lithostratigraphic correlation between the scattered outcrops of the MDF is permitted by their common stratigraphic position above the Stac Fada Member of the upper Bay of Stoer Formation, which comprises a regionally extensive event bed of either meteorite-impact ejecta (Amor et al., 2008; Simms, 2015) or volcanic origin (Lawson, 1972; Stewart, 2002). However, the possibility remains that the units at each locality are not necessarily time equivalents, particularly as individual exposure areas of the unit (as mapped) do not always stratigraphically extend to the Stac Fada Member due to drift cover or local faulting. The MDF has not been directly dated, but its age is stratigraphically bracketed between 1177 ± 5 Ma (Stenian Period of the Mesoproterozoic) and 977 ±39 Ma (Tonian Period of the Neoproterozoic), based on 40Ar/39Ar dating of the underlying Stac Fada Member and Rb–Sr whole-rock regressions of the overlying Diabaig Formation (Turnbull et al., 1996; Parnell et al., 2011). This age indicates that the MDF was deposited during the Grenvillian Orogeny, along the margins of the supercontinent Rodinia (Rainbird et al., 2012). This deposition on the edge of the Laurentian Shield meant that it largely avoided later Caledonian deformation (Williams and Foden, 2011).

The MDF is interpreted to have been deposited in a narrow rift basin with detritus sourced from local fault scarps (Stewart 1982, 1990; Rainbird et al., 2001). Palaeomagnetic (Torsvik and Sturt, 1987) and geochemical (Stewart, 1990) data suggest that deposition occurred in a semi-arid climate at a palaeolatitude of 10 – 20°N.

5.3. Sedimentology of the Meall Dearg Formation

5.3.1. Facies associations

Two facies associations (FA) are recognized in strata of the MDF (Fig. 5.2). The facies associations are mutually exclusive, with FA1 cropping out at Rubha Réidh, Balchladich Bay and Stoer and FA2 at Enard Bay.

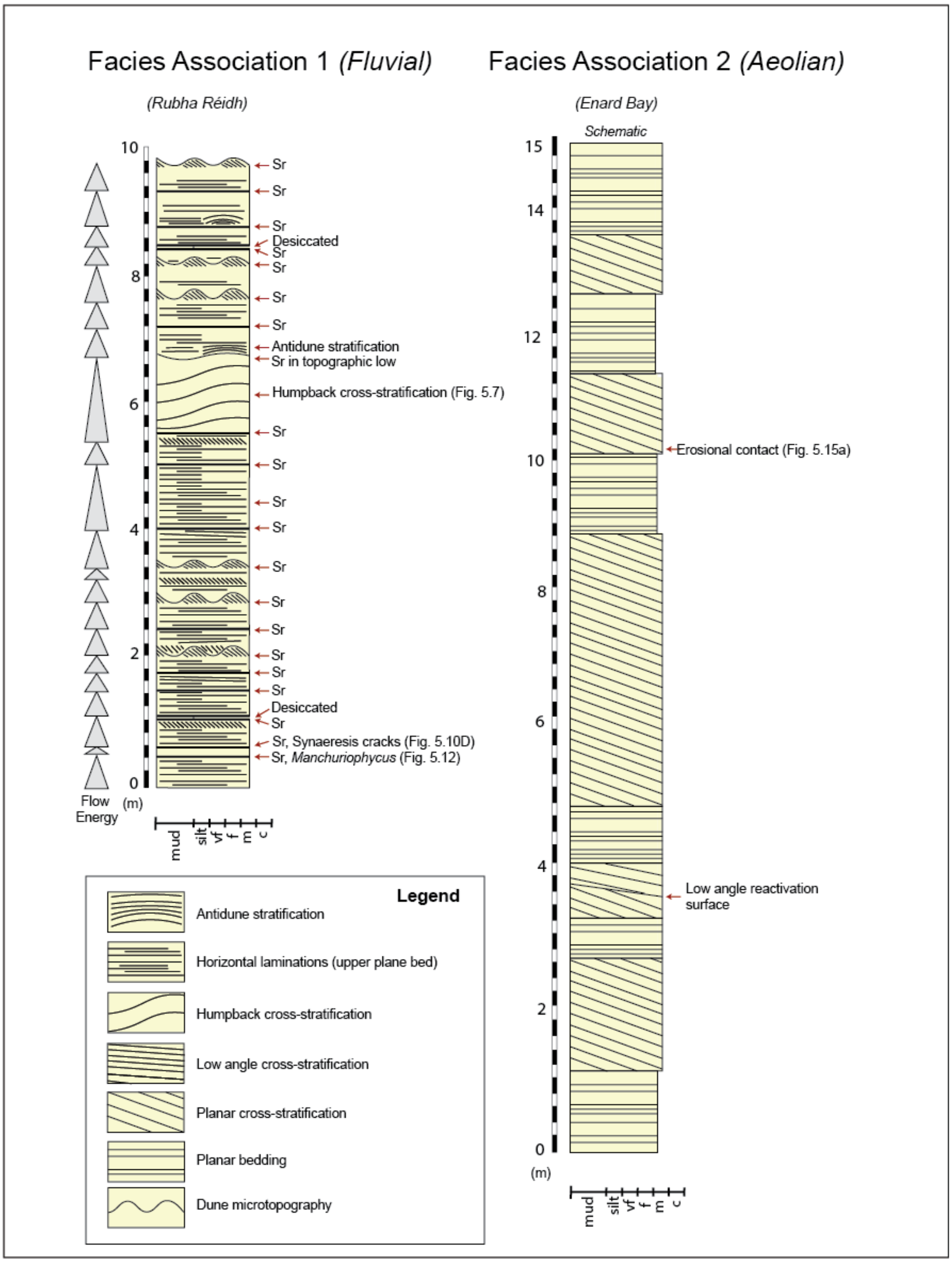

Figure 5.2. Representative stratigraphic logs of Facies Association 1 and 2. Sr, ripple marks

5.3.1.1. Facies Association 1 (Rubha Réidh, Balchladich Bay and Stoer)

Strata of FA1 form the majority of the exposed MDF, and all of the facies at Rubha Réidh, Balchladich Bay and Stoer. The contiguous Stoer–Balchladich Bay section is 200 – 300 m thick, and is underlain by the Bay of Stoer Formation and unconformably overlain by the Applecross Formation. At Rubha Réidh, the succession is truncated to 100 m thickness, with a faulted lower contact, and is unconformably overlain by the Diabaig Formation (Stewart 2002). FA1 consists nearly entirely of sandstone (>99% of total strata). Mudstones (<1%) are restricted to millimetre-thick, often desiccated, laterally discontinuous layers or intraformational mud clasts. Sandstones are medium-grained, with the exception of the lowest 7 m of stratigraphy at Stoer, where pebbly sandstones occur. Lower bounding surfaces either are flat (Fig. 5.3B), or drape and preserve an underlying dune topography (Fig. 5.3C). Erosion between sand-bodies is restricted to localized scours, no more than 50 cm deep. Various stratification types and bedding plane features are present (Table 5.1). Three-dimensional outcrops permit the identification of both foreset and backset (cross-stratification dipping up local palaeoflow) stratification and foreset dips indicate that palaeoflow was towards 279° (n = 41, S = 32.4). The description and interpretation of each stratification type and bedding plane feature are as follows.

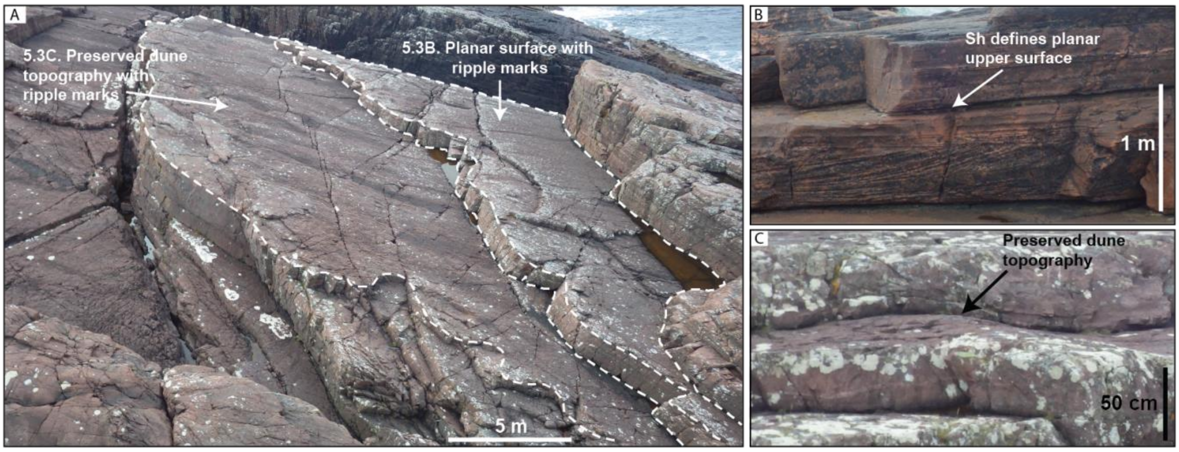

Figure 5.3. A) Planform surfaces of the Meall Dearg Formation at Rubha Réidh. The microtopography of the surface is dictated by the underlying lithofacies. If horizontal laminae (Sh) form the topmost lithofacies of the underlying sand-body, topography is flat (B). If dune cross-stratification forms the topmost lithofacies of the underlying sand-body, dune microtopography is preserved (C). Each planform surface is near ubiquitously covered in ripple marks.

Table 5.1. Stratification types and bedding plane features observed in the Meall Dearg Formation at each location of study. The table does ont give any indication of abundance.

Location	Stoer	Rubha Réidh	Bachladich Bay	Enard Bay
Facies association	FA1	FA1	FA1	FA2
Exposure type	Vertical Cliffs	Wave-cut platforms	Wave-cut platforms	Wave-cut platforms
Horizontal laminae	Y	Y	Y	
Antidune stratification		Y	Y	
Chute & pool structures	Y	Y		
Humpback cross-stratification		Y		
Low angle cross-stratification	Y	Y	Y	
Planar cross-stratification	Y	Y	Y	Y
Trough cross-stratification	Y			
Ripple marks	Y	Y	Y	Y
Adhesion marks	Y	Y	Y	Y
Manchuriophycus		Y		
Reticulate marks		Y		
Planar bedding				Y

5.3.1.1a. Sandstone stratification types

Stratification types in this section are documented in order of progressively decreasing associated flow strength.

1) Backset laminae associated with an upstream-dipping scour surface (chute and pool structures).

Asymmetric scoured surfaces, filled by upstream-inclined cross laminae, are present at Rubha Réidh and Stoer (Fig. 5.4). Backsets truncate against steep, downstream-dipping scoured margins, and are succeeded vertically by horizontal laminae and convex-up bedding. At Stoer, convex-up bedding passes down-flow into horizontal laminae with soft-sediment deformation structures (Fig. 5.4B).

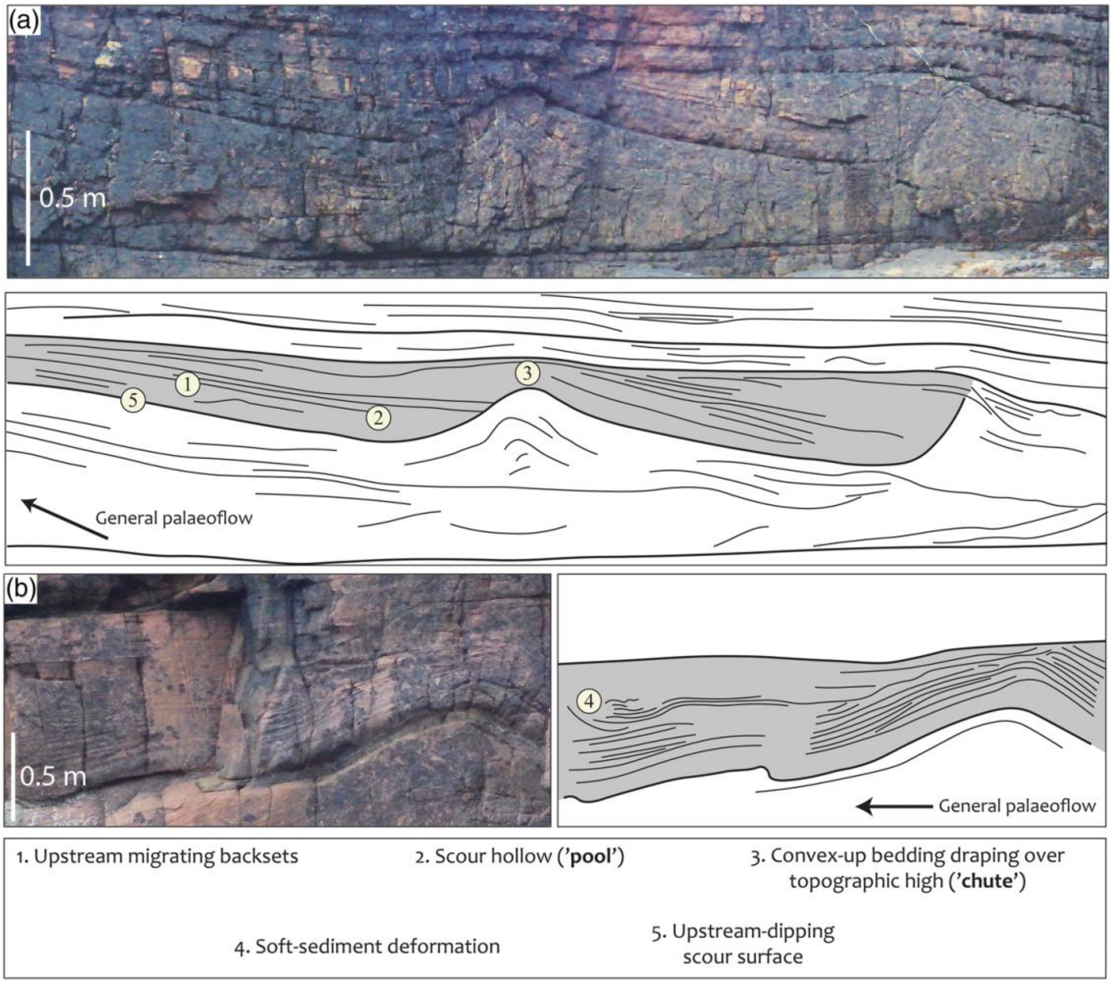

Figure 5.4. Possible chute and pool structures at (A) Rubha Réidh and (B) Stoer (inaccessible cliff exposure). Upstream-dipping bedding truncates against the steeper, down-flow dipping surfaces ('Pool'). Convex-up bedding passes over topographic high ('Chute').

Comparable features are rarely reported from the rock record (Fralick, 1999; Fielding, 2006; Lowe and Arnott, 2016; Winston, 2016), but are analogous to chute and pool structures formed in laboratory experiments (Alexander et al., 2001; Cartigny et al., 2014). Chute and pool structures form as a result of a temporary hydraulic jump within a localized scour when shallow, faster flowing waters (the chute) pass immediately into deeper, slower flowing waters (the pool) (Fielding, 2006). Their relationship with juxtaposed bedforms in the MDF indicate that the pools were filled prior to flow waning to regimes associated with the deposition of antidune stratification and horizontal laminae. High-velocity and turbulent flow conditions account for the association of chute and pool structures with soft-sediment deformation.

2) Convex-up bedding containing backset cross-laminae (antidunes).

Convex-up bedding is occasionally associated with otherwise horizontal beds (Fig. 5.5). Convex-up beds are low-relief (20 – 25 cm), symmetrical and internally characterized by cross-laminae that dip upstream (compared with palaeocurrents from nearby dune cross-stratification). They are solitary and do not form larger concavo-convex sets. Widths of convex-up portions range from 200 to 225 cm.

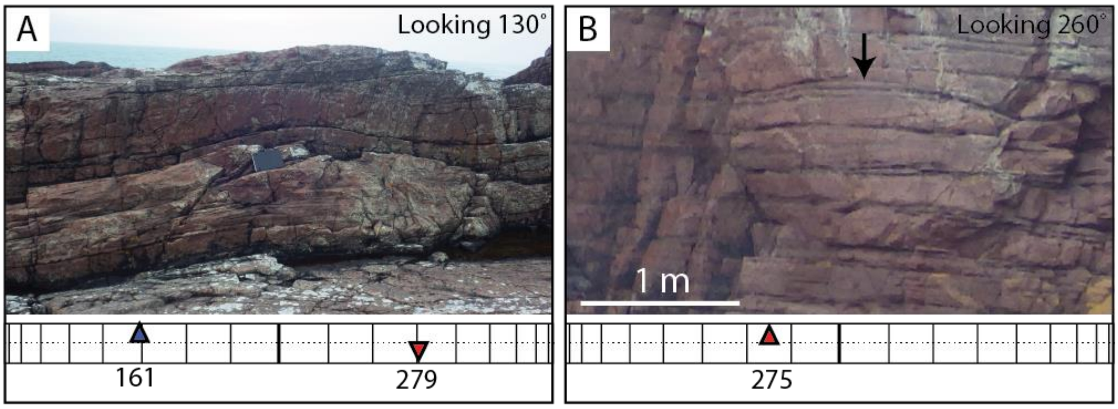

Figure 5.5. A) Solitary antidune stratification, with backset cross-bedding dipping against prevailing palaeoflow. Red arrowhead indicates local palaeoflow. Blue arrowhead indicates upstream-directed outbuilding of antidune stratification; B) convex-up bedding possibly representative of antidune stratification. Red arrowhead highlights local palaeoflow. Both images from Rubha Réidh.

Symmetrical, convex-up beds with internal upflow-dipping cross-laminae suggest that they formed in the antidune stability field (e.g., Fielding, 2006; Cartigny et al., 2014). Antidune stratification has been produced in experimental flows underneath transient standing waves (e.g., Kennedy, 1963; Alexander et al., 2001), suggesting that standing waves developed in supercritical flow conditions during the deposition of the MDF. Their comparative scarcity compared with horizontal laminae (see below) reflects the transient nature of such flow conditions and the relatively low preservation potential of antidune stratification. Additionally, confident diagnosis of antidune stratification requires full preservation of the bedform under aggrading sedimentation (Cartigny et al., 2014), meaning that the number of identifiable antidune deposits in the MDF is probably an under-representation of their true abundance.

3) Horizontal laminae (upper plane bed).

Horizontal laminae constitute the basal parts of the majority of FA1 sand-bodies (>95%) (Fig. 5.6). Thin (<4 mm), ungraded laminae occur in sets 5 – 110 cm thick. Sets are tabular in depositional-dip and -strike sections. Underlying bounding surfaces are flat and exhibit no evidence of incision into the underlying bed (at outcrop scale). In large depositional-dip outcrops, horizontal laminae occasionally show a lateral transition to low-angle, down-flow dipping cross-stratification (see below).

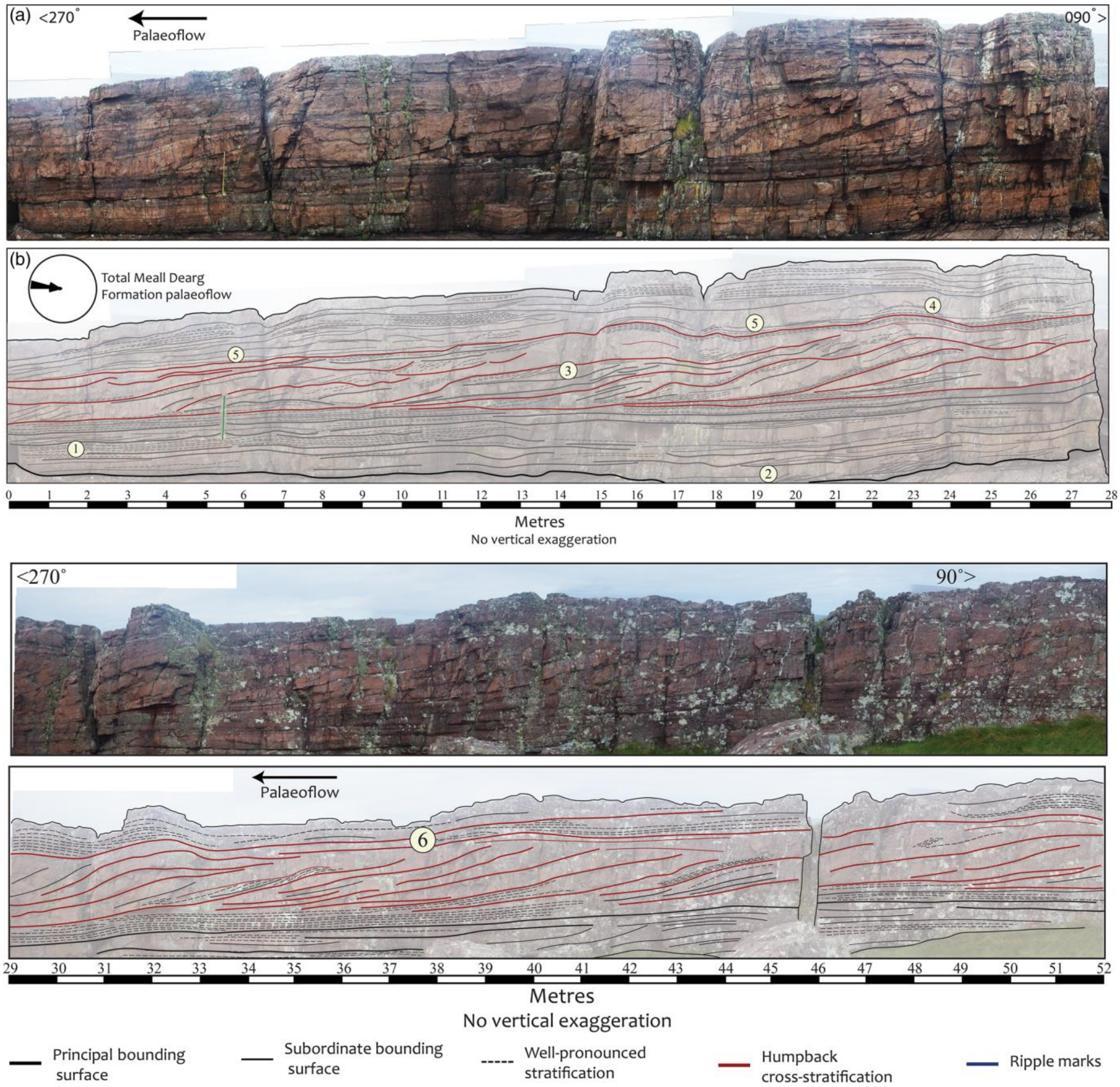

Figure 5.6. Architectural panel of Meall Dearg outcrop (Rubha Réidh)

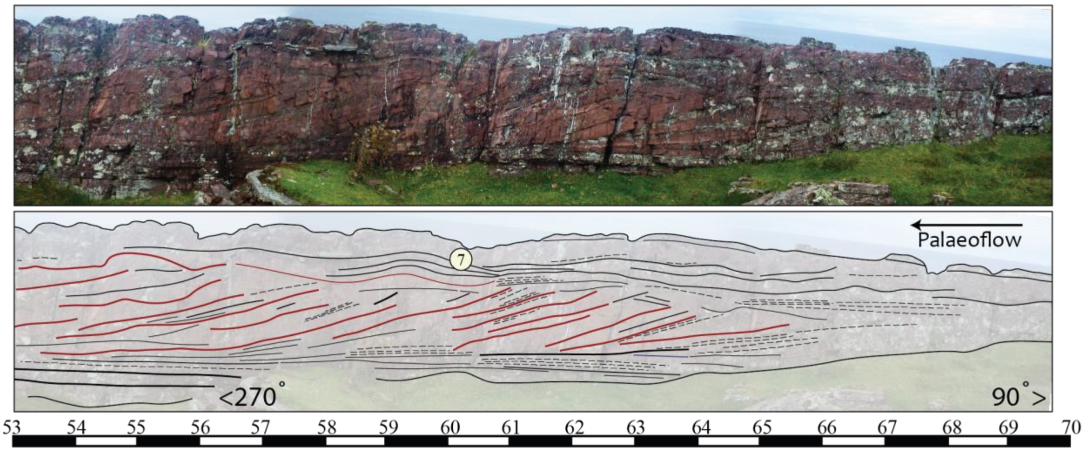

Figure 5.6. *(continued)*

Horizontal laminae record upper flow regime plane bedding (Paola et al., 1989). Upward transitions from upper to transitional upper flow regime sedimentary structures are interpreted as the product of waning floods. Similarly, down depositional-dip transitions from horizontal laminae to low-angle cross-stratification represent lateral decreases in flow strength (upper to transitional upper flow regime) (Fielding, 2006).

4) Asymmetrical sigmoidal sets of cross-stratification (humpback dunes).

Cross-stratification exhibiting a downflow-divergent sigmoidal geometry is present in multiple sand-bodies at Rubha Réidh (Figs 5.6 and 5.7A). The sigmoidal geometry permits the differentiation of discrete topset, foreset and bottomset elements. Convex-up bed topography is apparent at the top of each set (Fig. 5.7A), a stratification type referred to as humpback cross-stratification (Saunderson and Lockett, 1983; Fielding, 2006). Sets are up to 2.2 m high and can be traced down depositional-dip for >65 m (Fig. 5.6). Ripple marks are frequently preserved in topographic lows associated with preserved convex-up topography (Fig. 5.6). In 3D sections, it is clear that humpback sets comprise wedge-shaped packages that built out in a westwards direction (Fig. 5.7B).

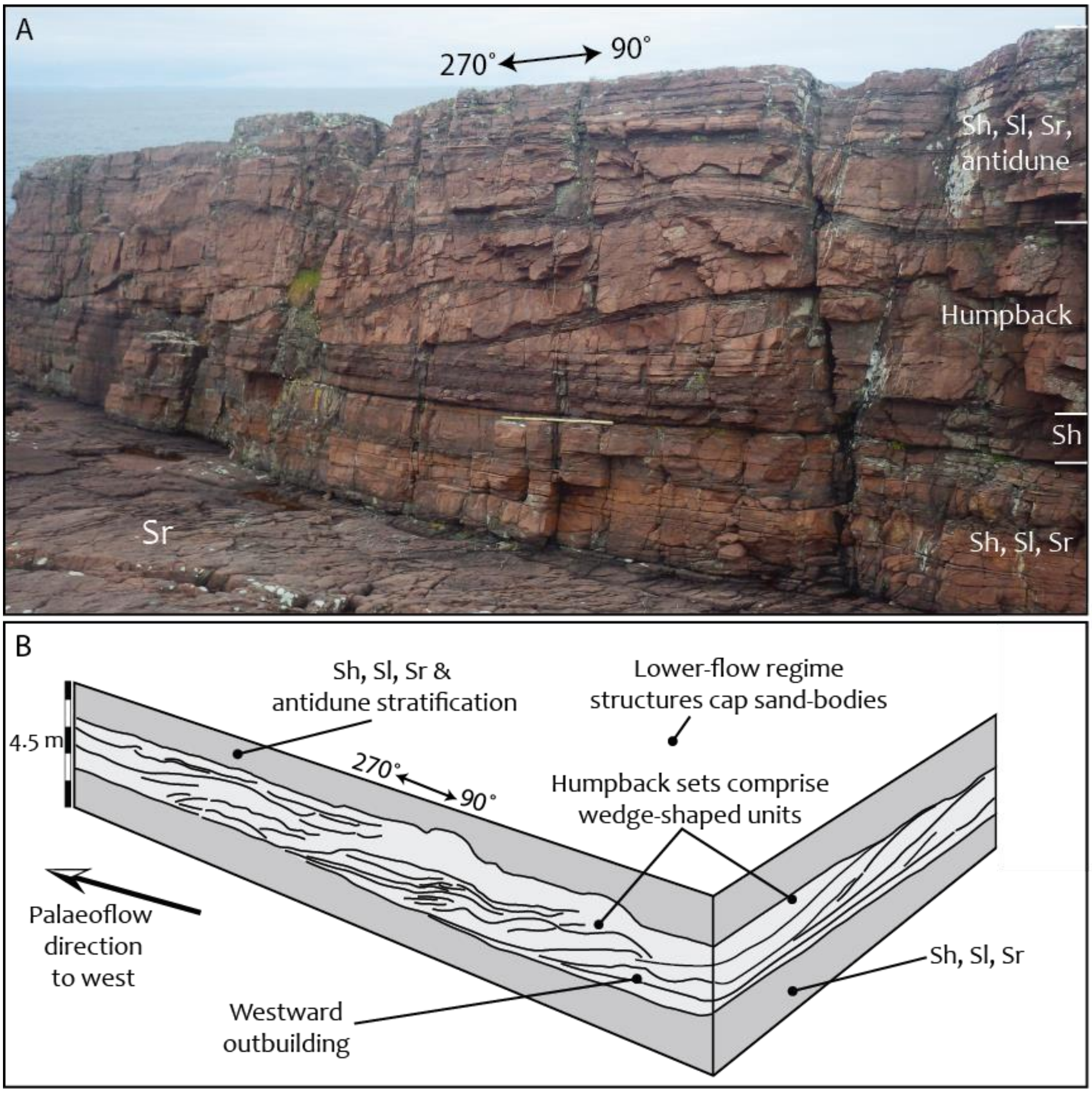

Figure 5.7. A) Humpback cross-stratification at Rubha Réidh; B) Line drawing of exposure in (A). 3D exposure illustrates the westward outbuilding of wedge-shaped humpback cross-stratified packages. Sh, horizontal laminae; Sl, Low-angle cross-stratification; Sr, ripple marks.

Humpback ‘form-sets’ develop when deposition dominates over erosion at flow conditions transitional between the dune stability field and the upper plane bed field (Saunderson and Lockett, 1983). Convex-up bed topography at the top of each set implies that the bedforms are fully preserved (‘form-sets’) (Reesink et al., 2015).

5) Low-angle (<20°) cross-stratification (transitional upper flow regime dunes).

Low angle cross-stratification occurs throughout the MDF (Fig. 5.8A). Foreset dip angles range from 5° to 15°. In depositional-dip sections, low-angle foresets occasionally merge into horizontal laminae up-flow.

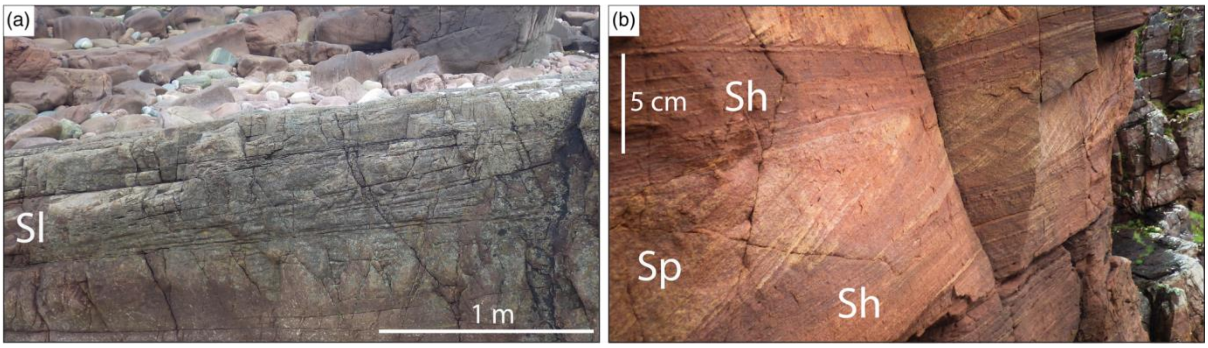

Figure 5.8. A) Low-angle cross-stratification at Balchladich Bay (Sl); B) alternating sets of horizontal-laminated (Sh) and planar cross-stratified (Sp) sandstones at Stoer.

Low-angle cross-stratification develops at flow conditions transitional between dune stability field and upper plane bed stability (Fielding 2006). Lateral transitions between horizontal laminae and low-angle cross-stratification reflect localized variations in flow energy.

6) High-angle (>20°) cross-stratification (lower flow regime dunes).

Planar cross-stratification occurs in solitary sets of 10 – 30 cm thickness. Cosets of planar cross-stratification do not occur; instead, sets are intercalated with sedimentary structures associated with upper flow regime flows (most abundantly horizontal laminae) (Fig. 5.8B). Sets are highly tabular and show minimal lateral thickness changes in both depositional-dip and depositional-strike sections. Trough cross-stratification was observed only at the base of the formation at Stoer (coincident with the only pebbly interval observed in the MDF).

At Rubha Réidh, in instances where cross-bedded units occur at the top of a major sand-body, dune topography is preserved (Fig 5.2, Fig. 5.3A, Fig. 5.9A). Dunes are spaced 0.5 – 1.5 m apart and have heights of 10 – 30 cm. Abundant ripple marks are superimposed onto the dune microtopography (see Section 5.3.1.1b).

The migration of lower flow regime 2D and 3D subaqueous dunes produces planar and trough cross-beds respectively. The existence of tabular sets with minimal lateral variation in relief implies that flow depths were consistent across large areas. Cosets of high-angle cross-stratification are entirely absent, with cross-stratification most commonly occurring between upper flow regime sedimentary structures, suggesting that their deposition relates to waning high-energy floods.

5.3.1.1b. Bedding plane features

In the MDF, ripple marks and other sedimentary surface textures are common on some bedding surfaces, which record the preservation of primary substrates. Sedimentary surface textures exhibit a wide variety of morphologies, owing to their formation on substrates that persisted for variable intervals of sedimentary stasis (Davies et al., 2017b). This morphological variability may hamper the determination of whether the textures had a microbial or abiotic origin, so in this section they are classified following the technique described by Davies et al. (2016): Category A structures are demonstrably abiotic in origin; Category Ba is used where circumstantial evidence suggests that structures may be biotic, but an abiotic origin cannot be ruled out; Category Ab is used for the opposite situation to this; Category ab is used where there is no clear evidence to support abiotic or biotic origin. This descriptive approach brings certain inferred microbially induced sedimentary structures (MISS) firmly back into the fold of geological agnosticism. Its scientific merit lies in the fact that it leaves open the possibility of multiple explanations, biogenic or abiotic (or both), until one or the other can be corroborated assuredly through other lines of investigation.

1) Ripple marks (A).

Symmetrical ripple marks are nearly ubiquitous on each studied planform surface (n = 12) at Rubha Réidh, Balchladich Bay and Stoer (Fig. 5.9). The largest of these exposed surfaces has an area of >1000 m^2. Ripple marks are frequently seen superimposed on top of dune topography, where they have weakly anastomosing sinuous crests that rarely extend >2 m (Fig. 5.9A). On flat surfaces that lack dune microtopography, crests are subparallel and extend for >10 m (Fig. 5.9B). Ripple marks record unidirectional flow on individual bedding planes, but a near 360° dispersal is apparent when all rippled surfaces are considered (Fig. 5.9B). The modal east–west strike-line is perpendicular to the prevailing westward flow ($\theta = 279°$; n = 41). Many ripple marks have clear drainage lines etched into their flanks, indicating emergence and drainage subsequent to their formation (Fig. 5.10A-B). Crests are mostly well-rounded or flat-topped. Sharp crested ripple marks are rare (Fig. 5.10C) and contain synaeresis cracks within their troughs (Fig. 5.10D). Infrequent interference ripple marks occur (Fig. 5.10E). Ripple marks located within dune troughs are often draped by mud (Fig. 5.10F). In addition to planform exposures of ripple marks, trains of ripple crests can be observed within vertical sections (Figs 5.6, Fig. 5.10G). Above humpback dunes, sharp crested ripple marks are present in dune troughs and form ripple trains that extend laterally for up to 4 m (Fig. 5.6). In rare instances ripple crests display uneven oversteepening (Fig. 5.10H).

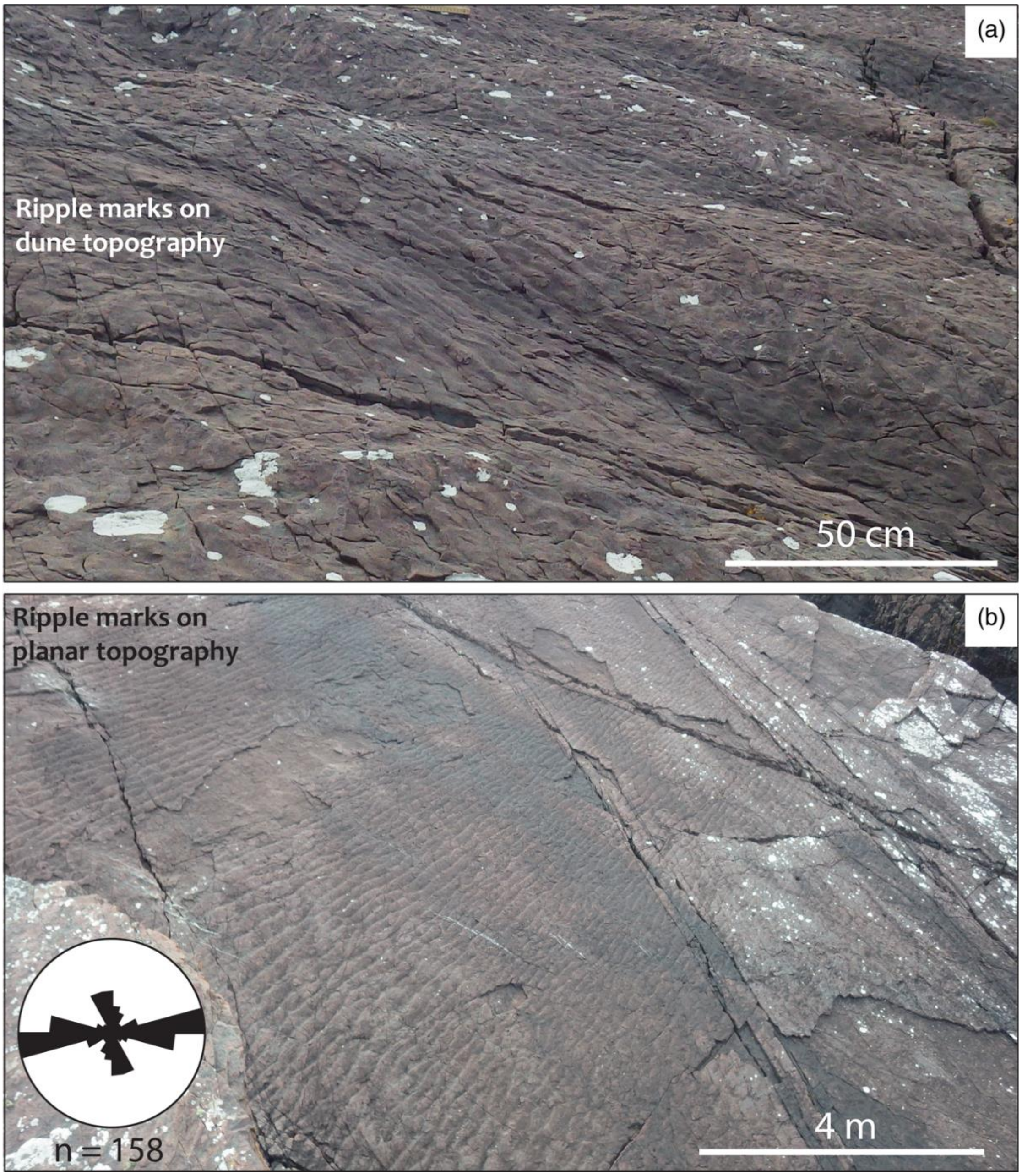

Figure 5.9. A) Ripple marks superimposed onto dune topography; B) planar surface with ripple marks

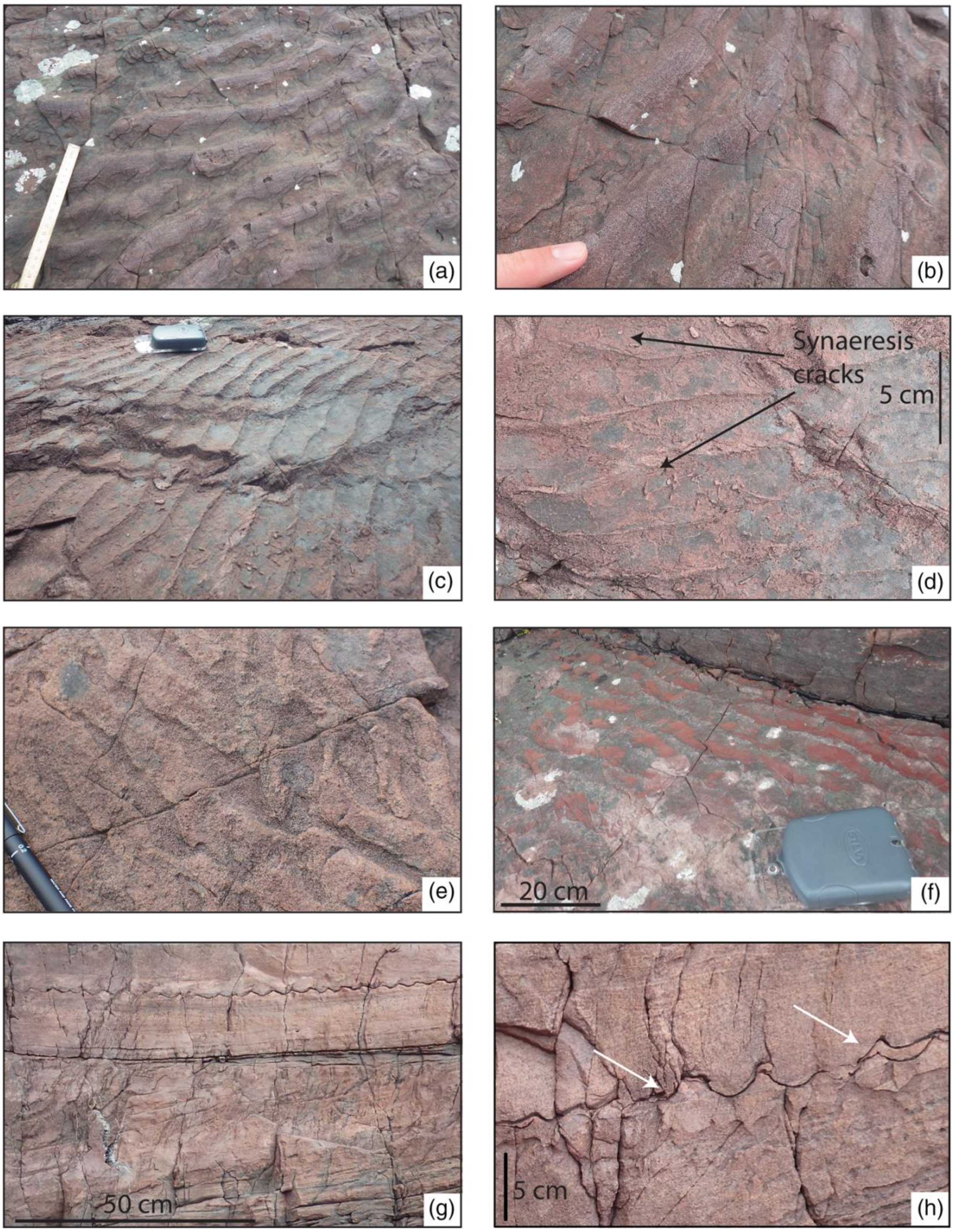

Figure 5.10. Morphology of preserved ripple marks: A) Sinuous-crested ripple marks with etched drainage marks; B) drainage marks etched in flanks of ripple marks; C) sharp crested ripple crests; D) synaeresis cracks in ripple troughs; E) interference ripple marks; F) mud-draped ripple marks; G) ripple marks preserved within vertical section; H) oversteepened ripple marks. All photographs from Rubha Réidh.

Symmetrical ripple marks record bedform stability under low flow regime, representing falling flood stage. Their near-ubiquitous positioning above sand-bodies that contain upper and transitional upper flow regime sedimentary structures suggests that flood waters receded to leave pools of standing water across the depositional plain. Their comparatively greater abundance within humpback dune troughs (compared with crests) lends further credence to this notion, suggesting more pervasive pooling of water within pre-existing topographic lows. Variations in ripple-crest strike-line suggest that this ponded water drained and moved in different directions, depending on localized slope and wind conditions. Soft-sediment deformation of some ripple crests may have been caused by current drag over the rippled surface during subsequent flooding events. Alternatively, the oversteepening may be seismically induced.

2) Adhesion marks (A).

Adhesion marks are frequently seen to be superimposed upon ripple-marked surfaces (Fig. 5.11). They occur as 2 – 5 mm wide, 1 – 3 mm high positive epirelief mounds that are irregular in form (i.e., adhesion marks and not adhesion ripples; Kocurek and Fielder, 1982). Their spatial distribution across any given bedding surface is strongly dependent on the associated dune and ripple microtopography (Fig. 5.11). On dune crests (topographic highs), ripple marks are densely blanketed by adhesion marks across their crests and troughs (Fig. 5.11A). Within dune troughs (topographic lows), adhesion marks are only ever restricted to ripple crests, or are absent entirely (Fig. 5.11B). On flat beds lacking dune microtopography, adhesion marks occur on both ripple crests and troughs, but are more common on the former (Fig. 5.11C).

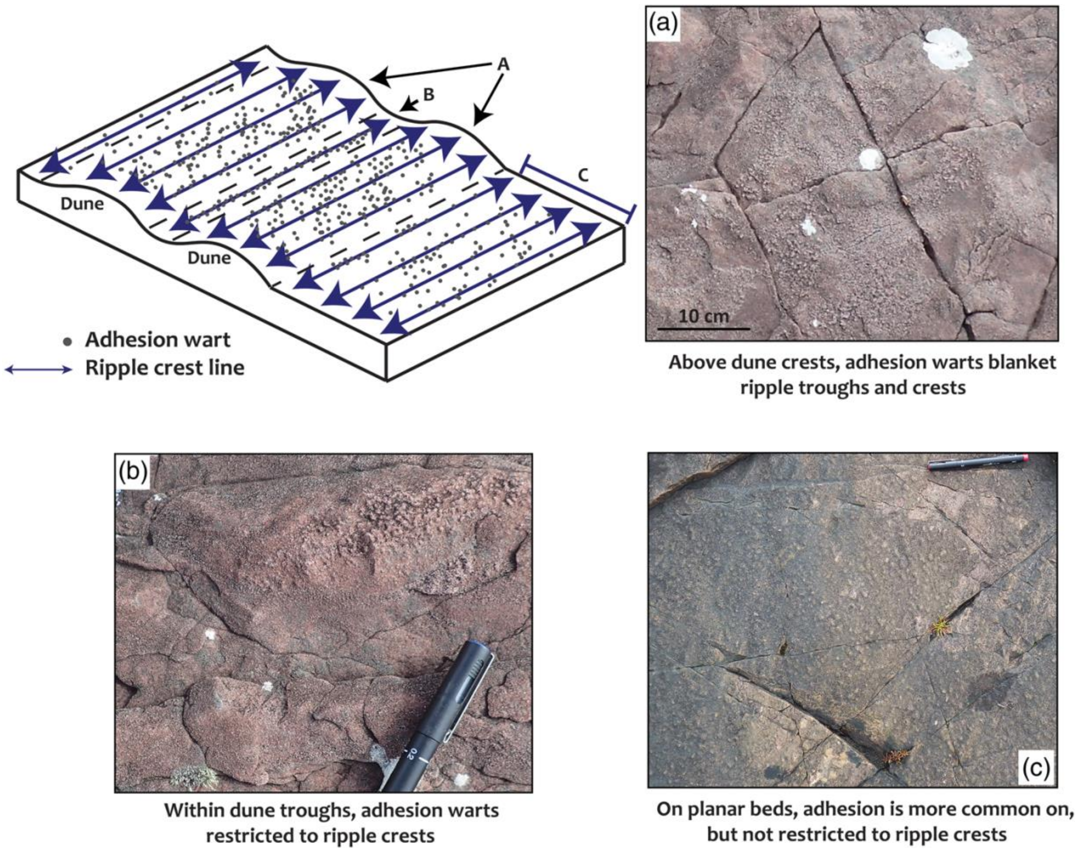

Figure 5.11. Schematic illustration and photographs of adhesion mark distribution across Meall Dearg fluvial facies

Adhesion marks indicate that water-lain sands were intermittently subaerially exposed, permitting the accretion of wind-blown sand grains onto moist substrates (Kocurek and Fielder, 1982). Adhesion marks are progressively more common with height above the surface (i.e., most common on ripple crests on dune crests; least common in ripple troughs in dune troughs), indicating that they can be used to locally determine how extensive the recession of pooled water was between flood events. The total absence of adhesion marks in some dune troughs suggests that, in some instances, no subaerial exposure occurred and that pooled water persisted until the subsequent flood event (Fig. 5.11A-C).

3) Sinuous shrinkage cracks (Manchuriophycus) (Ba).

Sinuous shrinkage cracks were observed at one ripple-marked surface at Rubha Réidh. Cracks are up to 1 cm wide and 25 cm long. They most commonly occur within, and parallel to, ripple troughs, but single cracks may also cross ripple crests (Fig. 5.12). They are preserved in positive epirelief, although post-depositional erosion often results in accompanying negative epirelief impressions.

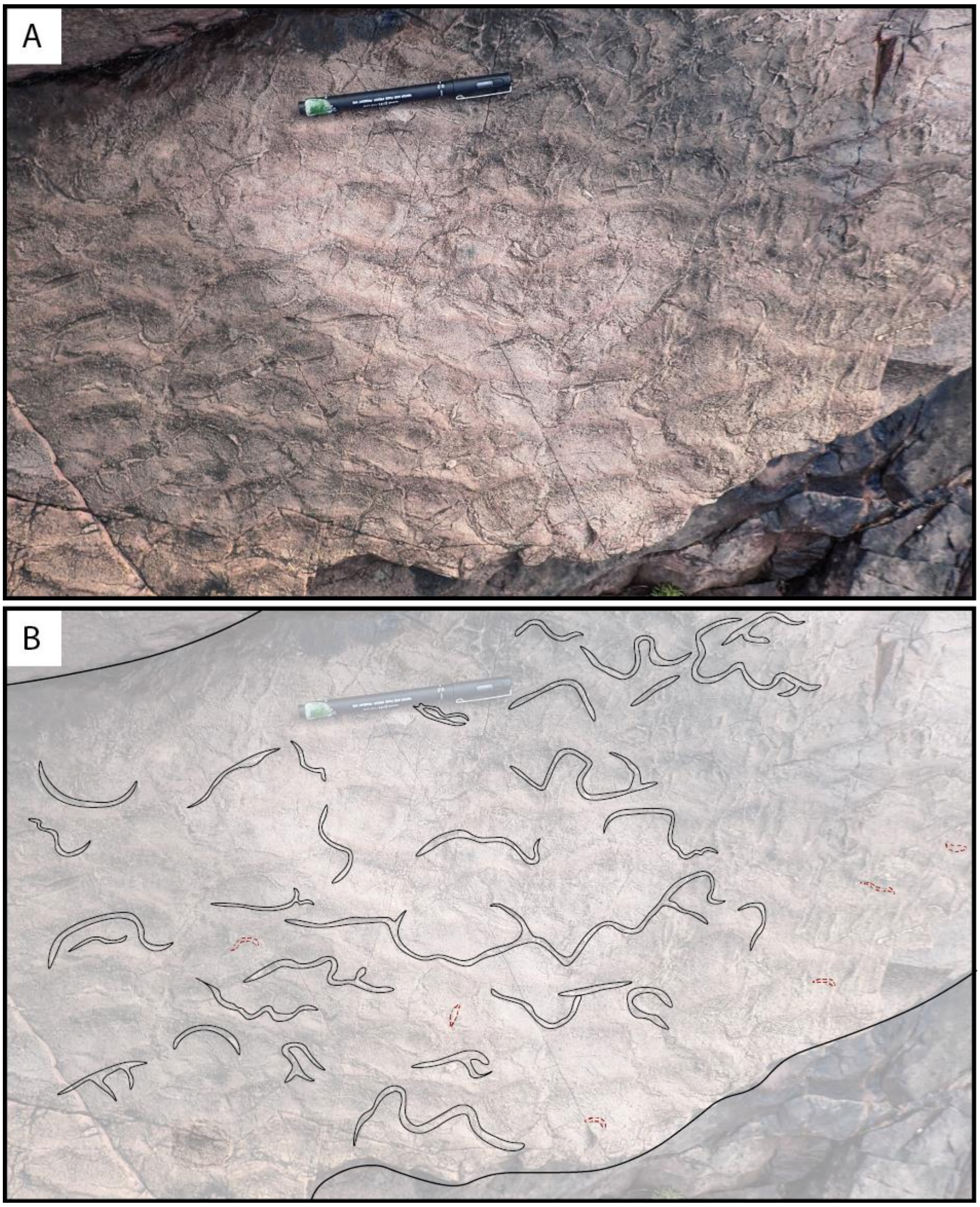

Figure 5.12. A) Examples of *Manchuriophycus* at Rubha Réidh. B) Line drawings of *Manchuriophycus* in (A). Fragments of possible 'Manchuriophycus' dashed and highlighted in red.

The sinuous shrinkage cracks fit the type description of the 'pseudofossil' *Manchuriophycus* (Endo, 1933). *Manchuriophycus* has variously been interpreted as fossilized algae, a burrow structure, or an inorganic desiccation crack (see Häntzschel, 1962); although is now more commonly thought to be a type of microbially induced sedimentary structure (sensu Noffke et al., 2001) arising as a result of the shrinkage of microbial mats with very high strengths and elasticity within wave ripple troughs (Koehn et al., 2014). In the absence of a mat, grains would more probably have accommodated stress by moving past one another rather than opening cracks (McMahon et al., 2016). If the MDF examples have a microbial origin, their preferential development in ripple troughs would imply that matgrounds were thicker within topographic lows (Schieber, 2007). There is no assured evidence that shrinkage accurred subaerially or subaqueoulsy through dewatering.

Prave (2002) reported similar features ('irregular- to rod-shaped fragments of variable length and curvature concentrated within ripple troughs', p. 813) and interpreted these as fragments of microbially bound sand layers that had been entrained and rolled during ephemeral flows (his Fig. 4A). Surfaces with well-formed *Manchuriophycus* identified during this study also host positive epirelief fragments similar in morphology to the fragments described by Prave (2002) (Fig. 5.12).

4) Reticulate markings (Ba)

Reticulate ridges occur on multiple planform surfaces (Fig. 5.13A-B). Single nets are 2 – 6 mm wide and 1 – 2 mm high.

Figure 5.13. Possible microbial sedimentary surface textures at Rubha Réidh: (A, B) reticulate markings preserved at Rubha Réidh; (C) clear margin separating sandstone with and without adhesion marks.

Reticulate markings have modern analogues in cyanobacteria and eukaryotic algae, where they arise from filament tangling (Shepard and Sumner, 2010; Davies et al., 2016).

5) Serrated margins (ab).

In rare instances, clear serrated margins several millimetres thick separate bedding plane surfaces with and without adhesion marks (Fig. 5.13C).

Prave (2002) interpreted the serrated margins as remnants of microbially bound layers, where sand grains had adhered to a microbial crust (owing to the presence of sticky extracellular polymeric substances and cyanobacterial filaments). Possible alternative abiotic explanations for the margins could include: (1) post-depositional partial erosion of overlying sediment layers; or (2) original patchy distribution of moist sands resulting in localized adhesion.

6) Desiccated sandstone (ab).

In rare instances, desiccated polygons overprint ripple marks without a muddy matrix (Fig. 5.14A). Polygons are 15 – 25 cm wide and a few centimetres deep.

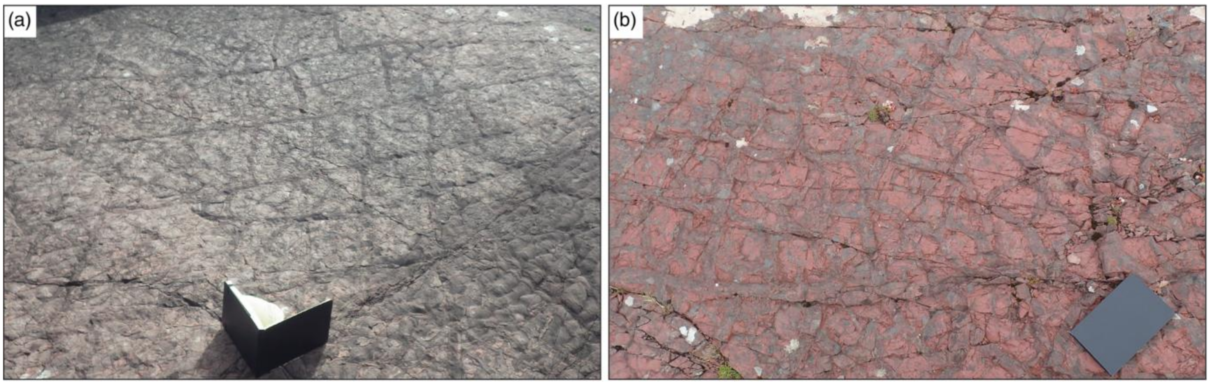

Figure 5.14. A) Desiccated sandstone surface; B) desiccated mudstone surface. Both Rubha Réidh

Desiccation cracks develop only in materials with sufficient cohesive strength (e.g., Van Mechelen, 2004). Within moist (abiotic) sands, such cohesion can be attained only if grains have high textural maturity (Chavdarian and Sumner, 2011; Glumac et al., 2011). To date, desiccation experiments on clay-poor sand substrates with angular grains have been unsuccessful (Kovalchuk et al., 2017). However, microbiota can increase sand cohesion by stabilizing grains with cyanobacterial filaments and extracellular polymeric substances (e.g., De Boer, 1981) and, in doing so, enable polygon formation (Prave, 2002; Eriksson, 2007; McMahon et al., 2016; Kovalchuk et al., 2017). Although this is a viable formation mechanism, the absence of proximal microbial fabrics on the desiccated sandstone bed at Rubha Réidh means that no direct evidence for a microbial origin has been conclusively ascertained in this study.

7) Desiccated mudstone (A)

The mudstones that account for <1% of FA1 are ubiquitously desiccated, with single polygons up to 1 m in diameter (Fig. 5.14B).

Desiccated mudstones result from a reduction in volume as muds dry out when emerged (Bradley 1933), indicating that all the preserved Meall Dearg mudstones were deposited immediately prior to subaerial exposure.

5.3.1.1c. Interpretation of Facies Association 1 (high-energy alluvial events)

Sand-bodies at Stoer, Rubha Réidh and Balchladich Bay are interpreted as the deposits of multiple high-energy alluvial flood events. During peak flow, upper flow regime conditions prevailed (Fielding, 2006), occasionally entering the chute and pool or antidune stability regimes (Alexander et al., 2001; Cartigny et al., 2014). As floods waned, flows progressively operated under transitional upper and subcritical flow conditions, resulting in the vertical stacking of sedimentary structures in accordance with decreasing flow velocity (Fig. 5.2). At Stoer, stratification types are typically limited to intercalated horizontal laminae and planar cross-stratification, with each package the result of a single flood. Packages at Stoer are rarely greater than 20 cm thick, implying either shallow flow depths or partial erosion by successive flood events. This is in contrast to the variety of preserved stratification at Rubha Réidh, where humpback form-sets are up to 2.2 m thick and must have been submerged in deeper water during deposition. During high flood stages, it is implicit that the critical flow velocity for coarse-sediment transport was exceeded, so the absence of such sediment grades indicates either: (1) only medium-grained sediment in the primary sediment supply (e.g., owing to a significant distance from the sediment source); or (2) bypass of coarser sediment fractions. Variably striking ripple crestlines are superimposed on nearly all studied sand-bodies, reflecting unconfined post-flood pooling of quiescent waters.

Abundant adhesion marks and desiccation cracks indicate intermittent subaerial exposure. The diversity of reticulate markings, *Manchuriophycus* and other surface textures with ambiguous origin offer strong circumstantial evidence for microbial colonization of substrates during sedimentary stasis (Schieber, 1999; Prave, 2002; Davies et al., 2016).

No apparent unconformity exists between the MDF and the underlying Bay of Stoer Formation, but the boundary marks a major change in sedimentary lithofacies. Bay of Stoer Formation fluvial facies consist of stacked, lower flow regime, 3D sedimentary structures (Stewart, 2002; Ielpi et al., 2016), typical of perennial fluvial flow (Bristow, 1987; Best et al., 2003), and are overlain by the shallow lacustrine Poll a'Mhuilt Member (Stewart, 2002). In contrast, MDF deposition occurred as high-energy events; a lithofacies shift that probably reflects changes in the regional temperature and seasonality of precipitation (e.g., Fielding, 2006; Lowe and Arnott, 2016) within the low-latitude, semi-arid climate belt where the formation was deposited (Torsvik and Sturt, 1987; Stewart, 1990). Alternatively, the stratigraphic appearance of these features may be a preservational artefact related to changes in basin accommodation, but, as the duration of hiatus at the Poll a'Mhuilt–Meall Dearg boundary is not understood, such a control cannot be confidently assessed.

5.3.1.2. Facies Association 2 (Enard Bay)

The 150 – 250 m thick MDF succession at Enard Bay overlies the Poll a'Mhuilt Member (not exposed in continuous coastal section) and is unconformably overlain by the Diabaig Formation (Stewart, 2002). Owing to lithofacies dissimilarity, Gracie and Stewart (1967) and Stewart (2002) did not correlate these strata with those described in the section on FA1, but the locality is now the British Geological Survey reference section for the MDF (British Geological Survey Lexicon of Named Rock Units, http://www.bgs.ac.uk/lexicon/lexicon.cfm?pub=TAD, accessed 2017). Here, the Enard Bay strata are recorded as Facies Association 2. FA2 deposits are near-ubiquitously composed of fine- or medium-grained sandstones (Fig. 5.2, Fig. 5.15A, Fig. 5.17B). No mudstones were observed in this study. Planar cross-beds occur in sets 1 – 5 m thick, intercalated with laterally extensive planar beds up to 2.8 m thick (Fig. 5.15A-B). These sedimentary characteristics indicate an aeolian origin for FA2, which was probably deposited coevally with the FA1 alluvial deposits. Although an aeolian interpretation was previously discarded by Stewart (2002) on the basis that 'convex-upward aeolian reactivation surfaces comparable in size with those figured by McKee (1966) were not observed' (p. 72), an absence of such features is not diagnostic proof against aeolian deposition. Two sedimentary facies are described, in support of an aeolian origin: (1) large-scale planar cross-bedded; and (2) planar-bedded. These facies are exclusive of the southernmost outcrop currently mapped as MDF; a singular exposure of occasionally pebbly, coarse-grained, cross-bedded sandstone separated from the described succession by 250 m (Krabbendam, 2012). This c. 5 m high and c. 30 m wide partially exposed outcrop forms a prominent small knoll, apparently faulted into contact with the rest of the MDF at Enard Bay (Fig. 5.16). Given the dissimilarity of its facies to the remainder of the succession, the inability to confirm a genetic relationship with the rest of the MDF strata at Enard Bay, and the local presence of faulted slivers of pebbly sandstones of the Applecross Formation, the exposure is here considered most likely to be a previously unrecognized outcrop of the latter formation. However, even if the outcrop records a basal pebbly fluvial facies to the remainder of the local MDF, this lithology is never seen to be interbedded with the overlying aeolian facies.

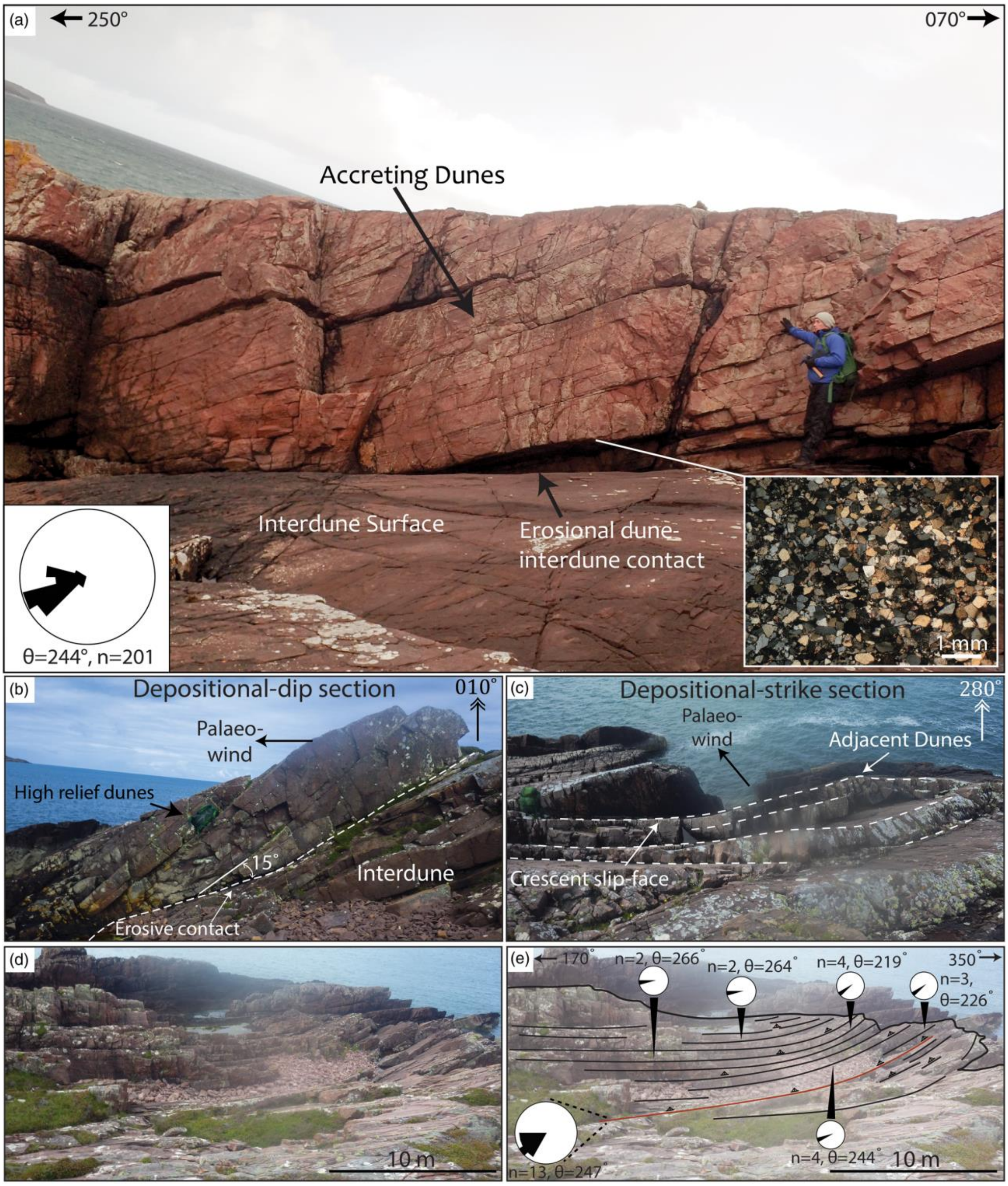

Figure 5.15. A) Intercalated planar cross-stratified dunes and planar-bedded interdunes at Enard Bay. Height of person 187 cm. Insets: Rose diagram of paleowind directions measured at Enard Bay; Representative thin section under cross-polarised light of aeolian facies at Enard Bay. Restored to horizontal; B) Aeolian dune geometry in depositional-dip sections; C) Aeolian dune geometry in depositional-strike sections; D) Large-scale arcuate aeolian dune-forms; E) Palaeoflow dispersal across a single aeolian dune-form. All Enard Bay.

Figure 5.16. Exposure of occasionally pebbly, coarse-grained, cross-bedded sandstone apparently faulted into contact with the rest of the Meall Dearg Formation at Enard Bay

5.3.1.2a. Large-scale planar cross-bedded sandstones (aeolian dunes)

Large-scale planar cross-bedding occurs within fine- to medium-grained well-rounded arkosic arenites. Cross-beds occur in sets of 1.2 – 5 m thickness (Fig. 5.15A), which are planar in depositional-dip sections (Fig. 5.15B) and curved in depositional-strike sections (Fig. 5.15C). Curved foresets demonstrate palaeoflow spreads of up to 40° across single sets (Fig. 5.15D-E), although the dispersal does not detract from the highly unimodal WSW-directed stacking of dune foresets (θ = 248°, n = 201). Sets are up to 40 m wide, with typical angles of climb between 15 and 25° (maximum 34°). Foresets are characterized by 1 – 4 mm thick, steeply dipping cross laminae with subtle inverse grading (Fig. 5.17A) or planar laminae with no discernible grain-size trends (Fig. 5.17C). Cross-bedded sets are typically bound by planar-bedded sandstones (Fig. 5.15A-B). When planar beds are absent, dune sets are separated by low-angle, erosional reactivation surfaces (Fig. 5.18A).

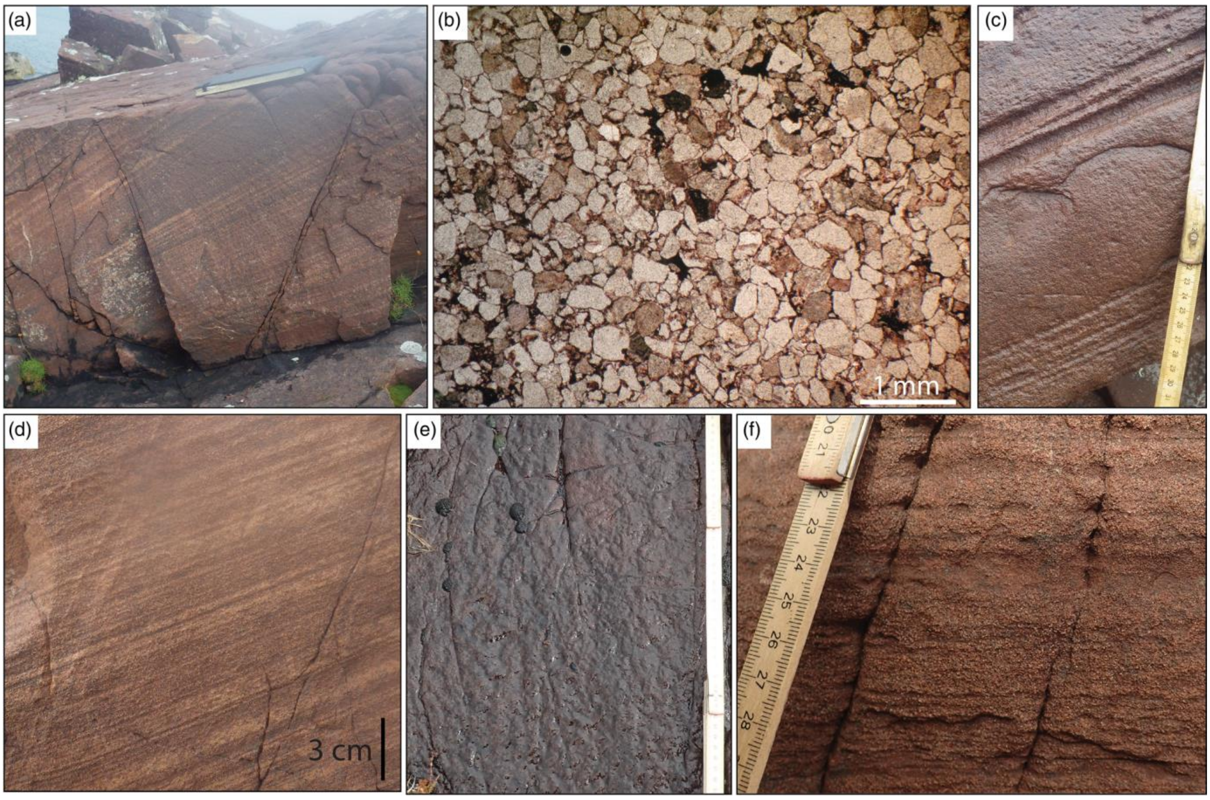

Figure 5.17. Sedimentary structures at Enard Bay: A) Cross laminae in dune facies (interpreted grainflow deposits). Restored to horizontal; B) Textural and mineralogical character of dune facies as observed in sample thin-section under polarized light; C) Planar laminae in dune facies (interpreted grainfall deposits); D) wind-ripple horizontal laminae define pinstripe lamination; E) Adhesion warts preserved on interdune surface; F) Possible adhesion lamination in interdune facies.

Figure 5.18. A) Dune sets separated by low-angle, erosional reactivation surface (dashed line). Height of person is 187 cm; B) Channel-form incising into 2.4 m thick planar-bedded package (Enard Bay).

The presence of fine- to medium-grained sandstones with well-rounded grains, arranged in cross-strata sets that are composed of cross-laminae (grainflow) and planar laminae (grainfall), suggests that the planar cross-bedded facies represent aeolian dune deposits (e.g., Hunter, 1977; Kocurek, 1981, 1996). High dispersal of palaeoflow measurements across single dune sets, and curved crest lines (Fig. 5.15C) suggest that the dunes were arcuate.

5.3.1.2b. Planar-bedded sandstones (aeolian interdunes)

Planar bedding occurs in packages of fine- and subordinate medium-grained arkosic arenites, 0.1 – 2.4 m thick, and display near ubiquitous pinstripe lamination (Fig. 5.17D). Adhesion lamination is uncommon (Fig. 5.17F). Planform surfaces are largely featureless, but sometimes contain adhesion marks (Fig. 5.17E) or, rarely, poorly developed ripple marks (n = 4) exhibiting a near 90° spread of strike lines.

Within the planar-bedded facies, one known example of a coarse-grained, apparently massive channelized sand-body incises into a 2.4 m thick planar-bedded package (Fig. 5.18B). Exposure constraints restrict full dimensions from being determined, but the preserved sand-body is at least 9 m wide and has a relief of 1.5 m.

Planar-bedded facies are interpreted as aeolian interdunes. Pinstripe lamination and climbing ripple stratification can form by aeolian ripple migration under aggrading conditions (Fryberger et al., 1988; Hunter, 1977). Adhesion marks record moist interdune surfaces. The interpreted interdune packages are comparatively thinner (predominantly <1 m, maximum 2.4 m) and less laterally extensive than dune surfaces. The channelized sand-body may be (the only) evidence for fluvial deposition in FA2, but the absence of internal structure prevents further interpretation. If fluvial in origin, it differs from the FA1 alluvium at Rubha Réidh, Balchladich Bay and Stoer through its coarser grain size and presence of channel margins.

5.3.2. Mutual exclusion of aeolian and fluvial deposits

The mutual geographical exclusion of the aeolian facies association at Enard Bay (FA2) and fluvial facies association at Rubha Réidh, Balchladich Bay and Stoer (FA1) is not unexpected. In many modern mixed fluvial–aeolian systems, there is a high propensity for fluvial flood-reworking of neighbouring aeolian dune deposits (e.g., Kocurek and Nielson, 1986; Langford, 1989), biasing the resultant sedimentary record towards alluvial dominance. This preservation bias may have been particularly acute in pre-vegetation systems, when plant-related factors that can buffer against reworking (such as sediment binding and baffling by roots, and the reduction of near-surface flow velocities by above-ground structures) were absent (Tirsgaard and Øxnevad, 1998; Rodríguez-López et al., 2014). Furthermore, wind-blown sands may have been more readily deflated from the alluvial realm in the absence of vegetation (Dalrymple et al., 1985; Lancaster and Baas, 1998; Mountney, 2004). Deflation may also have been locally promoted by a low groundwater table (as suggested by the absence of wet interdune facies in the MDF) (Fryberger et al., 1988; Kocurek and Havholm, 1993; Tirsgaard and Øxnevad, 1998). In such a scenario, the aeolian strata at Enard Bay would represent exceptional preservation of deposits that were originally more common when the MDF depositional environments were active, their absence at Rubha Réidh, Balchladich Bay and Stoer reflecting the biasing effects of high-energy flood events. The limited outcrop of the MDF at Enard Bay does not permit a robust explanation for their exceptional preservation to be determined, but any one of a number of potential preservation mechanisms may have been responsible (e.g., relating to climate, sediment supply, rate of dune migration or accommodation space generation; Mountney, 2012).

5.4. Discussion: Aggradation and stasis

Preserved Meall Dearg stratification types and sedimentary surface textures have allowed the identification of high-energy flood events, but this interpretation was permitted only because the strata contain direct evidence for: (1) upper flow regime bedforms deposited by rapidly decelerating flows under highly aggrading bed conditions; and (2) bedding plane records of intervals of sedimentary stasis. Upper flow regime bedforms such as antidunes have traditionally been considered to be transient sedimentary features, with limited long-term preservation potential (e.g., Reid and Frostick, 1994). However, they can be preserved, unmodified, when the rate of deceleration does not permit bedforms to equilibrate with flow regime (McKee et al., 1967; Alexander and Fielding, 1997; Alexander et al., 2001); conditions that may have been more frequent during Earth history than has traditionally been assumed (Fielding, 2006). The stacking of stratification types recording progressively lower flow regime conditions, as can be seen in the MDF, is attributable to such conditions of rapid sediment fall-out during falling flood stages. The preservation of these signatures, in addition to the full preservation of convex lamina sets within antidunes, attests to high rates of bed aggradation during sedimentation (Alexander and Fielding, 1997; Fielding, 2006; Cartigny et al., 2014).

The exceptional aggradational preservation of antidunes and related bedforms provides direct evidence that supercritical flow conditions developed during alluvial deposition, but cannot determine whether such conditions were perennial or whether they instead reflect discrete high-energy flood events. The determination of event deposition requires separate evidence that the sedimentary system repeatedly reverted to background conditions of low flow regime or sedimentary stasis (neither deposition nor erosion; Tipper, 2015) subsequent to the development of supercritical flow. In the MDF, the packages of sediment revealing supercritical flow are sandwiched between strata that preserve bedding plane evidence for prolonged intervals of sedimentary stasis. Such features include sedimentary surface textures of both abiotic (adhesion marks and desiccation cracks) and probable microbial origin (e.g., reticulate marks, *Manchuriophycus*), analogous to modern features that develop during sedimentary stasis in ephemeral streams (Davies et al., 2017b). For such original substrate features to have become preserved in the sedimentary record, the succeeding flows must have lacked the capacity to erode the underlying substrate. In sparsely vegetated modern and ancient ephemeral alluvial settings, rapidly aggraded sediment piles can change the locus of subsequent sedimentary events, thus escaping erosional truncation (Field, 2001; Cain and Mountney, 2009). In the MDF, evidence for such conditions can be seen in the way in which bounding surfaces are rarely erosional; succeeding packages of strata, most often floored with upper flow regime elements, are deposited directly above preserved topography (Fig. 5.3). This indicates that, despite the surpassing of a critical threshold for the deposition of upper flow bedforms, the critical threshold for erosion of underlying strata was not exceeded. The only erosional contacts in the entire succession are restricted to laterally discontinuous <50 cm scour-cuts. These characteristics of the MDF suggest that highly aggrading bed conditions can enhance the preservation potential of strata recording sedimentary stasis, in addition to supercritical bedforms.

5.5. Meall Dearg Formation: Concluding remarks

The spatial distribution of stratification types and bedding plane features across the Mesoproterozoic Meall Dearg Formation indicates deposition by high-energy alluvial events and, subordinately, as aeolian dunes. The alluvial and aeolian sedimentary facies are mutually exclusive, potentially suggesting that aeolian sediments were preserved only in regions less prone to reworking by alluvial activity. The 'sheet-braided' alluvial sandstones contain a variety of stratification types relating to upper flow regime (chute and pool structures, antidune stratification, horizontal laminae), transitional upper flow regime (humpback cross-stratification, low-angle cross-stratification) and lower flow regime conditions (planar cross-stratification, trough cross-stratification, ripple marks). Bedding surfaces separating major sand-bodies include primary substrates that host desiccation cracks, adhesion marks and putative microbial sedimentary surface textures (e.g., *Manchuriophycus*, reticulate marks), which developed during prolonged intervals of sedimentary stasis. The vertical stacking of sedimentary structures in accordance with decreasing associated flow velocity, as well as evidence of periodic emergence and non-deposition, suggests event sedimentation during episodic floods. This degree of interpretation was achievable only because of specific sedimentary conditions at the time of deposition; namely the combination of: (1) rapidly decelerating flows acting under aggrading bed conditions; and (2) intervals of non-deposition, during which primary sedimentary surface textures were imparted onto the substrate. The depositional characteristics of the Meall Dearg Formation are in line with classical facies models for pre-vegetation alluvium, but it is emphasized that these observations do not reveal universal characteristics of Precambrian rivers; they reflect one of a multitude of depositional conditions that could lead to the deposition of 'sheet-braided', pre-vegetation alluvium.

5.6. Alluvial signatures of ephemeral pre-vegetation rivers - Summary

Ancient ephemeral rivers are recognisable in alluvium as stacked beds, with each bed bearing evidence of waning flow conditions and possible intervening intervals of sedimentary stasis (e.g., Tunbridge, 1984; Stear, 1985; Olsen, 1987; Gall et al., 2017). The observation of upper flow regime elements alone is insufficient to interpret ephemerality as such elements also widely develop in perennially flowing regimes (e.g., on bar-tops; Bristow, 1993). It has been considered that pre-vegetation rivers would have been most similar to those operating today in very arid environments (e.g., Schumm, 1968; Fuller, 1985; Miall, 1996; Long, 2004; Owen and Santos, 2014) where ephemeral rivers predominate (e.g., McKee et al., 1967; Stear, 1985; Tooth, 2000; Stromberg et al., 2017). Whilst ephemeral systems likely developed across a broader range of climates before plant evolution, due to expected higher runoff rates (Tirsgaard and Øxnevad, 1998), clearly not all pre-vegetation rivers were ephemeral, as is demonstrated by the many global examples of interpreted perennial pre-vegetation river deposits (Chapter 4). The

Meall Dearg Formation case study demonstrates, however, that this understanding cannot be used to dispute the existence of ephemeral pre-vegetation rivers, or to make any assumption that all previous interpretations of ephemeral pre-vegetation rivers were incorrect, because ephemeral flow conditions can be confidently diagnosed from pre-vegetation alluvium in certain instances.

Increased runoff rates and decreased upstream water retention may have increased the likelihood for flashy discharge events (e.g., Long, 1978, 2002, 2004; Miall, 1980; Fuller, 1985; Trewin, 1993; Love and Williams, 2000; Gouramanis et al., 2003; Bose et al., 2012). As upper flow regime elements are more readily preserved if flows decelerate faster than sediment equilibrates (Alexander et al., 2001; Fielding, 2006), expected higher discharge variability may have resulted in a preservation bias towards upper flow regime elements within pre-vegetation alluvium. Upper flow regime elements have been proposed to be unusually abundant within pre-vegetation alluvium (Long, 2011), and pre-vegetation successions which entirely comprise these elements are regularly explained as a consequence of increased runoff rates in the absence of land plants (e.g., Hjellbakk, 1993, 1997; Lowe and Arnott, 2016). However, many syn-vegetation alluvial successions are also dominated by upper flow regime elements (e.g., Tunbridge, 1981; Gall et al., 2017), such that this characteristic is not a pre-vegetation motif. The presented dataset of Palaeoarchean-upper Cambrian alluvium (Table A3) combined with data on Devonian alluvium previously compiled by Davies and Gibling (2010a) finds that there is little change in the abundance of upper and transitional upper flow regime elements preserved in alluvium after the onset of vegetation (Fig. 5.19). This suggests that high-energy floods were not more abundant before the evolution of land plants (contra Long, 2011). Future investigations should consider more fully the effects of upstream water retention and increased runoff rates on fluvial style in the downstream-reaches of riverscapes (the areas of the sedimentary systems with highest preservation potential).

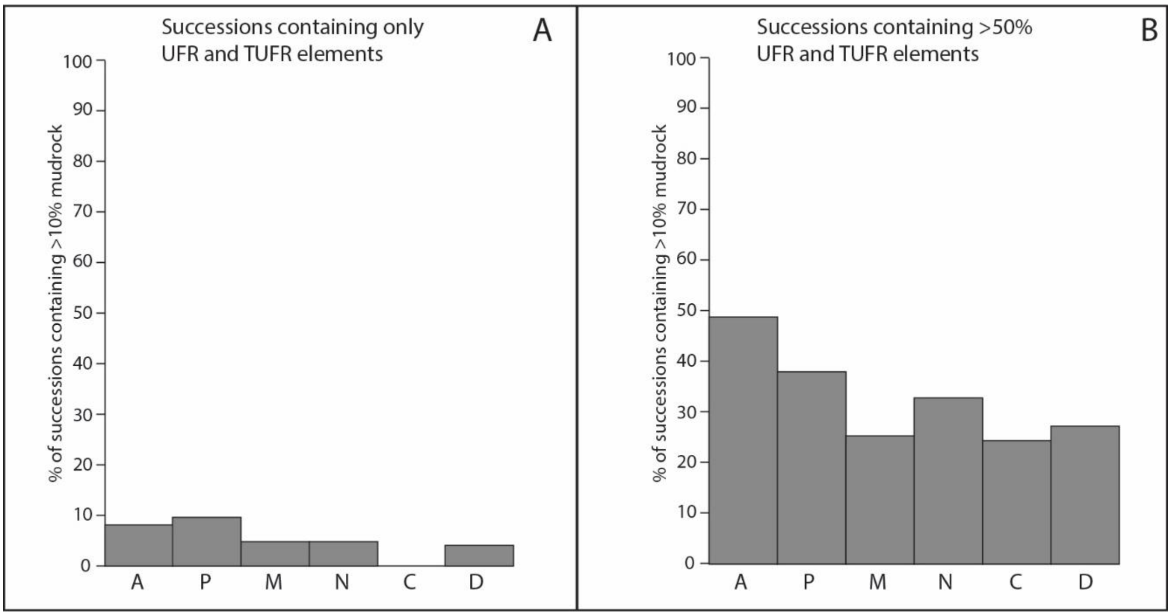

Figure 5.19. Percentage of case studies for each Era/Period that contain: (A) Only upper flow regime and transitional upper flow regime elements; (B) >50% upper flow regime and transitional upper flow regime sedimentary structures. Archean-Cambrian data presented in Table A3. Devonian data presented in Davies and Gibling (2010a).

Chapter 6

BIOTIC INFLUENCES ON PRE-VEGETATION RIVERS AND ALLUVIUM: EVIDENCE FROM THE 'SERIES ROUGE', FRANCE

Despite the distinct nature of pre-vegetation alluvium, it is now recognised that the landscapes in which such deposits were laid down were not wholly abiotic. Prior to their 'greening' by embryophytes and other higher land plants, Earth's non-marine environments likely hosted abundant microbial mats and biofilms (e.g., Horodyski and Knauth, 1994; Noffke, 2010; Wellman and Strother, 2015). In light of this, an increasing number of studies have postulated that microbiota may have influenced geomorphic stability and processes in Precambrian and early Palaeozoic rivers (e.g., Medaris et al., 2003; Sarkar et al., 2005; Eriksson et al., 2009; Bose et al., 2012; Petrov, 2014, 2015; Ielpi, 2016; Santos and Owen, 2016). These assertions are primarily made by combining: (1) the recognition that mats would have been present in the pre-vegetation realm; with (2) reference to observations of microbial influences on sedimentary processes in modern environments or laboratory experiments. Such modern observations include: 1) demonstrations of how extracellular polymeric substances (EPS), secreted by microbiota, alter the thresholds of sediment entrainment, transport and deposition (e.g., Vandevivere and Baveye, 1992; Tolhurst et al., 2002; Friend et al., 2008; Malarkey et al., 2015); or 2) observations of how microbial mats prolong substrate stabilization under moving fluids, prior to their catastrophic failure (Krumbein et al., 1994; Hagadorn and McDowell, 2012; Vignaga et al., 2013).

Understanding exactly how a microbial influence may have been exerted on pre-vegetation rivers is currently hampered by a paucity of studies that provide direct supporting physical evidence from the geological record. In part this is because Precambrian and early Palaeozoic alluvial strata only rarely preserve fossil evidence for the presence of microbial mats during deposition (Schieber, 1999; Noffke et al., 2001; Davies and Gibling, 2010a; Davies et al., 2011, 2016). A survey of pre-vegetation fluvial units includes only 9 formations which simultaneously host evidence for microbial life, including the previously discussed Meall Dearg Formation (Chapter 5) and Copper Harbour Formation (see Fig. 2.7) (Prave, 2002; Parizot et al., 2005; Yeo et al., 2007; Rasmussen et al., 2009; Sheldon, 2012; Beraldi-Campesi et al., 2014; Wilmeth et al., 2014; Petrov, 2014, 2015). Even fewer studies have directly used sedimentary geological evidence to support assertions of how these ancient mats may have influenced fluvial processes. In part this may be due to outcrop constraints. For example, such an undertaking was not possible for the Meall Dearg Formation because large-scale exposures undissected by faults were sparse, such that architectural analysis was rarely possible (although high-energy flood events would have almost inevitably torn up any microbiota present in the flow path).

Petrov (2015) interpreted a microbial mat influence on fluvial landscapes in the 1.58 Ga Mukun Basin of Russia, but the sedimentary architecture of the associated strata was not detailed, and many of the 'microbial-related structures' he reported within the fluvial facies are more parsimoniously interpreted as abiotic features (adhesion marks, ladder ripples, accretionary dunes and soft sediment deformation (his Plates 9 and 10); see Davies et al., 2016). Santos and Owen (2016) postulated that the development and preservation of Precambrian fine-grained meandering rivers could have been promoted by microbial mats. This was supported by the presence of an 8 m thick fine-grained interval (including inclined heterolithic lateral accretion) preserved within pre-vegetation alluvium (discussed in Chapter 7).

With these notable exceptions, most other reports of a microbial influence on Precambrian sedimentation are wholly hypothetical (e.g., Bose et al., 2012) and there is thus a knowledge gap arising from a scarcity of studies which directly use sedimentary geological evidence to support or contend assertions of microbial influence on pre-vegetation rivers. This chapter attempts to redress this with reference to the Ediacaran-Cambrian ''Series Rouge" of northwest France, which provides an excellent opportunity to study the interactions between matgrounds, pre-vegetation river systems, and preserved alluvial architecture. The Series Rouge is well-suited for such a purpose in that it contains both well exposed outcrop of alluvial architecture, in addition to multiple lines of evidence for former microbial mat colonies. This chapter is organised as follows: (1) an introduction to the geological context of the Series Rouge; (2) an analysis of the lines of evidence for microbial life within the succession; (3) an analysis of the sedimentary architecture and facies of the succession; and (4) a discussion of how microbial life (evidenced in Section 6.2) influenced the sedimentary characteristics of the Series Rouge (evidenced in Section 6.3).

6.1. Geological context of the Series Rouge

Neoproterozoic and lower Palaeozoic red bed successions, deposited during the terminal stages of the Cadomian Orogeny, crop out across northwest France and the Channel Islands (Renouf, 1974; D'Lemos et al., 1990; Went and Andrews, 1990). Stratigraphic nomenclature of the red beds is confused, in part due to the scattered nature of outcrop in isolated geological inliers and outliers, on islands, and in part due to the cross-border spread of outcrop in northern France and on the UK Channel Islands of Alderney and Jersey (Fig. 6.1). The stratigraphic terminology used for the French outcrops is localized to each individual outcrop belt, but they are informally grouped as the "Séries Rouges du Golfe Normano-Breton". The British Geological Survey recognises the Alderney Sandstone and Rozel Conglomerate (Jersey) as discrete mapping units, but does not relate them to one another or to the French outcrops. Here the term 'Series Rouge' is used to group the geographically-proximal red-bed outcrop areas on both the Channel Islands and French mainland. Formal stratigraphic correlation is presently impossible due to a lack of reliably dated markers, but the term is used to refer to all the unfossiliferous sandstones, conglomerates, and mudstones that share a common basal unconformity above deformed Neoproterozoic shales and volcanic rocks (the Brioverian Series) or plutonic igneous complexes in the region (summarised in Figure 6.2). The precise age of the Series Rouge is still subject to discussion. Red-bed sequences in Normandy unambiguously underlie Cambrian Stage 3 (521– 514 Ma) limestones (dated by the presence of the trilobite *Bigotina* (Pillola, 1993)) and pre-trilobite marine siliciclastics from Cambrian Stage 2 (529–521 Ma). The red beds in northern Brittany are less well constrained stratigraphically, but are lithologically similar to the Normandy red beds. The French Geological Survey considers them Early Ordovician, on the basis of radiometric data obtained from the intercalated Plourivo-Plouezec andesitic volcanics (Auvray et al., 1980). However, palaeogeographic considerations render an Early Ordovician age implausible. Palaeocurrent data demonstrate that alluvial strata of the Series Rouge were derived from the west ($\theta = 84°$; $n = 431$, $S = 40.8$), but there is no potential Early Ordovician source for such sediments in this direction, where well-dated marine shelf sediments (the Gres Armoricain) were being laid down during this interval (Paris et al., 1999; Dabard et al., 2007, 2009). The weight of evidence thus suggests that the Series Rouge were deposited between the latest Ediacaran and earliest Cambrian (although even if they were Early Ordovician they would still unambiguously represent pre-vegetation strata).

Deposits included in the Series Rouge cover a range of depositional environments (Fig. 6.2). Alluvial fan conglomerates dominate the stratigraphy on Jersey (Went et al., 1988; Went, 2005), whereas coeval sandy alluvium (and subordinate marine sandstone) comprises the Alderney succession (Todd and Went, 1991; Ielpi and Ghinassi, 2016). At Goëlo, the lower Port Lazo Formation passes upwards from alluvial fan-alluvial plain deposition into a subtidal setting, before transitioning into braided fluvial deposition of the Roche Jagu Formation (Went, 2016). At Baie de St-Brieuc, with the exception of a 30 m interval of mature marine quartzites representing nearshore marine environments (the Erquy Quartzite) (Went, 2013), braided alluvium predominates (the Fréhel Formation).

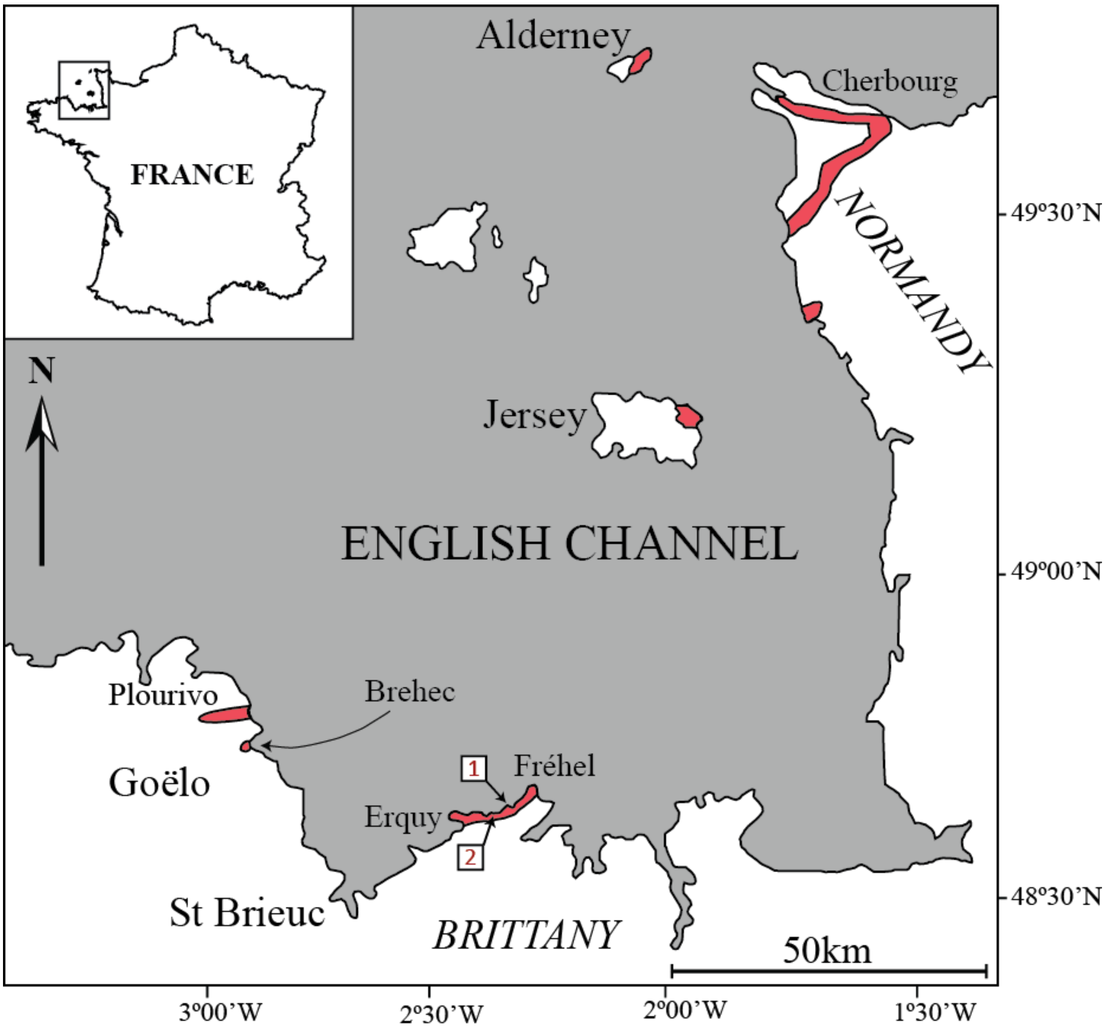

Figure 6.1. Location of Series Rouge 'Red Beds'. Numbered boxes indicate location of presented architectural panels: 1. Sables d'Or Quarry (Fig. 6.11); 2. Pointe aux Chèvres (Fig. 6.8).

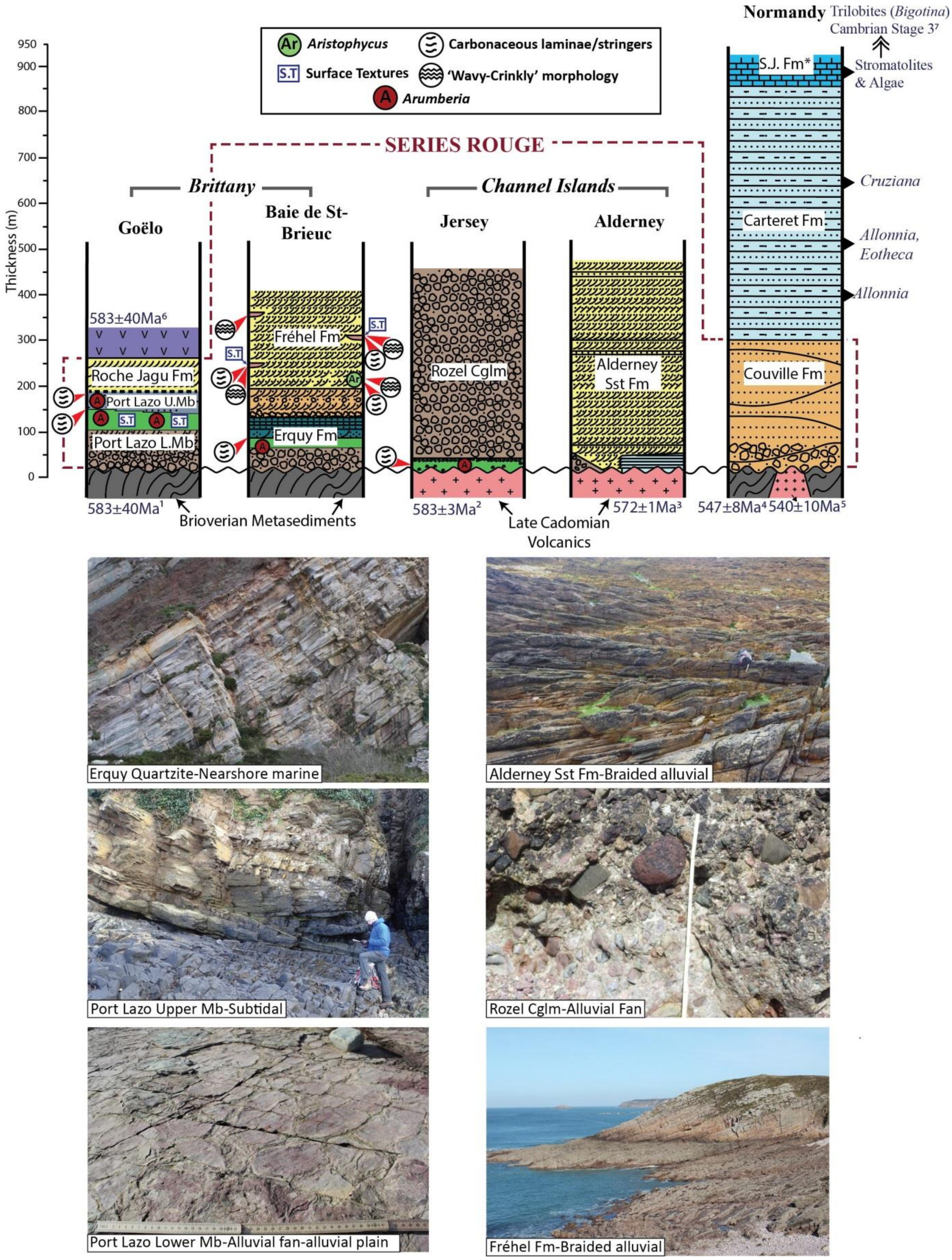

Figure 6.2. Top: Lithostratigraphic correlation of the formations which constitute the Series Rouge. Formations comprising Series Rouge boxed. Summaries of sedimentology presented in Section 6.3. Carteret Formation fauna from Doré (1994). Superscript numbers in the top diagram relate to the following publications: 1. Auvray (1979); 2. Miller et al. (2001); 3. D'Lemos et al. (2001); 4. Hagstrum et al. (1980); 5. Pasteels and Doré (1982); 6. Auvray et al. (1980); 7. Pillola (1993). S.J Fm = Saint-Jean-de-la-Rivière Formation. Bottom: Typical outcrops and interpreted environments for Series Rouge units.

The sedimentary characteristics of Series Rouge alluvium presented in this chapter entirely refer to the Fréhel Formation at Baie de St-Brieuc (Section 6.3). Coastal and quarry exposures of the Fréhel Formation permitted analysis of: (1) the dimensions, geometry and composition of constituent sediment bodies; (2) stacking patterns and lateral relationships from depositional-strike successions (perpendicular to palaeoflow); and (3) local downstream variation from depositional dip successions (parallel to palaeoflow), which were better suited for revealing details of lateral terminations and stacking patterns of individual interpreted barforms and channel-fills.

Photomosaics of laterally-extensive strata were constructed during a reconnaissance visit and later used in the field so that beds could be accurately traced and locations of palaeoflow measurements and architectural elements precisely recorded, permitting a three-dimensional reconstruction of alluvial deposits (Allen, 1983; Miall, 1985, 1996; Long, 2006, 2011).

Within the most extensive exposures, coset boundaries were seen to change in prominence laterally, passing into boundaries separating individual sand-bodies. In outcrop, such transitions can be picked out by variable weathering expressions of the bounding surface, and arise because larger barforms can separate into numerous smaller bars down-section (Allen, 1983). It has been suggested that annotation of bounding surfaces should leave no 'hanging lines' (Miall, 1996), but as the lateral transitions in these instances reflect original depositional processes, connecting lines is considered potentially misleading.

The cliff sections provide good lateral exposure of sedimentary architecture, but often at the expense of vertical access. However, coastal outcrops at Pointe aux Chèvre (Fig. 6.1) permitted detailed study of a c. 49 m thick vertical succession. The stepped nature of the exposure meant that architectural elements could still be accurately mapped laterally. Data collection was repeated for multiple vertically-stacked barforms, giving an indication of the temporal evolution of fluvial style.

Evidence for microbial life during Series Rouge deposition (petrography, sedimentary surface textures, pseudofossils (Section 6.2)) follow observations made from: 1) Fréhel Formation alluvium; and 2) Alluvial plain facies of the Port Lazo Formation (see Went (2016) for detailed descriptions of Port Lazo Formation sedimentary facies). Alluvial plain facies of the Port Lazo Formation are additionally included for discussion of ancient microbial life as the rivers responsible for depositing Fréhel alluvium would have had the potential to interact with microbial mats located in alluvial plain settings in both the quiescent parts of their channel belts, and within their distal coastal reaches. Observations made from the Fréhel and Port Lazo Formations are explicitly clarified throughout.

6.2. Evidence for microbial life in the Series Rouge

A suite of circumstantial evidence for microbial life is preserved in the Series Rouge. Rarely preserved mudstones in the Fréhel Formation contain petrographic evidence for reworked microbial mat fragments (Section 6.2.1). Bedding plane exposures of both the Fréhel Formation and Port Lazo Formation contain a variety of sedimentary surface textures with possible biogenic origins (Section 6.2.2). The Fréhel Formation also contains two instances of the enigmatic branching 'pseudofossil' *Aristophycus* (Section 6.2.3). The origin of *Aristophycus* is critically discussed, with a microbial formation mechanism shown to be favourable. Alluvial plain facies of the Port Lazo Formation also contain *Arumberia*, another enigmatic psuedofossil with multiple suggested formation mechanisms (Section 6.2.4). The origin of *Arumberia* is also briefly discussed, and is suggested to be strong evidence for the former colonisation of microbial matgrounds in certain, low-energy sedimentary environments.

6.2.1. Petrographic evidence

Positive identification of microbial mat features from petrographic thin sections can be challenging because they share similarities with other laminated structures produced by purely physical means (e.g., differential compaction of anisotropic sediment (Schieber, 1999)). Despite this, circumstantial petrographic evidence for the presence of matgrounds during deposition exists within fine-grained alluvial sedimentary rocks of the Fréhel Formation, which occur either as discontinuous layers, or as red or white blocky intraformational mud clasts in sandstones. Such mudstones and siltstones contribute <1% of the thickness of the formation, yet, where these have been sampled, they always contain features in thin sections that may be characteristic of former microbial mats, including abundant detrital mica and probable carbonaceous material.

Detrital biotite mica is a near ubiquitous component of both red and white mudstones of the Fréhel Formation (Fig. 6.3). The biotite micas are most commonly weathered and degraded, and present as aligned, near-isotropic (due to alteration to ferric oxide), <0.5 mm flakes with little or no observable cleavage (Fig. 6.3A). The weathered biotite contrasts with locally-present fresher biotite, which exhibits a pale green colour and characteristic cleavage planes (Fig. 6.3B). Mica flakes vary in abundance between sampled mudstones, either displaying an even distribution across the sample (Fig. 6.3A), or occurring as discrete, dense layers in which mica flakes surround grains in an anastomosing fashion (Fig. 6.3C-D). The segregation of mica results from settling velocities that are much lower than for quartz grains of similar size (Doyle et al., 1983). For this reason they tend to float and accumulate preferentially in quiet water settings along with silts and clays. Such low energy fluvial subenvironments (such as floodplain ponds) are most suited to matground development. Here, mica may have avoided resuspension and become trapped and bound in these environments due to the secretion of EPS by microbial matgrounds, termed the 'fly paper effect' (e.g., Gerdes and Krumbein, 1987; Schieber, 1999, 2004; Schieber et al., 2007).

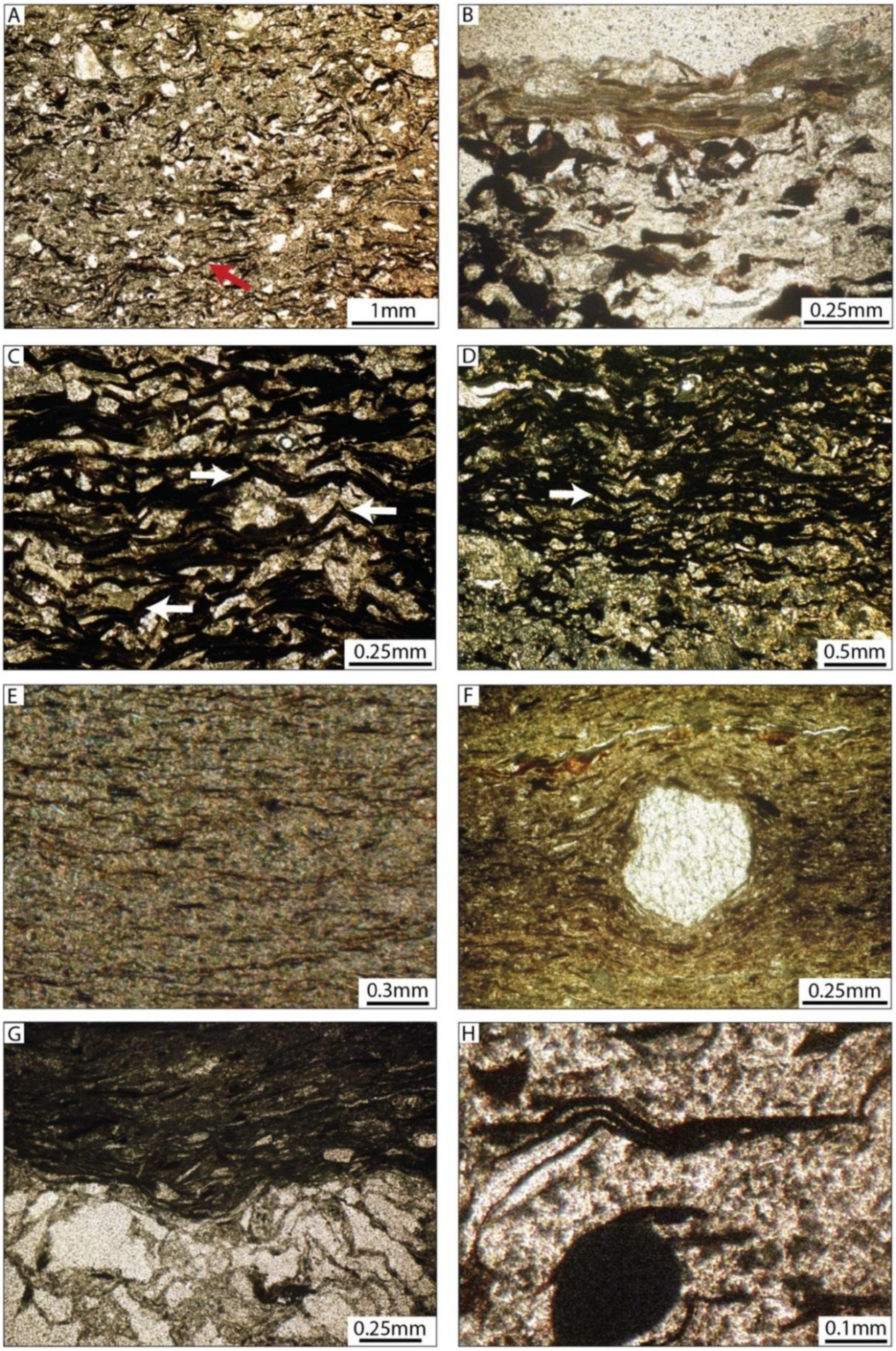

Figure 6.3. Petrographic evidence for matground colonisation in the Fréhel Formation: (A) Detrital biotite mica with approximately aligned long-axes (red arrow indicates wavy-crinkly morphology); (B) Pale green biotite with cleavage planes; (C–D) Wavy-crinkly morphology exhibited by detrital biotite mica (examples arrowed); (E) Fréhel Formation mudstone with interpreted carbonaceous stringers; (F) Differential compaction of carbonaceous stringers surrounding suspended quartz grain; (G)

Petrographic thin section of mud clast hosting carbonaceous material present; (H) Delaminating oxidised biotite mica fraying towards its lateral margin.

The association between densely packed mica and microbial matgrounds is further suggested by abrupt, convex-upward features within mica layers (Fig. 6.3B-C). This morphology is frequently described as 'wavy-crinkly' (e.g., Gerdes and Krumbein, 1987; Schieber, 1999, 2004) and is sometimes cited as evidence for microbial mats where present in the sedimentary record (Schieber, 1999; Sur et al., 2006; Deb et al., 2007; Samanta et al., 2011), on the basis that modern microbial mat laminae regularly display a similar morphology (Horodyski et al., 1977; Krumbein and Cohen, 1977).

Fragments of carbonaceous material are also present in petrographic thin sections of the Fréhel Formation and may represent comminuted microbial mats. Carbonaceous material is predominantly isotropic (Fig. 6.3E–G). Carbonaceous material occurs in two ways: (1) as elongate laminae, potentially representing in situ matgrounds (Fig. 6.4E); or, (2) more commonly, as <0.25 mm long stringers, potentially representing reworked fragments of matgrounds (Fig. 6.3F). In instances where the material is present as laminae, these usually occur in isolation and are separated by up to 0.5 mm of background sediment (Fig. 6.3E). Carbonaceous laminae are particularly common in thin sections made from intraformational mud clasts, where they exhibit discrete internal laminae that may have strengthened the clasts against physical attrition (Fig. 6.3G). In contrast, stringers occur in isolation, with evidence for internal cohesion and rigidity, such that they were able to bend and fold prior to and during deposition; some carbonaceous stringers are differentially compacted around isolated quartz grains (Fig. 6.3F) (Schieber et al., 2010).

Caution is required in visually distinguishing carbonaceous flakes from degraded biotite in thin section. Detrital biotite tends to fray at its margins, break along cleavage planes and become isotropic when altered to iron oxide (Fig. 6.3H) (Fordham, 1990). In the Fréhel Formation, carbonaceous stringers may be distinguished from detrital biotites by: (1) lower relief (Fig. 6.3A v Fig. 6.3E); (2) more continuous laminae (Fig. 6.3E); and (3) a lack of evidence for cleavage planes.

6.2.2. Sedimentary surface textures

Mudrocks within the braided alluvium of the Fréhel Formation and the probably marine-influenced alluvial plain deposits of the Port Lazo Formation display a variety of sedimentary surface textures. Some of these may be related to microbial processes and would thus be referred to as referred to as 'microbially induced sedimentary structures' or MISS (sensu Noffke et al., 2001). Obtaining conclusive proof of a microbial origin for a particular sedimentary surface texture in the ancient record during initial field observation can be problematic, as many abiotic mechanisms can produce MISS-like textures (Davies et al., 2016). As a result, each surface texture described below is assigned a sedimentary surface texture category, indicating the degree of certainty of a microbial formation mechanism (Davies et al., 2016) (introduced in Section 5.3.1.1b). Category B are definitively biotic (microbial) and category A are definitively abiotic. Category Ba is assigned for structures with evidence for a biotic origin, but an abiotic origin cannot be ruled out (Ab for the converse situation). Surface textures with a plausible biotic origin, but where there is no clear evidence are classed ab.

6.2.2.1. Transverse wrinkles (ab); (Fréhel and Port Lazo Formations)

Wrinkles (sensu Davies et al., 2016) may have abiotic or microbial origins. Within the Fréhel Formation, wrinkles are irregular, broadly subparallel and occur superimposed on irregular mm-relief topographic highs that are spaced approximately 1 cm apart (Fig. 6.4A). The long axes of these structures trend E-W, perpendicular to the predominant eastward flow orientation observed from cross-strata and rippled surfaces. Within the Port Lazo Formation, wrinkles display strong, parallel alignment, have mm-scale spacing and are highly discontinuous (individual ridges are predominantly <2.5 cm long) (Fig. 6.4B). The strike lines are highly variable (unlike those in the Fréhel Formation). Individual ridges are spaced 1–1.4 mm apart and have heights <0.5 mm.

6.2.2.2. 'Bubble' texture (ab); (Fréhel Formation)

Multiple, circular, epirelief 'bubbles' are no more than 1 mm in diameter and have a patchy distribution across the surface, but when present occur as densely spaced clusters (Fig. 6.4C). They differ to epirelief bulges (Section 6.2.2.3) by being smaller and more densely packed. The structures have a near uniform size distribution and rarely overlap. Similar textures may be formed by a respiring matground (Noffke et al., 1996), though abiotic origins cannot be ruled out. For example, within modern intertidal sediments, air escape bubbles frequently form near the strandline during falling tide, as well as beneath clay veneers (De Boer, 1979; Davies et al., 2016).

6.2.2.3. Epirelief bulges (Ba); (Fréhel Formation)

Simple isolated bulges occur on numerous bedding planes (Fig. 6.4D). They occur as sub-circular domes preserved in positive epirelief, typically 2–4 mm in diameter. The formation of similar bulges has been previously attributed to gas release from within a microbial surface (Dornbos et al., 2007; Gerdes, 2007). Oxygen rich bubbles may remain stable for weeks or months if they are not disturbed, permitting them to become enmeshed by filamentous cyanobacteria (if present), and potentially preserved (Bosak et al., 2010).

6.2.2.4. Ruptured domes (Ba) (Port Lazo Formation)

Ruptured domes occur alongside *Arumberia* (Section 6.2.3.2) on desiccated surfaces within in the Port Lazo Formation Lower Member. These are discoidal ring shaped bulges no more than 30 mm in diameter and 3 mm in height. Each dome contains a central depression (Fig. 6.4E). Shape varies from circular to fairly elongate. Domes are typically clustered. Ruptured domes are probably the result of burst bubbles that could occur either within a matground or clay veneer.

6.2.2.5. 'Elephant skin texture' (Ba); (Port Lazo Formation)

The term 'elephant skin texture' has become a bucket term for many different textures, having been consistently misapplied in recent years (Davies et al., 2016), but the Port Lazo Upper Member contains infrequent examples of the texture that match the original description of Runnegar and Fedonkin (1992). The texture consists of a tight network of reticulate ridges (Fig. 6.4F). Width of individual polygons within the network is <5 mm. Orientation of individual ridges are highly irregular. The origin of the structure is uncertain, but it has been described from multiple microbial matground facies, particularly in Ediacaran strata (e.g., Gehling, 1999; Steiner and Reitner, 2001).

6.2.2.6. Curved shrinkage cracks (ab) (Port Lazo Formation)

Curved cracks with tapering edges are preserved in the Port Lazo Formation (upper Member only) (Fig. 6.4G). It has been proposed that such cracks require a microbial binding of surface sediment to form (Gerdes, 2007; Harazim et al., 2013), though abiotic mechanisms have also been proposed (e.g., contraction of the mineral lattice in swelling clay in response to a change in pore-water salinity, seismic shock) (Allen, 1982; Astin and Rogers, 1991; Pratt, 1998).

6.2.2.7. Reticulate markings (Ba) (Port Lazo Formation)

Reticulate markings are occasionally associated with *Arumberia* in the Port Lazo Formation (Fig. 6.4H). Such markings may develop on a microbial mat when filamentous bacteria glide, collide and amalgamate (Shepard and Sumner, 2010), or from the tangling of algal filaments (Davies et al., 2016).

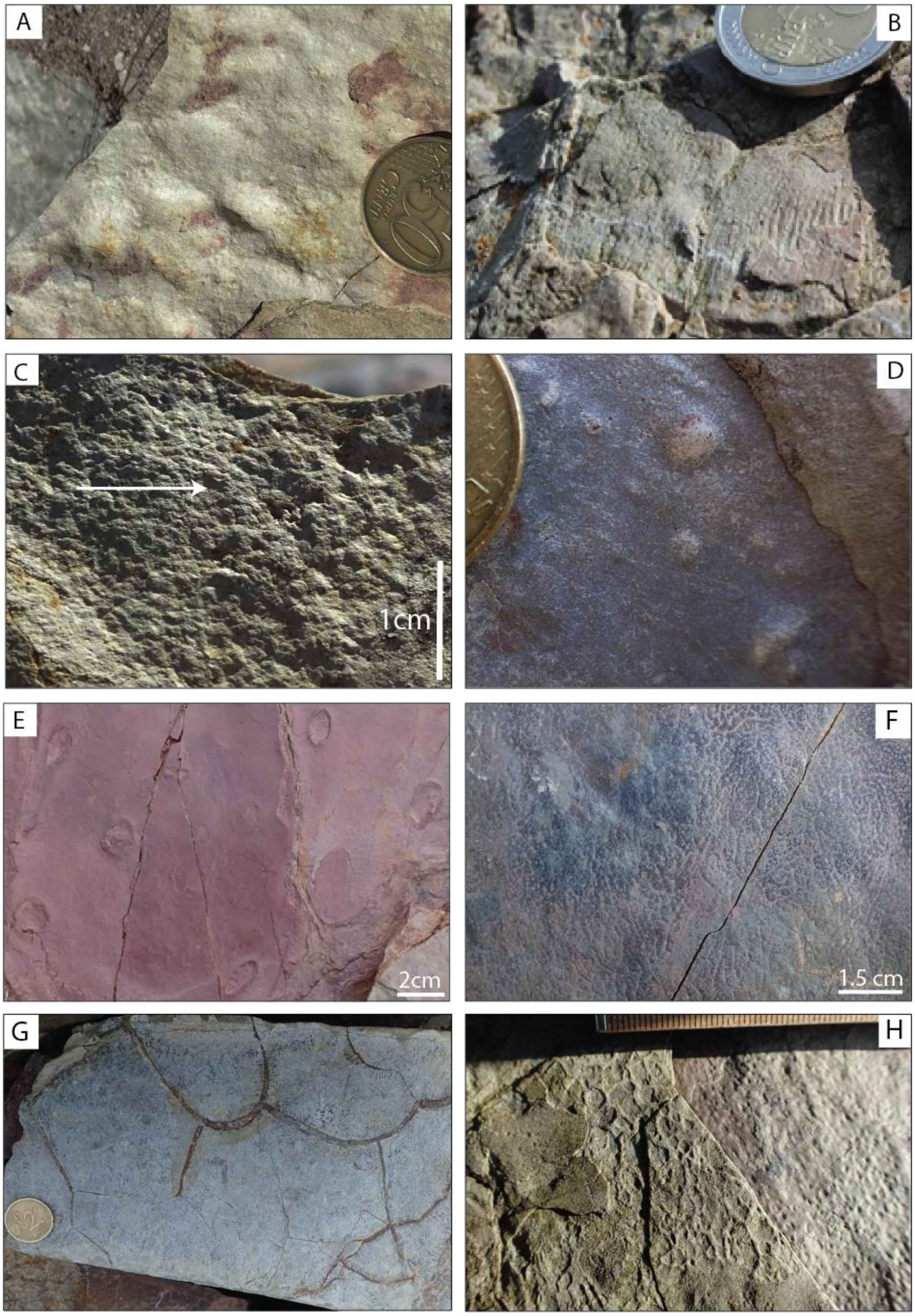

Figure 6.4. A) Transverse wrinkles. Fréhel Formation. Diameter of coin is 24 mm; B) Transverse wrinkles. Port Lazo Formation. Diameter of coin is 27 mm; C) ‘Bubble-texture’. Fréhel Formation; D) Epirelief bulges. Fréhel Formation. Diameter of coin is 24 mm; E) Ruptured domes. Port Lazo Formation; F) Elephant skin texture. Port Lazo Formation; G) Curved shrinkage cracks. Port Lazo Formation. Diameter of coin is 24 mm; H) Reticulate markings (pimple structures to right of image associated with *Arumberia*-Fig. 6.6). Port Lazo Formation.

6.2.2.8. Assessing microbial origins for the sedimentary surface textures

Interpretations of microbial origins for these sedimentary surface textures are made with a caveat of reasonable uncertainty. The majority of the surface textures described above can be classified as ‘ab’ (Davies et al., 2016) as there is no unambiguous evidence to support either a definite biotic or abiotic formation mechanism. However, the high abundance and diversity of enigmatic ab and Ba sedimentary surface textures within close spatial proximity may lend support to a microbial origin for at least some of the textures because: (1) microbial mats broaden the potential range of interaction between physico-chemical processes and a sedimentary surface; and (2) can be interred at different stages of their morphological development (Schieber, 1999; Gehling and Droser, 2009; Davies et al., 2016, 2017b).

6.2.3. ‘‘Pseudofossils”

6.2.3.1. Aristophycus

Two examples of the enigmatic branching structure *Aristophycus* (Osgood, 1970; Davies et al., 2016) occur on a single bedding plane of very coarse-grained, trough cross-stratified alluvial sandstone (Fig. 6.5A), 50 m above the base of the Fréhel Formation (Fig. 6.2). The sediment immediately overlying the structures is considerably finer (fine to medium sand) and more micaceous (Fig. 6.5E). Petrographic evidence demonstrates that the composition of the raised *Aristophycus* structure is predominantly quartz and feldspar (Fig. 6.5B), but the sandstone underlying the branching structure hosts densely packed detrital mica flakes (Fig. 6.5D). Detrital mica is less common within the host sandstone at greater distances, both laterally (Fig. 6.5C) and vertically (Fig. 6.5D) from the *Aristophycus* structures.

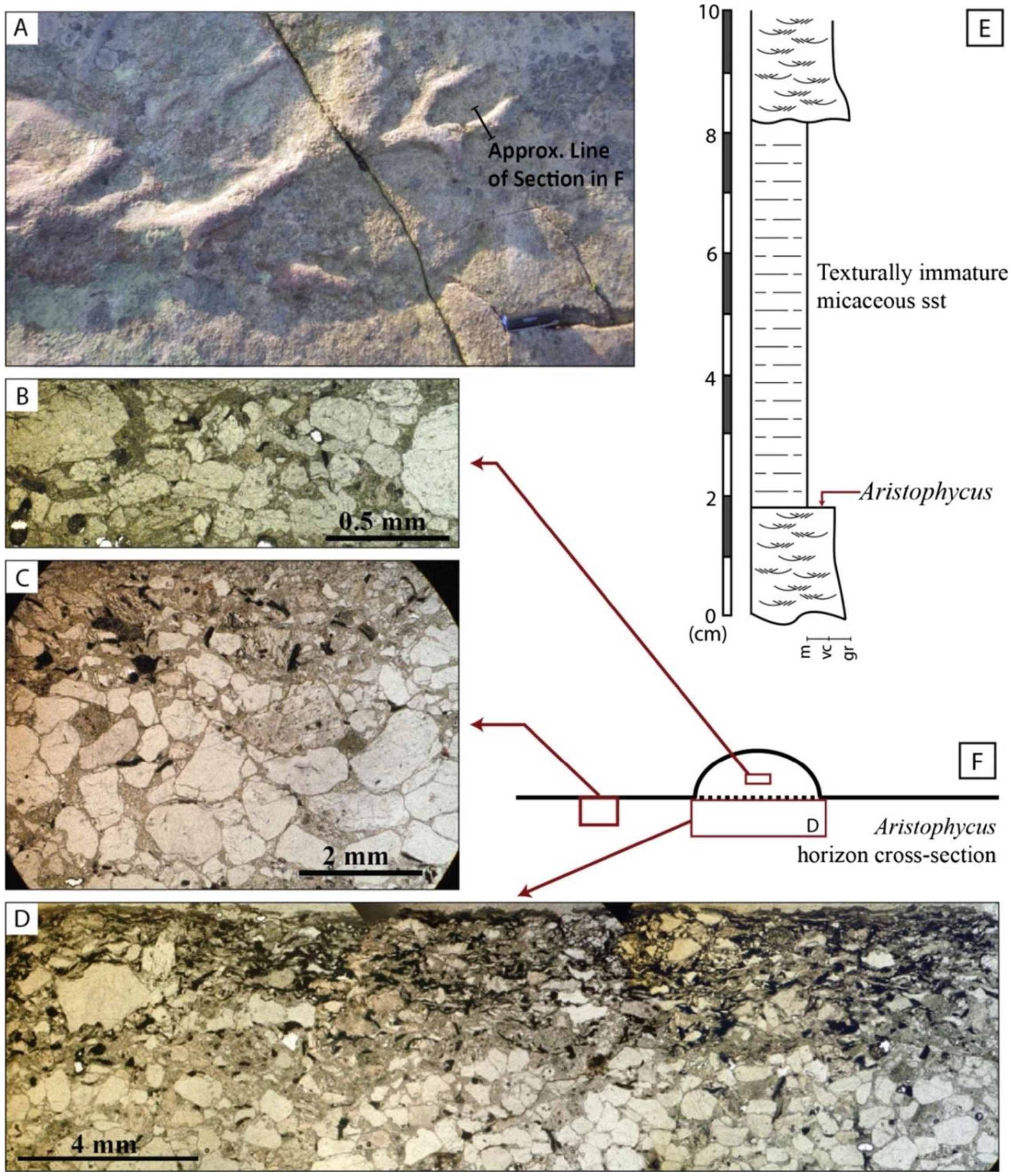

Fig. 6.5. A) *Aristophycus* structures. Fréhel Formation. Pen lid is 38 mm long; B) Petrographic thin section of *Aristophycus*; C) Petrographic thin section of sandstone horizon immediately adjacent to *Aristophycus*; D) Petrographic thin section of sandstone horizon immediately underlying *Aristophycus*; E) Vertical log of *Aristophycus* bearing section; F) Schematic line of section across *Aristophycus*.

Three hypotheses for *Aristophycus* formation have been proposed: (1) expulsion of pore water through burrow cavities (Seilacher, 1982); (2) dewatering of unconsolidated sands beneath an impermeable clay seal (Knaust and Hauschke, 2004); and (3) the movement of fluidized sediment trapped beneath an impermeable microbial mat (Seilacher, 2007; Kumar and Ahmad, 2014). The sandstones of the Fréhel Formation pre-date terrestrial burrows so the first hypothesis can be rejected in this instance. The two described examples of *Aristophycus* are interpreted as dewatering structures incorporating elements of hypotheses (2) and (3) above. Expelled pore fluid appears to have been unable to migrate vertically upwards through the micaceous sandstone and instead moved laterally from a point source in the very coarse sandstone along a conduit before dissipating into a small number of breach points in the overlying bed.

Thus, *Aristophycus* is interpreted to mark the route of water escape through this locally heterogeneous system. The isolated stratigraphic occurrence of the structure is explained by the fact that the bulk of the Fréhel Formation records more high energy fluvial deposition, and is unsuited to the formation of *Aristophycus* by virtue of being homogenous with regard to permeability. The role of mats in the origin is inferred from the densely packed detrital mica immediately underlying *Aristophycus* (Fig. 6.5D) (see Section 6.2.1).

6.2.3.2. Arumberia

Multiple red or reduced drab mudstones within the Port Lazo Formation contain examples of the enigmatic sedimentary surface texture, *Arumberia* (Fig. 6.6). The most prominent *Arumberia* location occurs near the top of the Lower Member of the Port Lazo Formation at Bréhec (Fig. 6.2), where multiple examples are spread extensively across a 300 m^2 desiccated surface within a heterolithic mottled red bed succession that records probable tidally influenced alluvial plain facies (Went, 2016). Previous reports have also noted *Arumberia* within basal red mudstones of the Rozel Conglomerate at Tête des Hougues, Jersey and in red mudstones overlying the Erquy Conglomerate at Pointe des Trois Pierres, Brittany (Bland, 1984).

Arumberia was originally interpreted as an Ediacaran metazoan (Glaessner and Walter, 1975) before being reinterpreted as a physical sedimentary structure (Brasier, 1979), and is now more commonly described as a microbially-induced sedimentary structure (McIlroy and Walter, 1997). It comprises a series of parallel or subparallel, occasionally bifurcating rugae (<1 mm relief), spaced c. 1–3mm from one another (Fig. 6.6A, Fig. 6.6B). In the vast majority of instances, the rugae are seen as parallel lines, often in association with small 'spheroid impressions' (Bland, 1984), 0.5–1.5mm in diameter and <1mm in relief (Fig. 6.6C). Petrographic thin sections demonstrate that carbonaceous laminae occur in close association with the *Arumberia* (Fig. 6.6D, Fig. 6.6E).

The structure remains enigmatic, but its tight global stratigraphic range between 630–520 Ma (Bland, 1984), association with carbonaceous laminae, desiccated nature within subaerially-exposed facies, and morphological complexity suggest that it likely represents a preserved fossilized matground organism (Kolesnikov et al., 2012; Davies et al., 2016).

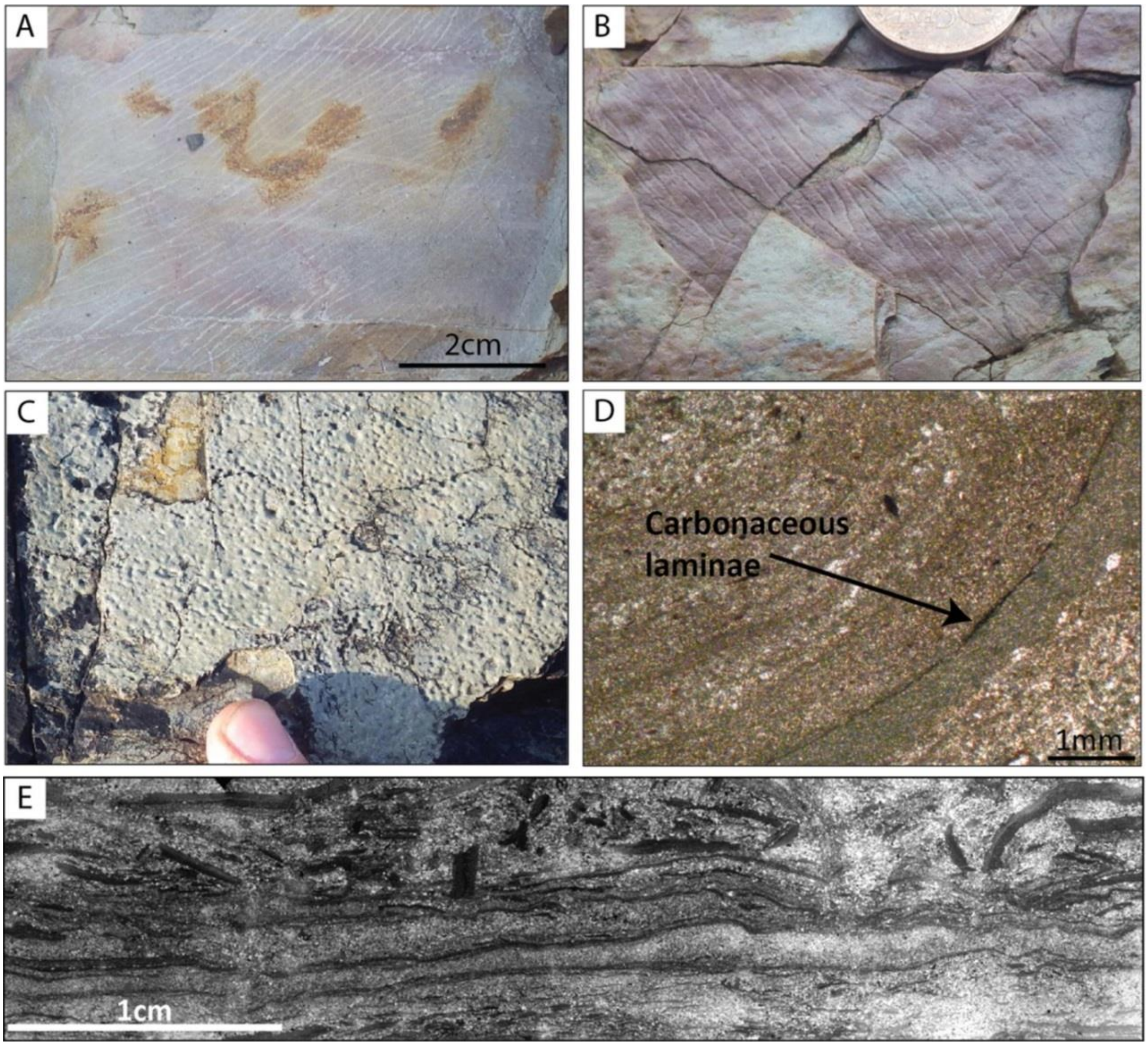

Fig. 6.6. A–B) *Arumberia* lines. Diameter of coin is 21 mm; C) Spherical impressions in association with *Arumberia*; D) Carbonaceous material (arrowed) draped over mud laminae; (E) Petrographic thin section of drab mudstone hosting *Arumberia*, showing clearly deformed mud laminae and carbonaceous material. All images from the Port Lazo Formation.

6.2.4. Microbial landscapes of the Series Rouge

With the possible exception of *Arumberia*, none of the characteristics described in the above sections are definitive proof of microbial matgrounds, when taken in isolation. However, taken together, the co-occurrence of a variety of lines of circumstantial evidence, including petrographic signals, sedimentary surface textures, *Aristophycus and Arumberia*, lend support to the contention that the depositional environments of the Series Rouge were colonized by matgrounds. There is a strong facies-dependency to these signatures. Within braided alluvial facies (Fréhel Formation), evidence for matgrounds is restricted to more quiescent subenvironments, rather than higher energy sandy channels. In coastal alluvial plain facies (Port Lazo Formation), a variety of sedimentary surface textures, *Arumberia*, and petrographic signatures all occur in close-proximity within desiccated, subaerially exposed mudstones. Thus it appears that rivers operating in the Series Rouge depositional environments would have had the potential to interact with microbial mats in both quiescent parts of their channel belts, and within their distal coastal reaches. The effect that these mats had on hydrodynamic processes is assessed below through study of the sedimentary architecture of the Series Rouge alluvium.

6.3. Sedimentary characterisitcs of the Fréhel Formation

Detailed accounts of the sedimentary facies of the Series Rouge have previously been published and are summarised in Figure 6.2 (Doré, 1972; Todd and Went, 1991; Went and Andrews, 1991; Went et al., 1988; Went, 2005, 2013, 2016; Went and McMahon, 2018) but the sedimentary architecture has been less comprehensively studied. A detailed evaluation of sedimentary architecture requires high quality, extensive exposures. The most suitable exposures in the Series Rouge occur in the Fréhel Formation. The sedimentary characteristics presented in this section entirely refer to the Fréhel Formation.

The Fréhel Formation is characterised by repetitive stacked 0.2–1.0 m thick cosets of trough cross-stratified sandstone, separated by erosional bounding surfaces (Figs. 6.7A). The spacing between bounding surfaces decreases up through the formation concomitant with a decrease in average cross-set size. Conglomerates are common towards the base of the formation, but higher up the section they are limited to laterally discontinuous lenses or layers overlying down-flow dipping accretion surfaces (Fig. 6.7B). Fine argillaceous sandstone and mudstone are scarce, restricted to very thin, discontinuous lenses and contributes <1% of total thickness. Palaeocurrents display a strongly unimodal eastwards palaeoflow direction (θ= 84°; n = 431; variance = 021°–165°), consistent with previous studies (Went and Andrews, 1991).

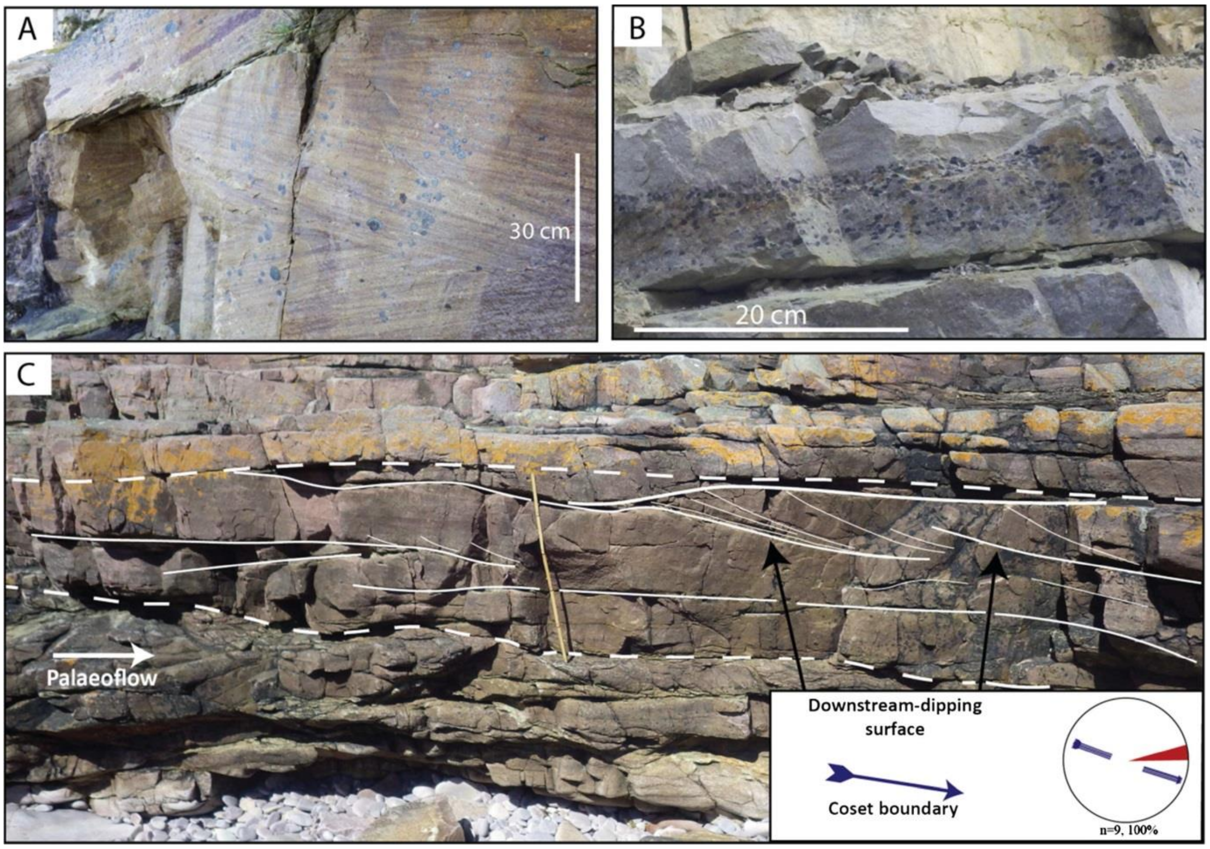

Figure 6.7. (A) Trough-cross stratification; (B) Conglomerate lying above down-flow dipping reactivation surface; (C) Example of downstream-accretion element. Percentage values under rose indicate scale of external ring. Dashed lines indicate interpreted barform top and bottom surfaces. All Fréhel Formation.

6.3.1. 'Sheet-braided' architecture of the Fréhel Formation

Sedimentary bodies in the Fréhel Formation either occur as simple sheets with aspect ratios regularly exceeding 75:1 (determining precise ratios is usually constrained by exposure), mostly recording in-channel dune migration, or as more complex interpreted barforms, representing various modes of barform accretion as well as in-channel dune migration. The majority of simple sheets consist of 1–3 stacked sets of trough cross-stratification, with planar and laterally extensive set, coset and sand-body bounding surfaces. Interpreted barforms are differentiated from simple-sheets by the presence of low-angle, inclined surfaces representing the incremental growth of individual bars. These architectural-units comprise multiple different elements: while downstream-accretion (DA) elements are by far the most abundant, lateral-accretion (LA), downstream-lateral accretion (DLA) and upstream accretion (UA) elements also occur (Table 2.2). Coset and set boundaries are typically inclined at greater angles than underlying incremental surfaces, and the lateral extent of individual surfaces is far less than in simple sheet-sandstones.

6.3.1.1. Stacked bar-forms at Pointe aux Chèvres

Stacked barforms crop out in coastal sections orientated parallel to depositional dip at Pointe aux Chèvres (Fig. 6.8). Figure 6.8A shows accretion elements within 20 successive interpreted barforms. Low-sinuosity accretion elements (DA, DLA) dominate the succession. Lateral-accretion surfaces (non-heterolithic) are apparent but uncommon. Some barforms display significant morphodynamic variation. For example, Fig. 6.9A displays a preserved barform within which the mode of bedform migration can be seen to transition from net DLA (inclined cosets 30–60° from the underlying surface) to net DA (inclined cosets 0–30° from the underlying surface) over a distance of 15 m.

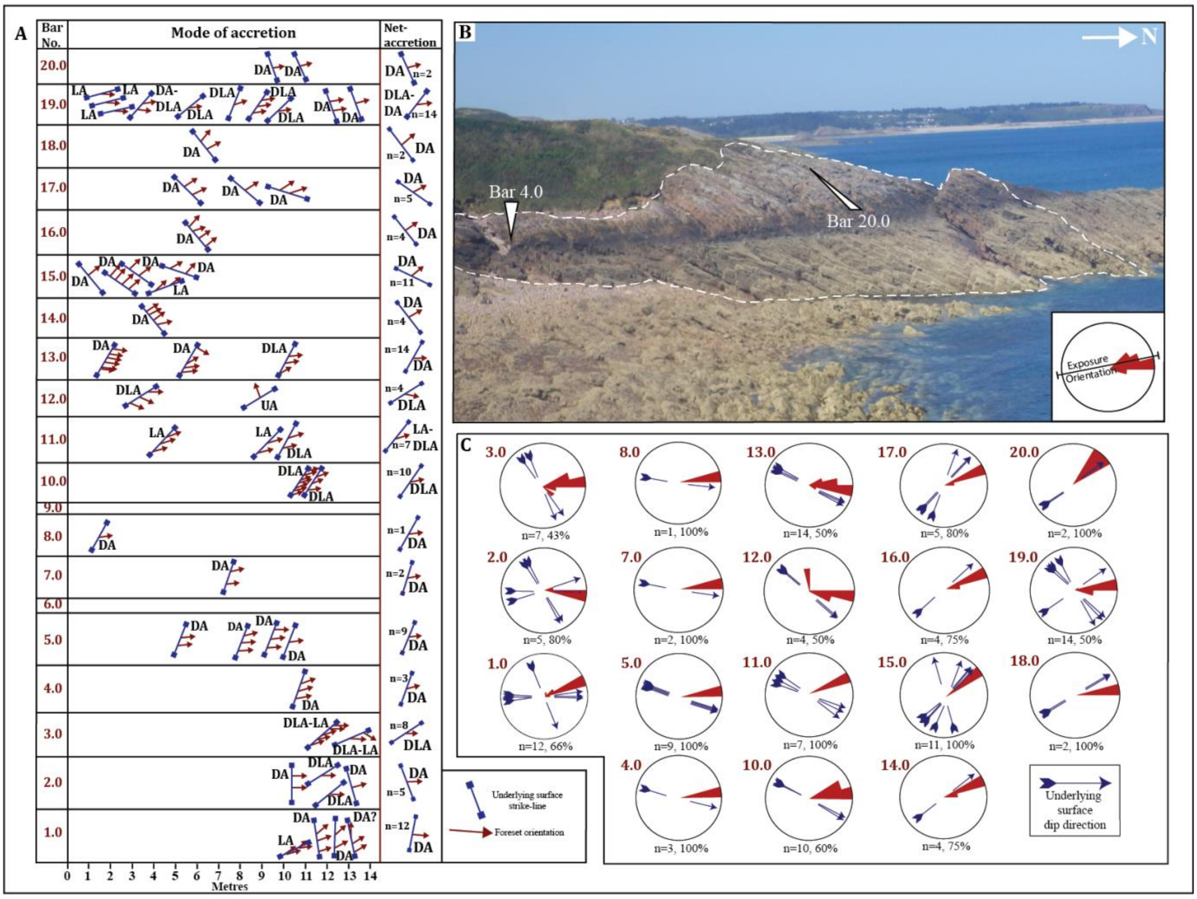

Fig. 6.8. A) Architectural analysis of Fréhel Formation cropping out at Point aux Chévres. Successive sand-bodies identified by number. The displayed data shows the relationship between set/coset inclinations (red arrows) to their respective underlying surfaces (strike-lines represented by blue barb). Accretion elements are mapped on in their exact lateral position within the respective sandbody (horizontal scale). No vertical scale intended. Acronyms relate to inferred architectural element (Fig. 2.2; Section 2.1.2). Sandy bedforms are not included in diagram; B) Succession presented in (A); C) Rose plots of sandbodies from (A). Blue arrows show dip direction of genetically related surfaces (presented as strike-lines in (A)). Percentage values under rose diagrams display circumference scale. Measurements: Palaeoflow, n = 116; Bounding surfaces, n = 51.

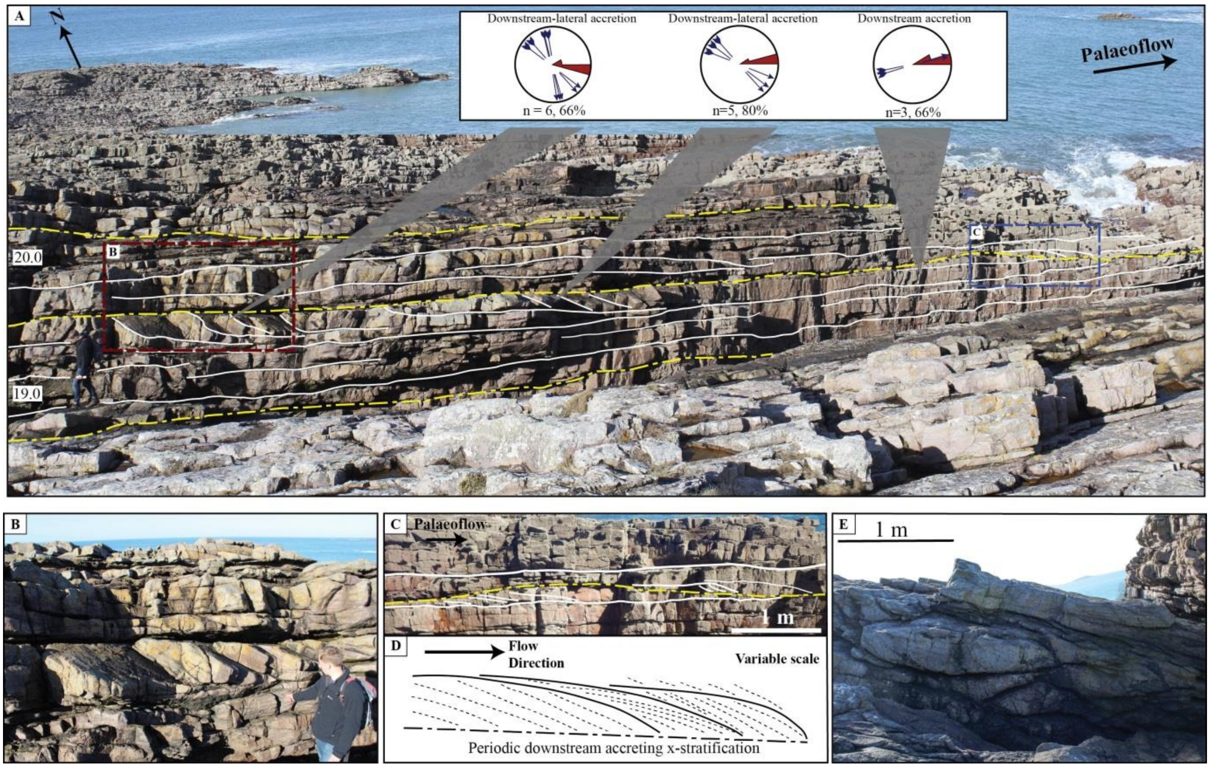

Fig. 6.9. A) Proximal down-flow variations of accretion within individual barform. Person is 187 cm tall. Yellow lines denote lower and upper surfaces of interpreted barform; B) Example of a downstream-lateral accretion element. Person is 187 cm tall; C) Downstream-accretion element; D) Schematic diagram of prograding stack of downstream-accretion elements; E) Trough-cross stratification. All images from Fréhel Formation, Series Rouge.

Depositional-strike exposures were also studied at Pointe aux Chèvres. These most commonly display a 'sheet-braided' architecture, with thin, tabular sand-bodies extending laterally for at least 55 m. Channel-margins are notably rare (2 occurrences), but where present they exhibit <1 m in erosional relief and are gently-dipping. Subordinate discontinuous bedding is apparent (Fig. 6.10), typically characterised by planar cross-stratification which diminishes in thickness towards sand-body margins. In one instance, discontinuous bedding is succeeded by a thin (<10 cm) red mudstone (possible bar-top hollow fill) (Fig. 6.10C). In thin section, this mud bore carbonaceous material and abundant detrital mica (see Section 6.2.1; Fig. 6.10D).

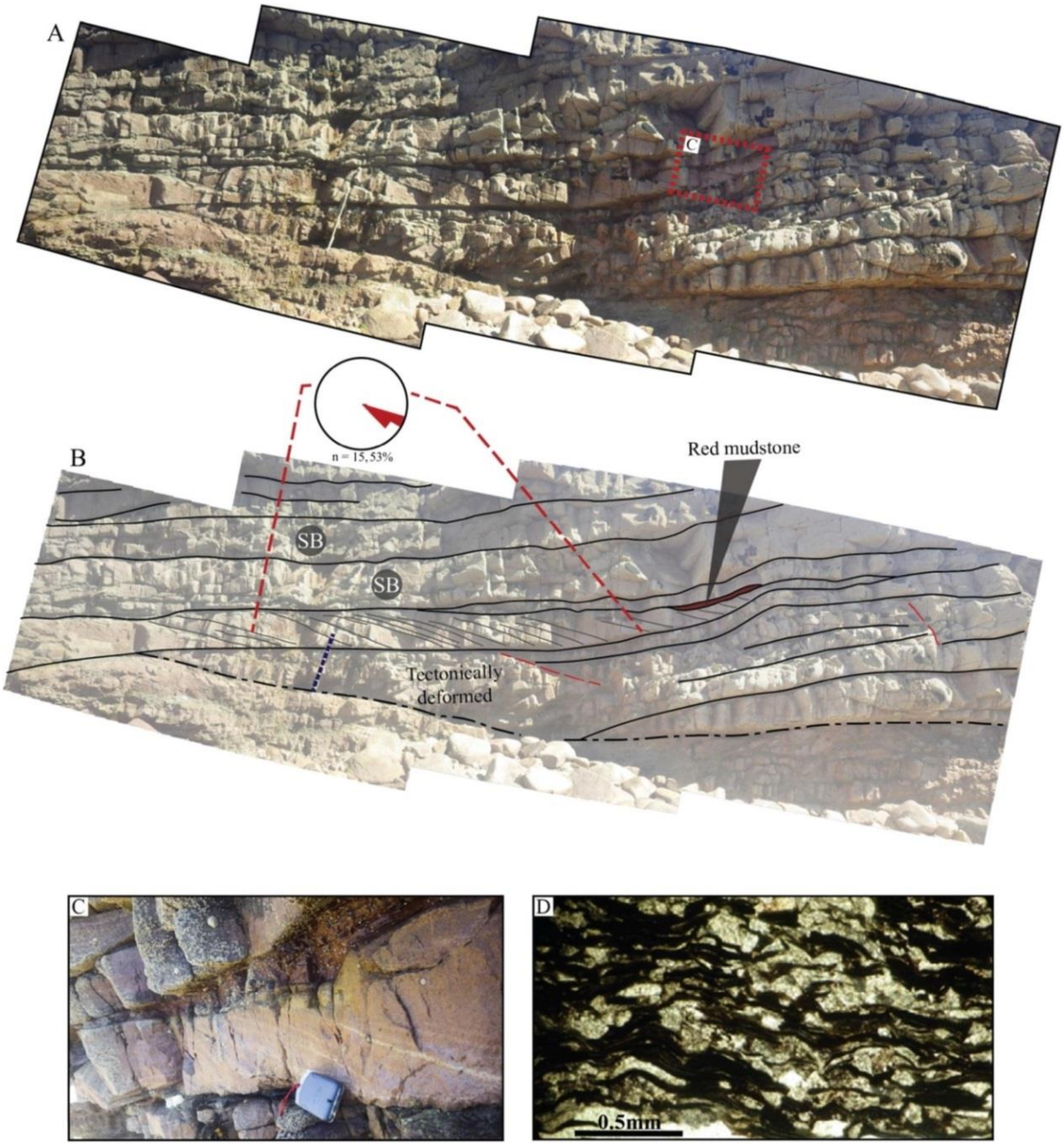

Fig. 6.10. A) Discontinuous sandstone body within along-strike section at Pointe aux Chèvre, Fréhel Formation. Metre rule for scale; B) Interpretative line drawing of A; C) Thin mudstone layer highlighted in B. Compass-clinometer is 10.5 cm long; D) Petrographic thin section of mudstone in C, displaying wavy-crinkly laminae constituted by detrital mica. SB = Sandy-bedform (see section 2.1.1.1)

6.3.1.2. Oblique to depositional-strike architecture at Sables d'or quarry

Quarry faces at Sables d'Or (regional location indicated on Fig. 6.1) provide intermittent depositional-dip and depositional-strike exposure of both simple sheets and interpreted barforms, extending 1.3 km in total and >125 m continuously. Sand-bodies are 1–3.5 m thick and commonly exceed exposure width. No fine grained horizons were observed, but mud clasts are common.

Typical sand-body architecture is presented in Fig. 6.11. Vertical cliff exposures were inaccessible in their upper levels; palaeocurrents were not estimated in these levels as they could not be directly measured (note, the prefix 'i' before element acronyms in the upper portion of the outcrop, indicating that these elements were 'interpreted' only and not directly measured, see Section 2.1.2 for methodology).

Trough cross-stratification is near-ubiquitous, with cross-set thickness displaying no upwards decrease within individual bodies. No facies transition occurs across major surfaces, even on inclined surfaces representing barform growth. Major erosional bounding surfaces are dominantly planar. Reactivation surfaces bounding cosets vary significantly in their lateral extent. In simple sheets, these surfaces are predominantly planar, and regularly extend laterally for over 60 m. Within interpreted barforms, gently dipping accretion surfaces rarely exceed 30 m before terminating against major erosional surfaces (Fig. 6.11). Gently inclined erosional scours also dissect individual sand-bodies, possibly representing fluctuating stages and bedform alignment within the overall system (e.g., Fahnestock, 1965; Cant and Walker, 1978; Miall, 1985).

Sandy-bedforms are the dominant element in depositional-strike/oblique exposures. Clear DA and DLA elements are discernible in places. Inclined surfaces representing possible sandy lateral accretion (iLA) are present but have minimal contribution to the overall architecture (Fig. 6.11). Preserved channel margins are rare (4 occurrences) (Fig. 6.11). Maximum dip of channel margins varies from 5° - 18°.

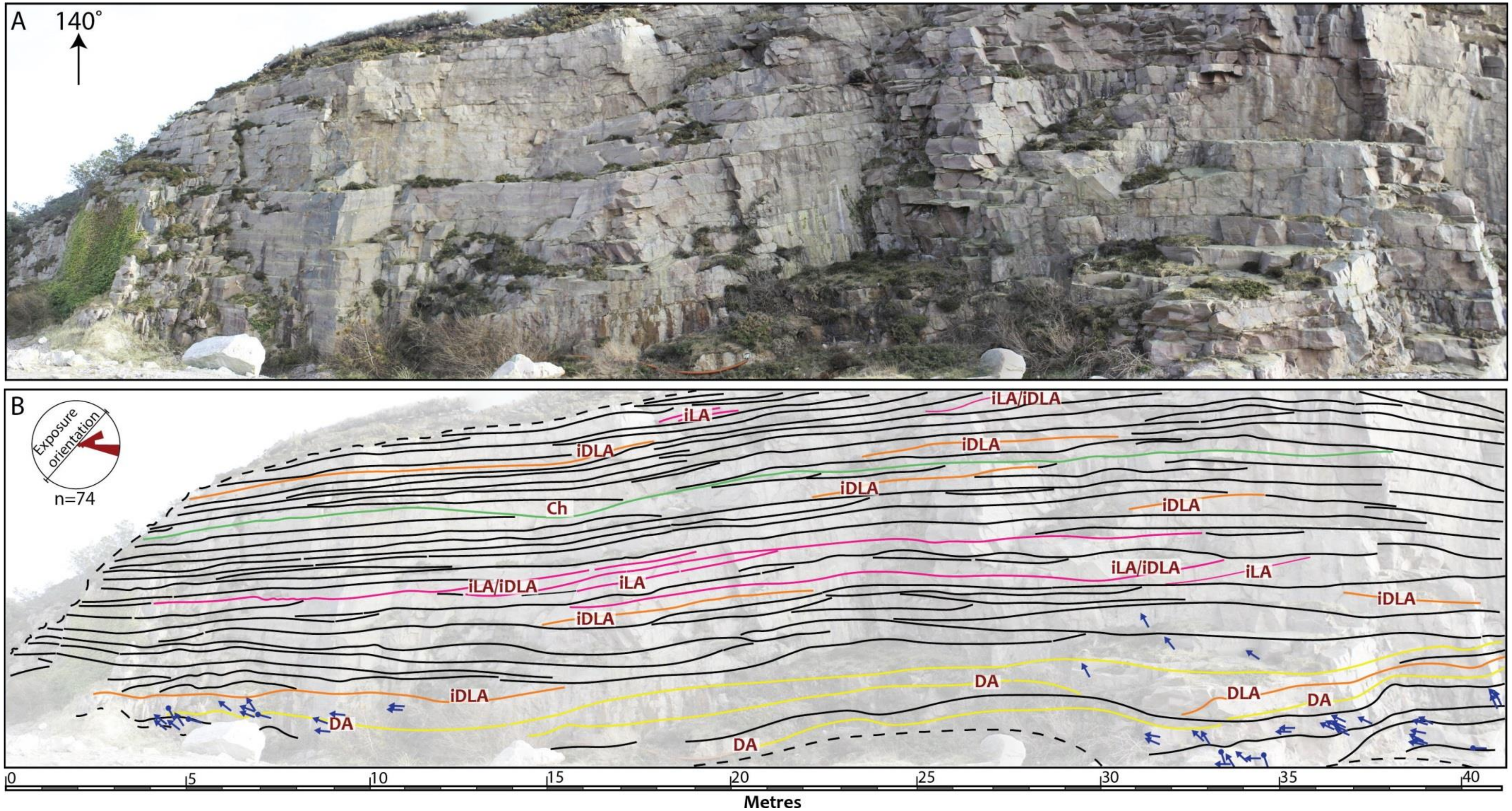

Figure. 6.11. A) Photograph of alluvium at Sables d'Or quarry; B) Interpreted architecture of alluvium. Panel demonstrates the high lateral continuity of sandbodies. Blue arrows represent palaeoflow orientations measured from cross-bed foresets. Blue pins represent dip directions of set/coset boundaries. The directions indicated by the arrows and pins have been corrected for tectonic tilt, and are organized with respect to the architectural panel so that arrows pointing up indicate dip directions away from the observer, and those pointing down indicate dip directions towards the observer. Procedure after Long (2006). Architectural elements annotated (lines denote architectural element type: Yellow, DA; Orange, DLA/iDLA; Pink, LA/iLA; Green, Channel; Black, SB/iSB).

6.3.2. Interpretation of fluvial style

The Fréhel Formation almost exclusively consists of stacked, sandstone sheets, typically 1–2 m thick, with sedimentation dominated by in-channel dune migration, and with rarely observed channel margins less than 0.5 m high. Stacked accretion elements (Fig. 6.8A) demonstrate that not all sand-bodies were deposited in single episodes of flooding so flow may have been perennial (Bristow, 1987; Best et al., 2003; Long, 2006) (Chapter 4). Mudrock is scarce in the Fréhel Formation. This may relate to the poor preservation of bar top and floodplain facies: most sandbodies are erosionally truncated, indicating only partial preservation of alluvium during river aggradation. Alternatively, the paucity of mudrock may reflect sediment bypass (due to highly variable discharge or aeolian winnowing; Long, 1978; Dalrymple et al. 1985; Aspler and Chiarenzelli, 1997; Went, 2005) or a lack of mud in the system (i.e., inherently low mud production due to the absence of vegetation-mediated weathering; Davies and Gibling, 2010a). The rare discontinuous mud lenses that are present are interpreted to have been deposited in slackwater parts of the channel belt.

Barform orientations indicate that there was an overall low-sinuosity to the sand-dominated fluvial system, with the majority of identified accretion elements only migrating 0–30° relative to underlying, down-flow dipping surfaces. The near ubiquity of trough cross-stratification throughout the sequence can be seen to be the result of normal in-channel sedimentation dominated by migrating sinuous-crested dunes. Rare sandy lateral-accretion surfaces likely reflect lateral accretion on in-channel bars within this low-sinuosity system (Bristow, 1987).

The predominant sedimentary style of the Fréhel Formation is thus one of ‘sheet-braided’ architecture with very low mud content, likely reflecting sedimentation from a large, low-sinuosity, perennial braided river. The sedimentary characteristics of the formation are consistent with typical pre-vegetation sandy alluvial successions in that they present an overall ‘sheet-braided’ architecture (discussed in Section 7.2.2) at normal outcrop scale (e.g., Long, 1978, 2006; Fedo and Cooper, 1990; Rainbird, 1992; McCormick and Grotzinger, 1993; Nicholson, 1993; MacNaughton et al., 1997; Eriksson et al., 1998; Köykkä, 2011; Marconato et al., 2014; Ielpi and Rainbird, 2015). This remains the case even in the rare instances where small discontinuous mudstone lenses which host evidence of microbial life occur.

6.4. Reasons to doubt matgrounds as stabilizing agents

The meso-scale 'sheet-braided' architecture of the Fréhel Formation (Section 6.3) demonstrates that there is no evidence suggesting that matgrounds (Section 6.2) offered any level of landscape stability to the Series Rouge fluvial systems that could be compared to that provided by land plants in Silurian and younger counterparts. This is contrary to studies that have hypothesised that microbial mats might have fulfilled a similar role to land plants, as geomorphic stabilizers, on pre-vegetation Earth (e.g., Bose et al., 2012; Petrov, 2014, 2015; Ielpi, 2016; Santos and Owen, 2016). However, this is perhaps unsurprising as, in order for biostabilization to significantly affect fluvial deposits, it is vital that any biological cohesion exceeds physical erosive forces. Four lines of evidence suggest that microbial mats do not and could not have provided such requisite levels of cohesion, and are discussed in the following sections.

6.4.1. Matgrounds are surficial features

One key difference between matgrounds and higher land plants is that the latter have deep substrate anchorage, accentuated by palimpsesting of multiple generations of roots. The increased cohesion associated with such underground roots has been demonstrated to provide reinforcement of bank sediments (e.g., Smith, 1976; Bridge, 1993), increasing the critical shear stress of river banks and limiting undercutting. In a classic study, Smith (1976) demonstrated that, within the Alexandra Valley (Canada), grass roots on the floodplain margins of river channels accumulated down to depths of 7.6 m; far in excess of the depth required to reinforce banks against caving (in this instance, 3.5 m – the depth of the adjacent channel). Conversely, modern microbial mats attain maximum thicknesses of several centimetres and only persist near the substrate surface (de Beer and Kühl, 2001) due to their rapid decomposition following burial by even thin event layers of sediment (e.g., Black, 1933; Krumbein and Swart, 1983; Chafetz and Buczynski, 1992; Konhauser, 2007).

Considering that the limited root penetration of the earliest embryophytes (Edwards et al., 2015) had a limited effect on alluvial architecture, and that bank stabilization by roots did not develop until deeper rooting near the Siluro-Devonian boundary (e.g., Gensel et al., 2001; Hillier et al., 2008; Davies and Gibling, 2010a; Kennedy et al., 2012), it is unsurprising that even less-penetrative surficial mats left no evidence for having any effect on bank stability. Microbial mats can offer no protection against the undercutting of substrates on which they rest, yet bank undercutting is the primary erosive mechanism of lateral fluvial channel migration.

A further difference between microbial mats and land plants is the latter frequently alter surface microtopography which in turn reduces flow velocity (Bouma et al., 2013; Moor et al., 2017).

6.4.2. Matground properties change when emergent

A further difference between microbial mats and land plants is that the latter have the capacity to develop structure above the water-table and do not necessarily undergo changes to their physical properties (as mechanical components of the fluvial system) whether they are submerged, wet, or dry. In contrast, matgrounds exist in an elastic state when they are respiring, but only respire when they are submerged in water. When they dry out and stop respiring, they behave in a brittle fashion and may easily become detached from a substrate through desiccation, shrinkage and curling. The bulk of studies that have looked at the sedimentological influences of microbiota are usually only concerned with mats in their elastic state (e.g., Gerdes, 2007; Hagadorn and McDowell, 2012; Vignaga et al., 2013). Even when substrates are wet, matgrounds may still detach: 1) if the physical forces acting on them exceed their biological cohesiveness (Moulin et al., 2008; Graba et al., 2010, 2013, 2014); or 2) by autogenic buoyancy-mediated detachment processes (Boulêtreau et al., 2006; Mendoza-Lera et al., 2016).

As river channel migration occurs primarily through undercutting of emergent substrates, it should be expected that those mats on raised banks adjacent to active channels would usually comprise dried, surficial microbial mats that would provide negligible reinforcement against bank erosion (although biological soil crusts may be an exception).

6.4.3. There are no modern analogues of matground-stabilized rivers

No published studies of modern rivers were identified which suggested that microbial mat or biological soil crust communities can stabilize river banks. Modern rivers that exist in the complete absence of any form of vegetation are rare or non-existent at the present day (Davies et al., 2011).

6.4.4. There is no physical evidence in the rock record for matground stabilized rivers

There are relatively few records of observed microbial matground fabrics within pre-vegetation alluvial strata (Prave, 2002; Parizot et al., 2005; Yeo et al., 2007; Rasmussen et al., 2009; Sheldon, 2012; Beraldi-Campesi et al., 2014; Wilmeth et al., 2014; Petrov, 2014, 2015) (Chapter 5). Modern examples of microbiota from the sparsely vegetated Mimer River, Spitsbergen (Davies, personal communication) provide a potentially analogous explanation for this paucity of matground evidence in ancient alluvium. If their pre-vegetation counterparts occupied similar reaches of ancient braidplains, it should be expected that they would have very limited preservation potential in the rock record: lacking the capacity to resist physical reworking, they essentially occupy erosional, rather than depositional, subenvironments of the fluvial system. Their occurrence in the rock record is thus limited to fortuitous instances where components of such subenvironments have only undergone partial erosion (e.g., the rare mud horizons or intraformational clasts of the Fréhel Formation).

The limitations of microbial mats as pre-vegetation stabilizers of alluvial landscapes are further revealed by the global stratigraphic record of microbially-induced sedimentary structures. In a table demonstrating previously-published reports of MISS, and the facies from which they were recorded, Davies et al. (2016, their Table 1) listed only 5 instances of pre-vegetation fluvial MISS (8.2% of the total Precambrian to mid Silurian records across all sedimentary environments (n=61)), compared to 11 instances of post-vegetation MISS (31.4% of the total late Silurian to Cretaceous records (n=35)). This suggests that, while MISS were present in Earth's fluvial environments since at least the Proterozoic, they were far more commonly preserved after the evolution of land plants. That is, once the more muddy and quiescent fluvial subenvironments most commonly colonized by microbial mats (floodplains, etc.) began to become deeply stabilized by roots, less prone to wholesale reworking during deposition, and more readily preserved in the rock record. This observation provides further circumstantial evidence that the stabilization, and preservation potential, of certain fluvial facies afforded by terrestrial vegetation was several orders of magnitude greater than that afforded by microbial mats alone.

6.5. Microbiota of the Series Rouge - Conclusion

The Series Rouge of northwest France contains a wealth of individual circumstantial lines of evidence for the presence of microbial mats which, combined, suggest that the fluvial systems active during deposition operated within a 'microbial landscape'. Despite this, there is no evidence that microbial mats increased the stability of any components of the fluvial system. The fluvial deposits are characterised by repetitively stacked beds of trough cross-stratified sandstone representing deposition from migrating sinuous crested dunes in low sinuosity channels and on predominantly downcurrent-dipping barforms. Frequent channel-switching led to selective preservation of deep channel-bar deposits such that the preserved sedimentary architecture is 'sheet-braided' at outcrop scale; the typical stratigraphic record of many other pre-vegetation fluvial systems.

Through a critical understanding of the ways in which microbial mats may affect sedimentation, coupled reference to the global stratigraphic record of alluvial microbially induced sedimentary structures, it is shown that microbial mats alone were very weak agents of geomorphic stabilization. In the pre-vegetation world, they were several orders of magnitude less effective at buffering against erosion when compared to the land plants that began to share their non-marine habitats from the Palaeozoic onwards (Fig. 6.12). The influence of microbial mats on the sedimentary characteristics of pre-vegetation alluvium is thus shown to have been negligible. As a result, the stratigraphic sedimentary record is biased in only preserving a record of the dominant purely physical processes in such systems.

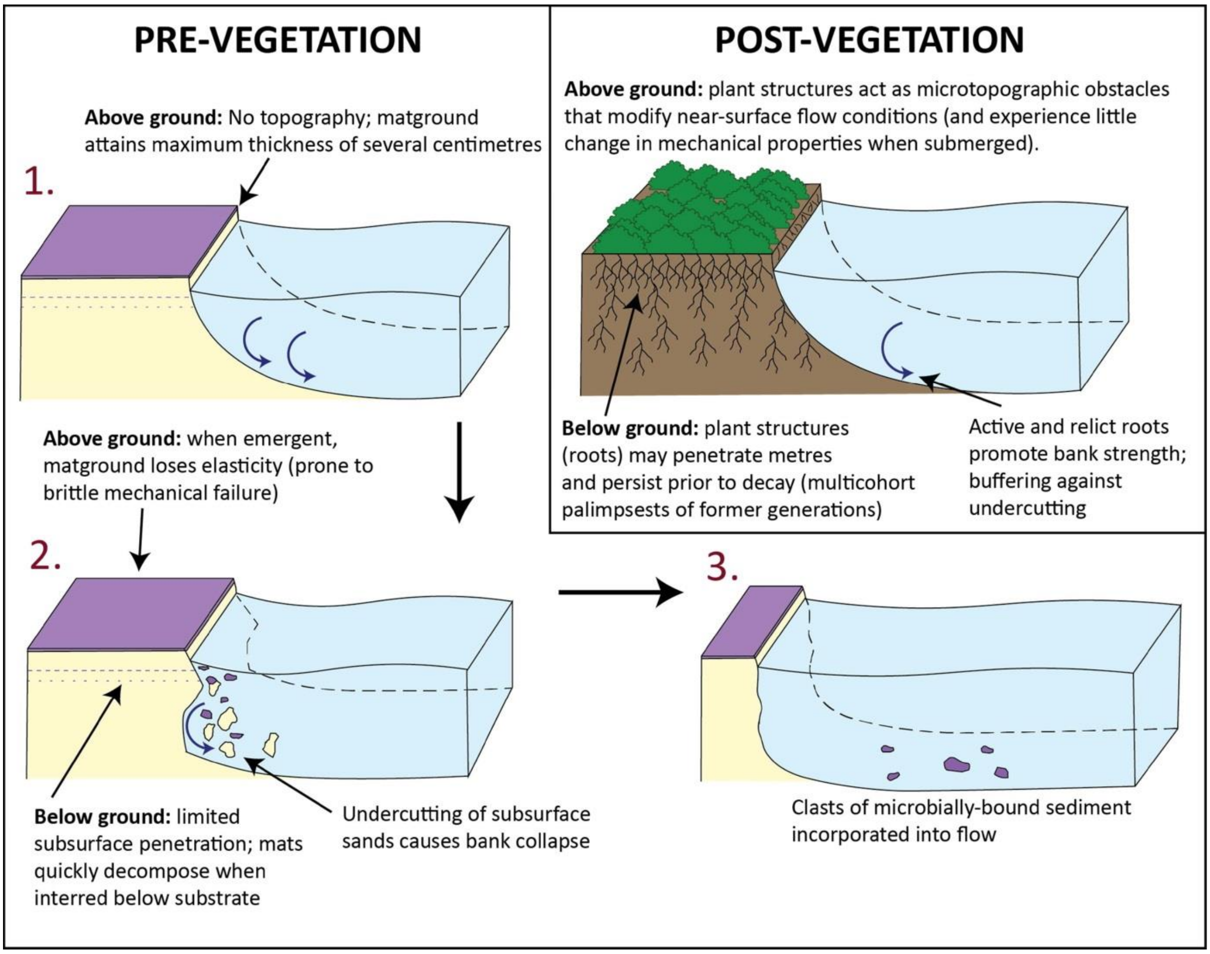

Fig. 6.12. Schematic reconstruction of the relationships between: 1) matgrounds and unvegetated river channels; and 2) embryophytes and other higher land plants and river channels.

Despite this, surficial microbiota did apparently leave much smaller scale clues to their presence and activity within pre-vegetation systems. In the Series Rouge, these include a suite of potential microbial sedimentary surface textures, distinct ‘‘pseudofossils” such as *Aristophycus* and *Arumberia*, and petrographic indicators, such as biotite accumulations and associated carbonaceous laminae. This indicates that some of the oldest communities of life on land were able to bestow an influence on the long-term rock record, even though they lacked an ecosystem engineering capacity to geomorphically sculpt the landscapes that they once inhabited.

6.6. Chapter summary

Earth’s Precambrian continents likely hosted abundant microbial mats and biofilms (e.g., Horodyski and Knauth, 1994). Chapter 6 aims to understand how a microbial influence may have been exerted on pre-vegetation rivers as perceived in the alluvial rock record, with specific reference to the Ediacaran-Cambrian ‘Series Rouge’ of northwest France. The Series Rouge is well-suited for this study as it contains both extensive exposures of alluvial architecture and multiple lines of evidence for former microbial mat colonies. Series Rouge deposits cover a range of depositional environments (Fig. 6.2), though this chapter considers Fréhel Formation alluvium most fully. Evidence for microbial life during deposition is made from multiple differing observations (petrography, sedimentary surface textures and pseudofossils). Rarely preserved mudstones contain petrographic evidence for reworked microbial mat fragments (Section 6.2.1) and, when exposed, mudstone bedding planes host a variety of sedimentary surface textures with possible biogenic origins (transverse wrinkles, 'bubble' textures, epirelief bulges, ruptured domes, 'elephant skin texture', curved shrinkage cracks, reticulate markings; see Section 6.2.2). Two instances of the enigmatic branching 'pseudofossil' *Aristophycus* also occur (Section 6.2.3), with petrographic evidence demonstrating a microbial formation mechanism. Additionally, alluvial plain facies contain *Arumberia*, another enigmatic psuedofossil with a preferred microbial origin (Section 6.2.4).

The co-occurrence of a variety of lines of circumstantial evidence for former microbial mats lend support to the contention that the depositional environments of the Series Rouge were colonized by matgrounds. Despite this, preserved alluvium contains no evidence of significant bank stability. The predominant sedimentary style is one of 'sheet-braided' architecture with very low mud content, likely reflecting sedimentation from a large, low-sinuosity braided river. These sedimentary characteristics are entirely consistent with typical pre-vegetation sandy alluvium at normal outcrop scale (discussed in Section 7.2.2) thus alluvial architecture provides no evidence to suggest that matgrounds offered any level of significant landscape stability. Furthermore, there is a strong facies-dependency to microbial signatures within alluvial facies, with matground evidence being restricted to more quiescent subenvironments, rather than higher energy sandy channels.

Through a critical understanding of the ways in which microbial mats may affect sedimentation, Section 6.4 discusses why microbial mats alone lacked the ecosystem engineering capacity to sculpt the landscapes they occupied. Microbiota did have the capacity to leave smaller scale clues to their presence (e.g., sedimentary surface textures, pseudofossils) thus demonstrating that some of the oldest communities of life on land were capable of bestowing a minor influence on the ancient sedimentary record.

Chapter 7

PLANFORM DIVERSITY OF PRE-VEGETATION RIVERS

7.1. Introduction

It is not possible to see a pre-vegetation river: these geomorphic entities went extinct c.473 Ma when the first embryophytes began to colonize alluvial settings (Rubinstein et al., 2010). This truism is important to concede when aiming to understand what fluvial planform looked like prior to the evolution of vegetation: it means the question can only ever be approached indirectly. Three lines of reasoning have been employed to hypothesize the nature of pre-vegetation rivers: 1) modern geomorphological observations; 2) numerical and analogue modelling; and 3) geological evidence. Each of these methods is not without limitations: 1) geomorphological approaches are hampered by an absence of modern fully unvegetated rivers and an inability to observe systems operating outside of the present Earth condition (i.e., a post-glacial world with a specific tectonic configuration, on which plants have existed, and potentially accumulated effects [e.g., mudrock], for 473 Ma); 2) modelling approaches are reliant on an accurate understanding of the pre-vegetation laws of nature, which are only inferable from these partial modern analogues, and additionally suffer from practical scaling problems (e.g., Kleinhans, 2009); and 3) geological approaches rely on deferring to the 'best possible' explanation, and are thus at risk of becoming overly qualitative in the process of adjudging what 'best possible' means (particularly as the 'best possible' explanation may fundamentally not yet be knowable, or be knowable but not be thought about, during the reasoning process). Of these approaches however, the third is the only one which directly deals with the tangible sedimentary record of pre-vegetation rivers (i.e., it is the only path of reasoning to utilise physical material that actually existed when pre-vegetation rivers were in operation). This chapter is based solely on such a geological approach, reviewing: 1) the means by which ancient fluvial planform may be inferred using geological observations; 2) trends in sedimentary rock character that distinguish pre-vegetation and syn-vegetation alluvium; and 3) a case study from the Torridonian in which a rare example of pre-vegetation strata previously interpreted as the deposits of a meandering river system occur.

7.1.1. Rocks vs. Rivers

Geological studies of ancient alluvium aim to describe preserved sedimentary characteristics and give an explanation for their formation. Frequently, this explanation involves an attempt to interpret the geomorphic planform of ancient river channels: an interpretation made possible because modern rivers with different geomorphic planforms (e.g., braided vs. meandering (end-members)) are known to accrete sediment in different ways, due to differences between the flow patterns within their channels and fluctuations in their discharge. The notion that ancient alluvial strata may be diagnosed as being deposited by a particular channel planform can be traced back to precursor facies models such as those of Allen (1964, 1970), in which particular heterolithic vertical successions of the Anglowelsh Old Red Sandstone were interpreted as having been deposited in point bars of sinuous streams (Fig. 7.1). Allen's (1964, 1970) interpretations were made possible by detailed bed-by-bed lithological and palaeocurrent analysis (of outcrops with limited exposure) (Fig. 7.1). Following the subsequent development of conceptual models for the deposits of 'typical' braided rivers (Cant and Walker, 1976), Allen's (1964, 1970) models (originally erected for specific Anglowelsh Old Red Sandstone examples) became adopted as archetypal counterpoints during the development of the 'facies model' paradigm (Walker, 1976) and have since been widely promoted in sedimentology textbooks. Hereafter, strata that bear similar signatures to Allen's (1964, 1970) examples are described as belonging to the 'classic meandering facies model' (CMFM).

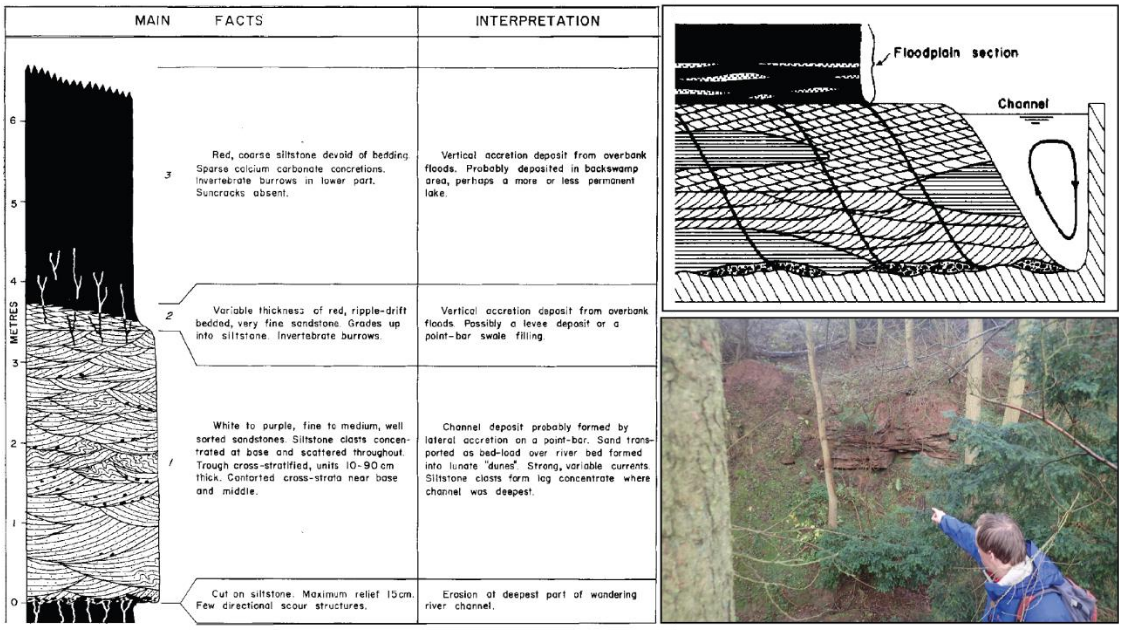

Figure 7.1. Clockwise starting from the left: Allen's (1964) generalized succession and interpretation of a cyclothem at Ludlow; Allen's (1970) generalized composite cyclothem sequence; Typical exposure quality of the Anglowelsh Old Red Sandstone at Ludlow described by Allen (geologist is 187 cm tall). Allen (1964) summarized that each cyclothem recorded a floodplain sequence at its simplest: point-bar sands overlain by topstratum deposits (i.e., overbank deposits).

Even early proponents of facies models noted that the universal applicability of the CMFM was limited without further integrated work (Walker and Cant, 1979). However, further testing has raised questions about the CMFM, because its characteristics may be equivocal for diagnosing meandering, especially when the full complexity and diversity of fluvial sedimentary environments are considered (e.g., Jackson, 1977; Bridge, 1985, 1993; Ethridge, 2011; Colombera et al., 2013; Hartley et al., 2015). In other words, "meandering facies" (e.g., CMFM strata) can be a recurring geological characteristic of sedimentary rock, but cannot always be considered synonymous with geomorphic "meandering rivers": CMFM strata need not always have been deposited by meandering rivers, and meandering rivers need not always deposit CMFM strata. Yet, even with this caveat, CMFM strata are hugely significant for our understanding of pre-vegetation alluvium. This is because it has been recognised for four decades that sedimentary rock successions bearing the signatures of the CMFM are apparently absent (or at least exceedingly rare) in strata that pre-date the evolution of land plants (Cotter, 1978; Davies and Gibling, 2010a). While there are exceptions (see Section 7.3), a general approximation is that whilst syn-vegetation strata may or may not bear the hallmarks of the CMFM, pre-vegetation strata almost uniformly do not. Coevally with this major stratigraphic shift in the frequency distribution of CMFM strata, other architectural signatures of alluvium are seen to change. Chief amongst these are 'sheet-braided' strata (sedimentary successions composed primarily of beds with >20:1 aspect ratio (Cotter, 1978, Davies et al., 2011), see section 7.2.2), which in the Silurian become extremely uncommon (Gibling and Davies, 2012) having been the near-ubiquitous architectural style since the Archean (Fig. 7.2).

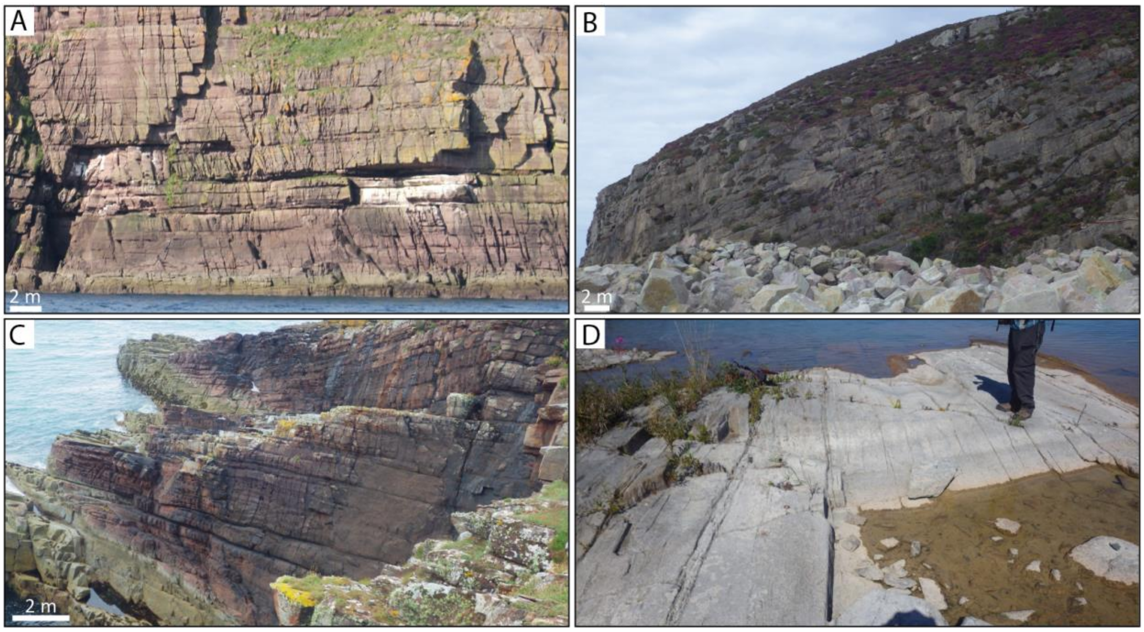

Figure 7.2. Examples of 'sheet-braided' architecture: A) Neoproterozoic Applecross Formation, Scotland (Chapter 4); B) Ediacaran-Cambrian Series Rouge, France (Chapter 6); C) Mesoproterozoic Meall Dearg Formation, Scotland (Chapter 5); D) Archean Jackson Lake Formation, NW Territories, Canada. Person for scale is 196 cm.

To clarify, throughout this chapter, both the CMFM and the 'sheet-braided' style refer solely to *sedimentary rock characteristics* and not geomorphology. The terms used to describe them carry false interpretive baggage regarding fluvial planform, but this is an artefact of their erection during the facies model boom of the 1970s and 80s, during which diagnostic models were often over-confidently prescribed. This clarification is essential because, in recent years, a conflation between rock signature and river has become commonplace in published literature (e.g., Ielpi and Ghinassi, 2015; de Almeida et al., 2016; Ielpi and Rainbird, 2016a).

7.2. Interpreting pre-vegetation river planform from outcrop

In recent years there has been ongoing dispute about whether or not meandering rivers existed prior to the evolution of land plants (Eriksson et al., 1998; Els, 1998; Retallack et al., 2014, 2015; Ielpi, 2016; Santos and Owen, 2016; Santos et al., 2017a,b). In order to evaluate the merits of a geological approach to answering the question as to whether pre-vegetation meandering rivers existed, it is first necessary to understand: 1) the character of sedimentary rock that has previously been placed within the classic meandering facies model; and 2) the history of the term "sheet-braided", which has led to recent contentions regarding pre-vegetation alluvium, despite being the dominant architectural style.

7.2.1. Classic meandering facies: lateral accretion and inclined heterolithic strata

As noted in Section 7.1.1, identifying channel planform from ancient alluvium may not be as simple as was thought during the inception of the facies model paradigm (e.g., Ethridge, 2011; Colombera et al., 2013; Hartley et al., 2015). From modern analogue, these were known to comprise laterally accreting inclined heterolithic stratification (LA-IHS), in association with other characteristics such as: 1) thick mudstones interbedded with channelized sandstones, thought to record the dominance of overbank floodplain deposits relative to in-channel sediment; 2) palaeocurrent variance, which may indicate channel sinuosity; and 3) channel bodies displaying a degree of organisation, usually with upward fining and change in sedimentary structures, related to meandering channel-planforms (Bernard et al., 1962; Allen, 1963; Ore, 1964; Thomas et al., 1987). The most robust interpretations of ancient meandering rivers identify multiple of these criteria, with a particular emphasis on LA-IHS; although it should be noted that a number of earlier publications based 'meandering' interpretations on only weak evidence.

Inclined heterolithic stratification (IHS) are typically seen in vertical cross-section in the sedimentary record where they consist of packages of sigmoidal beds of alternating grain-size inclined relative to the local tectonic dip (Fig. 7.3). If fully preserved, a gently dipping topset passes through an inflection point to a steeper dipping foreset and then through another inflection point to a gently dipping bottomset which terminates asymptotically against a basal erosion surface. Overlying strata often erosionally truncate topsets. Where the steepest part of the foresets of IHS can be determined to dip near orthogonal to neighbouring palaeocurrent directions, they are classified as heterolithic examples of the lateral accretion (LA) architectural elements (Miall, 1985; originally termed 'epsilon cross-stratification' by Allen, 1963) (Section 2.1.2; Fig. 2.2).

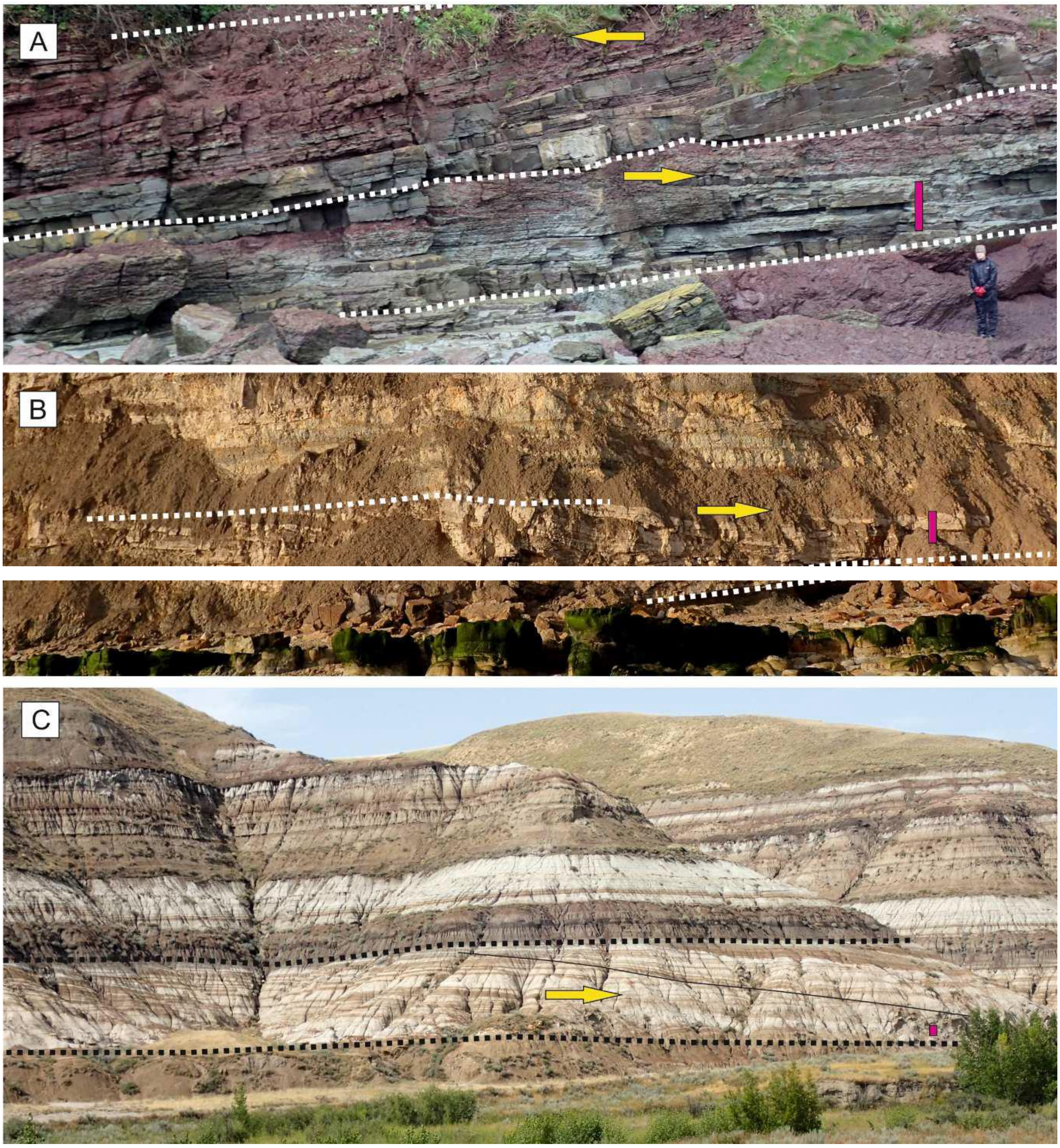

Figure 7.3. Outcrop expressions of LA-IHS recording point bar deposits of various scales. In each image, dashed line shows bounding surfaces of the LA-IHS element, yellow arrow shows general direction of migration, and pink bar represents one metre vertically: A) Two superimposed LA-IHS packages in broadly opposed directions. Underlying mudrock contains vertisol structures; strata deposited in a fluvial floodplain environment. Late Silurian (Pridolian) Milford Haven Group, Llansteffan, Carmarthenshire, Wales; B) Isolated LA-IHS within estuarine facies. Early Cretaceous Ashdown Formation, Fairlight, East Sussex, England; C) Large scale LA-IHS with internal erosion surface, recording deposition within a tidally-influenced meandering point bar. Late Cretaceous Horseshoe Canyon Formation, Willow Creek, Alberta, Canada.

The subtle distinction between IHS and LA should not be overlooked: although certain stratal packages may be diagnosed as both IHS and LA sets, not all IHS are LA sets and not all LA sets are IHS (Fig. 7.4). Individually, both IHS and LA sets can develop in low-sinuosity systems, whereas LA-IHS packages appear to require the existence of channel meanders in order to develop. This is because, in meandering channels, lateral accretion sets are deposited when flowing water is centrifugally deflected from the inner to outer bank of a curve, forcing helical overturn within the water body and inner bank accretionary sedimentation by the secondary current that moves obliquely up slope of the inner channel bend (e.g., Leopold and Wolman, 1960). This process, combined with outer bend erosion, leads to lateral movement of the channel position and point bars that develop with the shift in the position of the inner bank. Such point bars are often internally composed of LA-IHS, and prolonged migration into a former channel leads to a 2D stratigraphic vertical profile (e.g., in core or log) in which an erosional lower bounding surface (the original channel floor) is overlain by coarser-grained IHS bottomsets, succeeded by younger iterations of IHS foresets and ultimately finer-grained topsets.

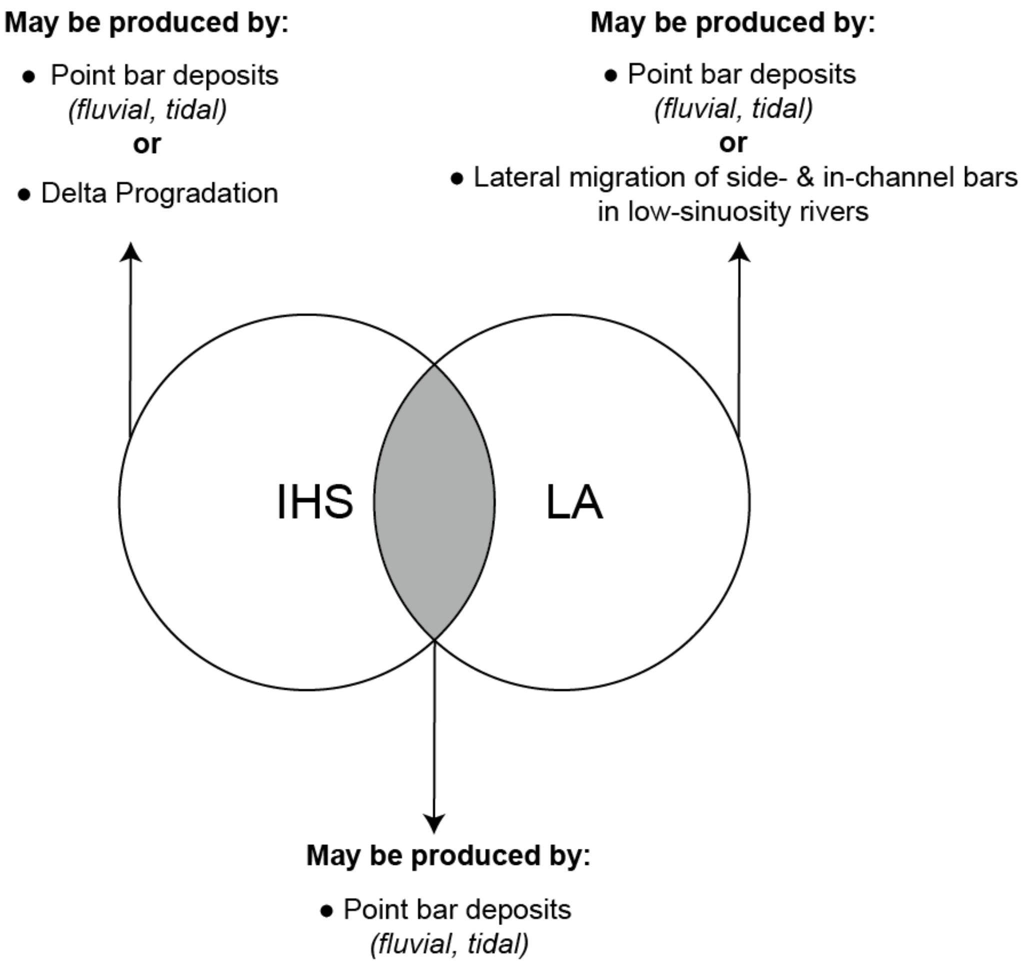

Figure 7.4. Conceptual model illustrating the difference between inclined heterolithic stratification (IHS), lateral accretion (LA) and laterally accreting inclined heterolithic stratification (LA-IHS), and the depositional circumstances that each can potentially represent.

Interpretations of ancient fluvial IHS deposits have suggested the origin of heterolithic components relates to varying discharge (Nami, 1976) and discontinuous point bar growth (Puigdefabregas and Van Vliet, 1978), though observations of modern fluvial point bars suggest that IHS deposits received an additional coarser-to-fine couplet every flood event (e.g., Bridge and Jarvis, 1976). The common overall upwards decrease in grain-size and internal bedform scale (e.g., Tyler and Ethridge, 1983) reflects the fact that these vertical profiles effectively record shoaling upwards from the former channel thalwegs and the decrease in flow velocity and depth encountered towards the upper slope of original geomorphic point bars (Allen, 1965). Ultimately, LA-IHS deposits are succeeded by fine-grained mudrock deposits representing overbank deposition once the channel has migrated away from its original locus. Thus, the presence of LA-IHS can be used to suggest the presence of an ancient point bar in a meandering river. However, it is essential to recognise that not all meanders result in the deposition of LA-IHS. For example, Hartley et al. (2015) documented exhumed amalgamated meander belt deposits from the upper Jurassic Morrison Formation, Utah. Despite point bar morphology being visible in planview, lateral accretion sets were estimated to comprise <5% of the total outcrop area and showed no significant heterolithic component. Thus the presence of LA-IHS can recognise the presence of meandering in a certain instance, but its absence within alluvium does not necessarily preclude a meandering planform to the river that deposited it.

An additional caveat to the use of LA-IHS is that its confident recognition requires a certain extent of exposure of strata. Outcrop (rather than core of seismic data) is required in order to ascertain criteria such as palaeocurrent data and complete sedimentary bedforms. Vertically, the extent of stratal exposure is required to be equivalent to the depth (or erosionally truncated remnant) of the original channel and, laterally, it must extend for a recognizable fraction of the total point-bar length. The scale of natural sedimentary rock exposure on Earth is highly variable but it is clear that the sedimentary-stratigraphic record of LA-IHS (and, thus, the record of positively identified meandering rivers) is biased to stratal packages that occur at outcrop scale. In other words, if we can identify LA-IHS in the rock record, we can be confident in our interpretation that a meander point bar existed at that point, but we are only ever likely to identify LA-IHS if the complete element is preserved at outcrop scale: thus the CMFM is biased towards the identification of small muddy meandering streams. In contrast, the physical dimensions of rock outcrops are usually vastly inferior to many geomorphic components of large river systems. For example, today one of the world's largest extant meander belt (up to c. 12 km wide) occurs in the Mississippi River. This meander-belt is associated with river widths of up to 1000 m and point-bars reaching up to 3750 m in length: it is speculative to assess how this would be recorded in a natural geological outcrop, subjected to vagarious truncation by faulting, erosion, and masking (e.g., by drift deposits or vegetation). Attempts are increasingly being made to understand how large-scale entrenched fluvial systems may present signatures in the pre-vegetation rock record (e.g., Ielpi et al., 2017), but, at present, there are few analogous datasets from Phanerozoic strata, and the observations are not directly comparable with the better understood outcrop-scale record of small- to moderate-sized channels (which may form a nested internal component of larger entrenched systems).

In rare instances where exhumed fluvial planforms are preserved, it is possible to directly relate IHS deposits to palaeochannel dimensions. One such example is the well-studied Jurassic Scalby Formation, England (e.g., Nami, 1976; Leeder and Nuami, 1979; Alexander, 1992; Ielpi and Ghinassi, 2014;

Ghinassi et al., 2016) (Fig. 7.5). Scalby Formation IHS deposits have a maximum thickness of 4 metres which match estimated channel widths and bankfull depths of 21 and 4 metres respectively (Nami, 1976). The fact that, even in such exceptionally exposed examples, clearly defined LA-IHS elements record only the deposits of relatively small rivers (Fig. 7.5 inset), emphasizes that the sedimentary geological record, and the CMFM are more suited for the positive recognition of deposits of small- to moderate-sized meandering rivers.

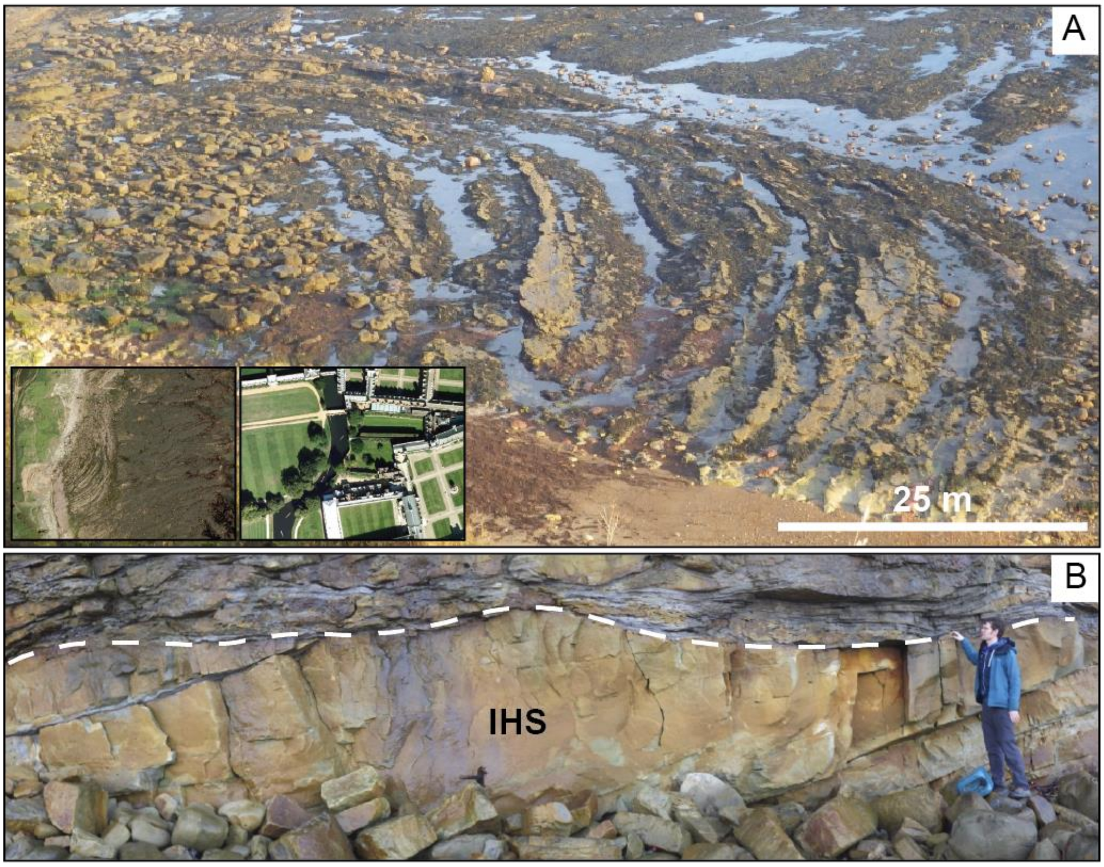

Figure 7.5. Example of an exhumed meander plain in which LA-IHS can be related to ancient channel dimensions: A) Exhumed meander plain. Jurassic Scalby Formation, Yorkshire, England. Inset satellite images (at same scale) show how the Scalby meander plain reflects a river with comparable dimensions to the moderate-sized lowland River Cam, eastern England, rather than a major river system. Images: Google Earth, Infoterra and Bluesky; B) Vertical cross-section displaying inclined heterolithic stratification, with undulating scroll bar top. Jurassic Scalby Formation, Yorkshire, England.

To summarize, certain sedimentary characteristics, such as those found within the CMFM can be confidently recognised, in both modern and ancient strata, to represent the deposit of meandering rivers. Their recognition in the rock record is sufficient for confident reasoning that meandering rivers exist. However, other isolated characteristics (e.g., thick mudrock) without LA-IHS are weak evidence: in instances where these have been used in isolation to infer the presence of ancient meanders, conclusions must be treated with caution. Additionally, because not all meanders will deposit sediment that conforms to the CMFM, the absence of LA-IHS or CMFM strata is not proof of the absence of river meanders. The acceptance of these subtle but crucial details is key to answering the question about whether or not pre-vegetation meandering rivers existed.

7.2.2. 'Sheet-braided' alluvium

In his study of the evolution of fluvial style in the Palaeozoic, Cotter (1978) recognised that pre-vegetation alluvial successions in the Central Appalachians consisted predominantly of stacked, laterally extensive beds, whereas syn-vegetation successions contained a greater number of complex, amalgamated channel-shaped strata. To emphasize the distinct nature of the pre-vegetation alluvium at this location, Cotter (1978) introduced the term 'sheet-braided' to describe single genetic units of sandstone with width:depth ratios exceeding 20:1. He explicitly stated that 'sheet-braided' was a subdivisional classification of the 'fluvial style' of an alluvial sedimentary package (Cotter 1978, p. 364), and that 'fluvial style' referred to the character of an alluvial rock sequence (Cotter 1978, p. 362). Cotter (1978) suggested that the 'sheet-braided' fluvial style was the dominant geological signature of pre-vegetation alluvium in the Appalachian Basin. Later, Davies and Gibling (2010a) and Davies et al. (2011) used original fieldwork-based case studies and a database of publications published in the intervening 30 years to demonstrate that the 'sheet-braided' style held true for the majority of pre-vegetation alluvium worldwide.

The inclusion of the word 'braided' in the term is regrettable because its formal definition, in reference to rock character alone, has recently become forgotten. It is important to note that, apparently at least until 2015, the term 'sheet-braided' was reserved solely for a rock characteristic, but multiple recent papers have begun to refer to a previously unknown concept: 'sheet-braided rivers' (e.g., Ielpi and Ghinassi, 2015; de Almeida et al., 2016; Ielpi and Rainbird, 2016b), sometimes even as the eponymous topic of a paper (Ielpi and Rainbird, 2016a). These papers have argued against the predominance of 'sheet-braided' pre-vegetation alluvium, on the basis that special circumstances of outcrop and exposure may permit a more refined interpretation of fluvial planform during deposition (e.g., Ielpi and Ghinassi, 2015; Ielpi and Rainbird, 2016a,b). However, these arguments are actually only against (mythical) sheet-braided rivers, in almost all of the instances cited, the strata (despite their interpreted depositional diversity) are almost always 'sheet-braided' alluvium (e.g., minimum 30:1 aspect ratio forest bar sandbodies (Ielpi and Rainbird, 2016b); 20:1-80:1 channel sand-bodies (Ielpi and Ghinassi, 2015)).

'Sheet-braided' architectures are independent of any conceptual models of fluvial planform and have been proven polygenetic (Santos et al., 2014). To date, 'sheet-braided' sandstones are known which bear signatures of having been deposited by: 1) highly mobile channels (e.g., McMahon et al., 2017) (Chapter 4, Chapter 6); 2) wide channels (e.g., Nicholson, 1993); 3) unconfined flow (e.g., Winston, 2016); 4) high-energy flood events (e.g. McMahon and Davies, 2018) (Chapter 5); 5) deep channels (e.g., Ielpi et al., 2016); and 6) very shallow channels (Section 4.2).

The term ‘sheet-braided’, despite its misleading wording, still has value, provided that it is used as a passive descriptor of architectural properties rather than carrying implications of fluvial geomorphology. In many natural geological outcrops, the low diagnostic bar for the identification of ‘sheet-braided’ architecture (>20:1 aspect ratio) means that this architectural characteristic can still be identified or rejected even when more refined architectural interpretation is prohibited. Throughout this thesis it is used in this way (Table 2.1).

7.2.3. The stratigraphic distribution of the ‘classic meandering facies model’ and ‘sheet-braided’ strata

There is another factor that supports the retention of the term “sheet-braided”: in that the characteristic retains importance as a key distinction between alluvium deposited before and after the evolution of land plants: the near ubiquity of ‘sheet-braided’ alluvium in pre-vegetation alluvium means that it may be mistakenly perceived as a bucket term, but its true merit lies in the converse fact that there are no known examples of syn-vegetation alluvial successions that are dominated by such architecture (Gibling and Davies, 2012). Thus, in a holistic view of alluvium through time, the Precambrian dominance and Phanerozoic diminishment of ‘sheet-braided’ alluvium attests to the significance of the evolution of a terrestrial flora in promoting a wider diversity of preserved alluvial phenomena.

Stratigraphic trends shown by the CMFM also conform to this notion. A global paucity of reported “interpretations” of pre-vegetation meandering fluvial styles was first demonstrated by Cotter (1978) and subsequently by Davies and Gibling (2010a). Both of these studies recognized that “interpretations” of braided fluvial styles were curtailed at the expense of interpretations of meandering from the onset of the first appearance of fossil plants in the sedimentary record. Further scrutiny utilizing an even larger dataset than those used by Cotter (1978) and Davies and Gibling (2010a) (Table A3 [Appendix]) provides additional evidence of these stratigraphic trends (Fig. 7.6). Of the few reports of pre-vegetation meandering river deposits that do exist (Table 7.1), the most compelling case has been described from the Neoproterozoic Allt-na-Béiste Member of the Torridon Group in NW Scotland, suggested to record the deposits of long-lived meandering rivers, from the positive identification of LA-IHS (i.e., conforming to the CMFM) within well-exposed outcrop (Santos and Owen, 2016) (discussed in Section 7.3). All other interpretations of pre-vegetation meandering river deposits in published literature have been made on the basis of limited evidence, or from 2D vertical facies that lack clear evidence for large-scale architecture or palaeocurrents (Table 7.1). While comparably weak ‘interpretations’ of fluvial style have also been made in younger strata, the lack of strong evidence in these particular examples is critical as it may validate the contention that meandering rivers were rare on pre-vegetation Earth.

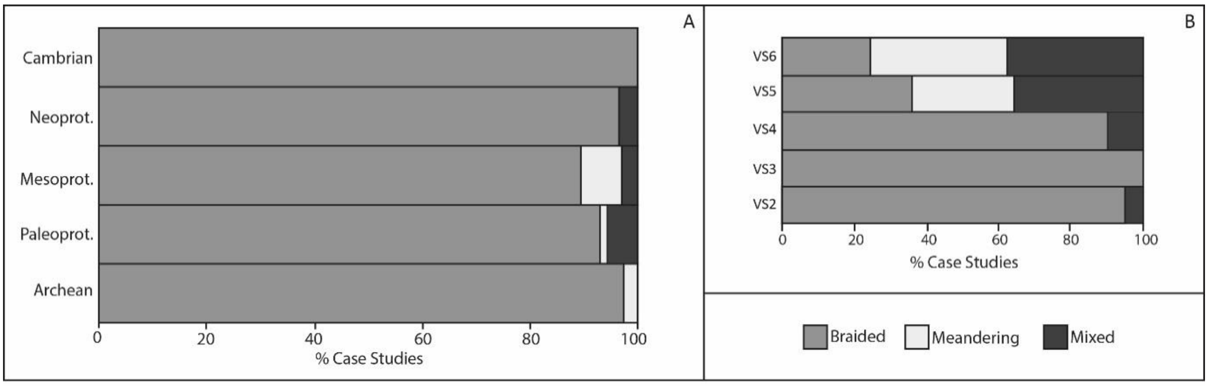

Figure 7.6. A) Previous interpretations of fluvial style for each Era/Period. "Mixed" represents case studies for which previous authors inferred that both braided and meandering styles were present. (n=38 [Archean], n=72 [Paleoproterozoic], n=40 [Mesoproterozoic], n=70 [Neoproterozoic], n=37 [Cambrian]). Data presented in Table A3; B) From Davies and Gibling (2010a). Previous interpretations of fluvial style for each vegetation stage (n=23 [VS2], 9 [VS3], 11 [VS4], 14 [VS5], 24 [VS6]). VS = Vegetation stage (Davies and Gibling, 2010a). VS2 to VS6 = Early Cambrian to Upper Devonian.

Table 7.1. Previous interpretations of pre-vegetation meandering rivers, justification for the interpretations, and problems with the criteria used. Note list also includes the 'mixed' fluvial planforms graphically illustrated in Figure 7.6.

Formation	**Authors**	**Age (Ma)**	**Explanation for meandering fluvial interpretation**	**Potential issues with interpretation**
Allt-na-Béiste Member	Santos and Owen (2016)	850-1000 Ma	LA-IHS deposits; presence of mudrock, interpreted as floodplain material; interpreted crevasse splay elements	Only 6 examples of IHS observed in c. 180 m of alluvium. Maximum thickness 41 cm. Sandy-bedforms dominant component of stratigraphy.
Hatches Creek Group	Sweet (1988)	1870-1846 Ma	1 fining up cycle; 'probable lateral accretion surfaces' capped with 3 m of mudstone	LA surfaces restricted to one 9 m thick sand-body. 'Insufficient outcrop' exposure prohibits accurate understanding of the relationship between inclined foresets and their underlying surface. Surfaces may alternatively represent local lateral-accretion on an in channel bar within a sandy braided system (Long, 2011).

The Transvaal Sequence	Pretorius (1974)	2500 – 2100 Ma	None given	Conceptual model of system only
Nelson Head Formation (in the Brock Inlier).	Long (1978)	c. 1000 Ma	'Possible meandering stream deposit'. Palaeocurrents in sets of cross-stratified sandstone are at a high angle to underlying surface, and change systematically up section.	Minor overbank fines; no crevasse elements (Long, 2011)
Katherine Group	Long (1978)	c. 1000 Ma	LA surfaces associated with 3.17 m thick CH element.	Minor overbank fines; no crevasse elements (Long, 2011)
Mount Currie Conglomerate	Long (2011)	Ediacaran-Lower Cambrian	iLA (see Figure 2.2 for definition) can be traced across laterally extensive tabular beds.	No palaeoflow measurements could be obtained.
Orienta Formaion	Morey and Ojakangas (1982)	c. 1000 Ma	Fining up cycles	Vertical sequence analysis only. No evidence for LA surfaces, levee facies, or systematic upsection deviation in palaeocurrent direction
Fond du Lac Formation	Morey and Ojakangas (1982)	c. 1000 Ma	171 fining up cycles, ranging from 0.3 – 18.6 m thick	Vertical sequence analysis only. No evidence for LA surfaces, levee facies, or systematic upsection deviation in palaeocurrent direction.
Solor Church Formation	Morey and Ojakangas (1982)	c. 1000 Ma	Fining up cycles	Vertical sequence analysis only. No evidence for LA surfaces, levee facies, or systematic upsection deviation in palaeocurrent direction. Palaeocurrent measurements are strongly unimodal (Morey, 1967).

Red Castle Formation	Wallace and Crittenden (1969)	Neoproterozoic	Fining up cycles	Vertical sequence analysis only. No evidence for LA surfaces, levee facies, or systematic upsection deviation in palaeocurrent orientation.
Serpent Formation	Long (1978)	2200-2400 Ma	Santos et al. (2017a) state that Long (1976) interpreted the Serpent Formation as the product of a sandy meandering fluvial system.	Long (1978) states the Serpent Formation is 'interpreted as the product of deposition in a (braided) stream system with low to intermediate sinuosity'.

In summary, geological observations find little conclusive evidence for pre-vegetation meanders in the rock record, but the limitations of the CMFM should not be misunderstood, such that it is entirely possible that many pre-vegetation meandering river deposits have so far gone unrecognised. The results confirm earlier claims that 'sheet braided' strata are common before the evolution of vegetation and formations conforming to the CMFM are common thereafter. There is clear proof in the rock record that something switches in the Silurian. Pre-vegetation alluvium have a certain frequency distribution of character (i.e., near ubiquitous sheet-braided architecture, very rare CMFM) and syn-vegetation alluvium have another (i.e., very rare sheet-braided, not uncommon CMFM). Much of the debate regarding (unobservable) pre-vegetation meandering rivers misses this key point: the advent of vegetation created a wholesale change in the nature of the rock record, which can be preserved and recognised.

7.3. Case study: The Allt-na-Béiste Member, Scotland

Of the 387 compiled Archean-Cambrian alluvial successions (Table A3), the Allt-na-Béiste Member is the only succession in which LA-IHS is recorded. This so far unique occurrence justifies the need to revisit the succession here, in order to place these sedimentological signatures into their regional context with reference to the rest of the Torridonian Sandstones.

7.3.1. Stratigraphic setting

The Allt-na-Béiste (ANB) Member, NW Scotland, forms part of the Mesoproterozoic-Neoproterozoic Torridonian Sandstones (Section 2.1.1) (Fig. 7.7). It is a minor component of this stratigraphy, accounting for 295 m of the >10 km-thick succession, and measures only 18 m at its type section (Fig. 7.8). Unambiguous ANB exposures crop out at three locations: Diabaig, Gairloch and Torridon (Fig.

7.7). The type section at Diabaig is the only location where the sedimentary context of the ANB Member can be studied in full as both the underlying Diabaig Formation lacustrine rocks and overlying Applecross Formation braided alluvium are exposed (Fig. 7.8, Fig. 7.9). At Gairloch, the base of the succession is faulted out whereas at Torridon, neither the section top nor base is exposure (Fig. 7.10).

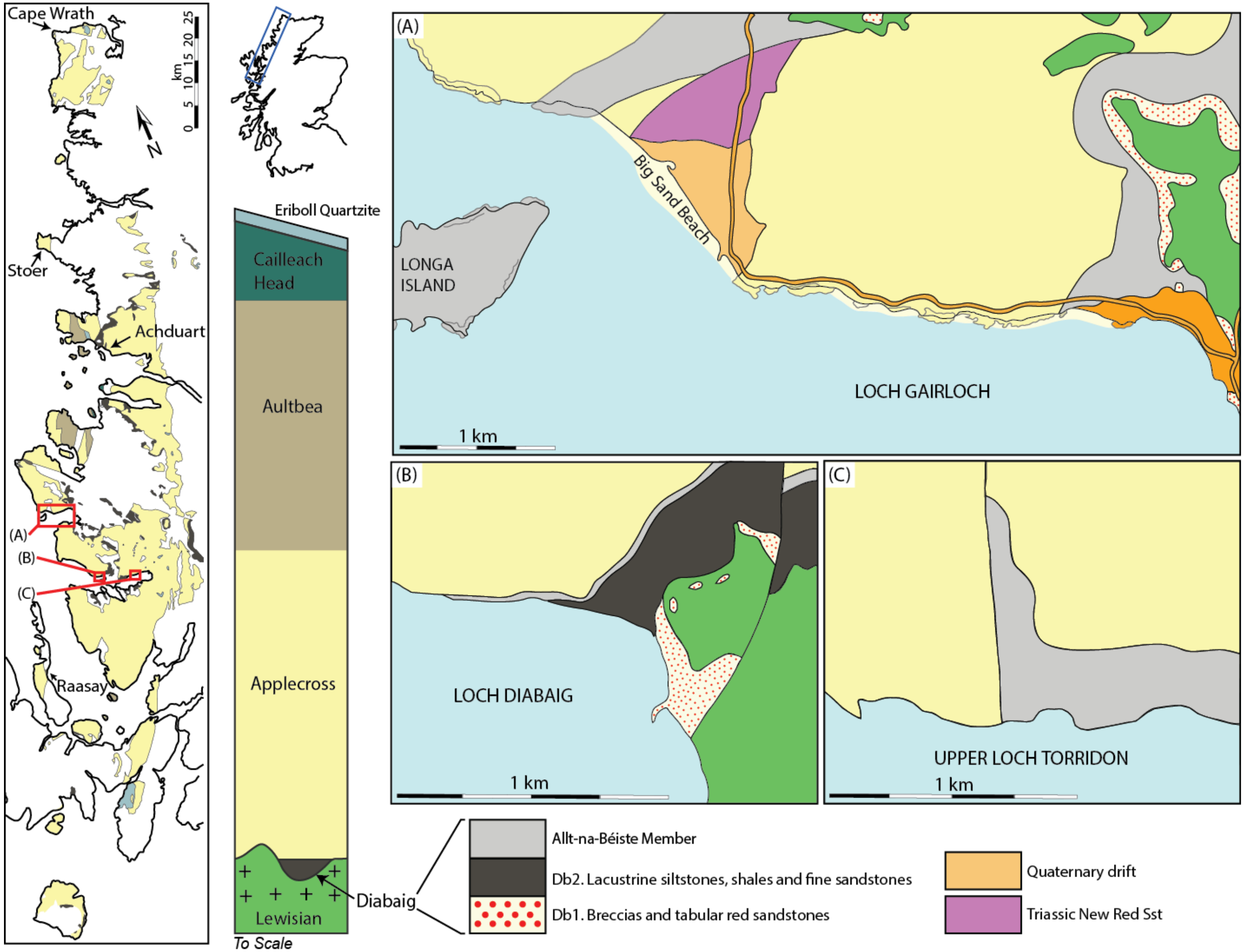

Figure 7.7. Geological map and stratigraphic section of the Torridon Group, Scotland. Locations of study indicated in higher resolution inset maps: A) Gairloch; B) Diabaig; C) Torridon

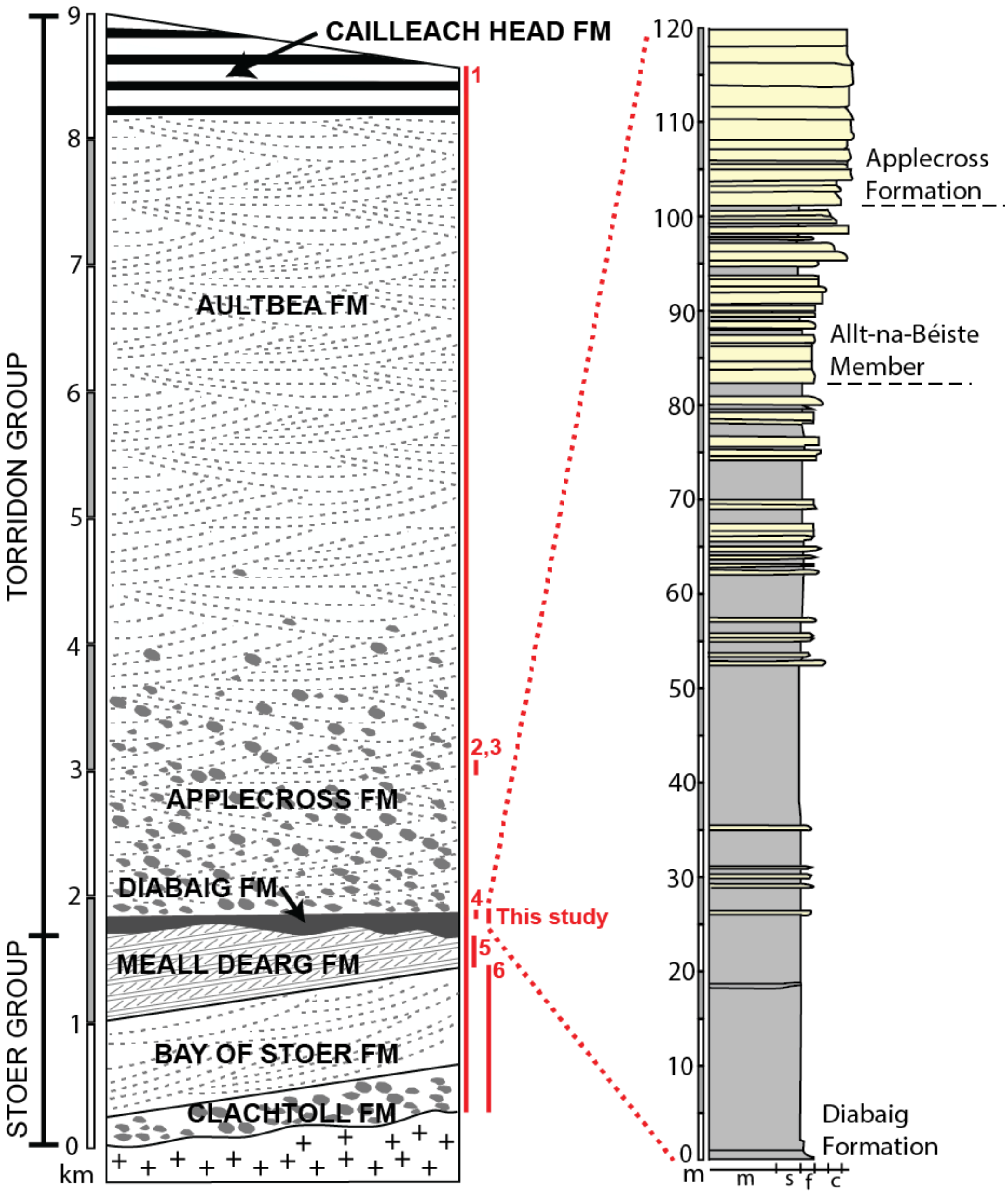

Figure 7.8. Torridonian lithostratigraphy. Red lines mark the stratigraphic extent of recent sedimentological studies of Torridonian strata: 1) Stewart (2002); 2) Ielpi and Ghinassi (2015); 3) Ghinassi and Ielpi (2018); 4) Santos and Owen (2016); 5) McMahon and Davies (2018); 6) Ielpi et al. (2016). Inset sedimentary log shows a measured section of the Diabaig Formation, Allt-na-Béiste Member and Applecross Formation at the Allt-na-Béiste types section at Diabaig.

Figure 7.9. Sedimentary deposits at Diabaig: A) Diabaig Formation lacustrine mudrocks. Geologist is 187 cm tall; B) The contact between Diabaig lacustrine facies and the Allt-na-Béiste Member. Geologist is 187 cm tall; C) Sandstone and mudstone dominated sedimentary facies preserved in the Allt-na-Béiste. Box denotes location of Figure 7.15A.

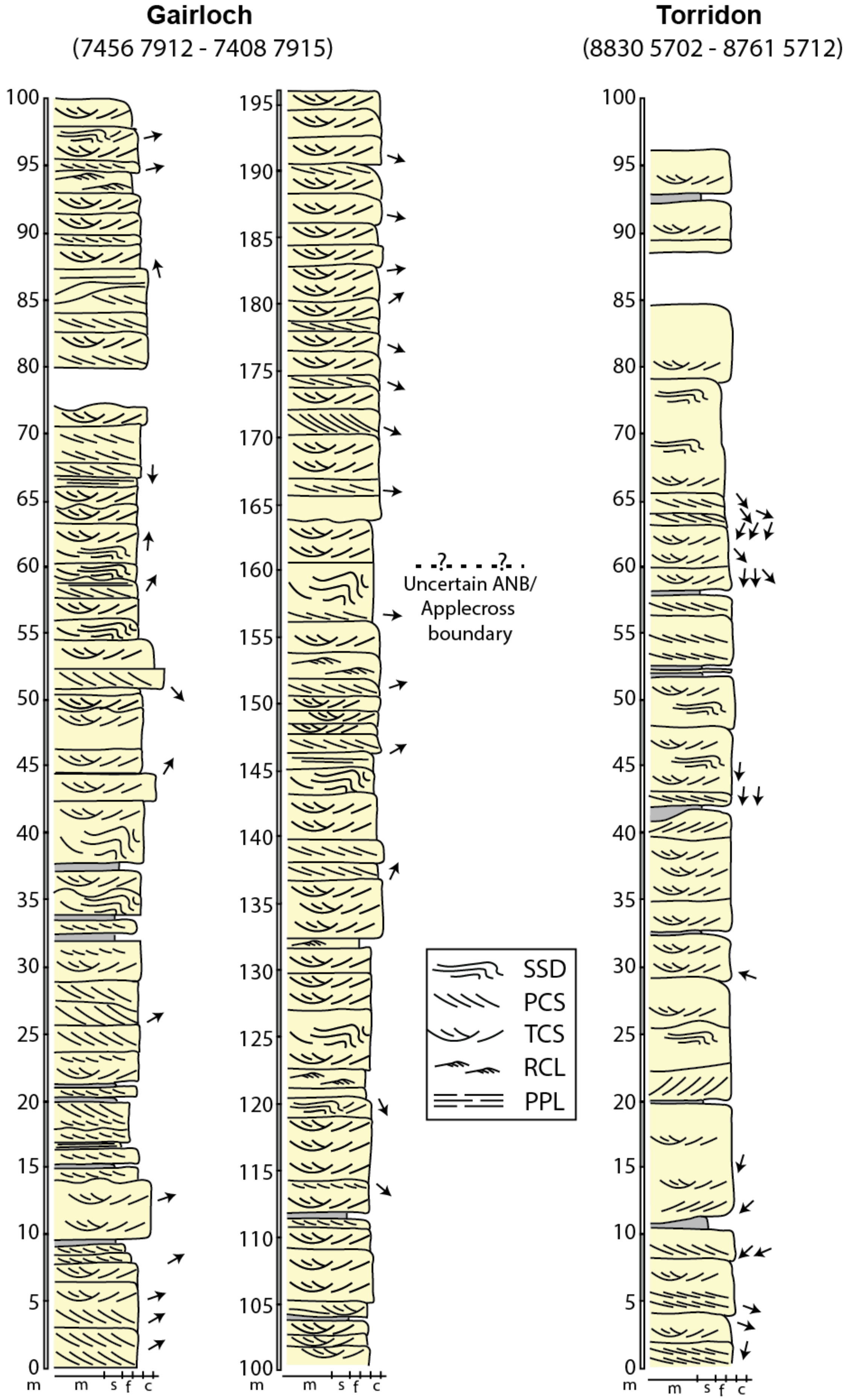
Gairloch
(7456 7912 - 7408 7915)
Torridon
(8830 5702 - 8761 5712)
Uncertain ANB/ Applecross boundary
SSD
PCS
TCS
RCL
PPL
m
m s f c

Figure 7.10. Measured sedimentary logs of the Allt-na-Béiste Member at Gairloch and Torridon. SSD = Soft-sediment deformation; PCS = Planar cross-stratification; TCS = Trough cross-stratification; RCL = Ripple cross-lamination; PPL = Plane parallel lamination. Black arrows denote palaeoflow orientation

7.3.2. Sedimentary facies

Sand-grade or coarser sediment account for an average of 98% of the ANB Member's total stratigraphic thickness (varying between 83% at Diabaig, 98% at Torridon, and 99% at Gairloch). Trough cross-bedded arkosic sandstones are most abundant, with troughs ranging between 0.1-0.6 m in height (Fig. 7.11A). Cross-strata are concave-up and occasionally associated with rare soft-sediment deformation (<5%) (Fig. 7.11B) (which is far less common than in the overlying Applecross Formation despite the medium-sand modal grain-size (Owen, 1995; Owen and Santos, 2014) (Fig. 4.4)). Planar cross-stratification is subordinate and occurs in either <0.15 m sets (Fig. 7.11C) or larger 0.6 – 1.6 m sets which, if traced down-dip, transition laterally into planar stratification. Planar-cross strata are usually top-truncated, either by low-angle to horizontal cross-stratification (Fig. 7.11C), further sets of planar-cross stratification, or tabular beds filled with trough-cross stratification. Low-angle cross-stratified packages are typically several cm-thick and extend laterally down-dip for up to 1.5 m. Sandstone beds in places have preserved 3D dune topography (Fig. 7.11E) capped by cm- to dm- thick lenses of finer grained, ripple cross-laminated sandstone with siltstone intercalations (Fig. 7.11D).

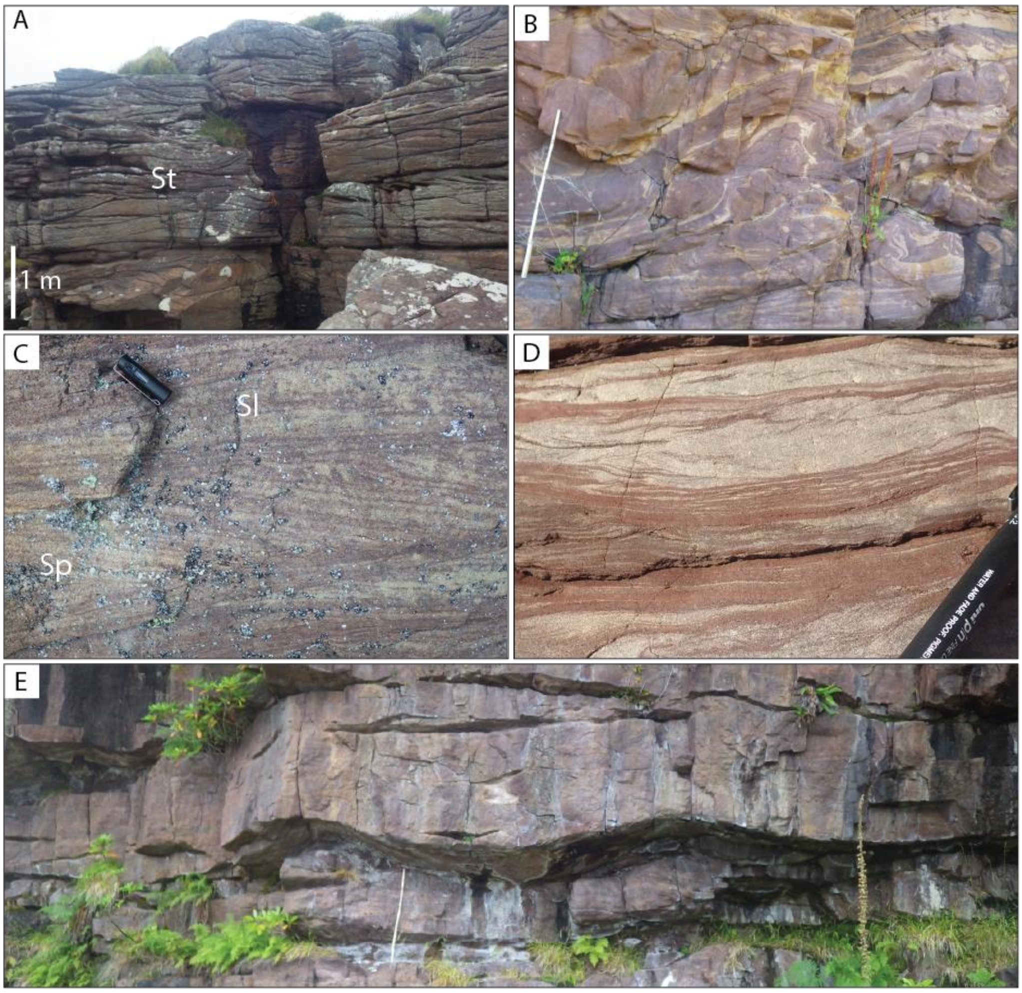

Figure 7.11. Sandstone dominated sedimentary facies of the Allt-na-Béiste Member: A) Trough cross-stratified sandstones (Gairloch); B) Soft-sediment deformation (Gairloch). Metre rule for scale; C) Small sets of planar cross-stratification and low-angle cross-stratification (Torridon). Pen lid is 4 cm long; D) Ripple cross-laminated sandstone with siltstone intercalations (Gairloch). Pen is 1 cm wide; E) Preserved dune topography (Torridon). Metre rule for scale. St = Trough cross-stratified sandstone; Sp = Planar cross-stratified sandstone; Sl = Low-angle cross-stratified sandstone.

Silt and mud-grade sediment contribute <2% of total ANB alluvium (c. 13% at Diabaig, <1% at Gairloch, 2% at Torridon) and occur as laterally discontinuous packages up to 1.6 m thick (Fig. 7.12A) (but typically <0.1 m thick (Fig. 7.12B)). Packages have planar bases on top of underlying sandstones, whereas the package tops are erosional and irregular. In some areas, cm-thick silty-sandstones alternate with cm-dm thick medium-grained sandstones. Mud clasts are also relatively common (Fig. 7.12C-D).

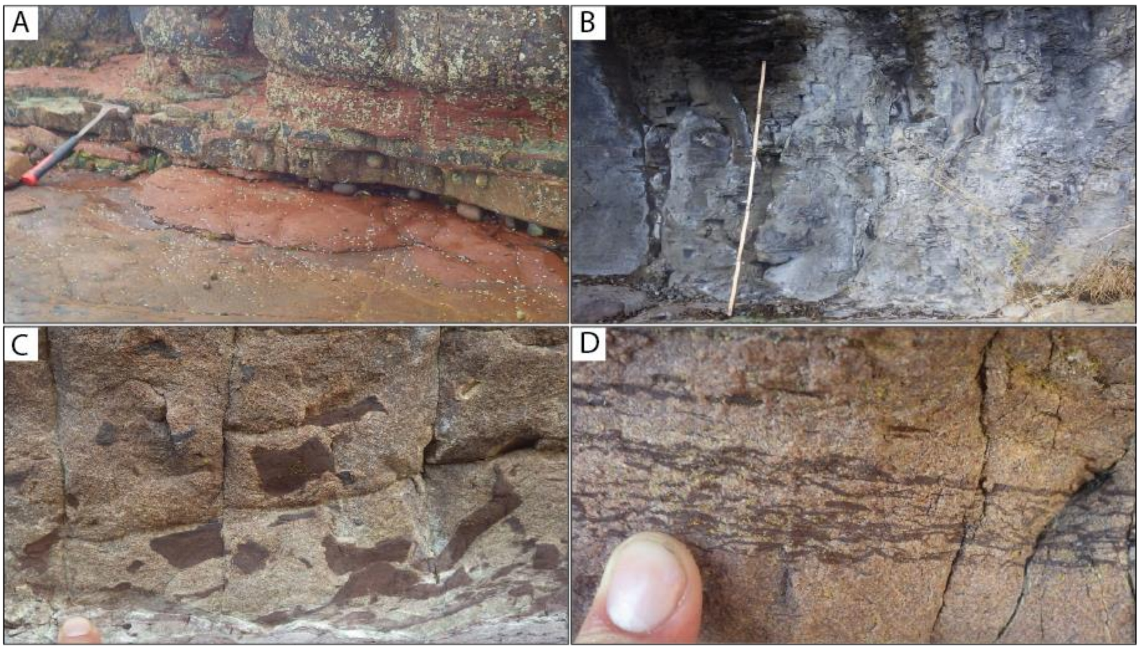

Figure 7.12. Mudstone and siltstone sedimentary facies of the Allt-na-Béiste Member: A) Intercalated sandstone and silty-mudstone packages (Gairloch). Hammer is 31 cm long; B) Silty-mudstone package (Diabaig). Metre rule for scale; C, D) Intraformational mud clasts (both Gairloch).

7.3.3. Architectural elements

Sandstone packages are predominantly classified as sandy-bedforms (SB, Miall, 1985) or interpreted sandy-bedforms (Fig. 2.2, Fig. 7.13) (Table 7.2). These are 10 – 51 cm thick tabular bodies that are typically trough cross-stratified, though packages displaying intercalations of small, planar cross-stratification and low-angle cross-stratification occur locally (Fig. 7.11C). Downstream-accretion elements (DA; Miall, 1985) are also present. These consist of successive sets of large-scale planar cross-stratification that can be traced down-dip from foreset avalanche surfaces to planar-bedded stratification, without a break (Fig. 7.13, Fig. 7.14). Predominant downstream-migration is indicated by the low disparity between stratification sets and genetically related bounding surfaces (Miall, 1985) (Fig. 7.13). DA elements range in thickness between 0.3-2.8 m and can be traced up to 20 m in a down-flow direction.

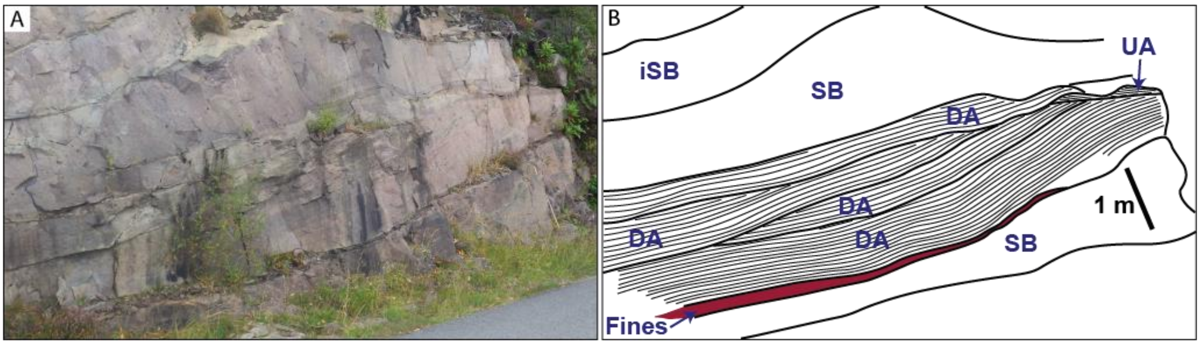

Figure 7.13. Allt-na-Béiste Member downstream accretion elements at Torridon: A) Field photograph. Metre rule for scale; B) Interpreted architectural panel. See Figure 2.2 for acronym definitions.

Table 7.2. A comparison of the sedimentary characteristics of the Allt-na-Béiste Member and the Applecross Formation. Description of elements in Figure 2.2. LA-IHS defined in Section 7.2.1.

Element	**Allt-na-Béiste Member**	**Applecross Fm**
Channels (CH)	Not recorded	Rare
Sandy-bedforms (SB)	Common	Abundant
'Interpreted' Sandy-bedforms (iSB)	Common	Abundant
Downstream-accretion element (DA)	Present locally	Common
Homogeneous lateral-accretion deposit (LA)	Present locally	Rare
Laterally-accreting inclined heterolithic stratification (LA-IHA)	6 recorded sets	Not recorded
Floodplain fines (FF)	<2% total vertical thickness	Extremely rare

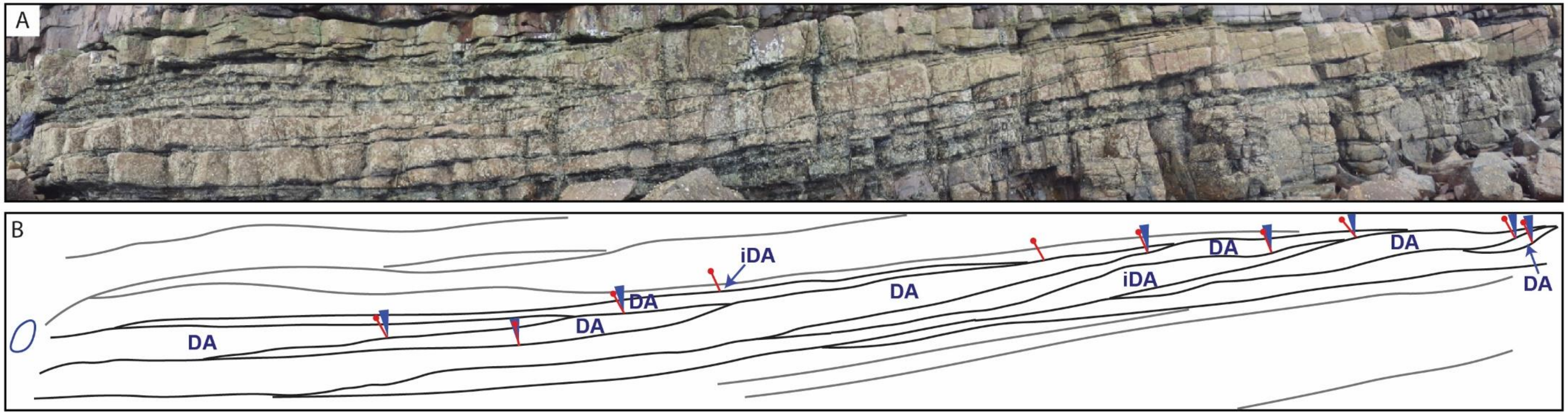

Figure 7.14. Allt-na-Béiste Member downstream-accretion elements at Diabaig: A) Field photograph; B) Interpreted architectural panel. Blue rose diagram indicates palaeoflow measured from cross-bed foresets. Red pins indicate direction of dip of genetically underlying bounding surfaces. Bag for scale is 35 cm high.

While the member's architecture is dominated by SB/iSB with subordinate DA elements, both LA-IHS (Fig. 7.15, Fig. 7.16) and non-heterolithic LA occur locally. Six LA-IHS sets have been recognised at two locations within the ANB (4 at Diabaig, 2 at Gairloch). The combined thickness of these isolated sets equates to 210 cm (maximum individual thickness 41 cm), with individual widths of 157 – 278 cm; representing less than 1% of the total 295 m-thickness of the member. Individual LA-IHS sets display little grading but consist of a distinct coarse-to-fine couplet (medium-grained sandstone and silty, very fine-grained sandstone; with no mud-grade couplets (Fig. 7.15, Fig. 7.16). LA-IHS sets either overlie thin beds of mudstone (3 cm – 31 cm) or erosionally downlap channel-fill deposits. When fully preserved, sets have gradational contacts with overlying mudstones (up to 150 cm) (Fig. 7.12A, Fig. 7.15A). In other instances, LA-IHS deposits are erosively overlain by succeeding channel sandstones (Fig. 7.16). Internally, most LA-IHS sets are crudely stratified, but in instances where exposure is fresh, foreset orientations indicate that accretion occurred at a high angle to palaeoflow. Cosets of vertically stacked LA-IHS sets do not occur: instead, LA-IHS deposits are solitary and occur at intervals where mudrock is most abundant (Fig. 7.9C). Two non-heterolithic lateral accretion packages were identified (both at Gairloch). These packages are wedge shaped, up to 70 cm thick and 300 cm wide and are erosively overlain by sandy-bedforms.

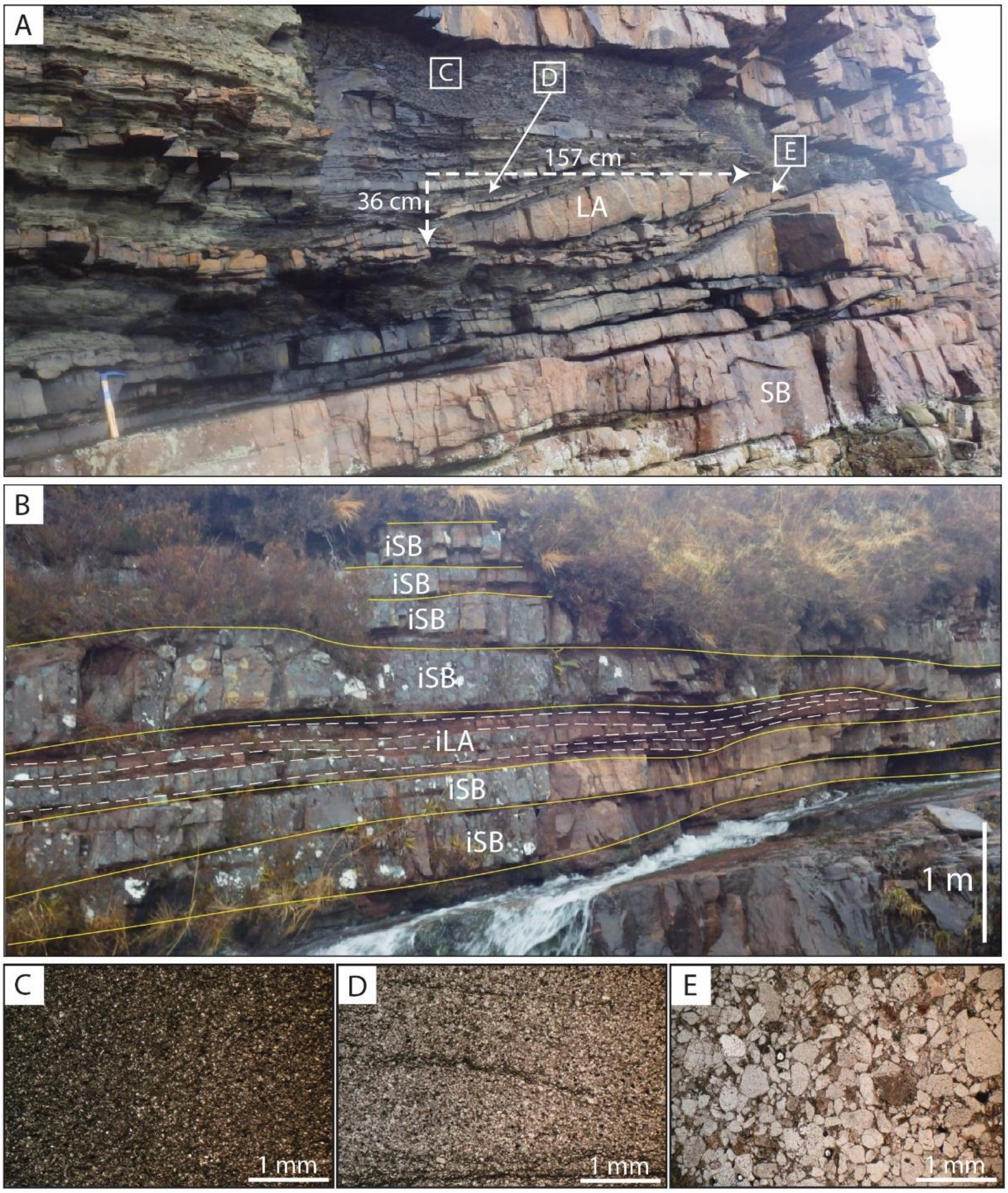

Figure 7.15. Allt-na-Béiste Member laterally accreting inclined heterolithic stratification deposits: A) 41 cm thick inclined heterolithic stratification deposits at Diabaig, overlain by muddy-siltstones interpreted as overbank material (locations of thin sectioned samples shown in C-E illustrated); B) Inclined heterolithic stratification erosively overlain by sandy-bedform elements (road section between Alligin and Diabaig); C) Thin section of muddy-siltstones interpreted as overbank material; D) Thin section of fine component of inclined heterolithic stratification (siltstone); E) Thin section of coarse component of inclined heterolithic stratification (medium-coarse sandstone).

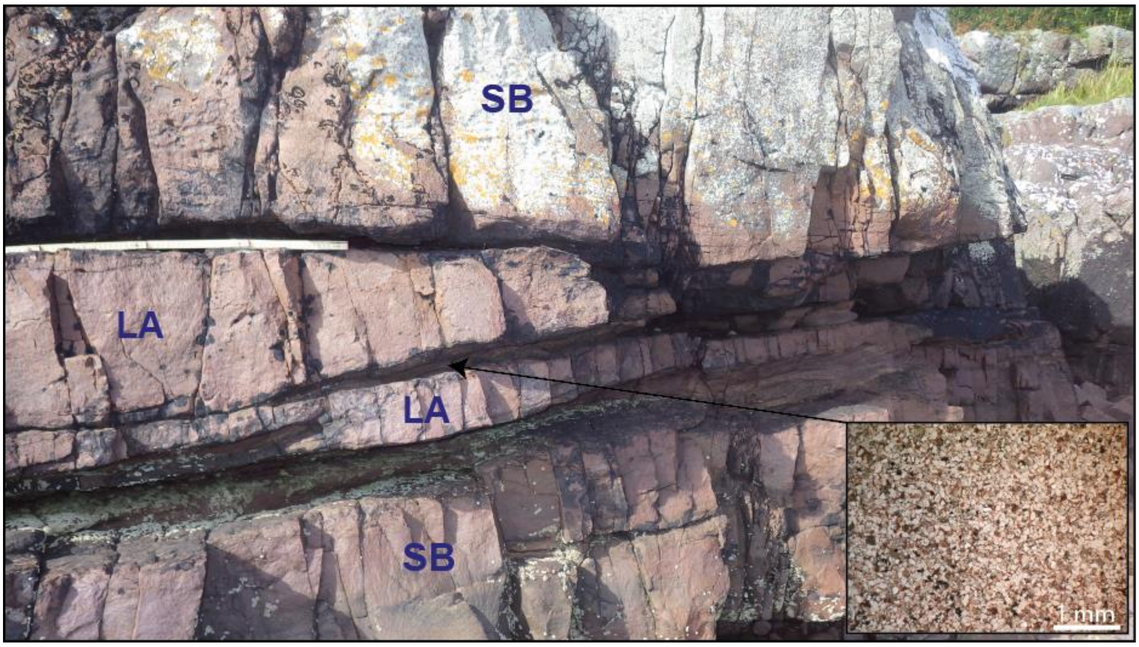

Figure 7.16. Allt-na-Béiste Member laterally accreting inclined heterolithic stratification deposits at Gairloch. Inset demonstrates that fine-sand grade sediment constitutes the fine-grained component of the inclined heterolithic stratification couplet.

7.3.4. Interpretation of the depositional environment of the Allt-na-Béiste Member

Santos and Owen (2016) interpreted the ANB as recording meandering channels on long-lived floodplains, at the onset of fluvial deposition by large-scale rivers (though figured outcrops suggesting this interpretation were based predominantly from observations of one exposure (Fig. 7.17)). They interpreted a variety of components of ancient meandering streams (crevasse splays, point bars, overbank deposits) from a number of individual photo-mosaics (though some of these interpretations are contradictory; e.g., the same horizon shown as “point bar 2” in their Figure 4, is shown as crevasse splays and overbank deposits in their Figure 9). While the data presented in this chapter affirms that this succession is of significance for pre-vegetation studies (as contended by Santos and Owen (2016)) in that it contains isolated, small sinuous channels, here it is argued that the negligible scale and frequency of these constituent architectural elements should be taken into account when interpreting the depositional environment of the member as a whole.

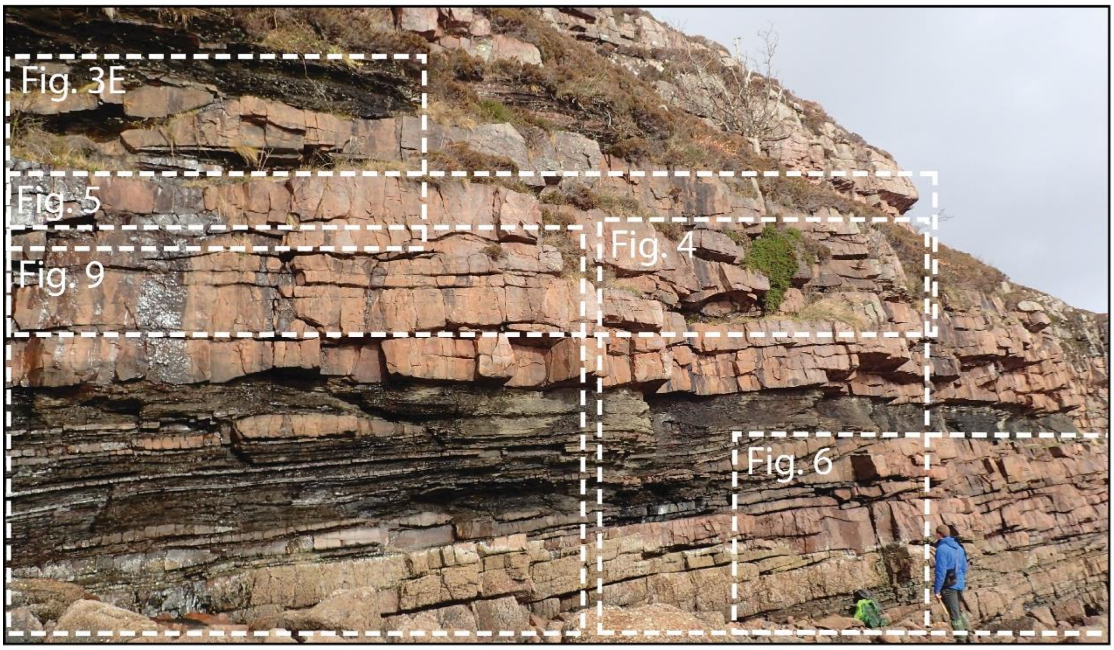

Figure 7.17. Outcrop of Allt-na-Béiste Member alluvium at Diabaig. Rectangles outline the locations of 6 of the figures presented in Santos and Owen (2016). This outcrop at Diabaig is dissimilar from the vast majority of the Allt-na-Béiste Member stratigraphic thickness such that interpretations based on the exposure cannot be considered diagnostic of the member as a whole.

The bulk of the ANB does not record meandering fluvial deposition. SB and iSB elements were deposited by migrating low amplitude three-dimensional dunes; their upwards transitions into ripple cross-laminae relate to long-term changes in aggradation rate and water depth shallowing. The tabular, stacked nature of the trough cross-stratified sets, and their broadly unimodal transport directions, imply that channel planforms had low sinuosity and that sediment accreted largely by vertical aggradation. Preserved barforms also indicate modal downstream accretion. Downstream accreting barforms are ubiquitously top-truncated, such that the depth of the water body cannot be estimated. Most examples are overlain by low-angle cross-stratification, indicating flow conditions transitional between dune and upper plane bed stability (Fielding, 2006).

As noted by Santos and Owen (2016), most of the fine-grained packages are likely overbank deposits: although two instances of silty-mudstone packages with concave-up lower bounding surfaces are likely abandoned channel deposits. However, these packages are typically <0.1 m-thick (maximum 1.6 m), so claims of long-lived floodplains (Santos and Owen, 2016) cannot be supported from sedimentological evidence. Even though fine-grained facies are highly subordinate (accounting for <2% of stratigraphy), the ANB is markedly more mudrock-rich than the overlying Applecross Formation (<1%), suggesting a contrasting depositional style for the two units (Table 7.2).

The LA-IHS deposits support the proposed existence of meandering channels during certain intervals of deposition of the ANB (Santos and Owen, 2016). Palaeoflow measurements from IHS surfaces indicate that flow was near orthogonal to their strike, suggesting deposition on point-bars during high water or rapidly falling water stages. The sigmoidal form of the majority of sets (4 of the 6) indicates that the packages are not truncated and that they may relate to gently curved meanders rather than high-sinuosity planforms (Bridge and Leeder, 1976). Whilst palaeohydraulic reconstructions must be treated with suitable caveats of uncertainty, the complete set thicknesses of 36-41 cm approximately equate to similar bankfull water-depths (e.g., Allen, 1965; Bridge and Leeder, 1976; Miall, 2006). Thus the channels that deposited the ANB LA-IHS were of very negligible size and depth, even in comparison with the small- to moderate-sized meandering channels that are possible to identify in Phanerozoic strata (Fig. 7.18; compare also Fig 7.5). It is argued here that isolated channels with a maximum depth of 41 cm are best interpreted as rarely developing, small, moderately sinuous creeks draining mud-rich plains during intervals of low-sedimentation. Modern fluvial IHS packages receive an additional coarse-fine couplet every flood event (Bridge and Jarvis, 1976), so the maximum five coarse-fine couplets seen in the ANB examples may imply that these small sinuous creeks were short-lived. Additionally, limited lateral movement of the ANB point bars is suggested by the lack of lateral erosional amalgamation in 5 of the 6 examples (Thomas et al., 1987).

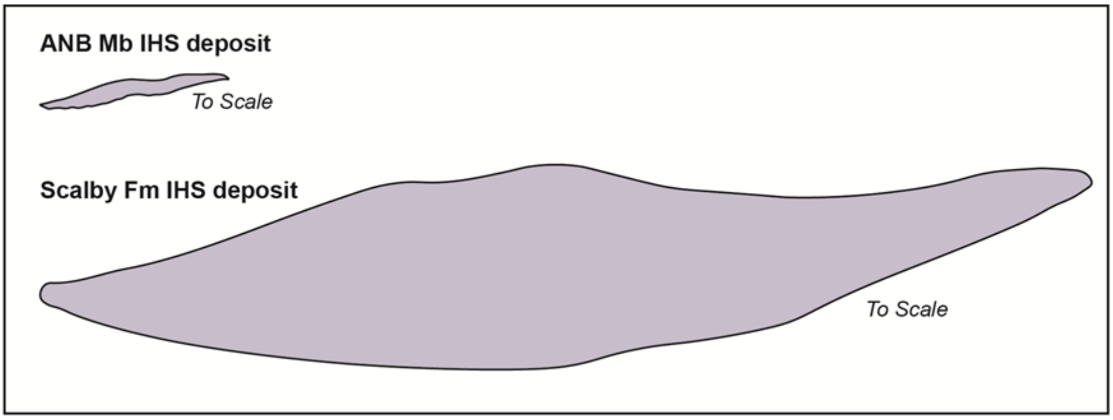

Figure 7.18. Line tracing showing the comparative scale of examples of inclined heterolithic stratification from the Neoproterozoic Allt-na-Béiste Member and the Jurassic Scalby Formation (shown in Figure 7.5B).

In summary, preserved ANB alluvium is characterized by: 1) stacked sandy-bedforms; 2) subordinate, <2.8 m thick, low sinuosity interpreted barform deposits; 3) rare mudrock and LA-IHS sets; and 4) predominantly unidirectional palaeoflow directions. Such depositional characteristics suggest that the member was predominantly deposited by shallow, low-sinuosity rivers. Instances where sandstone-dominated packages, deposited by low-sinuosity systems, transition upwards to the fine-grained packages, associated with the rare occurrences of LA-IHS ‘creeks’, may be associated with intervals of decreasing channel gradient.

7.3.5. Discussion of the ANB LA-IHS

Although the sinuous creeks that deposited the LA-IHS in the ANB were minor components of the bulk sedimentary landscape, their existence is still anomalous in comparison with other pre-vegetation sedimentary successions. While bank stability due to mud may have played a role in their formation, this appears unlikely to be the complete explanation for their occurrence. Other (relatively) mudrock-rich pre-vegetation successions apparently lack such architectural elements (even within the Torridonian Supergroup: e.g., certain horizons of the Clachtoll Formation (Ielpi et al., 2016); Poll a'Mhuilt Member (Stewart, 2002; Stueeken et al., 2017); and Cailleach Head Formation (Stewart, 2002)).

One possible explanation for the ANB LA-IHS occurrences is that they formed locally as small lacustrine basins became overfilled with sediment. Recently, the ANB has been considered to be the basal member of the overlying Applecross Formation (Stewart, 2002; Santos and Owen, 2016), which has a distal provenance and occurs across much of the Torridonian outcrop area with little variation in lithology or palaeoflow (Nicholson, 1993; Stewart, 2002; Williams, 2001; Kinnaird et al., 2007; Williams and Foden, 2011; Krabbendam et al., 2017) (Section 4.1, Figure 4.13). Within this stratigraphic context, the ANB is viewed as recording the onset of the fluvial deposition of the Applecross Formation (which has a dominant 'sheet-braided' architecture) (Stewart, 2002; Santos and Owen, 2016). However, traditionally (and formally) the ANB is the uppermost member of the underlying Diabaig Formation (Peach et al., 1907; British Geological Survey, 2017), which infills palaeotopographic depressions in the Lewisian Gneiss basement, has a more local Lewisian provenance, and exhibits dramatic regional variation in its lithology and thickness (Fig. 7.19). Sedimentary rocks of the Diabaig Formation record highly localized alluvial fan deposition followed by lacustrine deposition. Considering the ANB as being more genetically associated with the Diabaig Formation than the Applecross Formation potentially explains two key characteristics of the member: 1) its variable palaeoflow indicators at each of its outcrop localities (Diabaig, $\theta = 331°$, $n = 31$; Gairloch, $\theta = 92°$, $n = 56$; Torridon, $\theta = 181°$, $n = 42$; compared with the uniform southeastwards palaeoflow of the Applecross Formation (Fig. 4.13)); and 2) its marked thickness variation between outcrop areas, which corresponds with how much of the local palaeotopography was previously filled with more typical Diabaig Formation strata (and its absence from lows that are fully filled with classic Diabaig Formation sediments (e.g., Rùm, Rasaay, Scoraig), and areas where Lewisian topography is flat (e.g., between Cape Wrath and the Stoer Peninsular (Williams, 1966)) (Fig. 7.19, Fig. 7.20). At the Diabaig locality, where LA-IHS is most common in the ANB, Stewart (2002) estimated that palaeovalley relief was approximately 250 m when sedimentation started. Alluvial fan and lacustrine facies account for 216 m of the local stratigraphy (Fig. 7.8): such sediments would have filled nearly all the available accommodation space, resulting in low-gradient alluvial plains where fine-grained cohesive sediment could sometimes accumulate. In this scenario, at this location, the 19 m thick ANB would represent the final stages of filling of a local topographic low. Small creeks draining into the Diabaig lakes could feasibly have temporarily attained high sinuosity planforms during intervals of low sedimentation, with bank stability afforded by the mud-rich plains.

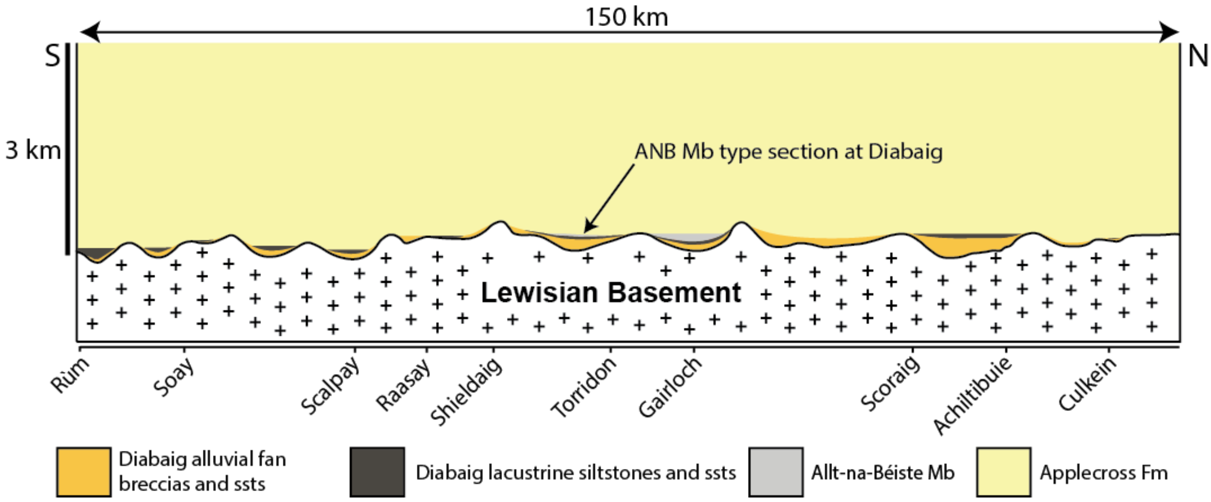

Figure 7.19. Spatial distribution and representative thicknesses of Diabaig Formation, Allt-na-Béiste Member and Applecross Formation deposits across the Torridonian outcrop belt. Lewisian Basement Complex topography redrawn from Stewart (2002).

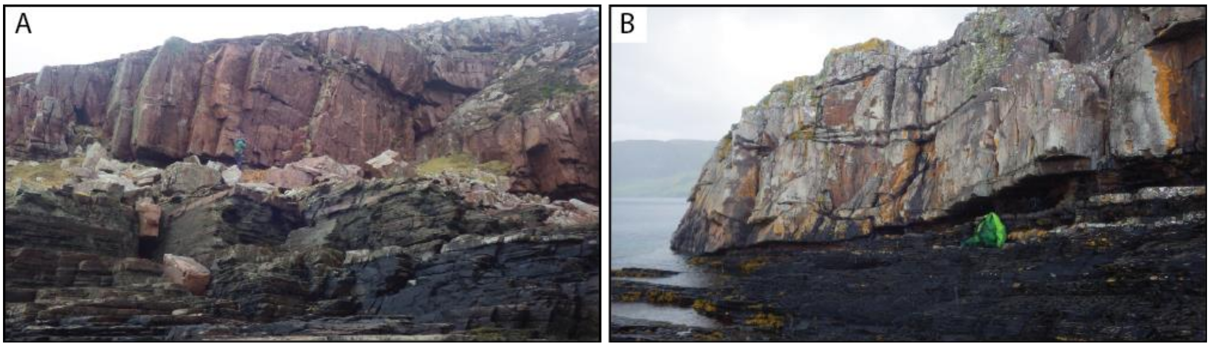

Figure 7.20. Erosive contact between Diabaig Formation lacustrine facies and Applecross Formation braided alluvium at: A) Achduart. Geologist is 196 cm tall; B) Raasay. Bag is 37 cm high. Allt-na-Béiste Member absent.

It is suggested here that the ANB reflects fluvial and terminal lacustrine-marginal deposition at the top of the Diabaig Formation. In this model its deposition precedes the hiatus between the Diabaig and Applecross Formations (Muirhead et al., 2017). The highly localized development of the 6 known <41 cm-deep sinuous creeks within isolated topographic depressions, seen in the ANB, are thus far less typical of pre-vegetation alluvium than the rest of the ANB succession and the 3000 metres of 'sheet-braided' alluvium in the overlying Applecross Formation, which blankets almost the entire outcrop area of the Torridonian Supergroup.

Chapter 8

PRE-VEGETATION ALLUVIUM AS AN ANALOGUE FOR MARS

There has recently been an increased contention that a better understanding of pre-vegetation alluvium may inform our understanding of fluvial systems apparent from rover and satellite imagery of Mars (Owen and Santos, 2014; Santos and Owen, 2016; Ielpi and Rainbird, 2016a; Ielpi et al., 2017). This chapter discusses the merit and limitations of such analogy and the common ground in which pre-vegetation and Martian sedimentary geology may inform one another.

Certain Martian landforms, identified in orbital imagery, have long been suspected to have a fluvial origin (e.g., Mars Channel Working Group, 1983; Malin and Edgett, 2003; Baker et al., 2015), although unequivocal Martian alluvium has only been confidently identified in recent years, since the advent of surface rover missions (Williams et al., 2013). This delayed proof highlights the inadequacy of satellite images for the recognition of lithofacies and sediment stacking patterns, both of which characteristics are prerequisite for the positive identification of alluvium. The examination of grain size, texture, sedimentary facies, bedding architecture and palaeoflow are presently only achievable with use of ground-based rovers (e.g., Squyres and Knoll, 2005; Williams et al., 2013; Grotzinger et al., 2015), but thus far such collected data is of limited geographic extent. For example, the *Curiosity* rover (active since 2014) has only covered 18.13 km (as of 05/02/2018, Sol 1956) (Fig. 8.1). Regardless, rover images have provided us with unprecedented direct access to extra-terrestrial strata that were deposited in (presumably) unvegetated settings (e.g., Squyres and Knoll, 2005; Williams et al., 2013; Grotzinger et al., 2015) and upcoming rover missions (*ExoMars* (Vago et al., 2006), *Mars 2020* (Mustard et al., 2013)) mean that the direct comparison of terrestrial and Martian strata will become possible in coming years.

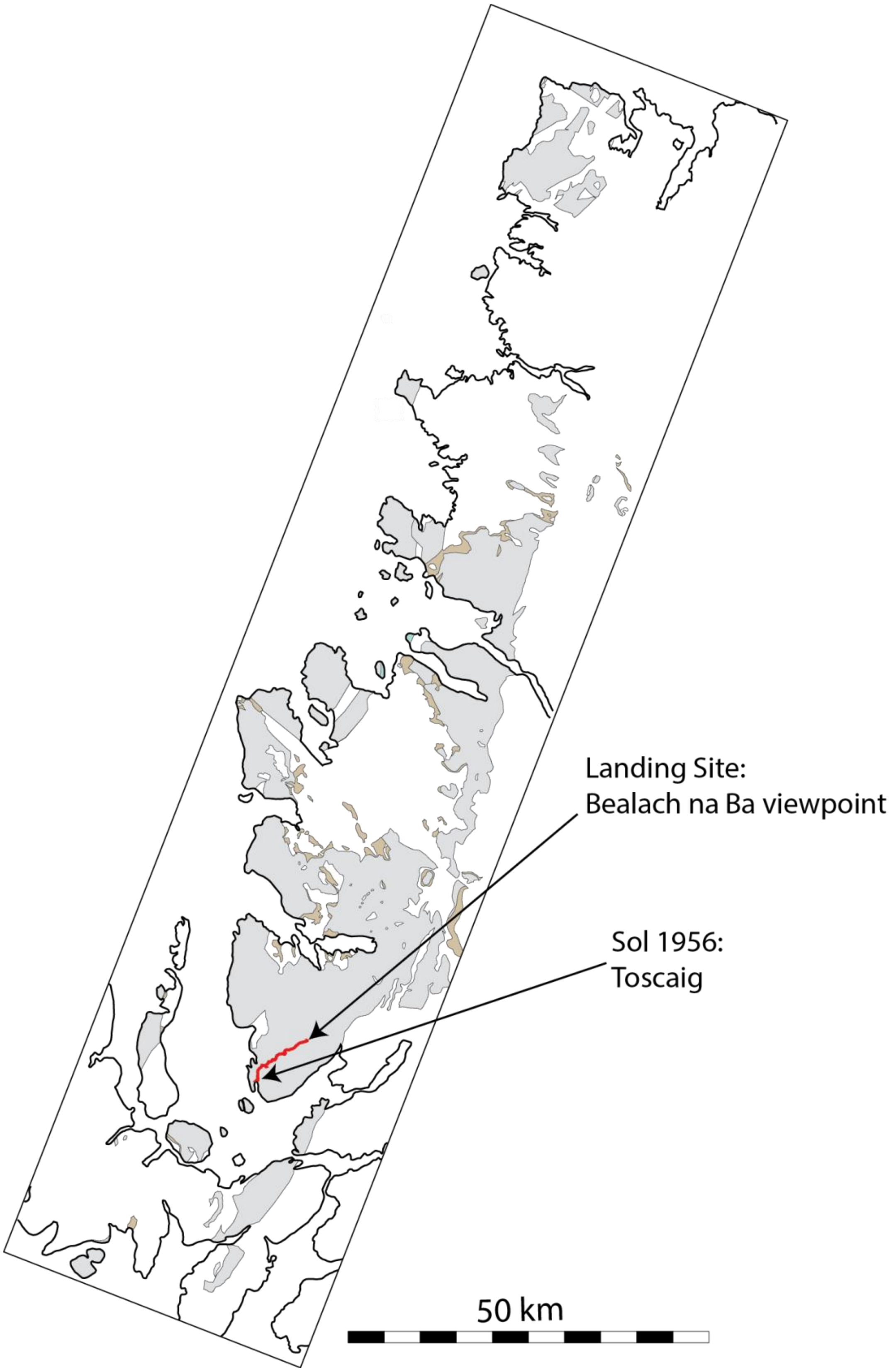

Figure 8.1. Comparison of the distance travelled by NASA's Mars rover *Curiosity* with the outcrop extent of the Torridonian Sandstones. Red line: Route driven through to the 1956 Martian day, or sol, of the rover's mission on Mars (February 5th, 2018). Hypothetically, had the rover landed at the Bealach na Ba viewpoint (24 on Figure 2.1), it would currently be located at Toscaig (25 on Figure 2.1).

In the few studies carried out to date, the possible consequences of the complete absence of vegetation on deposition and preservation have been acknowledged (e.g., Grotzinger et al., 2014; Edgar et al., 2018). Tangible characteristics of the terrestrial pre-vegetation alluvial record have even been used as supportive evidence for environmental interpretations on Mars (e.g., scarcity of fine-grained out-of-channel material in pre-vegetation alluvium (Chapter 3) was used to recommend a lacustrine, not overbank, origin of the Sheepbed mudstone at Gale Crater (Grotzinger et al., 2014)).

The terrestrial pre-vegetation sedimentary record remains the most relevant, directly accessible, repository of information for studies of planetary sedimentary geology. However, this record does not account for the many other differences between Mars and Earth which may affect sedimentation and ultimately preserved sedimentary strata (Table 8.1). For example, reduced gravity conditions relative to Earth will have affected the physical laws governing fluvial fluid-sediment interaction (e.g., acceleration due to gravity is an integral parameter for determining factors as diverse as the Froude Number or Reynold's Number of a flow, and is incorporated into predictions arising from Stokes' Law of Settling). Lower Martian gravity will result in generally lower sediment settling velocities, implying that in a layer of water of a given depth and velocity, sediment sorting will be less pronounced on Mars than on Earth (Kuhn, 2014). Reduced gravity would also likely reduce flow velocities on any given slope; suggesting that the formation of sinuous planforms would have been less reliant on bank cohesion than on Earth (Matsubara et al., 2015).

Table 8.1. Basic data of Mars and Earth. Source: http://solarsystem.jpl.nasa.gov/planets/ (unless stated). List of differences and effects not exhaustive.

	Earth	**Mars**	**Effect**
Vegetation	Yes	Presumably no	No biostabilization; increased sediment yield and erodibility
Gravity (m/s^2)	9.8	3.7	Influences flow hydraulics (e.g., reduces flow velocity) and the behaviour of sediment in water (e.g., reduces sediment settling velocity) (Kuhn, 2014); increases the static angle of repose of loose material (Kleinhans et al., 2011)
Atmospheric Pressure (kPa)	101	0.8	May permit liquid water only for a few hours and few days per year
Surface temperature range (°C)	-88/+58	-87/-5	May permit liquid water only for a few hours and few days per year

As well as different depositional controls, at present there are methodological differences between terrestrial and Martian sedimentary geology. Many characteristics used to study Earth's alluvial record are not available on Mars (Table 8.2), and basic tasks on Earth may take days on Mars (because of the technical aspects involved in oprating a rover mission) such that studies of even small outcrops can take months (e.g., Schieber et al., 2017). Even when employing similar techniques, they are employed at vastly different scales. For example, Edgar et al. (2018) analysed bed-scale sedimentary textures and geometries for the Shaler outcrop, an interpreted fluvial deposit identified by the *Curiosity* rover (Grotzinger et al., 2014). The study was restricted to a single 70 centimetre thick, 20 metre wide sand-body (Fig. 8.2), from which, Edgar et al. (2018) recognised 7 sedimentary facies and measured 57 foreset directions. This level of detail is rarely matched in studies of alluvium on Earth: the abundance of strata, even within a poorly exposed outcrop, usually exceeds these dimensions. As such, data is normally gathered from a wider area without such a high-resolution focus. Even in instances where this detail is undertaken, it is because the terrestrial strata have been identified as unique or interesting relative to surrounding strata: as opposed to the Shaler outcrop, which was studied because it happened to be in the path of *Curiosity*. This may raise questions regarding the comparability of interpretations between Mars and Earth.

Table 8.2. Methods of studying alluvium on Mars and Earth.

Technique	How applied in this study	Possible on Mars using NASA'S Mars rover *Curiosity*?
Measuring and describing vertical stratigraphic sections	Sedimentary logs were constructed at multiple locations. Various scales were used, depending on the detail required. In instances where multiple sections were accessible, the cleanest face was typically used. Logs were always measured up a stratigraphic section. For large outcrops, logs were supplemented by examination from a distance (where possible).	Yes. Scale is dependent on the available outcrop. Detail is dependent on accessibility and presentation of the available outcrop. Direction of measurement is dependent on the direction of travel (i.e., not necessarily up-section) (rovers rarely backtrack).
The construction of architectural panels	Architectural panels were constructed to document the details of large outcrops. Photographs were frequently taken during a reconnaissance visit. Photomosaics were later constructed and returned to the field so the details of architectural elements could be accurately mapped on the panels whilst in the field. Architectural panels were constructed to deduce complex facies changes occurring across large outcrops.	No. Large outcrops usually unavailable. Limited ability to study outcrops from different orientations. The vast majority of architectural elements would not be able to be directly measured, thus only allowing for interpretations of architectural elements (see Section 2.1.2). No revisiting of outcrop to ascertain stratigraphic relationships.
Description of lithological characteristics.	Lithologic classification was done by visual observation directly in the field. Colour was described using a fresh rock surface. Descriptions of sedimentary structures utilized 3D exposures whenever possible. Samples were readily obtained if further study was desired (e.g., thin section analysis) and could be used or discarded when fit.	Limited ability to describe lithological characteristics. On-board cameras cannot resolve grains finer than 42.1 microns (coarse silt). Fresh rock surfaces are rarely available (no use of rock hammer). On-board instruments unable to conduct a full assessment of composition and/or minerology and time and cost constraints means any concerted attempts to do so must be carefully assessed. Sampling unavailable.
Palaeocurrent analysis	Palaeocurrent directions were measured whenever reliable 3D surfaces were available. Numerous measurements were taken in order to give an indication of regional transport directions (e.g., n = 2333, Torridon alluvium; n = 431, Series Rouge)	Limited ability to study outcrops from multiple orientations in order to ascertain true dip direction.
Study of global stratigraphy	A database of 704 Archean-Carboniferous aged alluvial units was compiled in order to observe and quantify shifts in the frequency of sedimentary facies, structures, architectures and lithologies across this duration	Not available.

Figure 8.2. 'Shaler outcrop' detailed in Edgar et al. (2018) drawn to scale above alluvial successions studied in this project. Shaler outcrop dimensions graphically illustrated using red bar: A) Detail of cross-stratified sandstone, Shaler outcrop (Mastcam mosaic acquired on Sol 120, mcam00752). Image credit: NASA/JPL-Caltech/MSSS; B) Torridon alluvium at Bealach na Ba (Fig. 2.1); C) Series Rouge alluvium at Sables d'Or Quarry (Fig. 6.11).

Despite detailed facies analysis, the limited Shaler outcrop dimensions: 1) makes it difficult to determine the exact depositional setting of the fluvial deposit; and 2) prevents any hypotheses of the larger-scale fluvial morphology. Given these constraints, when it comes to making comparisons with pre-vegetation alluvium, it appears more detailed work on small alluvial outcrops on Earth may be of greater benefit to studies of small Martian outcrops than studies which reconstruct fluvial morphology based on observations across large stratigraphic successions.

The *in situ* analysis by Edgar et al. (2018) represent a major advance in sedimentology, although it also serves to emphasize that the study of Martian sedimentary rocks is still in its infancy. The amount of data that can be collected remains minimal, restricted to the limited ground-coverage provided by rovers. For example, following the *Opportunity* rover's investigation of Meridiani Planum, it is possible to estimate that only 2% of the approximated thickness of the sequence was studied (Edgett and Malin, 2002; Squyres et al., 2004; Grotzinger et al., 2005; Edgar et al., 2012). Without more detailed records of Martian alluvium, comparisons with pre-vegetation Earth landscapes will likely remain equivocal or simplistic. However, only an understanding of the abiotic skeleton behind rivers will permit a better understanding of the base palette of alluvial facies that are commonly shared by Earth and Mars, and the variants on each planet arising from the presence/absence of major differences in boundary conditions, including vegetation (Table 8.1).

Chapter 9

SUMMARY OF CONCLUSIONS

The ‘Torridonian Sandstones’, the main field site of this study, offers one of the best opportunities to study the sedimentary record of pre-vegetation rivers as the succession contains some of the most extensive and easily accessible exposures of pre-vegetation alluvial strata worldwide. Sedimentological analyses of pre-vegetation alluvium was also conducted on the Ediacaran-Lower Cambrian Series Rouge (NW France and the UK Channel Islands) and the Neoproterozoic Jacobsville Formation, with all results (after cross-comparison with multiple syn-vegetation successions) attesting to the distinct character of pre-vegetation alluvium.

Further proof of this claim is provided through a compilation of Earth’s 704 globally-distributed Archean-Carboniferous alluvial stratigraphic units. Analysis of this database unequivocally demonstrates that pre-vegetation alluvium is lithologically distinct from syn-vegetation alluvium. The long-held anecdotal contention that mudrock is rare in pre-vegetation alluvium was quantitatively tested and proven to be true: mudrock is on average 1.4 orders of magnitude less common in pre-vegetation alluvium than in syn-vegetation alluvium. This increase in global alluvial mudrock is a significant characteristic of the global rock record. The onset of the increase, coeval with the first appearance of plants in the fossil record, is unlikely to be a coincidence as plants can greatly contribute to the development and retention of alluvial mudrocks. The source-to-sink deposition of pre-vegetation mud was thus profoundly different to that seen at the present day.

In the absence of widespread mudrock, pre-vegetation alluvial successions predominantly consist of stacked, laterally extensive beds of coarser grained sediment, widely described as being ‘sheet-braided’. Despite seemingly repetitive sedimentology at outcrop scale, the ‘sheet-braided’ successions studied over the course of this project contain evidence of multiple fluvial styles: ‘sheet-braided’ architectures are polygenetic.

Torridon alluvium is dominated by laterally-extensive beds bound by planar basal erosion surfaces that are marked by coarser-lags and mudstone-rip-up clasts. Dominant trough cross- and subordinate planar-cross bedding record deposition from sinuous- and straight-crested dunes that migrated under lower-flow regime conditions. Thick successions of cross-bedded deposits are analogous to modern sediments deposited in the deeper portion of channels during active flow, and this is a likely origin for the prevalent Torridon facies. Less frequently, inclined cosets of cross-stratified sandstone were witnessed abutting a common underlying bounding surface, such that the packages could be interpreted as the deposits of barforms. The relative dominance of packages consisting of bedforms which accumulated predominantly by vertical aggradation, compared with the relative infrequency of packages of accretionary strata which could be interpreted as the deposits of barforms, suggests channels were laterally mobile, efficiently reworking barforms and biasing the depositional record towards the deposits of the deeper portion of channels during active flow. Low-dispersal of palaeocurrent directions across the entire outcrop belt and throughout its entire thickness indicates that the fluvial system was low-sinuosity. The profusion of cross-bedding, combined with evidence for barforms, which would have accreted during flood stages, suggests the fluvial system was perennial.

In stark contrast to Torridon alluvium, the Mesoproterozoic Meall Dearg Formation contains direct evidence for high-energy ephemeral floods. This interpretation can be permitted because the strata contain evidence of widespread upper and transitional upper flow regime bedforms deposited by rapidly decelerating flows, alongside bedding plane records of intervals of sedimentary stasis. The stacking of stratification types recording progressively lower flow regime conditions, as can be seen in the Meall Dearg Formation, is attributable to conditions of rapid sediment fall-out during falling flood stages. Rapid rates of deceleration also enabled the full preservation of convex lamina sets within antidunes. The preservation of both these sedimentary signatures attests to high rates of bed aggradation during sedimentation. The Meall Dearg Formation also contains evidence for deposition by aeolian dunes. These aeolian sedimentary facies are mutually exclusive to alluvium, possibly indicating that aeolian sediments were preserved only in regions less prone to reworking by alluvial activity.

The Ediacaran-Cambrian Series Rouge contains multiple circumstantial lines of evidence for the presence of microbial mats which, combined, suggest that the fluvial system operated within a 'microbial landscape'. Despite this, there is no evidence that microbial mats increased the stability of any components of the fluvial system, an observation in contrast to recent speculation. The fluvial deposits are characterised by repetitively stacked beds of trough cross-stratified sandstone representing deposition from migrating sinuous crested dunes in low sinuosity channels and subordinately on predominantly downcurrent-dipping barforms. Frequent channel-switching led to selective preservation of deep channel-bar deposits such that the preserved sedimentary architecture is characteristically 'sheet-braided'. The influence of microbial mats on preserved sedimentary architecture was negligible, such that the stratigraphic sedimentary record is biased in only preserving a record of the dominant purely physical processes in such systems.

The aforementioned case studies, combined with surveys of the wider literature, attest that pre-vegetation alluvial formations have a certain frequency distribution of character. While 'sheet-braided' architectures are nearly ubiquitous regardless of fluvial style, reports of classic meandering facies are extremely rare. One reported instance of interpreted pre-vegetation meandering channel deposits, the Allt-na-Béiste Member, was revisited in order to assess its significance. 'Sheet-braided' sedimentary packages recording the migration of low amplitude three-dimensional dunes dominate the succession. The tabular, stacked nature of the trough cross-stratified sets, and their broadly unimodal transport directions, imply that channel planforms were characteritically low sinuosity. Evidence for higher-sinuosity channels was rare but not absent entirely: sets of laterally accreting inclined heterolithic stratification (LA-IHS), the architectural element most frequently related to point bar deposition, were observed on six occassions. This element type contributes less than one percent of the total succession thickness, and when present, are no more than 41 cm thick. These isolated channels are interpreted as rarely developing, small, moderately sinuous creeks draining mud-rich plains during intervals of low-sedimentation. They are unrepresentative of the remainder of the formation, whose depositional character otherwise suggests deposition by shallow, low-sinuosity rivers. The existence of LA-IHS is in the Allt-na-Béiste Member is still significant in that it is entirely anomalous in comparison to other global pre-vegetation alluvium. Consequently, their recognition has added fuel into the debate surrounding how abundant pre-vegetation meandering rivers actually were. Geological observations find little conclusive evidence for pre-vegetation meanders, besides rare (and inconsequential) instances such as the LA-IHS in the Allt-na- Béiste Member.

The terrestrial pre-vegetation sedimentary record is the most relevant, directly accessible, repository of information for studies of Martian sedimentary geology. However, this record does not account for the many other differences between Mars and Earth which may affect sedimentation and ultimately preserved sedimentary strata (e.g., differences in acceleration due to gravity). As well as different depositional controls, there are methodological differences between terrestrial and Martian sedimentary geology. Many characteristics used to study Earth's alluvial record are not available on Mars and basic tasks on Earth may take days on Mars and cost significant sums on money. However, the data that is collected is usually to a level of detail unmatched in studies of alluvium on Earth. Martian sedimentary geology is still in its infancy, but upcoming rover missions and inevitable scientific advances will surely mean that the direct comparison of terrestrial and Martian strata will become possible in coming years.

REFERENCES

Alexander, J., 1992. Nature and origin of a laterally extensive alluvial sandstone body in the Middle Jurassic Scalby Formation. *Journal of the Geological Society*, ***149***, 431-441.

Alexander, J., Bridge, J.S., Cheel, R.J. & Leclair, S.F. 2001. Bedforms and associated sedimentary structures formed under supercritical water flows over aggrading sand beds. *Sedimentology,* ***48***, 133–152.

Alexander, J. & Fielding, C. 1997. Gravel antidunes in the tropical Burdekin River, Queensland, Australia. *Sedimentology,* ***44***, 327–337.

Allen, J.R. 1963. The classification of cross-stratified units. With notes on their origin. *Sedimentology*, ***2***, 93-114.

Allen, J.R.L. 1964. Studies in fluviatile sedimentation: six cyclothems from the Lower Old Red Sandstone, Anglowelsh Basin. *Sedimentology,* ***3***, 163-198.

Allen, J.R. 1965. A review of the origin and characteristics of recent alluvial sediments. *Sedimentology,* ***5***, 89-191.

Allen, J.R.L. 1970. Studies in fluviatile sedimentation: a comparison of fining-upwards cyclothems, with special reference to coarse-member composition and interpretation. *Journal of Sedimentary Research*, ***40***, *298-323*.

Allen, J.R.L., 1978. Keynote address: achievements and prospects in fluvial sedimentology. *In*: Miall, A.D. (ed). *Fluvial Sedimentology: Canadian Society of Petroleum Geologists Memoir*, ***5***, 849

Allen, J.R.L. 1982. *Sedimentary Structures: Their Character and Physical Basis.* Elsevier, Amsterdam.

Allen, J.R.L. 1983. Studies in fluviatile sedimentation: bars, bar-complexes and sandstone sheets (low-sinuosity braided streams) in the Brownstones (L. Devonian), Welsh Borders. *Sedimentary Geology*, ***33***, 237-293.

Alroy, J., Aberhan, M., Bottjer, D.J., Foote, M., Fürsich, F.T., Harries, P.J., Hendy, A.J., Holland, S.M., Ivany, L.C., Kiessling, W. & Kosnik, M.A. 2008. Phanerozoic trends in the global diversity of marine invertebrates. *Science*, ***321***, 97-100.

Amor, K., Hesselbo, S.P., Porcelli, D., Thackrey, S. & Parnell, J. 2008. A Precambrian proximal ejecta blanket from Scotland. *Geology*, ***36***, 303–306.

Aspler, L.B., Chiarenzelli, J.R. 1997. Initiation of 2.45–2.1 Ga intracratonic basin sedimentation of the Hurwitz Group, Keewatin Hinterland, Northwest Territories, Canada. *Precambrian Research, **81***, 265–297.

Astin, T.R., Rogers, D.A. 1991. ‘‘Subaqueous shrinkage cracks” in the Devonian of Scotland reinterpreted. *J. Sediment. Res.* ***61***, 850–859.

Auvray, B., 1979. *Genese et Evolution De La Croftte Continentale Dans Ie Nord Du Massif Armoricain.* Rennes University, These.

Auvray, B., Macé, J., Vidal, P., Vander Voo, R. 1980. Rb-Sr dating of the Plouézec volcanics, N Brittany: implications for the age of red beds (‘Series Rouges’) in the northern Armorican Massif. *Journal of the Geological Society*, ***137***, 207–210.

Baas, J.H. and Best, J.L. 2008. The dynamics of turbulent, transitional and laminar clay-laden flow over a fixed current ripple. *Sedimentology*, ***55***, 635-666.

Basu, A. 1981. Weathering before the advent of land plants: Evidence from unaltered detrital K-feldspars in Cambrian-Ordovician arenites. *Geology,* ***9***, 132-133.

Battison, L. & Brasier, M.D. 2012. Remarkably preserved prokaryote and eukaryote microfossils within 1 Ga-old lake phosphates of the Torridon Group, NW Scotland. *Precambrian Research,* ***196***, 204–217.

Beraldi-Campesi, H., Farmer, J.D., Garcia-Pichel, F. 2014. Modern terrestrial sedimentary biostructures and their fossil analogs in Mesoproterozoic subaerial deposits. *Palaios,* ***29***, 45–54.

Bernard, H.A., LeBlanc, R.J. & Major, C.F. 1962. *Recent and Pleistocene Geology of Southeast Texas: Field Excursion No. 3, November 10 and 11*.

Berner, R.A., 2004. *The Phanerozoic Carbon Cycle: CO^2 and O^2*. Oxford University Press.

Best, J.L., Ashworth, P.J., Bristow, C.S. & Roden, J. 2003. Three-dimensional sedimentary architecture of a large, mid-channel sand braid bar, Jamuna River, Bangladesh. *Journal of Sedimentary Research,* ***73***, 516–530.

Black, M. 1933. The algal sediments of Andros Island, Bahamas. *Philos. Trans. R. Soc. London Ser.* ***222***, 165–192.

Bland, B.H. 1984. Arumberia Glaessner & Walter, a review of its potential for correlation in the region of the Precambrian-Cambrian boundary. *Geol. Mag.* ***121***, 625–633.

Bluck, B.J. 1971. Sedimentation in the meandering River Endrick. *Scottish Journal of Geology*, ***7***, 93-138.

Blundell, D.J., Hurich, C.A. & Smithson, S.B. 1985. A model for the MOIST seismic reflection profile, N Scotland. *Journal of the Geological Society, London*, ***142***, 245–258.

Bogoni, M., Putti, M. & Lanzoni, S. 2017. Modeling meander morphodynamics over self-formed heterogeneous floodplains. *Water Resources Research*, ***53***, 5137-5157

Bosak, T., Bush, J.W.M., Flynn, M.R., Liang, B., Ono, S., Petroff, A.P. & Sim, M.S., 2010. Formation and stability of oxygen-rich bubbles that shape photosynthetic mats. *Geobiology,* ***8***, 45–55.

Bose, P.K., Eriksson, P.G., Sarkar, S., Wright, D.T., Samanta, P., Mukhopadhyay, S., Mandal, S., Banerjee, S. & Altermann, W. 2012. Sedimentation patterns during the Precambrian: a unique record?. *Marine and Petroleum Geology*, ***33***, 34-68.

Boulêtreau, S., Garabetian, F., Sauvage, S. & Sanchez-Perez, J.M. 2006. Assessing the importance of a self-generated detachment process in river biofilm models. *Freshwater Biol.* ***51***, 901–912.

Bouma, T.J., Temmerman, S., van Duren, L.A., Martini, E., Vandenbruwaene, W., Callaghan, D.P., Balke, T., Biermans, G., Klaassen, P.C., van Steeg, P., & Dekker, F. 2013. Organism traits determine the strength of scale-dependent biogeomorphic feedbacks: a flume study on three intertidal plant species. *Geomorphology,* ***180***, 57–65.

Boyce, C.K. & Lee, J.E. 2017. Plant Evolution and Climate Over Geological Timescales. *Annual Review of Earth and Planetary Sciences*, ***45***, 61-87.

Bradley, D.C. 2011. Secular trends in the geologic record and the supercontinent cycle. *Earth-Science Reviews*, ***108***, 16-33.

Bradley, W.H. 1933. Factors that determine the curvature of mud-cracked layers. *American Journal of Science*, 55–71.

Brasier, A.T., Culwick, T., Battison, L., Callow, R.H.T. & Brasier, M.D. 2016. Evaluating evidence from the Torridonian Supergroup (Scotland, UK) for eukaryotic life on land in the Proterozoic. *In*: Brasier, A.T., McIlroy, D. & McLoughlin, N. (eds) *Earth System Evolution and Early Life: A Celebration of the Work of Martin Brasier. Geological Society, London, Special Publications*, ***448***, 121–144.

Brasier, M.D. 1979. The Cambrian radiation event. *In*: House, M.R. (ed), *The Origin of the Major Invertebrate Groups, vol. 12. Academic Press London Systematics Association Sp*., 103–159.

Braudrick, C.A., Dietrich, W.E., Leverich, G.T. & Sklar, L.S. 2009. Experimental evidence for the conditions necessary to sustain meandering in coarse-bedded rivers. *Proceedings of the National Academy of Sciences*, ***106***, 16936-16941.

Briant, R.M., Bateman, M.D., Russell Coope, G. & Gibbard, P.L. 2005. Climatic control on Quaternary fluvial sedimentology of a Fenland Basin river, England. *Sedimentology*, ***52***, 1397-1423.

Bridge, J.S. 1985. Paleochannel Patterns Inferred From Alluvial Deposits: A Critical Evaluation Perspective: Perspective. *Journal of Sedimentary Research*, ***55***, 579-589

Bridge, J.S. 1993. The interaction between channel geometry, water flow, sediment transport and deposition in braided rivers. *Geol. Soc. London Spec. Publ.* ***75***, 13–71.

Bridge, J.S. & Jarvis, J. 1976. Flow and sedimentary processes in the meandering river South Esk, Glen Clova, Scotland. *Earth Surface Processes and Landforms*, ***1***, 303-336.

Brierley, G.J. & Hickin, E.J. 1991. Channel planform as a non-controlling factor in fluvial sedimentology: the case of the Squamish River floodplain, British Columbia. *Sedimentary geology*, ***75***, 67-83.

Bristow, C.S. 1987, Brahmaputra River: Channel migration and deposition. *In*: Ethridge, F.G., Flores, R.M. and Harvey, M.D. (ed). *Recent Developments in Fluvial Sedimentology: Contributions from the Third International Fluvial Sedimentology Conference: SEPM (Society for Sedimentary Geologists), Special Publication*, ***39***, 63–74.

Bristow, C.S. 1993. Sedimentary structures exposed in bar tops in the Brahmaputra River, Bangladesh. *Geological Society, London, Special Publications*, ***75***, 277-289.

Bristow, C. 1996. Reconstructing fluvial channel morphology from sedimentary sequences. *In*: Carling, P.A., Dawson, M.R. (eds). *Advances in Fluvial Dynamics and Stratigraphy. John Wiley & Sons, Ltd*., 351–371

Bristow, C.S. & Best, J.L. 1993. Braided rivers: perspectives and problems. *Geological Society, London, Special Publications*, ***75***, 1-11.

Cain, S.A. & Mountney, N.P. 2009. Spatial and temporal evolution of a terminal fluvial fan system: the Permian Organ Rock Formation, South-east Utah, USA. *Sedimentology*, ***56***, 1774–1800.

Callow, R.H., Battison, L. & Brasier, M.D. 2011. Diverse microbially induced sedimentary structures from 1 Ga lakes of the Diabaig Formation, Torridon Group, northwest Scotland. *Sedimentary Geology, **239***, 117–128.

Cant, D.J. & Walker, R.G. 1976. Development of a braided-fluvial facies model for the Devonian Battery Point Sandstone, Quebec. *Canadian Journal of Earth Sciences, **13***, 102-119.

Cant, D.J. & Walker, R.G. 1978. Fluvial processes and facies sequences in the sandy braided South Saskatchewan River, Canada. *Sedimentology, **25***, 625–648.

Carling, P.A., Golz, E., Orr, H.G. & Radecki-Pawlik, A. 2000. The morphodynamics of fluvial sand dunes in the River Rhine, near Mainz, Germany. I. Sedimentology and morphology. *Sedimentology, **47***, 227-252.

Cartigny, M.J., Ventra, D., Postma, G. & Den Berg, J.H. 2014. Morphodynamics and sedimentary structures of bedforms under supercritical-flow conditions: New insights from flume experiments. *Sedimentology, **61***, 712–748.

Chafetz, H.S. & Buczynski, C., 1992. Bacterially induced lithification of microbial mats. *Palaios, **7***, 277–293.

Chavdarian, G.V. & Sumner, D.Y. 2011. Origin and evolution of polygonal cracks in hydrous sulphate sands, White Sands National Monument, New Mexico. *Sedimentology, **58***, 407–423.

Church, M., 2006. Bed material transport and the morphology of alluvial river channels. *Annu. Rev. Earth Planet. Sci.*, ***34***, 325-354.

Church, M. & Rice, S.P. 2009. Form and growth of bars in a wandering gravel-bed river. *Earth Surface Processes and Landforms*, ***34***, 1422-1432.

Clarke, J.T., Warnock, R. & Donoghue, P.C. 2011. Establishing a time-scale for plant evolution. *New Phytologist*, ***192***, 266-301.

Collinson, J.D. 1970. Bedforms of the Tana river, Norway. *Geografiska Annaler. Series A. Physical Geography*, 31-56.

Colombera, L., Mountney, N.P. & McCaffrey, W.D. 2013. A quantitative approach to fluvial facies models: methods and example results. *Sedimentology*, ***60***, 1526-1558.

Constantine, J.A. & Dunne, T. 2008. Meander cutoff and the controls on the production of oxbow lakes. *Geology*, ***36***, 23-26.

Corcoran, P.L. & Mueller, W.U. 2002. The effects of weathering, sorting and source composition in Archean high-relief basins: examples from the Slave Province, Northwest Territories, Canada. *In*: Altermann, W. & Corcoran, P.L. (eds), *Precambrian Sedimentary Environments: A modern Approach to Ancient Depositional Systems, Special Publication*, ***33***, 183-211.

Corcoran, P.L., Mueller, W.U. & Chown, E.H. 1998. Climatic and tectonic influences on fan deltas and wave-to tide-controlled shoreface deposits: evidence from the Archaean Keskarrah Formation, Slave Province, Canada. *Sedimentary Geology*, ***120***, 125-152.

Cotter, E. 1978. The evolution of fluvial style, with special reference to the central Appalachian Paleozoic. *In*: Miall, A.D. (ed), *Fluvial Sedimentology: Canadian Society of Petroleum Geologists Memoir*, ***5***, 361–383.

Crowley, K.D. 1983. Large-scale bed configurations (macroforms), Platte River Basin, Colorado and Nebraska: primary structures and formative processes. *Geological Society of America Bulletin*, ***94***, 117-133.

D'Lemos, R.S., Strachan, R.A.& Topley, C.G. 1990. The Cadomian orogeny in the North Armorican Massif: a brief review. *Geol. Soc. London Spec. Publ.* ***51***, 3–12.

D'Lemos, R.S., Miller, B.V. & Samson, S.D. 2001. Precise U-Pb zircon ages from Alderney, Channel Islands: growing evidence for discrete Neoproterozoic magmatic episodes in northern Cadomia. *Geol. Mag.* ***138***, 719–726.

Dabard, M.P., Loi, A., & Paris, F. 2007. Relationship between phosphogenesis and sequence architecture: sequence stratigraphy and biostratigraphy in the Middle Ordovician of the Armorican Massif (W France). *Palaeogeogr. Palaeoclimatol. Palaeoecol.* ***248***, 339–356.

Dabard, M.P., Guillocheau, F., Loi, A., Paris, F., Balèvre, M. 2009. Evolution de la plate-forme paléozoïque centre-armoricaine del'Ordovicien au Dévonien. *12ème Congrès Français de Sédimentologie, Rennes, 2009. Livret d'excursions. Presqu'Ile de Crozon. Publication ASF*, ***65***, 55–102.

Dalrymple, R.W., Narbonne, G.M. & Smith, L. 1985. Eolian action and the distribution of Cambrian shales in North America. *Geology*, ***13***, 607-610.

Damuth, J.E., Kolla, V., Flood, R.D., Kowsmann, R.O., Monteiro, M.C., Gorini, M.A., Palma, J.J. & Belderson, R.H. 1983. Distributary channel meandering and bifurcation patterns on the Amazon deep-sea fan as revealed by long-range side-scan sonar (GLORIA). *Geology*, ***11***, 94-98.

Davies, N.S. & Gibling, M.R. 2010a. Cambrian to Devonian evolution of alluvial systems: the sedimentological impact of the earliest land plants. *Earth-Science Reviews*, ***98***, 171-200.

Davies, N.S. & Gibling, M.R. 2010b. Paleozoic vegetation and the Siluro-Devonian rise of fluvial lateral accretion sets. *Geology*, ***38***, 51-54.

Davies, N.S. & Gibling, M.R. 2012. Early Cambrian metazoans in fluvial environments, evidence of the non-marine Cambrian radiation: COMMENT. *Geology*, ***40***, 270.

Davies, N.S. & Gibling, M.R. 2013. The sedimentary record of Carboniferous rivers: Continuing influence of land plant evolution on alluvial processes and Palaeozoic ecosystems. *Earth-Science Reviews*, ***120***, 40-79.

Davies, N.S., Gibling, M.R., McMahon, W.J., Slater, B.J., Long, D.G., Bashforth, A.R., Berry, C.M., Falcon-Lang, H.J., Gupta, S., Rygel, M.C. & Wellman, C.H. 2017a. Discussion on 'Tectonic and environmental controls on Palaeozoic fluvial environments: reassessing the impacts of early land plants on sedimentation'Journal of the Geological Society, https://doi. org/10.1144/jgs2016-063. *Journal of the Geological Society*, pp.jgs2017-004.

Davies, N.S., Gibling, M.R. & Rygel, M.C., 2011. Alluvial facies evolution during the Palaeozoic greening of the continents: case studies, conceptual models and modern analogues. *Sedimentology*, ***58***, 220-258.

Davies, N.S., Liu, A.G., Gibling, M.R. & Miller, R.F. 2016. Resolving MISS conceptions and misconceptions: A geological approach to sedimentary surface textures generated by microbial and abiotic processes. *Earth-Science Reviews*, ***154***, 210–246.

Davies, N.S., McMahon, W.J., Shillito, A.S., 2018. A graphic method for depicting horizontal direction data on vertical outcrop photographs. *Journal of Sedimentary Research*, ***88,*** 516-521.

Davies, N.S., Rygel, M.C. & Gibling, M.R. 2010. Marine influence in the Upper Ordovician Juniata Formation (Potters Mills, Pennsylvania): implications for the history of life on land. *Palaios*, ***25***, 527-539.

Davies, N.S., Shillito, A.P. & McMahon, W.J. 2017b. Short-term evolution of primary sedimentary surface textures (microbial, ichnological) on a dry stream bed: modern observations and ancient implications. *Palaios*, ***32***, 125–134.

Davies, N.S., Turner, P. & Sansom, I.J. 2005. Soft-sediment deformation structures in the Late Silurian Stubdal Formation: the result of seismic triggering. *Norwegian Journal of Geology/Norsk Geologisk Forening*, ***85***, 233-243.

Davis, J.M., Balme, M., Grindrod, P.M., Williams, R.M.E. & Gupta, S., 2016. Extensive Noachian fluvial systems in Arabia Terra: Implications for early Martian climate. *Geology*, ***44***, 847-850.

de Almeida, R.P., Marconato, A., Freitas, B.T. & Turra, B.B. 2016. The ancestors of meandering rivers. *Geology*, ***44***, 203-206.

De Beer, D. & Kühl, M., 2001. Interfacial microbial mats and biofilms. *In*: Boudreau, B. P., Jørgensen, B.B. (eds), *The Benthic Boundary Layer.* Oxford University Press, New York.

De Boer, P. 1979. Convolute lamination of modern sands in the estuary of the Oosterschelde, the Netherlands, formed as a result of trapped air. *Sedimentology,* ***26***, 283–294.

De Boer, P.D. 1981. Mechanical effects of micro-organisms on intertidal bedform migration. *Sedimentology,* ***28***, 129–132.

Deb, S.P., Schieber, J. & Chaudhuri, A.K., 2007. Microbial Mat Features in Mudstones of the Mesoproterozoic Somanpalli Group. Pranhita-Godavari Basin, India. *In*: Schieber, J., Bose, P.K., Eriksson, P.G., Banerjee, S., Sarkar, S., Altermann, W. & Catuneanu, O. (eds) *Atlas of Microbial Mat Features Preserved Within the Siliciclastic Rock Record. Atlases in Geosciences, 39.* Elsevier, Amsterdam.

Dickinson, W.R. & Suczek, C.A. 1979. Plate tectonics and sandstone compositions. *Aapg Bulletin*, ***63***, 2164-2182.

Donaldson, J.A. & de Kemp, E.A. 1998. Archaean quartz arenites in the Canadian Shield: examples from the Superior and Churchill Provinces. *Sedimentary Geology*, ***120***, 153-176.

Doré, F. 1972. La transgression majeure du Paleozoique inferieur dans Ie Nord-Est du Massif armoricain. *Bull. Soc. Geol. Fr, **7***, 79-93.

Doré, F. 1994. *Cambrian of the Armorican massif. Pre-Mesozoic Geology in France and Related Areas*. Springer, Berlin Heidelberg, 136–141.

Dornbos, S.Q., Noffke, N. & Hagadorn, J.W. 2007. 4 (d). Mat-decay features. Atlas of microbial mats features preserved within the siliciclastic rock record. Atlases in Geosciences, ***2***, 106–110.

Dott, Jr, R.H. 2003. The importance of eolian abrasion in supermature quartz sandstones and the paradox of weathering on vegetation-free landscapes. *The Journal of geology*, ***111***, 387-405.

Dott Jr., R.H. & Byers, C.W. 1981. SEPM research conference on modern shelf and ancient cratonic sedimentation — the orthoquartzite-carbonate suite revisited. *Journal of Sedimentary Petrology*, ***51***, 329–347.

Dott Jr, R.H., Byers, C.W., Fielder, G.W., Stenzel, S.R. & Winfree, K.E. 1986. Aeolian to marine transition in Cambro-Ordovician cratonic sheet sandstones of the northern Mississippi Valley, USA. *Sedimentology*, ***33***, 345-367.

Doyle, L.J., Carder, K.L. & Steward, R.G. 1983. The hydraulic equivalence of mica. *J. Sediment. Res.* ***53***, 643–648.

Driese, S.G., Jirsa, M.A., Ren, M., Brantley, S.L., Sheldon, N.D., Parker, D. & Schmitz, M. 2011. Neoarchean paleoweathering of tonalite and metabasalt: implications for reconstructions of 2.69 Ga early terrestrial ecosystems and paleoatmospheric chemistry. *Precambrian Research, **189***, 1–17.

Edgar, L.A., Grotzinger, J.P., Hayes, A.G., Rubin, D.M., Squyres, S.W., Bell, J.F. & Herkenhoff, K.E. 2012. Stratigraphic architecture of bedrock reference section, Victoria crater, Meridiani Planum, Mars. *Sedimentary Geology of Mars, SEPM Special Publication*, ***102***, 195-209.

Edgar, L.A., Gupta, S., Rubin, D.M., Lewis, K.W., Kocurek, G.A., Anderson, R.B., Bell, J.F., Dromart, G., Edgett, K.S., Grotzinger, J.P. & Hardgrove, C. 2018. Shaler: In situ analysis of a fluvial sedimentary deposit on Mars. *Sedimentology*. doi:10.1111/sed.12370.

Edgett, K.S. & Malin, M.C. 2002. Martian sedimentary rock stratigraphy: Outcrops and interbedded craters of northwest Sinus Meridiani and southwest Arabia Terra. *Geophysical Research Letters*, ***29***, 2175

Edwards, D., Cherns, L. & Raven, J.A. 2015. Could land-based early photosynthesizing ecosystems have bioengineered the planet in mid-Palaeozoic times?. *Palaeontology, **58***, 803-837.

Els, B.G. 1990. Determination of some palaeohydraulic parameters for a fluvial Witwatersrand succession. *South African Journal of Geology*, ***93***, 531-537.

Els, B.G. 1998. The auriferous late Archaean sedimentation systems of South Africa: unique palaeo-environmental conditions?. *Sedimentary Geology*, ***120***, 205-224.

Els, B.G., Van den Berg, W.A. & Mayer, J.J. 1995. The Black Reef Quartzite Formation in the western Transvaal: sedimentological and economic aspects, and significance for basin evolution. *Miner. Deposita, **30***, 112–123.

Endo, R. 1933. *Manchuriophycus* nov. gen., from a Sinian formation of South Manchuria. *Japanese Journal of Geology and Geography, **11***, 1–2.

Eriksson, K.A. & Simpson, E.L., 1998. Controls on spatial and temporal distribution of Precambrian eolianites. *Sedimentary Geology*, **120**, 275-294.

Eriksson, P.G. 2007. Classification of structures left by microbial mats in their host sediments. *In*: Schieber, J., Bose, P.K., Eriksson, P.G., Banerjee, S., Sarkar, S., Altermann, W. & Catuneanu, O. (eds) *Atlas of Microbial Mat Features Preserved Within the Siliciclastic Rock Record. Atlases in Geosciences. Elsevier, Amsterdam, **39***.

Eriksson, P.G., Bumby, A.J., Brümer, J.J. & van der Neut, M. 2006. Precambrian fluvial deposits: enigmatic palaeohydrological data from the c. 2–1.9 Ga Waterberg Group, South Africa. *Sedimentary Geology*, ***190***, 25-46.

Eriksson, P.G., Condie, K.C., Tirsgaard, H., Mueller, W.U., Altermann, W., Miall, A.D., Aspler, L.B., Catuneanu, O. & Chiarenzelli, J.R. 1998. Precambrian clastic sedimentation systems. *Sedimentary Geology*, ***120***, 5-53.

Eriksson, P.G., Wright, D.T., Bumby, A.J., Catuneanu, O. & Mostert, P. 2009. Possible evidence for episodic epeiric marine and fluvial sedimentation (and implications for palaeoclimatic conditions), c. 2.3–1.8 Ga, Kaapvaal craton, South Africa. *Palaeogeogr. Palaeoclimatol. Palaeoecol.* ***273***, 153–173.

Ethridge, F.G. 2011. Interpretation of ancient fluvial channel deposits: review and recommendations. *In*: Davidson, S., Leleu, S., North, C.P. (eds), *From River to Rock Record: The Preservation of Fluvial Sediments and their Subsequent Interpretation*. *SEPM*, ***97***, 9-35.

Fahnestock, R.K. 1965. Stratification, bed forms, and flow phenomena (with an example from the Rio Grande). *In*: Middleton, G.V. (ed), *Soc. Econ. Paleontologists and Mineralogists, Spec. Pub*, ***12***, 84–115.

Fedo, C.M. & Cooper, J.D. 1990. Braided fluvial to marine transition: the basal Lower Cambrian Wood Canyon Formation, southern Marble Mountains, Mojave Desert, California. *Journal of Sedimentary Research*, ***60***, 220-234

Fedorchuk, N.D., Dornbos, S.Q., Corsetti, F.A., Isbell, J.L., Petryshyn, V.A., Bowles, J.A. & Wilmeth, D.T. 2016. Early non-marine life: evaluating the biogenicity of Mesoproterozoic fluvial-lacustrine stromatolites. *Precambrian Research*, ***275***, 105-118.

Field, J. 2001. Channel avulsion on alluvial fans in southern Arizona. *Geomorphology*, ***37***, 93–104.

Fielding, C.R. 2006. Upper flow regime sheets, lenses and scour fills: extending the range of architectural elements for fluvial sediment bodies. *Sedimentary Geology*, ***190***, 227-240.

Fisk, H.N. 1944. Geological Investigation of the Alluvial Valley of the Lower Mississippi River. *Mississippi River Commission, Vicksburg, Mississippi.*

Folk, R.L., 1980. *Petrology of sedimentary rocks*. Hemphill Publishing Company.

Fordham, A.W. 1990. Weathering of biotite into dioctahedral clay minerals. *Clay Miner*. ***25***, 51–63.

Fralick, P. 1999. Paleohydraulics of chute-and-pool structures in a Paleoproterozoic fluvial sandstone. *Sedimentary Geology,* ***125***, 129–134.

Fralick, P. & Zaniewski, K., 2012. Sedimentology of a wet, pre-vegetation floodplain assemblage. *Sedimentology,* ***59***, 1030-1049.

Friend, P,F. 1983. Towards the field classification of alluvial architecture or sequence. *In*: J.D, Collinson and J. Lewin (ed), *Modern and Ancient Fluvial Systems. Int. Assoc. Sediment. Spec. Publ.,* ***6***, 345-354.

Friend, P.F., Slater, M.J. & Williams, R.C. 1979. Vertical and lateral building of river sandstone bodies, Ebro Basin, Spain. *Journal of the Geological Society, London,* ***136***, 39–46,

Friend, P.L., Lucas, C.H., Holligan, P.M. & Collins, M.B. 2008. Microalgal mediation of ripple mobility. *Geobiology,* ***6***, 70–82.

Fryberger, S.G., Schenk, C.J. & Krystinik, L.F. 1988. Stokes surfaces and the effects of near-surface groundwater-table on aeolian deposition. *Sedimentology,* ***35***, 21–41.

Fryirs, K.A. & Brierley, G.J. 2012. *Geomorphic analysis of river systems: an approach to reading the landscape*. John Wiley & Sons.

Fuller, A.O. 1985. A contribution to the conceptual modelling of pre-Devonian fluvial systems. *South African Journal of Geology*, **88**, 189-194.

Gall, R.D., Birgenheier, L.P. & Berg, M.D.V. 2017. Highly Seasonal and Perennial Fluvial Facies: Implications For Climatic Control On the Douglas Creek and Parachute Creek Members, Green River Formation, Southeastern Uinta Basin, Utah, USA. *Journal of Sedimentary Research,* ***87***, 1019-1047.

Gao, C., Boreham, S., Preece, R.C., Gibbard, P.L. and Briant, R.M. 2007. Fluvial response to rapid climate change during the Devensian (Weichselian) Lateglacial in the River Great Ouse, southern England, UK. *Sedimentary Geology*, ***202***, 193-210.

Gehling, J.G. 1999. Microbial mats in terminal Proterozoic siliciclastics; Ediacaran death masks. *Palaios*, ***14***, 40–57.

Gehling, J.G., Droser, M.L. 2009. Textured organic surfaces associated with the Ediacara biota in South Australia. *Earth Sci. Rev.* ***96***, 196–206.

Gensel, P.G., Kotyk, M.E. & Basinger, J.F. 2001. Morphology of above- and belowground structures in Early Devonian (Pragian-Emsian) plants. *In*: Gensel, P.G., Edwards, D. (eds), *Plants Invade the Land: Evolutionary and Environmental Perspectives. Columbia University Press, New York*, 83–102.

Gerdes, G. 2007. Structures Left by Modern Microbial Mats in their Host Sediments. *In*: Schieber, J., Bose, P.K., Eriksson, P.G., Banerjee, S., Sarkar, S., Altermann, W. & Catuneanu, O. (eds) *Atlas of Microbial Mat Features Preserved Within the Siliciclastic Rock Record. Atlases in Geosciences, **39***, 5-38, Elsevier, Amsterdam.

Gerdes, G., Krumbein, W.E. 1987. Biolaminated Deposits. *Lecture Notes in Earth Sciences, **9***, 183. Springer, New York.

Germs, G.J.B. 1983. Implications of a sedimentary facies and depositional environmental analysis of the Nama Group in South West Africa (Namibia). *Spec. Publ. Geol. Soc. Afr.* ***11***, 89–114.

Ghazi, S. & Mountney, N.P. 2009. Facies and architectural element analysis of a meandering fluvial succession: The Permian Warchha Sandstone, Salt Range, Pakistan. *Sedimentary Geology, **221***, 99-126.

Ghinassi, M. & Ielpi, A. 2018. Precambrian snapshots: Morphodynamics of Torridonian fluvial braid-bars revealed by three-dimensional photogrammetry and outcrop sedimentology. *Sedimentology, **65***, 492-516

Ghinassi, M., Ielpi, A., Aldinucci, M. and Fustic, M. 2016. Downstream-migrating fluvial point bars in the rock record. *Sedimentary Geology*, ***334***, 66-96.

Gibling, M.R. 2006. Width and thickness of fluvial channel bodies and valley fills in the geological record: a literature compilation and classification. *Journal of sedimentary Research*, ***76***, 731-770.

Gibling, M.R. & Davies, N.S. 2012. Palaeozoic landscapes shaped by plant evolution. *Nature Geoscience*, ***5***, 99-105.

Gilliam, A.E. & Lerman, A. 2016. Formation mechanisms of channels on Titan through dissolution by ammonium sulfate and erosion by liquid ammonia and ethane. *Planetary and Space Science*, ***132***, pp.13-22.

Glaessner, M.F. & Walter, M.R. 1975. New Precambrian fossils from the Arumbera Sandstone, Northern Territory, Australia. *Alcheringa, **1***, 59–69.

Glumac, B., Curran, H.A., Motti, S.A., Weigner, M.M. & Pruss, S.B. 2011. Polygonal sandcracks: Unique sedimentary desiccation structures in Bahamian ooid grainstone. *Geology*, ***39***, 615–618.

Godin, P. 1991. Fining-upwards cycles in the sandy-braided river deposits of the Westwater Canyon Member (Upper Jurassic), Morrison Formation, New Mexico. *Sedimentary Geology*, ***70***, 61–82.

Gouramanis, C., Webb, J.A. & Warren, A.A., 2003. Fluviodeltaic sedimentology and ichnology of part of the Silurian Grampians Group, western Victoria. *Australian Journal of Earth Sciences*, ***50***, 811-825.

Graba, M., Moulin, F.Y., Boulêtreau, S., Garabétian, F., Kettab, A., Eiff, O., Sánchez-Pérez, J.M. & Sauvage, S., 2010. Effect of near-bed turbulence on chronic detachment of epilithic biofilm: experimental and modeling approaches. *Water Resour. Res.* ***46***, 1-15

Graba, M., Sanchez-Perez, J.M., Moulin, F.Y., Urrea, G., Sabater, S. & Sauvage, S. 2013. Interaction between local hydrodynamics and algal community in epilithic biofilm. *Water Res.* ***47***, 2153–2163.

Graba, M., Sauvage, S., Majdi, N., Mialet, B., Moulin, F.Y., Urrea, G. & Sanchez-Pérez, J.M. 2014. Modelling epilithic biofilms combining hydrodynamics, invertebrate grazing and algal traits. *Freshwater Biol.* ***59***, 1213–1228.

Gracie, A.J. & Stewart, A.D. 1967. Torridonian sediments at Enard Bay, Rossshire. *Scottish Journal of Geology*, ***3***, 181–194.

Grotzinger, J.P., Arvidson, R.E., Bell, J.F., Calvin, W., Clark, B.C., Fike, D.A., Golombek, M., Greeley, R., Haldemann, A., Herkenhoff, K.E. & Jolliff, B.L. 2005. Stratigraphy and sedimentology of a dry to wet eolian depositional system, Burns formation, Meridiani Planum, Mars. *Earth and Planetary Science Letters*, ***240***, 11-72.

Grotzinger, J.P., Gupta, S., Malin, M.C., Rubin, D.M., Schieber, J., Siebach, K., Sumner, D.Y., Stack, K.M., Vasavada, A.R., Arvidson, R.E. & Calef, F. 2015. Deposition, exhumation, and paleoclimate of an ancient lake deposit, Gale crater, Mars. *Science*, ***350***, 1-12.

Grotzinger, J.P., Sumner, D.Y., Kah, L.C., Stack, K., Gupta, S., Edgar, L., Rubin, D., Lewis, K., Schieber, J., Mangold, N. & Milliken, R., 2014. A habitable fluvio-lacustrine environment at Yellowknife Bay, Gale Crater, Mars. *Science*, ***343***, 1242777.

Gurnell, A. 2014. Plants as river system engineers. *Earth Surface Processes and Landforms*, ***39***, 4-25.

Hadlari, T., Rainbird, R.H. & Donaldson, J.A. 2006. Alluvial, eolian and lacustrine sedimentology of a Paleoproterozoic half-graben, Baker Lake Basin, Nunavut, Canada. *Sedimentary Geology*, ***190***, 47-70.

Hagadorn, J.W. Mcdowell, C. 2012. Microbial influence on erosion, grain transport and bedform genesis in sandy substrates under unidirectional flow. *Sedimentology*, ***59***, 795–808.

Hagstrum, J.T., Van der Voo, R., Auvray, B. & Bonhommet, N. 1980. Eocambrian—Cambrian palaeomagnetism of the Armorican Massif, France. *Geophys. J. Int.* ***61***, 489–517.

Hajek, E.A. & Heller, P.L. 2012. Flow-depth scaling in alluvial architecture and nonmarine sequence stratigraphy: example from the Castlegate Sandstone, central Utah, USA. *Journal of Sedimentary Research*, ***82***, 121-130.

Hajek, E.A. & Straub, K.M. 2017. Autogenic sedimentation in clastic stratigraphy. *Annual Review of Earth and Planetary Sciences,* ***45***, 681-709

Hamblin, W. K. 1958. Cambrian sandstones of northern Michigan. *Mich. Dept. Conserv., Geol. Surv. Div., Publ.,* ***51***, 146.

Häntzschel, W. 1962. Trace fossils and Problematica. *In*: Moore, R.C. (ed) *Treatise on Paleontology (Part W, Conodonts, Conoidal Shells of Uncertain Affinities, Worms, Trace Fossils, Problematica). Geological Society of America, Boulder, CO, and University of Kansas, Lawrence,* 177–245.

Harazim, D., Callow, R.H. & Mcilroy, D., 2013. Microbial mats implicated in the generation of intrastratal shrinkage ('synaeresis') cracks. *Sedimentology*, ***60***, 1621–1638.

Harden, D.R. 1990. Controlling factors in the distribution and development of incised meanders in the central Colorado Plateau. *Geological Society of America Bulletin*, ***102***, 233-242.

Harrison, P.A. 1979. *The structure and sedimentology of the Sinclair Group in the Awasib Mountains, Diamond Area No. 2, South West Africa/Namibia*, B.Sc. (Hons.) thesis (unpubl.). Rhodes University, Grahamstown, 69.

Hartley, A.J., Weissmann, G.S., Nichols, G.J. & Warwick, G.L. 2010. Large distributive fluvial systems: characteristics, distribution, and controls on development. *Journal of Sedimentary Research*, ***80***, 167-183.

Hartley, A.J., Owen, A., Swan, A., Weissmann, G.S., Holzweber, B.I., Howell, J., Nichols, G. & Scuderi, L. 2015. Recognition and importance of amalgamated sandy meander belts in the continental rock record. *Geology*, ***43***, 679-682.

Hatch, J.R. & Morey, G.B. 1985. Hydrocarbon source rock evaluation of Middle Proterozoic Solor Church Formation, North American Mid-Continent Rift System, Rice County, Minnesota. *AAPG Bulletin*, ***69***, 1208-1216.

Hazen, R.M., Sverjensky, D.A., Azzolini, D., Bish, D.L., Elmore, S.C., Hinnov, L. & Milliken, R.E. 2013. Clay mineral evolution. *American Mineralogist*, ***98***, 2007-2029.

Heller, P.L. & Paola, C. 1996. Downstream changes in alluvial architecture: an exploration of controls on channel-stacking patterns. *Journal of Sedimentary Research*, ***66***, 297-306.

Hillier, R.D., Edwards, D. & Morrissey, L.B. 2008. Sedimentological evidence for rooting structures in the Early Devonian Anglo-Welsh Basin (UK), with speculation on their producers. *Palaeogeogr. Palaeoclimatol. Palaeoecol.* ***270***, 366–380.

Hiscott, R.N., James, N.P. & Pemberton, S.G. 1984. Sedimentology and ichnology of the Lower Cambrian Bradore Formation, coastal Labrador: fluvial to shallow-marine transgressive sequence. *Bulletin of Canadian Petroleum Geology*, ***32***, 11-26.

Hjellbakk, A. 1997. Facies and fluvial architecture of a high-energy braided river: the Upper Proterozoic Seglodden Member, Varanger Peninsula, northern Norway. *Sedimentary Geology*, ***114***, 131-161.

Hoffman, P.F. 2009. Pan-glacial—a third state in the climate system. *Geology Today*, ***25***, 100-107.

Hofmann, H.J. 1966. Ordovician Paleocurrents near Cincinnati, Ohio. *The Journal of Geology*, ***74***, 868-890.

Horodyski, R.J. & Knauth, L.P. 1994. Life on land in the Precambrian. *Science-AAASWeekly Paper Edition-including Guide to Scientific Information,* ***263***, 494–498.

Horodyski, R.J., Bloeser, B. & Von der Haar, S. 1977. Laminated algal mats from a coastal lagoon, Laguna Mormona, Baja California, Mexico. *J. Sediment. Petrol.* ***47***, 680–696.

Hughes, Z.J., 2011. Tidal channels on tidal flats and marshes. *In*: Davis Jr, R.A. & Dalrymple, R.W. (eds), *Principles of Tidal Sedimentology, Springer Science and Buisness Media,* 269-300.

Hunter, R.E. 1977. Basic types of stratification in small eolian dunes. *Sedimentology,* ***24***, 361–387.

Ielpi, A. 2016. Lateral accretion of modern unvegetated rivers: remotely sensed fluvial–aeolian morphodynamics and perspectives on the Precambrian rock record. *Geological Magazine*, ***154***, 609-624.

Ielpi, A. & Ghinassi, M. 2014. Planform architecture, stratigraphic signature and morphodynamics of an exhumed Jurassic meander plain (Scalby Formation, Yorkshire, UK). *Sedimentology*, ***61***, 1923-1960.

Ielpi, A. & Ghinassi, M. 2015. Planview style and palaeodrainage of Torridonian channel belts: Applecross Formation, Stoer Peninsula, Scotland. *Sedimentary Geology*, ***325***, 1-16.

Ielpi, A. & Ghinassi, M. 2016. A sedimentary model for early Palaeozoic fluvial fans, Alderney Sandstone Formation (Channel Islands, UK). *Sediment. Geol.* ***342***, 31–46.

Ielpi, A. & Rainbird, R.H. 2015. Architecture and morphodynamics of a 1·6 Ga fluvial sandstone: Ellice Formation of Elu Basin, Arctic Canada. *Sedimentology,* ***62***, 1950–1977.

Ielpi, A. & Rainbird, R.H. 2016a. Reappraisal of Precambrian sheet-braided rivers: Evidence for 1· 9 Ga deep-channelled drainage. *Sedimentology,* ***63***, 1550-1581.

Ielpi, A. and Rainbird, R.H., 2016. Highly variable Precambrian fluvial style recorded in the Nelson Head Formation of Brock Inlier (Northwest Territories, Canada). *Journal of Sedimentary Research*, ***86***, 199-216.

Ielpi, A., Rainbird, R.H., Ventra, D. & Ghinassi, M., 2017. Morphometric convergence between Proterozoic and post-vegetation rivers. *Nature communications*, ***8***, 15250. https://doi.org/10.1038/ncomms15250.

Ielpi, A., Ventra, D. & Ghinassi, M. 2016. Deeply channelled Precambrian rivers: Remote sensing and outcrop evidence from the 1.2 Ga Stoer Group of NW Scotland. *Precambrian Research*, ***281***, 291-311.

Ilgen, A.G., Heath, J.E., Akkutlu, I.Y., Bryndzia, L.T., Cole, D.R., Kharaka, Y.K., Kneafsey, T.J., Milliken, K.L., Pyrak-Nolte, L.J. & Suarez-Rivera, R. 2017. Shales at all scales: Exploring coupled processes in mudrocks. *Earth-Science Reviews*, ***166***, 132-152

Jackson, R.G. 1975. Hierarchical attributes and a unifying model of bed forms composed of cohesionless material and produced by shearing flow. *Geological Society of America Bulletin*, ***86***, 1523-1533.

Jackson II, R.G. 1977. Preliminary evaluation of lithofacies models for meandering alluvial streams. *AAPG Memoir,* ***5***, 543-576

Jones, D.S., Creel, R.C., Rios, B. & Ramos, D.P.S. 2015. Chemostratigraphy of an Ordovician–Silurian carbonate platform: δ13C records below glacioeustatic exposure surfaces. *Geology,* ***43***, 59-62.

Kaiser, E. 1931. Der Grundsatz des Aktualismus in der Geologie. *Zeitschrift der Deutschen Geologischen Gesellschaft*, 389-407.

Kalliokoski, J. 1982. 7E: Jacobsville Sandstone. *Geological Society of America Memoirs*, ***156***, 147-156.

Karlstrom, L., Gajjar, P. & Manga, M. 2013. Meander formation in supraglacial streams. *Journal of Geophysical Research: Earth Surface*, ***118***, 1897-1907.

Karol, K.G., McCourt, R.M., Cimino, M.T. & Delwiche, C.F. 2001. The closest living relatives of land plants. *Science*, ***294***, 2351-2353.

Kelly, S.E.A.N. 2006. Scaling and Hierarchy in Braided Rivers and Their Deposits: Examples and Implications for Reservoir Modelling. *In:* Sambrook Smith, G.H., Best, J.L., Bristow, C.S. & Petts, G.E. (eds), *Braided Rivers: Process, Deposits, Ecology and Management. Special Publication of the International Association of Sedimentologists*, ***36***, 75–106. Blackwell, Oxford

Kemp, J. 1996. The Kuara Formation (northern Arabian Shield); definition and interpretation: a probable fault-trough sedimentary succession. *J. Afr. Earth Sc.* ***22***, 507–523.

Kennedy, J.F. 1963. The mechanics of dunes and antidunes in erodible-bed channels. *Journal of Fluid Mechanics*, ***16***, 521–544.

Kennedy, K.L., Gensel, P.G. & Gibling, M.R. 2012. Paleoenvironmental inferences from the classic Lower Devonian plant-bearing locality of the Campbellton Formation, New Brunswick, Canada. *Palaios*, ***27***, 424–438.

Kennedy, M.J., Droser, M., Mayer, L.M., Pevear, D. & Mrofka, D. 2006. Late Precambrian oxygenation; inception of the clay mineral factory. *Science*, ***311***, 1446-1449.

Kinnaird, T.C., Prave, A.R., Kirkland, C.L., Horstwood, M., Parrish, R. & Batchelor, R.A. 2007. The late Mesoproterozoic–early Neoproterozoic tectonostratigraphic evolution of NW Scotland: the Torridonian revisited. *Journal of the Geological Society*, ***164***, 541-551.

Kleinhans, M.G. 2010. Sorting out river channel patterns. *Progress in Physical Geography*, ***34***, 287-326.

Kleinhans, M.G., Buskes, C.J.J. & de Regt, H.W. 2009. Philosophy of Earth science. *In*: Allhoff, F. (ed), *Philosophies of the Sciences.* Wiley-Blackwell, N.Y, 213–235.

Kleinhans, M.G., Markies, H., De Vet, S.J. & Postema, F.N. 2011. Static and dynamic angles of repose in loose granular materials under reduced gravity. *Journal of Geophysical Research: Planets*, ***116***, *E11004*, http://dx.doi.org/10.1029/2011JE003865.

Knaust, D. & Hauschke, N. 2004. Trace fossils versus pseudofossils in Lower Triassic playa deposits, Germany. *Palaeogeogr. Palaeoclimatol. Palaeoecol.* ***215***, 87–97.

Kocurek, G. 1981. Significance of interdune deposits and bounding surfaces in aeolian dune sands. *Sedimentology, **28***, 753–780.

Kocurek, G. 1996. Desert aeolian systems, *In*: Reading, H.G. (ed) *Sedimentary Environments: Processes, Facies and Stratigraphy. 3rd edn.* Oxford, Blackwell Science, 125–153.

Kocurek, G. & Fielder, G. 1982. Adhesion structures. *Journal of Sedimentary Petrology, **52***, 1229–1241.

Kocurek, G. & Havholm, K.G. 1993. Eolian sequence stratigraphy—a conceptual framework. Chapter 16: Recent Developments in Siliciclastic Sequence Stratigraphy. *In*: Weimer, P. & Posamentier, H.W. *Siliciclastic Sequence Stratigraphy: Recent Developments and Applications. AAPG Memoirs, **58***, 393–409.

Kocurek, G. & Nielson, J. 1986. Conditions favourable for the formation of warm-climate aeolian sand sheets. *Sedimentology, **33***, 795–816.

Koehn, D., Bons, P., Montenari, M. & Seilacher, A. 2014. The elastic age: rise and fall of Precambrian biomat communities. *In*: *EGU General Assembly Conference Abstracts, Abstract 16, Vienna*, EGU2014-13793.

Komatsu, G. & Baker, V.R., 1994. Meander properties of Venusian channels. *Geology, **22***, 67-70.

Konhauser, K. 2007. *Introduction to Geomicrobiology*. Blackwell, Oxford, p. 425.

Kovalchuk, O., Owttrim, G.W., Konhauser, K.O. & Gingras, M.K. 2017. Desiccation cracks in siliciclastic deposits: Microbial mat-related compared to abiotic sedimentary origin. *Sedimentary Geology, **347***, 67–78.

Köykkä, J. 2011. The sedimentation and paleohydrology of the Mesoproterozoic stream deposits in a strike–slip basin (Svinsaga Formation), Telemark, southern Norway. *Sediment. Geol. **236***, 239–255.

Krabbendam, M. 2012. Stoer Group at Enard Bay. *In*: Goodenough, K.M. & Krabbendam, M. (eds) *A Geological Excursion Guide to the North-West Highlands of Scotland. Edinburgh Geological Society, Edinburgh,* 74–84.

Krabbendam, M., Bonsor, H., Horstwood, M.S. & Rivers, T. 2017. Tracking the evolution of the Grenvillian foreland basin: Constraints from sedimentology and detrital zircon and rutile in the Sleat and Torridon groups, Scotland. *Precambrian Research*, ***295***, 67-89.

Krumbein, W.E. & Cohen, Y. 1977. Primary production, mat formation and lithification: contribution of oxygenic and facultative an oxygenic cyanobacteria. *In*: Flugel, E. (ed), *Fossil Algae. Springer, Berlin Heidelberg New York*, 37–56.

Krumbein, W.E. & Swart, P.K. 1983. The microbial carbon cycle. *In*: Krumbein, W.E. (ed), *Microbial Geochemistry.* Blackwell Scientific Publishers, Oxford, 5–62.

Krumbein, W.E., Paterson, D.M. & Stal, L., 1994. *Biostabilization of Sediments. Bibliotheks und Information system,* Oldenburg, Germany, p. 526.

Krynine, P.D. 1948. The megascopic study and field classification of sedimentary rocks. *Journal of Geology,* ***56***, 130–165.

Kuhn, N. 2014. *Experiments in Reduced Gravity: Sediment Settling on Mars*. Elsevier.

Kumar, S. & Ahmad, S. 2014. Microbially induced sedimentary structures (MISS) from the Ediacaran Jodhpur Sandstone, Marwar Supergroup, western Rajasthan. *J. Asian Earth Sci.* ***91****,* 352–361.

Lancaster, N. & Baas, A. 1998. Influence of vegetation cover on sand transport by wind: field studies at Owens Lake, California. *Earth Surface Processes and Landforms,* ***23***, 69–82.

Langford, R.P. 1989. Fluvial–aeolian interactions: Part I, modern systems. *Sedimentology,* ***36***, 1023–1035.

Lawson, D.E. 1972. Torridonian volcanic sediments. *Scottish Journal of Geology*, ***8***, 345-362.

Lazarus, E.D. & Constantine, J.A. 2013. Generic theory for channel sinuosity. *Proceedings of the National Academy of Sciences*, ***110***, 8447-8452.

Lebeau, L.E. & Ielpi, A. 2017. Fluvial channel belts, floodbasins, and aeolian ergs in the Precambrian Meall Dearg Formation (Torridonian of Scotland): Inferring climate regimes from pre-vegetation clastic rock records. *Sedimentary Geology,* ***357***, 53-71.

Leclair, S.F. & Bridge, J.S. 2001. Quantitative interpretation of sedimentary structures formed by river dunes. *Journal of Sedimentary Research*, ***71***, 713-716.

Leeder, M.R. & Nami, M., 1979. Sedimentary models for the non-marine Scalby Formation (Middle Jurassic) and evidence for late Bajocian/Bathonian uplift of the Yorkshire Basin. *Proceedings of the Yorkshire Geological and Polytechnic Society,* ***42***, 461-482.

Legler, B., Johnson, H.D., Hampson, G.J., Massart, B.Y., Jackson, C.A.L., Jackson, M.D., El-Barkooky, A. & Ravnas, R. 2013. Facies model of a fine-grained, tide-dominated delta: Lower Dir Abu Lifa Member (Eocene), Western Desert, Egypt. *Sedimentology*, ***60***, 1313-1356.

Leithold, E.L., Blair, N.E. & Wegmann, K.W. 2016. Source-to-sink sedimentary systems and global carbon burial: a river runs through it. *Earth-Science Reviews*, ***153***, 30-42.

Lenton, T.M. & Daines, S.J. 2017. Matworld–the biogeochemical effects of early life on land. *New Phytologist*, ***215***, 531-537.

Leopold, L.B. & Wolman, M.G. 1960. River meanders. *Geological Society of America Bulletin*, ***71***, 769-793.

Lewin, J. & Macklin, M.G. 2003. Preservation potential for Late Quaternary river alluvium. *Journal of Quaternary Science*, ***18***, 107-120.

Lindsey, K.A. & Gaylord, D.R. 1992. Fluvial, coastal, nearshore, and shelf deposition in the Upper Proterozoic (?) to Lower Cambrian Addy Quartzite, northeastern Washington. *Sedimentary Geology*, ***77***, 15-35.

Long, D.G.F. 1976. *The Stratigraphy and Sedimentology of the Huronian (Lower Aphebian) Mississagi and Serpent Formations*. PhD thesis. University of Western Ontario, London, ON.

Long, D.G. 1978. Proterozoic stream deposits: some problems of recognition and interpretation of ancient sandy fluvial systems. *In*: Miall, A.D. (ed), *Fluvial Sedimentology: Canadian Society of Petroleum Geologists Memoir*, ***5***, 313-341.

Long, D.G.F. 2002. Aspects of Late Palaeoproterozoic fluvial style: the Uairen Formation, Roraima Supergroup, Venezuela. *In*: Altermann, W. & Corcoran, P.L. (eds), *Precambrian Sedimentary Environments: A Modern Approach to Ancient Depositional Systems: International Association of Sedimentologists, Special Publication*, ***33***, 323–338.

Long, D.G.F. 2004. Precambrian rivers. *In*: Eriksson, P.G., Altermann, W., Nelson, D.R., Mueller, W.U., Catuneaunu, O. (eds), *The Precambrian Earth: Tempos and Events. Developments in Precambrian Geology*, ***12***, Elsevier, 660–663.

Long, D.G. 2006. Architecture of pre-vegetation sandy-braided perennial and ephemeral river deposits in the Paleoproterozoic Athabasca Group, northern Saskatchewan, Canada as indicators of Precambrian fluvial style. *Sedimentary Geology*, ***190***, 71-95.

Long, D.G.F. 2011. Architecture and depositional style of fluvial systems before land plants: a comparison of Precambrian, early Paleozoic and modern river deposits. *In*: Davidson, S., Leleu, S. & North, C.P. (eds), *From River to Rock Record: The Preservation of Fluvial Sediments and their subsequent Interpretation. SEPM*, 37–61.

Love, S.E. & Williams, B.P. 2000. Sedimentology, cyclicity and floodplain architecture in the Lower Old Red Sandstone of SW Wales. *Geological Society, London, Special Publications*, ***180***, 371-388.

Lowe, D.G. & Arnott, R.W.C. 2016. Composition and Architecture of Braided and Sheetflood-Dominated Ephemeral Fluvial Strata. *In*: the Cambrian–Ordovician Potsdam Group: A Case Example of the Morphodynamics of Early Phanerozoic Fluvial Systems and Climate. *Journal of Sedimentary Research*, ***86***, 587-612.

Lyons, T.W., Reinhard, C.T. & Planavsky, N.J. 2014. The rise of oxygen in Earth's early ocean and atmosphere. *Nature*, ***506***, 307-315.

MacCulloch, J. 1819. *A description of the western islands of Scotland, including the Isle of Man, comprising an account of their geological structures, with remarks on their agriculture, scenery and antiques.* Constable, London.

Macnaughton, R.B., Dalrymple, R.W. & Narbonne, G.M. 1997. Early Cambrian braid-delta deposits, Mackenzie Mountains, north-western Canada. *Sedimentology*, ***44***, 587-609.

Malarkey, J., Baas, J.H., Hope, J.A., Aspden, R.J., Parsons, D.R., Peakall, J., Paterson, D.M., Schindler, R.J., Ye, L., Lichtman, I.D. & Bass, S.J. 2015. The pervasive role of biological cohesion in bedform development. *Nature communications,* ***6***, 6257

Malin, M.C. & Edgett, K.S. 2003. Evidence for persistent flow and aqueous sedimentation on early Mars. *Science*, ***302***, 1931-1934.

Malone, D.H., Stein, C.A., Craddock, J.P., Kley, J., Stein, S. & Malone, J.E. 2016. Maximum depositional age of the Neoproterozoic Jacobsville Sandstone, Michigan: Implications for the evolution of the Midcontinent Rift. *Geosphere*, ***12***, 1271-1282.

Marconato, A., de Almeida, R.P., Turra, B.B. & dos Santos Fragoso-Cesar, A.R. 2014. Pre-vegetation fluvial floodplains and channel-belts in the Late Neoproterozoic–Cambrian Santa Bárbara group (Southern Brazil). *Sedimentary Geology,* ***300***, 49–61.

Mars Channel Working Group. 1983. Channels and valleys on Mars. *Geological Society of America Bulletin*, ***94***, 1035-1054.

Matsubara, Y. & Howard, A.D., 2014. Modeling planform evolution of a mud-dominated meandering river: Quinn River, Nevada, USA. *Earth Surface Processes and Landforms,* ***39***, 1365-1377.

Matsubara, Y., Howard, A.D., Burr, D.M., Williams, R.M., Dietrich, W.E. & Moore, J.M. 2015. River meandering on Earth and Mars: A comparative study of Aeolis Dorsa meanders, Mars and possible terrestrial analogs of the Usuktuk River, AK, and the Quinn River, NV. *Geomorphology*, ***240***, 102-120.

Matsunaga, K.K. & Tomescu, A.M. 2016. Root evolution at the base of the lycophyte clade: insights from an Early Devonian lycophyte. *Annals of botany*, ***117***, 585-598.

McCormick, D.S. & Grotzinger, J.P. 1993. Distinction of marine from alluvial facies in the Paleoproterozoic (1.9 Ga) Burnside Formation, Kilohigok Basin, N.W.T. *Canada. J. Sediment. Petrol.* ***63***, 398–416.

McIlroy, D. & Walter, M.R. 1997. A reconsideration of the biogenicity of Arumberia banksi Glaessner & Walter. *Alcheringa*, ***21***, 79–80.

McKee, E.D. 1966. Structures of dunes at White Sands National Monument, New Mexico (and a comparison with structures of dunes from other selected areas). *Sedimentology, **7***, 3–69.

McKee, E.D., Crosby, E.T. & Berryhill, H.L., Jr. 1967. Flood deposits, Bijou Creek, Colorado, June 1965. *Journal of Sedimentary Research*, ***37***, 829–851.

McLaurin, B.T. & Steel, R.J. 2007. Architecture and origin of an amalgamated fluvial sheet sand, lower Castlegate Formation, Book Cliffs, Utah. *Sedimentary Geology*, ***197***, 291-311.

McPherson, J.G., Shanmugam, G. & Moiola, R.J. 1987. Fan-deltas and braid deltas: varieties of coarse-grained deltas. *Geological Society of America Bulletin*, ***99***, 331-340.

McMahon, S., van Smeerdijk Hood, A. & McIlroy, D. 2016. The origin and occurrence of subaqueous sedimentary cracks. *In*: Brasier, A.T., McIlroy, D. & McLoughlin, N. (eds) *Earth System Evolution and Early Life: A Celebration of the Work of Martin Brasier. Geological Society, London, Special Publications*, ***448***, 285–309.

McMahon, W.J. and Davies, N.S., 2018. Evolution of alluvial mudrock forced by early land plants. *Science*, ***359***, 1022-1024.

McMahon, W.J. & Davies, N.S. 2018. High-energy flood events recorded in the Mesoproterozoic Meall Dearg Formation, NW Scotland; their recognition and implications for the study of pre-vegetation alluvium. *Journal of the Geological Society*, ***175***, 13-32.

McMahon, W.J., Davies, N.S. & Went, D.J. 2017. Negligible microbial matground influence on pre-vegetation river functioning: Evidence from the Ediacaran-Lower Cambrian Series Rouge, France. *Precambrian Research*, ***292***, 13-34.

McManus, J. & Bajabaa, S. 1998. The importance of air escape processes in the formation of dish-and-pillar and teepee structures within modern and Precambrian fluvial deposits. *Sedimentary Geology,* ***120***, 337–343.

Medaris Jr, L.G., Singer, B.S., Dott Jr, R.H., Naymark, A., Johnson, C.M. & Schott, R.C. 2003. Late Paleoproterozoic climate, tectonics, and metamorphism in the southern Lake Superior region and Proto-North America: evidence from Baraboo interval quartzites. *J. Geol.* ***111***, 243–257.

Mendoza-Lera, C., Federlein, L.L., Knie, M. & Mutz, M., 2016. The algal lift: Buoyancy-mediated sediment transport. *Water Resources Research*, ***52***, 108-118.

Miall, A.D. 1980. Cyclicity and the facies model concept in fluvial deposits. *Bulletin of Canadian Petroleum Geology*, ***28***, 59-80.

Miall, A.D. 1985. Architectural-element analysis: a new method of facies analysis applied to fluvial deposits. *Earth-Science Reviews*, ***22***, 261-308.

Miall, A.D. 1988. Architectural elements and bounding surfaces in fluvial deposits: anatomy of the Kayenta Formation (Lower Jurassic), southwest Colorado. *Sedimentary Geology*, ***55***, 233-262.

Miall, A.D. 1996. *The geology of fluvial deposits: sedimentary facies, basin analysis, and petroleum geology*. Springer.

Miall, A.D. 2006. How do we identify big rivers? And how big is big?. *Sedimentary Geology*, ***186***, 39-50.

Miall, A. 2014. The facies and architecture of fluvial systems. *In*: *Fluvial Depositional Systems* (9-68). Springer International Publishing.

Miller, B.V., Samson, S.D. & D'Lemos, R.S. 2001. U-Pb geochronological constraints on the timing of plutonism, volcanism, and sedimentation, Jersey, Channel Islands, UK. *J. Geol. Soc.* ***158***, 243–251.

Minter, N.J., Buatois, L.A. & Mángano, M.G. 2016. The conceptual and methodological tools of ichnology. *In*: Mángano, G. & Buatois, L. (eds) *The Trace-Fossil Record of Major Evolutionary Events.* Springer, Dordrecht, 1–26.

Mitchell, R.L., Cuadros, J., Duckett, J.G., Pressel, S., Mavris, C., Sykes, D., Najorka, J., Edgecombe, G.D. & Kenrick, P. 2016. Mineral weathering and soil development in the earliest land plant ecosystems. *Geology*, ***44***, 1007-1010.

Moor, H., Rydin, H., Hylander, K., Nilsson, M.B., Lindborg, R. & Norberg, J. 2017. Towards a trait-based ecology of wetland vegetation. *Journal of Ecology*, ***105****, 1623-1635*.

Morey, G.B. 1967. RI-07 Stratigraphy and Petrology of the Type Fond du Lac Formation Duluth, Minnesota. *Minnesota Geol. Surv. Rept. Invest.* ***7***, 35 pp.

Morey, G.B. & Ojakangas, R.W. 1982. 7D: Keweenawan sedimentary rocks of eastern Minnesota and northwestern Wisconsin. *Geological Society of America Memoirs,* ***156***, 135-146.

Moretti, M. & Sabato, L. 2007. Recognition of trigger mechanisms for soft-sediment deformation in the Pleistocene lacustrine deposits of the Sant'Arcangelo Basin (Southern Italy): seismic shock vs. overloading. *Sedimentary Geology,* ***196***, 31-45.

Morey, G.B. and Ojakangas, R.W., 1982. 7D: Keweenawan sedimentary rocks of eastern Minnesota and northwestern Wisconsin. *Geological Society of America Memoirs*, *156*, pp.135-146.

Morris, J.L., Leake, J.R., Stein, W.E., Berry, C.M., Marshall, J.E., Wellman, C.H., Milton, J.A., Hillier, S., Mannolini, F., Quirk, J. & Beerling, D.J. 2015. Investigating Devonian trees as geo-engineers of past climates: linking palaeosols to palaeobotany and experimental geobiology. *Palaeontology*, ***58***, 787-801.

Moulin, F.Y., Peltier, Y., Bercovitz, Y., Eiff, O., Beer, A., Pen, C., Boulêtreau, S., Garabétian, F., Sellali, M., Sànchez-Pérez, J. & Sauvage, S. 2008. Experimental study of the interaction between a turbulent flow and a river biofilm growing on macrorugosities. *Freshwater Biol.* ***36***, 249–263.

Mountney, N.P. 2004. Feature: The sedimentary signature of deserts and their response to environmental change. *Geology Today*, ***20***, 101–106.

Mountney, N.P. 2012. A stratigraphic model to account for complexity in aeolian dune and interdune successions. *Sedimentology*, ***59***, 964–989.

Mowbray, T. 1983. The genesis of lateral accretion deposits in recent intertidal mudflat channels, Solway Firth, Scotland. *Sedimentology*, ***30***, 425-435.

Mueller, W.U. & Corcoran, P.L. 1998. Late-orogenic basins in the Archaean Superior Province, Canada: characteristics and inferences. *Sedimentary Geology*, ***120***, 177-203.

Muirhead, D.K., Parnell, J., Spinks, S. & Bowden, S.A. 2017. Characterization of organic matter in the Torridonian using Raman spectroscopy. *Geological Society, London, Special Publications*, ***448***, 71-80.

Mukhopadhyay, S., Choudhuri, A., Samanta, P., Sarkar, S. & Bose, P.K., 2014. Were the hydraulic parameters of Precambrian rivers different?. *Journal of Asian Earth Sciences*, ***91***, 289-297.

Mustard, J.F., Adler, M., Allwood, A., Bass, D.S., Beaty, D.W., Bell, J.F., Brinckerhoff, W., Carr, M., Des Marais, D.J., Brake, B. & Edgett, K.S. 2013. Report of the mars 2020 science definition team. *Mars Explor. Progr. Anal. Gr*, 155-205.

Nadon, G.C. & Issler, D.R. 1997. The compaction of floodplain sediments: timing, magnitude and implications. *Geoscience Canada*, ***24***, 37-43.

Nami, M. 1976. An exhumed Jurassic meander belt from Yorkshire, England. *Geological Magazine*, ***113***, 47-52.

Nesbitt, H.W., Fedo, C.M. & Young, G.M. 1997. Quartz and feldspar stability, steady and non-steady-state weathering, and petrogenesis of siliciclastic sands and muds. *The Journal of Geology*, ***105***, 173-192.

Nicholson, P.G. 1993. A basin reappraisal of the Proterozoic Torridon Group, northwest Scotland. *In*: Frostick, L.E. & Steel, R.J (eds). *Tectonic Controls and Signatures in Sedimentary Successions*, Special Publication of the International Association of Sedimentologists, ***20***, 183-202.

Noffke, N., 2010. *Geobiology: Microbial Mats in Sandy Deposits From the Archean Era to Today. Springer-Verlag, Berlin*, p. 194.

Noffke, N., Gerdes, G., Klenke, T. & Krumbein, W.E. 1996. Microbially induced sedimentary structures-examples from modern sediments of siliciclastic tidal flats. *Zentralbl. Geol. Palaeontol.* ***1***, 307–316.

Noffke, N., Gerdes, G., Klenke, T. & Krumbein, W.E. 2001. Microbially induced sedimentary structures—a new category within the classification of primary sedimentary structures: perspectives. *Journal of Sedimentary Research*, ***71***, 649–656.

North, C.P. & Davidson, S.K. 2012. Unconfined alluvial flow processes: recognition and interpretation of their deposits, and the significance for palaeogeographic reconstruction. *Earth-Science Reviews*, ***111***, 199–223.

Olsen, H. 1987. Ancient ephemeral stream deposits: a local terminal fan model from the Bunter Sandstone Formation (L. Triassic) in the Tønder-3,-4 and-5 wells, Denmark. *In*: Frostick, R.I (eds). *Desert Sediments: Ancient and Modern*. Geological Society of London: London; Special Publication, ***35***, 69–86.

Ore, H.T. 1964. Some criteria for recognition of braided stream deposits. *Rocky Mountain Geology*, ***3***, 1-14.

Osgood, R.G. 1970. Trace fossils of the Cincinnati area. *Palaeontogr Americana*, ***6***, 281-444.

Owen, G. 1987. Deformation processes in unconsolidated sands. *Geological Society, London, Special Publications*, ***29***, 11-24.

Owen, G. 1995. Soft-sediment deformation in upper Proterozoic Torridonian sandstones (Applecross Formation) at Torridon, northwest Scotland. *Journal of Sedimentary Research*, ***281***, 495–504.

Owen, G. 1996. Experimental soft-sediment deformation: structures formed by the liquefaction of unconsolidated sands and some ancient examples. *Sedimentology*, ***43***, 279-293.

Owen, G. & Santos, M.G. 2014. Soft-sediment deformation in a pre-vegetation river system: the Neoproterozoic Torridonian of NW Scotland. *Proceedings of the Geologists' Association*, ***125***, 511-523.

Paola, C., Wiele, S.M. & Reinhart, M.A. 1989. Upper-regime parallel lamination as the result of turbulent sediment transport and low-amplitude bedforms. *Sedimentology,* ***36***, 47–59.

Paris, F., Robardet, M., Dabard, M.P., Feist, R., Ghienne, J.F., Guillocheau, F., Le Hérissé, A., Loi, A., Mélou, M., Servais, T., Shergold, J., Vidal, M. & Vizcaïno, D. 1999. Ordovician sedimentary rocks of France. Acta Universitatis Carolinae. *Geologica*, ***43***, 85–88.

Parizot, M., Eriksson, P.G., Aifa, T., Sarkar, S., Banerjee, S., Catuneanu, O., Altermann, W., Bumby, A.J., Bordy, E.M., van Rooy, J.L. & Boshoff, A.J. 2005. Suspected microbial mat-related crack-like sedimentary structures in the Palaeoproterozoic Magaliesberg Formation sandstones, South Africa. *Precambrian Research*, ***138***, 274–296.

Park, R.G., Stewart, A.D. & Wright, D.T. 2002. The Hebridean terrane. *In*: Trewin, N.H. (ed) *The Geology of Scotland. 4th edn. Geological Society, London*, 45–80.

Parker, G. 1998. River meanders in a tray. *Nature*, ***395***, 111-112.

Parnell, J., Mark, D., Fallick, A.E., Boyce, A. & Thackrey, S. 2011. The age of the Mesoproterozoic Stoer Group sedimentary and impact deposits, NW Scotland. *Journal of the Geological Society, London*, ***168***, *349–358*.

Parsons, D.R., Schindler, R.J., Hope, J.A., Malarkey, J., Baas, J.H., Peakall, J., Manning, A.J., Ye, L., Simmons, S., Paterson, D.M. & Aspden, R.J. 2016. The role of biophysical cohesion on subaqueous bed form size. *Geophysical research letters,* ***43***, 1566-1573.

Pasteels, P. & Doré, F. 1982. Age of the Vire-Carolles granite. *In*: Odin, G. (ed), *Numerical Dating in Stratigraphy. John Wiley, New York*, 784–790.

Peach, B.N., Horne, J., Gunn, W., Clough, C.T., Hinxman, L.W. & Teall, J.J.H. 1907. *The geological structure of the northwest highlands of Scotland.* Memoirs of the Geological Survey of Scotland.

Peters, S.E. & Gaines, R.R. 2012. Formation of the/Great Unconformity/'as a trigger for the Cambrian explosion. *Nature*, ***484***, 363-366.

Peters, S.E. & Husson, J.M. 2017. Sediment cycling on continental and oceanic crust. *Geology*, ***45***, 323-326.

Petrov, P.Y. 2014. The Mukun basin: Settings, paleoenvironmental parameters, and factors controlling the early mesoproterozoic terrestrial sedimentation (Lower Riphean section of the Anabar uplift, Siberia). *Lithol. Min. Resour.* ***49***, 55–80.

Petrov, P.Y. 2015. Microbial factor in the formation of sedimentary continental systems of the Proterozoic (Mukun Basin, Lower Riphean of the Anabar Uplift of Siberia). *Paleontol. J.* ***49***, 530–545.

Pillola, G.I. 1993. The Lower Cambrian trilobite Bigotina and allied genera. *Palaeontology,* ***36***, 855.

Porada, P., Lenton, T.M., Pohl, A., Weber, B., Mander, L., Donnadieu, Y., Beer, C., Pöschl, U. & Kleidon, A. 2016. High potential for weathering and climate effects of non-vascular vegetation in the Late Ordovician. *Nature communications,* ***7***. 10.1038/ncomms12113

Pratt, B.R. 1998. Syneresis cracks: subaqueous shrinkage in argillaceous sediments caused by earthquake-induced dewatering. *Sedimentary Geololgy,* ***117***, 1–10.

Prave, A.R. 2002. Life on land in the Proterozoic: evidence from the Torridonian rocks of northwest Scotland. *Geology*, ***30***, 811-814.

Press, W.H., Flannery, B.P., Teukolsky, S.A. & Vetterling, W.T. 1992. Kolmogorov-smirnov test. *Numerical recipes in FORTRAN: the art of scientific computing*, 617-620.

Pretorius, D.A. 1974. Gold in the Proterozoic sediments of South Africa: Systems, paradigms, and models. *University of the Witwatersrand, Economic Geology Research Unit, Information Circular*, ***87,*** 2.

Puigdefabregas, C. & Van Vliet, A. 1977. Meandering stream deposits from the Tertiary of the southern Pyrenees. *In*: Miall, A. D (ed), *Fluvial Sedimentology. Mere. Can. Soc. Pet. Geol.*, ***5***, 469-485.

Quirk, J., Beerling, D.J., Banwart, S.A., Kakonyi, G., Romero-Gonzalez, M.E. & Leake, J.R. 2012. Evolution of trees and mycorrhizal fungi intensifies silicate mineral weathering. *Biology letters*, ***8***, 1006-1011.

Quirk, J., Leake, J.R., Johnson, D.A., Taylor, L.L., Saccone, L. & Beerling, D.J. 2015, August. Constraining the role of early land plants in Palaeozoic weathering and global cooling. *In: Proc. R. Soc. B*, ***282***, 20151115. The Royal Society.

Rainbird, R.H. 1992. Anatomy of a large-scale braid-plain quartzarenite from the Neoproterozoic Shaler Group, Victoria Island, Northwest Territories, Canada. *Canadian Journal of Earth Sciences*, ***29***, 2537-2550.

Rainbird, R.H., Cawood, P. & Gehrels, G. 2012. The great Grenvillian sedimentation episode: Record of supercontinent Rodinia's assembly. In: Busby, C. & Azor, A. (eds) *Tectonics of Sedimentary Basins: Recent Advances. Blackwell, Oxford,* 583–601.

Rainbird, R.H., Hamilton, M.A. & Young, G.M. 2001. Detrital zircon geochronology and provenance of the Torridonian, NW Scotland. *Journal of the Geological Society*, ***158***, pp.15-27.

Rainbird, R.H., Hearnan, L.M. & Young, G. 1992. Sampling Laurentia: Detrital zircon geochronology offers evidence for an extensive Neoproterozoic river system originating from the Grenville orogen. Geology, ***20***, 351-354.

Rasmussen, B., Blake, T.S., Fletcher, I.R., Kilburn, M.R. 2009. Evidence for microbial life in synsedimentary cavities from 2.75 Ga terrestrial environments. *Geology*, ***37***, 423–426.

Reesink, A.J.H., Van den Berg, J.H., Parsons, D.R., Amsler, M.L., Best, J.L., Hardy, R.J., Orfeo, O. & Szupiany, R.N. 2015. Extremes in dune preservation: controls on the completeness of fluvial deposits. *Earth-science reviews*, ***150***, 652-665.

Reid, I. & Frostick, L.E. 1994. Fluvial sediment transport and deposition. *In*: Pye, K. (ed) *Sediment Transport and Depositional Processes*. Blackwell Scientific, Oxford, 89–156.

Renouf, J.T. 1974. The Proterozoic and Palaeozoic development of the Armorican and Cornubian provinces. *Proc. Ussher Soc.* ***3***, 6–43.

Retallack, G.J., Marconato, A., Osterhout, J.T., Watts, K.E. & Bindeman, I.N. 2014. Revised Wonoka isotopic anomaly in South Australia and Late Ediacaran mass extinction. *Journal of the Geological Society*, ***171***, 709-722.

Rice, M.S., Gupta, S., Treiman, A.H., Stack, K.M., Calef, F., Edgar, L.A., Grotzinger, J., Lanza, N., Le Deit, L., Lasue, J. & Siebach, K.L. 2017. Geologic overview of the Mars Science Laboratory rover mission at the Kimberley, Gale crater, Mars. *Journal of Geophysical Research: Planets*, ***122***, 2-20.

Rodd, J.A. & Stewart, A.D. 1992. Geochemistry, weathering and diagenesis of the Diabaig Formation (Torridon Group) in NW Scotland. *Scottish Journal of Geology, **28***, 27-35.

Rodríguez-López, J.P., Clemmensen, L.B., Lancaster, N., Mountney, N. P. & Veiga, G. D. 2014. Archean to Recent aeolian sand systems and their sedimentary record: current understanding and future prospects. *Sedimentology, **61***, 1487–1534.

Ronov, A.B. 1994. Phanerozoic transgressions and regressions on the continents; a quantitative approach based on areas flooded by the sea and areas of marine and continental deposition. *American Journal of Science*, ***294***, 777-801.

Rubinstein, C.V., Gerrienne, P., de la Puente, G., Astini, R.A. & Steemans, P. 2010. Early Middle Ordovician evidence for land plants in Argentina (eastern Gondwana). *New Phytologist*, ***188***, 365-369.

Rubinstein, R.Y. & Kroese, D.P. 2016. *Simulation and the Monte Carlo method* (Vol. 10). John Wiley & Sons.

Runkel, A.C., Miller, J.F., McKay, R.M., Palmer, A.R. & Taylor, J.F. 2007. High-resolution sequence stratigraphy of lower Paleozoic sheet sandstones in central North America: The role of special conditions of cratonic interiors in development of stratal architecture. *Geological Society of America Bulletin*, ***119***, 860-881.

Runnegar, B.N., Fedonkin, M.A., 1992. Proterozoic metazoan body fossils. *In*: Schopf, J.W. & Klein, C. (eds), *The Proterozoic Biosphere: A Multidisciplinary Study. Cambridge University Press*, 369–388.

Russell, R.J. 1956. Environmental changes through forces independent of man. *In*: Thomas, W.L. (ed). *Man's role in changing the face of the earth: Chicago, Univ. Chicago Press*, 453-470.

Sadler, P.M. 1981. Sediment accumulation rates and the completeness of stratigraphic sections. *The Journal of Geology*, ***89***, 569-584.

Samanta, P., Mukhopadhyay, S., Mondal, A. & Sarkar, S. 2011. Microbial mat structures in profile: the Neoproterozoic Sonia sandstone, Rajasthan, *India. J. Asian Earth Sci.* ***40***, 542–549.

Santos, M.G., Almeida, R.P., Godinho, L.P., Marconato, A. & Mountney, N.P. 2014. Distinct styles of fluvial deposition in a Cambrian rift basin. *Sedimentology*, ***61***, 881-914.

Santos, M.G., Mountney, N.P. & Peakall, J. 2017a. Tectonic and environmental controls on Palaeozoic fluvial environments: reassessing the impacts of early land plants on sedimentation. *Journal of the Geological Society*, ***174***, 393-404.

Santos, M.G., Mountney, N.P., Peakall, J., Thomas, R.E., Wignall, P.B. & Hodgson, D.M. 2017b. Reply to Discussion on 'Tectonic and environmental controls on Palaeozoic fluvial environments: reassessing the impacts of early land plants on. *Journal of the Geological Society*, ***174***, 950-952.

Santos, M.G. & Owen, G. 2016. Heterolithic meandering-channel deposits from the Neoproterozoic of NW Scotland: Implications for palaeogeographic reconstructions of Precambrian sedimentary environments. *Precambrian Research*, ***272***, 226-243.

Santos, M.L.D. & Stevaux, J.C. 2000. Facies and architectural analysis of channel sandy macroforms in the upper Parana river. *Quaternary International*, ***72***, 87-94.

Sarkar, S., Banerjee, S., Eriksson, P.G. & Catuneanu, O. 2005. Microbial mat control on siliciclastic Precambrian sequence stratigraphic architecture: examples from India. *Sediment. Geol.* ***176***, 195–209.

Saunderson, H.C. & Lockett, F.P. 1983. Flume experiments on bedforms and structures at the dune-plane bed transition. *In*: Collinson, J.D. & Lewin, J. (eds) *Modern and Ancient Fluvial Systems. International Association of Sedimentologists, Special Publications*, 49–58.

Schieber, J. 1999. Microbial mats in terrigenous clastics: the challenge of identification in the rock record. *Palaios*, ***14***, 3–13.

Schieber, J., 2004. Microbial mats in the siliciclastic rock record: a summary of the diagnostic features. *In*: Eriksson, P.G., Altermann, W., Nelson, D.R., Mueller, W. U., Catuneanu, O. & Catuneanu, O. (Eds), *The Precambrian Earth: Tempos and Events, vol. 12.* Newnes.

Schieber, J. 2007. Ripple patches in the Cretaceous Dakota Sandstone near Denver, Colorado, a classic locality formicrobially bound tidal sand flats. *In*: Schieber, J., Bose, P.K., Eriksson, P.G., Banerjee, S., Sarkar, S., Altermann,W. & Catuneanu, O. (eds) *Atlas of Microbial Mat Features Preserved Within the Siliciclastic Rock Record. Atlases in Geosciences.* Elsevier, Amsterdam, 222–225.

Schieber, J., Bish, D., Coleman, M., Reed, M., Hausrath, E.M., Cosgrove, J., Gupta, S., Minitti, M.E., Edgett, K.S. & Malin, M. 2017. Encounters with an unearthly mudstone: Understanding the first mudstone found on Mars. *Sedimentology*, ***64***, 311-358.

Schieber, J., Bose, P.K., Eriksson, P.G., Banerjee, S., Sarkar, S., Altermann, W. & Catuneanu, O. 2007. *Atlas of microbial mat features preserved within the siliciclastic rock record. Atlases in Geoscience, vol. 2.* Elsevier, Amsterdam, p. 311.

Schieber, J., Southard, J.B. & Schimmelmann, A. 2010. Lenticular shale fabrics resulting from intermittent erosion of water-rich muds—interpreting the rock record in the light of recent flume experiments. *Journal of Sedimentary Research,* ***80***, 119–128.

Schumm, S.A. 1968. Speculations concerning paleohydrologic controls of terrestrial sedimentation. *Geological Society of America Bulletin,* ***79***, 1573-1588.

Sedgwick, A. & Murchison, R.I. 1829. On the structure and the relations of the deposits constrained between the Primary rocks and the Oolitic Series in the north of Scotland. *Transactions of the Geological Society of London, 2nd Series, 3,* 125–160.

Seilacher, A. 1982. Distinctive features of sandy tempestites. *In*: Einsele, G., Seilacher, A. (eds), *Cyclic and Event Stratification.* Springer, Berlin Heidelberg, 333–349.

Seilacher, A. 2007. *Trace Fossil Analysis.* Springer, Berlin, p. 226.

Selley, R.C. 1965. Diagnostic characters of fluviatile sediments of the Torridonian formation (Precambrian) of northwest Scotland. *Journal of Sedimentary Research,* ***35***, 366–380.

Sheldon, N.D. 2012. Microbially induced sedimentary structures in the ca. 1100 Ma terrestrial midcontinent rift of North America. *In*. Chafetz, H. (eds). *Microbial mats in siliciclastic depositional systems through time. SEPM Special Publication,* ***101***, 153–162.

Shepard, R.N. & Sumner, D.Y. 2010. Undirected motility of filamentous cyanobacteria produces reticulate mats. *Geobiology,* ***8***, 179–190.

Simms, M.J. 2015. The Stac Fada impact ejecta deposit and the Lairg Gravity Low: evidence for a buried Precambrian impact crater in Scotland? *Proceedings of the Geologists' Association,* ***126***, 742–761.

Smith, D.G. 1976. Effect of vegetation on lateral migration of anastomosed channels of a glacier meltwater river. *Geol. Soc. Am. Bull.* ***87***, 857–860.

Smith, R.L., Stearn, J.E.F. & Piper, J.D.A. 1983. Palaeomagnetic studies of the Torridonian sediments, NW Scotland. *Scottish Journal of Geology,* ***19***, 29–45.

Sønderholm, M. & Tirsgaard, H. 1998. Proterozoic fluvial styles: response to changes in accommodation space (Rivieradal sandstones, eastern North Greenland). *Sedimentary Geology*, ***120***, 257-274.

Squyres, S.W., Grotzinger, J.P., Arvidson, R.E., Bell, J.F., Calvin, W., Christensen, P.R., Clark, B.C., Crisp, J.A., Farrand, W.H., Herkenhoff, K.E. & Johnson, J.R. 2004. In situ evidence for an ancient aqueous environment at Meridiani Planum, Mars. *Science*, ***306***,1709-1714.

Squyres, S.W. & Knoll, A.H. 2005. Sedimentary rocks at Meridiani Planum: Origin, diagenesis, and implications for life on Mars. *Earth and Planetary Science Letters*, ***240***, 1-10.

Stear, W.M. 1985. Comparison of the bedform distribution and dynamics of modern and ancient sandy ephemeral flood deposits in the southwestern Karoo region, South Africa. *Sedimentary Geology*, ***45***, 209-230.

Stein, A.M. 1988. Basement controls upon basin development in the Caledonian foreland, NW Scotland. *Basin Research*, ***1***, 107–119.

Stein, A.M. 1992. Basin development and petroleum potential in The Minches and Sea of the Hebrides Basins. *In*: Parnell, J. (ed) *Basins on the Atlantic Seaboard: Petroleum Geology, Sedimentology and Basin Evolution. Geological Society, London, Special Publications*, ***62***, 17–20.

Steiner, M. & Reitner, J. 2001. Evidence of organic structures in Ediacara-type fossils and associated microbial mats. *Geology*, ***29***, 1119–1122.

Stewart, A.D. 1962. On the torridonian sediments of colonsay and their relationship to the main outcrop in north-west Scotland. *Geological Journal*, ***3***, 121-156.

Stewart, A.D. 1963. On certain slump structures in the Torridonian sandstones of Applecross. *Geological Magazine*, ***100***, 205-218.

Stewart, A.D. 1966a. On the correlation of the Torridonian between Rhum and Skye. *Geological Magazine*, ***103***, 432-439.

Stewart, A.D. 1966. An unconformity in the Torridonian. *Geological Magazine*, ***103***, 462-465.

Stewart, A.D. 1969. Torridonian rocks of Scotland reviewed. *North Atlantic geology and continental drift*, ***12***, 595-608.

Stewart, A.D. 1972. Pre-Cambrian landscapes in Northwest Scotland. *Geological Journal*, ***8***, 111-124.

Stewart, A.D. 1982. Late Proterozoic rifting in NW Scotland: the genesis of the 'Torridonian'. *Journal of the Geological Society*, ***139***, 413-420.

Stewart, A.D. 1990. Geochemistry, provenance and climate of the Upper Proterozoic Stoer Group in Scotland. *Scottish Journal of Geology*, ***26***, 89–97.

Stewart, A.D. 1991. Geochemistry, provenance and palaeoclimate of the Sleat and Torridon groups in Skye. *Scottish Journal of Geology*, ***27***, 81–95.

Stewart, A.D. 1995. Well Preserved Late Precambrian Paleosols from Northwest Scotland: Discussion. *Journal of Sedimentary Research*, ***65***, *44*.

Stewart, A.D. 2002. The later Proterozoic Torridonian rocks of Scotland: their sedimentology, geochemistry and origin. *Geological Society Memoir*, ***24***. Geological Society of London.

Stewart, A.D. & Donnellan, N.C.B. 1992. Geochemistry and provenance of red sandstones in the Upper Proterozoic Torridon Group in Scotland. *Scottish Journal of Geology*, ***28***, 143-153.

Stewart, A.D. & Irving, E. 1974. Palaeomagnetism of Precambrian sedimentary rocks from NW Scotland and the apparent polar wandering path of Laurentia. *Geophysical Journal International*, ***37***, 51-72.

Stewart, A.D. & Parker, A. 1979. Palaeosalinity and environmental interpretation of red beds from the late Precambrian ('Torridonian') of Scotland. *Sedimentary Geology*, ***22***, 229-241.

Strand, K. 1988. Alluvial sedimentation and tectonic setting of the early Proterozoic Kurkikylä and Kainuu Groups in northern Finland. *Geol Surv Finl, Spec Pap*, ***5***, 75-90.

Straub, K.M. & Wang, Y. 2013. Influence of water and sediment supply on the long-term evolution of alluvial fans and deltas: Statistical characterization of basin-filling sedimentation patterns. *Journal of Geophysical Research: Earth Surface*, ***118***, 1602-1616.

Stromberg, J.C., Setaro, D.L., Gallo, E.L., Lohse, K.A. & Meixner, T. 2017. Riparian vegetation of ephemeral streams. *Journal of Arid Environments*, ***138***, 27-37.

Strother, P.K. & Wellman, C.H. 2016. Palaeoecology of a billion-year-old nonmarine cyanobacterium from the Torridon Group and Nonesuch Formation. *Palaeontology*, ***59***, 89–108.

Strother, P.K., Battison, L., Brasier, M.D. &Wellman, C.H. 2011. Earth's earliest non-marine eukaryotes. *Nature*, ***473***, 505–509.

Stueeken, E.E., Bellefroid, E., Prave, A.R., Asael, D., Planavsky, N. and Lyons, T., 2017. Not so non-marine? Revisiting the Stoer Group and the Mesoproterozoic biosphere. *Geochemical Perspectives Letters*, ***3***, 221-229

Sur, S., Schieber, J., Banerjee, S., 2006. Petrographic observations suggestive of microbial mats from Rampur Shale and Bijaigarh Shale, Vindhyan basin, *India. J. Earth Syst. Sci.* ***115***, 61–66.

Suttner, L.J., Basu, A. & Mack, G.H. 1981. Climate and the origin of quartz arenites. *Journal of Sedimentary Research,* ***51****, 1235-1246.*

Sweet, I.P. 1988. Early Proterozoic stream deposits: braided or meandering-evidence from central Australia. *Sedimentary Geology,* ***58***, 277–293.

Tal, M. & Paola, C. 2007. Dynamic single-thread channels maintained by the interaction of flow and vegetation. *Geology*, ***35***, 347-350.

Teall, J.J.H. 1907. *The Petrography of the Torridonian Formation. Memoirs of the Geological Survey of Great Britain*, 278–290.

Teles, G., Chemale, F. & de Oliveira, C. G. 2015. Paleoarchean record of the detrital pyrite-bearing, Jacobina Au–U deposits, Bahia, Brazil. *Precambrian Research*, **256**, 289-313.

Temmerman, S., Bouma, T.J., Van de Koppel, J., Van der Wal, D., De Vries, M.B. & Herman, P.M.J. 2007. Vegetation causes channel erosion in a tidal landscape. *Geology*, ***35***, 631-634.

Thomas, R.G., Smith, D.G., Wood, J.M., Visser, J., Calverley-Range, E.A. & Koster, E.H. 1987. Inclined heterolithic stratification—terminology, description, interpretation and significance. *Sedimentary Geology*, ***53***, 123-179.

Thorne, C.R. 1990. Effects of vegetation on Riverbank erosion and stability. *In*: Thornes, J.W. (Ed), *Vegetation and Erosion: Processes and Environments*. John Wiley and Sons, Chichester, 125–144.

Tipper, J.C. 2015. The importance of doing nothing: stasis in sedimentation systems and its stratigraphic effects. *In*: Smith, D.G., Bailey, R.J., Burgess, P.M. & Fraser, A.J. (eds) *Strata and Time: Probing the Gaps in our Understanding. Geological Society, London, Special Publications,* ***404***, 105–122.

Tirsgaard, H. & Øxnevad, I.E. 1998. Preservation of pre-vegetational mixed fluvio–aeolian deposits in a humid climatic setting: an example from the Middle Proterozoic Eriksfjord Formation, Southwest Greenland. *Sedimentary Geology*, ***120***, 295-317.

Todd, S.P. & Went, D.J. 1991. Lateral migration of sand-bed rivers: examples from the Devonian Glashabeg Formation, SW Ireland and the Cambrian Alderney Sandstone Formation, Channel Islands. *Sedimentology*, ***38***, 997-1020.

Tolhurst, T.J., Gust, G. & Paterson, D.M. 2002. The influence of an extracellular polymeric substance (EPS) on cohesive sediment stability. *In*: Winterwerp, J.C. & Kranenburg, C. (Eds), *Fine Sediment Dynamics in the Marine Environment.* Elsevier, Amsterdam, pp. 409–426.

Tooth, S. 2000. Process, form and change in dryland rivers: a review of recent research. *Earth-Science Reviews*, ***51***, 67-107.

Torsvik, T.H. & Cocks, L.R.M. 2004. Earth geography from 400 to 250 Ma: a palaeomagnetic, faunal and facies review. *Journal of the Geological Society*, ***161***, 555-572.

Torsvik, T.H. and Sturt, B.A., 1987. On the origin and stability of remanence and the magnetic fabric of the Torridonian Red Beds, NW Scotland. *Scottish Journal of Geology*, *23*(1), pp.23-38.

Tosca, N.J., Johnston, D.T., Mushegian, A., Rothman, D.H., Summons, R.E. & Knoll, A.H. 2010. Clay mineralogy, organic carbon burial, and redox evolution in Proterozoic oceans. *Geochimica et Cosmochimica Acta*, ***74***, 1579-1592.

Trewin, N.H. 1993. Controls on fluvial deposition in mixed fluvial and aeolian facies within the Tumblagooda Sandstone (Late Silurian) of Western Australia. *Sedimentary Geology*, ***85***, 387-400.

Tunbridge, I.P. 1981. Old Red Sandstone sedimentation—an example from the Brownstones (highest Lower Old Red Sandstone) of south central Wales. *Geological Journal*, ***16***, 111-124.

Tunbridge, I.P. 1984. Facies model for a sandy ephemeral stream and clay playa complex; the Middle Devonian Trentishoe Formation of North Devon, UK. *Sedimentology, **31***, 697-715.

Turnbull, M.J., Whitehouse, M.J. & Moorbath, S. 1996. New isotopic age determinations for the Torridonian, NW Scotland. *Journal of the Geological Society, London, **153***, 955–964,

Tyler, N. & Ethridge, F.G. 1983. Depositional setting of the Salt Wash Member of the Morrison Formation, southwest Colorado. *Journal of Sedimentary Research*, ***53***, 533-547

Vago, J., Gardini, B., Kminek, G., Baglioni, P., Gianfiglio, G., Santovincenzo, A., Bayón, S. & van Winnendael, M. 2006. ExoMars-searching for life on the Red Planet. *ESA bulletin*, ***126***, 16-23.

Van de Kamp, P.C. & Leake, B.E. 1997. Mineralogy, geochemistry, provenance and sodium metasomatism of Torridonian rift basin clastic rocks, NW Scotland. *Scottish Journal of Geology*, ***33***, 105–124.

Van Loon, A.J., Mazumder, R. & De, S. 2012. Unravelling the depositional environment of the Archaean Rajkharsawan conglomerate (Jharkhand, eastern India). *Netherlands Journal of Geosciences, **91***, 129-135.

Van Mechelen, J.L.M. 2004. Strength of moist sand controlled by surface tension for tectonic analogue modelling. *Tectonophysics*, ***384***, 275–284.

Vandevivere, P. & Baveye, P. 1992. Effect of bacterial extracellular polymers on the saturated hydraulic conductivity of sand columns. Appl. Environ. *Microbiol.* ***58***, 1690–1698.

Vignaga, E., Sloan, D.M., Luo, X., Haynes, H., Phoenix, V.R. & Sloan, W.T. 2013. Erosion of biofilm-bound fluvial sediments. *Nat. Geosci.* ***6***, 770–774.

Vogt, T., 1941. Geology of a Middle Devonian cannel coal from Spitsbergen. *Norsk Geologisk Tidsskrift*, ***21***, 1-12.

Walker, R.G. 1976. Facies and facies models, general introduction. *In*: Walker, R.G. (ed). *Facies Models. Geoscience Canada Reprint Series*, ***3***, 21-24.

Walker, R.G. & Cant, D.J. 1979. Facies Models 3: Sandy Fluvial Systems. *In*: Walker, R.G. (ed), *Facies Models. Geological Association of Canada*, 23-32.

Wallace, C.A. & Crittenden Jr, M.D., 1969. The stratigraphy, depositional environment and correlation of the Precambrian Uinta Mountain Group, western Uinta Mountains, Utah. *Geologic Guidebook of the Uinta Mountains: Utah's Maverick Range, Sixteenth Annual Field Conference,* 127-141.

Wang, Y., Straub, K.M. & Hajek, E.A. 2011. Scale-dependent compensational stacking: an estimate of autogenic time scales in channelized sedimentary deposits. *Geology,* ***39***, 811-814.

Weissmann, G.S., Hartley, A.J., Nichols, G.J., Scuderi, L.A., Olson, M., Buehler, H. & Banteah, R. 2010. Fluvial form in modern continental sedimentary basins: distributive fluvial systems. *Geology*, ***38***, 39-42.

Weller, O.M. & St-Onge, M.R. 2017. Record of modern-style plate tectonics in the Palaeoproterozoic Trans-Hudson orogen. *Nature Geoscience,* ***10****, 305-311*.

Wellman, C.H. & Strother, P.K. 2015. The terrestrial biota prior to the origin of land plants (embryophytes): a review of the evidence. *Palaeontology,* ***58***, 601–627.

Went, D.J. 2005. Pre-vegetation alluvial fan facies and processes: an example from the Cambro-Ordovician Rozel Conglomerate Formation, Jersey, Channel Islands. *Sedimentology,* ***52***, 693–713.

Went, D.J., 2013. Quartzite development in early Palaeozoic nearshore marine environments. *Sedimentology*, ***60***, 1036-1058.

Went, D.J., 2016. Alluvial fan, braided river and shallow-marine turbidity current deposits in the Port Lazo and Roche Jagu formations, Northern Brittany: relationships to andesite emplacements and implications for age of the Plourivo-Plouézec Group. *Geological Magazine, **154**, 1037-1060*

Went, D.J.& Andrews, M.J. 1990. Post-Cadomian erosion, deposition and basin development in the Channel Islands and northern Brittany. *In*: D'Lemos, R.S., Strachan, R.A., Topley, C.G. (eds), *The Cadomian Orogeny. Geological Society Special Publication, **51***, 293–304.

Went, D.J. & Andrews, M.J. 1991. Alluvial fan, braided stream and possible marine shoreface deposits of the Lower Palaeozoic Erquy-Fréhel Group, northern Brittany. *Proc. Ussher Soc. **7**,* 385–391.

Went, D.J., Andrews, M.J. & Williams, B.P.J. 1988. Processes of alluvial fan sedimentation, basal rozel conglomerate formation, la têcte des hougues, Jersey, Channel Islands. *Geol. J. **23***, 75–84.

Went, D.J. & McMahon, W.J. 2018. Facies, architecture and morphodynamics of pre-vegetation fluvial systems, Lower Cambrian Series Rouge, English Channel region. *Sedimentology*.

Wermund, E.G. 1965. Cross-bedding in the Meridian Sand. *Sedimentology*, ***5***, 69-79.

Wheaton, J.M., Fryirs, K.A., Brierley, G., Bangen, S.G., Bouwes, N. & O'Brien, G. 2015. Geomorphic mapping and taxonomy of fluvial landforms. *Geomorphology*, ***248***, 273-295.

Williams, G.E. 1966. Palaeogeography of the Torridonian Applecross group. *Nature, **209***, 1303-1306.

Williams, G.E. 1966. *The Precambrian Torridonian sediments of the Cape Wrath district, north-west Scotland. PhD thesis*, University of Reading.

Williams, G.E. 2001. Neoproterozoic (Torridonian) alluvial fan succession, northwest Scotland, and its tectonic setting and provenance. *Geological Magazine, **138***, 161–184.

Williams, G.E. & Foden, J. 2011. A unifying model for the Torridon Group (early Neoproterozoic), NW Scotland: Product of post-Grenvillian extensional collapse. *Earth-Science Reviews*, ***108***, 34–49.

Williams, G.E. & Schmidt, P.W. 1997. Palaeomagnetic dating of sub-Torridon Group weathering profiles, NW Scotland: verification of Neoproterozoic palaeosols. *Journal of the Geological Society, London, **154***, 987–997,

Williams, R.M., Grotzinger, J.P., Dietrich, W.E., Gupta, S., Sumner, D.Y., Wiens, R.C., Mangold, N., Malin, M.C., Edgett, K.S., Maurice, S. & Forni, O. 2013. Martian fluvial conglomerates at Gale crater. *Science, **340***, 1068-1072.

Wilmeth, D.T., Dornbos, S.Q., Isbell, J.L. & Czaja, A.D. 2014. Putative domal microbial structures in fluvial siliciclastic facies of the Mesoproterozoic (1.09 Ga) Copper Harbor Conglomerate, Upper Peninsula of Michigan, USA. *Geobiology*, ***12***, 99–108.

Winston, D. 2016. Sheetflood sedimentology of the Mesoproterozoic Revett Formation, Belt Supergroup, northwestern Montana, USA. *Geological Society of America Special Papers*, ***522***, 1-56.

Wolman, M.G. & Brush, L.M., 1961. *Factors controlling the size and shape of stream channels in coarse noncohesive sands*. US Government Printing Office.

Xu, J. 2002. River sedimentation and channel adjustment of the lower Yellow River as influenced by low discharges and seasonal channel dry-ups. *Geomorphology*, ***43***, 151-164.

Xue, J., Deng, Z., Huang, P., Huang, K., Benton, M.J., Cui, Y., Wang, D., Liu, J., Shen, B., Basinger, J.F. & Hao, S. 2016. Belowground rhizomes in paleosols: The hidden half of an Early Devonian vascular plant. *Proceedings of the National Academy of Sciences*, ***113***, 9451-9456

Yeo, G.M., Percival, J.B., Jefferson, C.W., Ickert, R. & Hunt, P. 2007. Environmental significance of oncoids and crypto-microbial laminates from the Late Paleoproterozoic Athabasca Group, Saskatchewan and Alberta. Bull. Geol. Surv. Canada, ***588***, 315.

Young, G.M. 1999. Some aspects of the geochemistry, provenance and palaeoclimatology of the Torridonian of NW Scotland. *Journal of the Geological Society, London*, ***156***, 1097–1111,

Zielinski, T., 2003. Catastrophic flood effects in alpine/foothill fluvial system (a case study from the Sudetes Mts, SW Poland). *Geomorphology*, ***54***, 293-306.

APPENDIX

Table A1. Grid references of all field sites studied over the course of this project

Table A2. Database of alluvial mudrock (Archean-Carboniferous)

Table A3. Database of pre-vegetation alluvium characteristics (Archean-Cambrian)

Table A1. Grid references of all field sites studied over the course of this project

Torridonian	
Cape Wrath	58° 37’ 33’’N, 4° 59’ 51’’W
Sandwood Bay	58° 32’ 14’’N, 5° 03’ 34’’W
Handa Island	58° 23’ 02’’N, 5° 11’ 14’’W
Quinag	58° 12’ 54’’N, 5° 03’ 00’’W
Assynt	58° 10’ 12’’N, 5° 01’ 57’’W
Stoer peninsular	58° 12’ 05’’N, 5° 20’ 15’’W
Suilven	58° 00’ 11’’N, 5° 07’ 59’’W
Inverpolly	58° 03’ 12’’N, 5° 11’ 44’’W
Enard Bay	58° 04’ 33’’N, 5° 19’ 12’’W
Reiff	58° 04’ 12’’N, 5° 20’ 51’’W
Achiltibuie	58° 01’ 81’’N, 5° 21’ 65’’W
Stac Pollaidh	58° 02’ 35’’N, 5° 12’ 20’’W
Tanera Beg	58° 00’ 26’’N, 5° 27’ 02’’W
Badrallach	57° 52’ 25’’N, 5° 16’ 62’’W
Cailleach Head	57° 55’ 46’’N, 5° 24’ 14’’W
Stattic Point	57° 52’ 11’’N, 5° 20’ 24’’W
Gruinard Island	57° 52’ 59’’N, 5° 28’ 20’’W
Aultbea-Rubha Mor	57° 50’ 32’’N, 5° 35’ 11’’W
Bac an Leth-choin	57° 50’ 50’’N, 5° 44’ 48’’W
Rubha Réidh	57° 51’ 17’’N, 5° 48’ 20’’W
Big Sand-North Erradale	57° 45’ 07’’N, 5° 48’ 09’’W
Diabaig	57° 34’ 43’’N, 5° 42’ 13’’W
Alligin	57° 35’ 25’’N, 5° 34’ 20’’W
Liathach	57° 33’ 04’’N, 5° 28’ 53’’W
Beinn Eighe	57° 35’ 27’’N, 5° 25’ 16’’W
Glac Dhorch	57° 32’ 12’’N, 5° 28’ 07’’W
Upper Loch Torridon	57° 31’ 39’’N, 5° 30’ 39’’W
Fearnmore	57° 344’ 39’’N, 5° 48’ 56’’W
Bealach na Ba	57° 25’ 08’’N, 5° 42’ 32’’W
Toscaig	57° 22’ 26’’N, 5° 48’ 49’’W
Raasay	57° 26’ 22’’N, 6° 02’ 10’’W
Kyle of Lochalsh	57° 16’ 53’’N, 5° 42’ 12’’W
Kyleakin	57° 16’ 18’’N, 5° 43’ 28’’W
Ord	57° 08’ 55’’N, 5° 56’ 26’’W
Camasunary	57° 11’ 40’’N, 6° 06’ 54’’W
Rùm	57° 01’ 14’’N, 6° 16’ 07’’W
Series Rouge	
Plourivo	48° 51’ 20’’N, 3° 08’ 35’’W
Bréhec	48° 43’ 14’’N, 2° 56’ 15’’W
Erquy	48° 38’ 38’’N, 2° 29’ 02’’W
Fréhel	48° 41’ 04’’N, 2° 19’ 01’’W
Pointe aux Chèvres	48° 39’ 27’’N, 2° 22’ 10’’W
Sables d’Or Quarry	48° 38’ 21’’N, 2° 24’ 10’’W
Rozel	49° 14’ 22’’N, 2° 02’ 43’’W
Alderney	49° 42’ 32’’N, 2° 13’ 52’’W
Jackson Lake Formation	
Yellowknife	62° 34’ 54’’N, 114° 18’ 44’’W
Baraboo Quartzite	
‘Point of Rocks’ on U.S. Highway 12, Wisconsin	43° 26’ 10’’N, 89° 46’ 32’’W
Le Rue Quarry, Wisconsin	43° 26’ 09’’N, 89° 51’ 21’’W
Ableman’s Gorge, Wisconsin	43° 29’ 18’’N, 89° 54’ 45’’W
Parfrey’s Glen, Wisconsin	43° 25’ 09’’N, 89° 38’ 05’’W
Copper Harbor Conglomerate	
Copper Harbor, Michigan	47° 28’ 36’’N, 87° 54’ 19’’W
Freda Sandstone	

Red cliff, Michigan	46° 37’ 58’’N, 90° 41’ 38’’W
Jacobsville Formation	
L’anse	46° 45’ 11’’N, 6° 05’ 29’’W
Jura Quartzite	
Jura	55° 52’ 32’’N, 6° 05’ 29’’W
Cap de la Chèvre Formation	
Cap de la Chèvre	48° 10’ 08’’N, 4° 33’ 13’’W
Eriboll Formation	
Ord	57° 08’ 55’’N, 5° 56’ 28’’W
Assynt	58° 10’ 12’’N, 5° 01’ 57’’W
Gog Group	
Spriral Tunnels, Kicking Horse Pass, Alberta	51° 27’ 11’’N, 116° 17’ 03’’W
Wrekin Quartzite	
Shropshire	52° 41’ 37’’N, 2° 46’ 44’’W
Milford Haven Group	
Llansteffan	51° 46’ 04’’N, 4° 23’ 19’’W
Brownstones Formation	
Ross-on-Wye	51° 54’ 51’’N, 2° 35’ 16’’W
Alston Formation	
Bamburgh	55° 36’ 51’’N, 1° 43’ 12’’W
Millstone Grit	
Summerbridge	54° 04’ 33’’N, 1° 40’ 38’’W
Scalby Formation	
Burniston	54° 19’ 27’’N, 0° 25’ 13’’W
Horseshoe Canyon Formation	
Willow Creek, Alberta	49° 58’ 17’’N, 113° 47’ 02’’W
Tumblagooda Sandstone	
‘Z-bend’, Kalbarri	27° 39’ 13’’S, 114° 27’ 58’’E
‘Four-ways’, Kalbarri	27° 40’ 58’’S, 114° 27’ 58’’E
‘The Loop, Kalbarri	27° 32’ 43’’S, 114° 27’ 38’’E

Table A2. Database of alluvial mudrock (Archean-Carboniferous). References are stored in the attached CD-ROM

	Oldest possible age	Youngest possible age	Unit	Location	Mudrock %	Mudstone %	Siltstone %	Shale %	Claystone %	References
1	Paleoarchean	Paleoarchean	Baviaanskop Formation	S.Africa/ Swaziland	<1	<1	<1	0	0	Anhaeusser 1976; Eriksson 1977, 1980; Heubeck and Lowe 1994; Eriksson et al. 2006b; Hessler and Lowe 2006
2	Paleoarchean	Paleoarchean	Clatha Formation	South Africa/ Swaziland	<1	<1	<1	0	0	Anhaeusser 1976; Eriksson 1977, 1980; Heubeck and Lowe 1994; Eriksson et al. 2006b; Hessler and Lowe 2006
3	Paleoarchean	Paleoarchean	Hooggenoeg Formation	South Africa	<1	<1	<1	0	0	De Wit et al. 2011; De Wit 2014
4	Paleoarchean	Paleoarchean	Joe's Luck Formation	South Africa/ Swaziland	<1	<1	<1	0	0	Anhaeusser 1976; Eriksson 1977, 1980; Heubeck and Lowe 1994; Eriksson et al. 2006b; Hessler and Lowe 2006
5	Paleoarchean	Paleoarchean	Serra do Córrego Formation	South Africa	0	0	0	0	0	Teles 2013; Teles et al. 2015
6	Mesoarchean	Mesoarchean	Bababudan Group (undivided)	India	0	0	0	0	0	Srinivasan and Ojakangas 1986
7	Mesoarchean	Mesoarchean	Blyvooruitzicht Formation	South Africa	<1	<1	<1	0	0	Eriksson et al. 1993; Guy et al. 2014
8	Mesoarchean	Mesoarchean	Maraisburg Formation	South Africa	0	0	0	0	0	Guy et al. 2014
9	Mesoarchean	Mesoarchean	Sinqeni Formation	South Africa/ Swaziland	<1	<1	<1	<1	0	Dix 1984; Beukes and Cairncross 1991; Hicks 2009; Hicks and Hofmann 2012
10	Mesoarchean	Mesoarchean	Woodburn Lake Formation	Canada (NWT)	<1	<1	<1	0	0	Donaldson and de Kemp 1998
11	Mesoarchean	Neoarchean	Bell Lake Group (undivided)	Canada (NWT)	0	0	0	0	0	Mueller et al. 2005; Mueller and Pickett 2005
12	Mesoarchean	Neoarchean	Elsburg Formation	South Africa	<1	<1	<1	0	0	Els and Mayer 1998; Karpeta and Els 1999; Guy et al. 2010, 2014
13	Mesoarchean	Neoarchean	Kimberley Formation	South Africa	<1	<1	<1	0	0	Els and Mayer 1998; Karpeta and Els 1999; Guy et al. 2010, 2014
14	Mesoarchean	Neoarchean	Manjeri Formation	Zimbabwe	9	9	0	0	0	Kusky and Kidd 1992; Eriksson et al. 1994
15	Mesoarchean	Neoarchean	Mondeor Formation	South Africa	<1	<1	<1	0	0	Els and Mayer 1998; Karpeta and Els 1999; Guy et al. 2010, 2014
16	Mesoarchean	Neoarchean	Pote Formation	Zimbabwe	2	0	2	0	0	Hofmann et al. 2002
17	Neorchean	Neoarchean	Águas Claras Formation	Brazil	no data	no data	no data	no data	no data	Nogueira et al. 1995; Texeira et al. 2007
18	Neoarchean	Neoarchean	Black Reef Formation	South Africa	<1	<1	0	0	0	Henry et al. 1990; Els 1995; Eriksson and Reczko 1995; Catuneanu 1999; Eriksson et al. 2001
19	Neoarchean	Neoarchean	Buffelsfontein Group (undivided)	South Africa	0	0	0	0	0	Tyler 1978; Eriksson et al. 1993
20	Neoarchean	Neoarchean	Casa Forte Formation	Brazil	<1	0	<1	0	0	Baltazar and Zucchetti 2007
21	Neoarchean	Neoarchean	Crowduck Lake Group (undivided)	Canada (Ontario)	10	<1	<10	0	0	Corcoran and Mueller 2007
22	Neoarchean	Neoarchean	English Subprovince	Canada (Ontario)	no data	no data	no data	no data	no data	Hrabi and Cruden 2006
23	Neoarchean	Neoarchean	Godwan Group (undivided)	South Africa	0	0	0	0	0	Myers 1990; Eriksson et al. 1993
24	Neoarchean	Neoarchean	Hardey Formation	Australia (Western Australia)	<1	no data	no data	no data	no data	Blake 1984b, 1990a, 1993; Thorne 1990; Rasmussen et al. 2009
25	Neoarchean	Neoarchean	Jackson Lake Formation	Canada (NWT)	0	0	0	0	0	Isachsen and Bowring, 1994; Mueller et al. 2002
26	Neoarchean	Neoarchean	Jones Creek Supersequence	Australia (Western Australia)	0	0	0	0	0	Krapez et al. 1997, 2000, 2008

27	Neoarchean	Neoarchean	Keskarrah Formation	Canada (NWT)	<1	<1	<1	0	0	Corcoran et al. 1998; Corcoran and Mueller 2002
28	Neoarchean	Neoarchean	Lalla Rookh Formation	Australia (Western Australia)	7.5	no data	no data	no data	no data	Krapez 1984; Krapez and Barley 1987; Rasmussen and Buick 1999
29	Neoarchean	Neoarchean	Merougil Formation	Australia (Western Australia)	0	0	0	0	0	Krapez 1997; Krapez et al. 2000, 2008
30	Neoarchean	Neoarchean	Midway Sequence	USA (Minnesota)	0	0	0	0	0	Jirsa 2000
31	Neoarchean	Neoarchean	Moeda Formation	Brazil	0	0	0	0	0	Minter et al. 1990
32	Neoarchean	Neoarchean	Ogishkemuncie Sequence	USA (Minnesota)	no data	no data	no data	no data	no data	Jirsa and Starns 2008; Driese et al. 2011
33	Neoarchean	Neoarchean	Ongers River Formation	South Africa	<1	<1	0	0	0	Grobler et al. 1989; Altermann and Lenhardt 2012
34	Neoarchean	Neoarchean	Raquette Lake Formation	Canada (NWT)	<1	<1	0	0	0	Mueller and Corcoran 2001
35	Neoarchean	Neoarchean	Renosterspruit Sandstone Formation	South Africa	14	0	0	14	0	Watchorn, 1980, 1981; Tankard et al. 1982; Burke et al. 1984; Burke 1986
36	Neoarchean	Neoarchean	Shivakala Formation	Kenya	no data	no data	no data	no data	no data	Ngecu and Gaciri 1995
37	Neoarchean	Neoarchean	Timiskaming Group (undivided)	Canada (Ontario, Quebec)	0	0	0	0	0	Hyde 1980; Thurston and Chivers 1990; Corfu et al. 1991; Mueller et al. 1994; Born 1995; Ayer et al. 2002; Corcoran and Mueller 2007
38	Neorchean	Paleoproterozoic	Harmony Formation	South Africa	0	0	0	0	0	Minter, 1978; Smith and Minter, 1980; Buck 1983
39	Archean	Archean	Beaulieu Rapids Formation	Canada (NWT)	<1	0	<1	0	0	Roscoe et al. 1989; Corcoran et al. 1999; Corcoran and Mueller 2002
40	Archean	Archean	Bothaville Formation	South Africa	2.5	1	1.5	0	0	Buck, 1980; Grobler et al. 1989
41	Archean	Archean	Duparquet Formation	Canada (Quebec)	<1	<1	<1	0	0	Mueller et al. 1991; Eriksson et al. 1994; Mueller and Corcoran 1998
42	Archean	Archean	Hauy Formation	Canada (Quebec)	<1	<1	0	0	0	Mueller and Dimroth 1987
43	Archean	Archean	Leadbetter Conglomerate	Canada (Ontario)	<1	<1	0	0	0	Wendland et al. 2011
44	Archean	Archean	Mount Roe Formation	Australia (Western Australia)	0	0	0	0	0	Blake 1993
45	Archean	Archean	North Spirit Lake Group (undivided)	Canada (Ontario)	<1	<1	0	0	0	Wood 1980
46	Archean	Archean	Rainy Lake Group (undivided)	Canada (Ontario)	<1	<1	0	0	0	Wood 1980
47	Archean	Archean	Rajkharsawan Conglomerate	India	0	0	0	0	0	Van Loon et al. 2012
48	Archean	Archean	Randfontein Formation	South Africa	<1	<1	<1	0	0	Clendenin et al. 1991; Eriksson et al. 1993; Guy et al. 2010
49	Archean	Archean	Schelem Formation	South Africa	no data	no data	no data	no data	no data	Eriksson et al. 1993
50	Archean	Archean	Scotty Creek Formation	Australia (Western Australia)	0	0	0	0	0	Krapez et al. 2008
51	Archean	Archean	Stella Formation	Canada (Quebec)	<1	<1	<1	<1	<1	Mueller and Dimroth 1987
52	Archean	Archean	Yandal Sandstone	Australia (Western Australia)	0	0	0	0	0	Krapez et al. 2008

53	Paleoproterozoic	Paleoproterozoic	Aasvoëlkop Formation	South Africa	<1	no data	no data	no data	no data	Callaghan 1987; Callaghan et al. 2001; Hanson et al. 2004; Eriksson et al. 2008
54	Paleoproterozoic	Paleoproterozoic	Ahven-Kivilampi Formation	Finland	0	0	0	0	0	Strand 1988; Laajoki et al. 1989; Strand 2012
55	Paleoproterozoic	Paleoproterozoic	Amarook Formation	Canada (Nunavut)	0	0	0	0	0	Donaldson 1968; Rainbird and Davis 2007
56	Paleoproterozoic	Paleoproterozoic	Arkosite Formation	Finland	7.5	7.5	0	0	0	Strand 1988
57	Paleoproterozoic	Paleoproterozoic	Bandeirinha Formation	Brazil	0	0	0	0	0	Chemale Jr et al. 2012; Santos et al. 2013
58	Paleoproterozoic	Paleoproterozoic	Banganapalli Formation	India	0	0	0	0	0	Deb et al. 2012
59	Paleoproterozoic	Paleoproterozoic	Baraboo Quartzite	USA (Wisconsin)	<1	0	<1	0	0	Brett 1955; Dott and Dalziel 1972; Dott 1983; Medaris et al. 2003; Van Wyck and Norman 2004
60	Paleoproterozoic	Paleoproterozoic	Barron Quartzite	USA (Wisconsin)	0	0	0	0	0	Dott 1983
61	Paleoproterozoic	Paleoproterozoic	Beasley River Quartzite	Australia (Western Australia)	<1	<1	0	0	0	Martin et al. 2000; Mazumder and Kranendonk, 2013
62	Paleoproterozoic	Paleoproterozoic	Bigie Formation	Australia (Queensland, Northern Territory)	<1	<1	0	0	0	Betts et al. 1999
63	Paleoproterozoic	Paleoproterozoic	Billstein Formation	Namibia	0	0	0	0	0	Schalk 1988; Hoffmann 1989; Becker et al. 2005
64	Paleoproterozoic	Paleoproterozoic	Bisrampur Formation	India	0	0	0	0	0	Bhattacharya and Mahapatra 2008; Van Loon and De 2015
65	Paleoproterozoic	Paleoproterozoic	Blouberg Formation	South Africa	<1	<1	0	0	0	Bumby 2000; Bumby et al. 2001a; 2004; Simpson et al. 2013
66	Paleoproterozoic	Paleoproterozoic	Bonner Formation	USA (Montana)	no data	no data	no data	no data	no data	Kidder 1992; Ross et al. 1992
67	Paleoproterozoic	Paleoproterozoic	Boshoek Formation	South Africa	0	0	0	0	0	Eriksson et al. 2001
68	Paleoproterozoic	Paleoproterozoic	Bottletree Formation	Australia (Queensland)	0	0	0	0	0	Eriksson et al. 1993c; Southgate et al. 2006
69	Paleoproterozoic	Paleoproterozoic	Bruco Formation	Angola	<1	<1	0	0	0	Kröner and Correia 1980; Pedreira and de Waele 2008; Pereira et al. 2011
70	Paleoproterozoic	Paleoproterozoic	Burnside River Formation	Canada (Nunavut)	0	0	0	0	0	Grotzinger and Gall 1986; McCormick 1992; McCormick and Grotzinger 1992, 1993; Ielpi and Rainbird, 2016b
71	Paleoproterozoic	Paleoproterozoic	Cangalongue Formation	Brazil	0	0	0	0	0	Pedreira and de Waele 2008
72	Paleoproterozoic	Paleoproterozoic	Changzhougou Formation	China	0	0	0	0	0	Lu et al. 2008
73	Paleoproterozoic	Paleoproterozoic	Cromwell Member	Australia (Queensland)	2	0	2	0	0	Eriksson and Simpson 1993
74	Paleoproterozoic	Paleoproterozoic	Daspoort Formation	South Africa	<1	<1	0	0	0	Eriksson et al. 1993; Eriksson and Catuneanu 2004
75	Paleoproterozoic	Paleoproterozoic	Deadman Quartzite	USA (Arizona)	0	0	0	0	0	Bayne 1987; Cox 2002
76	Paleoproterozoic	Paleoproterozoic	Deighton Quartzite	Australia (Queensland)	<1	<1	<1	0	0	Derrick et al. 1977; Neumann et al. 2009
77	Paleoproterozoic	Paleoproterozoic	Dhalbhum Formation	India	0	0	0	0	0	Mazumder 2005; Mazumder et al. 2012b
78	Paleoproterozoic	Paleoproterozoic	Dhanjori Formation	India	<1	<1	<1	<1	0	Gupta et al. 1985; Saha 1994; Mazumder 2002; Mazumder and Sarkar 2004; Mazumder 2005; Mazumder and Arima 2009; Mazumder et al. 2012b
79	Paleoproterozoic	Paleoproterozoic	Dodmanberget Formation	Sweden	0	0	0	0	0	Bauer et al. 2013
80	Paleoproterozoic	Paleoproterozoic	Droogedal Formation	South Africa	8	8	0	0	0	Eriksson et al. 1989
81	Paleoproterozoic	Paleoproterozoic	Dwaalheawel Formation	South Africa	<1	0	<1	0	0	Schreiber and Eriksson 1992; Eriksson et al. 1993; Eriksson et al. 2001

82	Paleoproterozoic	Paleoproterozoic	Echo Sandstone	Australia (Northern Territory)	no data	no data	no data	no data	no data	Polito et al. 2006
83	Paleoproterozoic	Paleoproterozoic	Ellice Formation	Canada (Nunavut)	<1	<1	0	0	0	Ielpi and Rainbird 2015
84	Paleoproterozoic	Paleoproterozoic	FA Formation	Gabon	<1	0	<1	0	0	Ossa et al. 2014
85	Paleoproterozoic	Paleoproterozoic	Fair Point Formation	Canada (Saskatchewan)	<1	0	<1	0	0	Ramaekers and Catuneanu 2004
86	Paleoproterozoic	Paleoproterozoic	Fish River Formation	Australia (Queensland, Northern Territory)	0	0	0	0	0	Bradshaw et al. 2000
87	Paleoproterozoic	Paleoproterozoic	Flambeau Quartzite	USA (Wisconsin)	0	0	0	0	0	Campbell 1986
88	Paleoproterozoic	Paleoproterozoic	Gulcheru Quartzite	India	<1	<1	0	0	0	Deb et al. 2012; Basu et al. 2014; Chakrabarti et al. 2015
89	Paleoproterozoic	Paleoproterozoic	Hutte Sauvage Group (Undivided)	Canada (Quebec)	0	0	0	0	0	Girard 1992
90	Paleoproterozoic	Paleoproterozoic	Kazan Formation	Canada (Nunavut)	<1	<1	<1	0	0	Donaldson 1965; Miller 1993; Rainbird et al. 1999; Aspler et al. 2004; Hadlari et al. 2006
91	Paleoproterozoic	Paleoproterozoic	Kazput Formation (middle)	Australia (Western Australia)	<1	<1	0	0	0	Martin et al. 1991, 2000; Thorne and Tyler 1996
92	Paleoproterozoic	Paleoproterozoic	Kiskonkoski Formation	Finland	<1	<1	<1	0	0	Strand 2005
93	Paleoproterozoic	Paleoproterozoic	Kiyuk Group (Undivided)	Canada (Nunavut)	0	0	0	0	0	Aspler et al. 1989
94	Paleoproterozoic	Paleoproterozoic	Kolhan Sandstone	India	<1	<1	0	0	0	Ghosh and Chatterjee 1994; Bandopadhyay and Sengupta 2004
95	Paleoproterozoic	Paleoproterozoic	Koolbye Formation	Australia (Western Australia)	<1	0	<1	0	0	Martin et al. 2000; Mazumder et al. 2015
96	Paleoproterozoic	Paleoproterozoic	Kunwak Formation	Canada (Nunavut)	<1	<1	<1	0	0	Miller 1993; Rainbird et al. 1999; Hadlari et al. 2006
97	Paleoproterozoic	Paleoproterozoic	Kurinelli Sandstone	Australia (Northern Territory)	no data	no data	no data	no data	no data	Sweet 1988
98	Paleoproterozoic	Paleoproterozoic	Laanhongikko Formation	Finland	no data	no data	no data	no data	no data	Strand 1988; Laajoki et al. 1989; Strand 2012
99	Paleoproterozoic	Paleoproterozoic	Lazenby Lake Formation	Canada (Manitoba)	<1	<1	0	0	0	Ramaekers and Catuneanu 2004
100	Paleoproterozoic	Paleoproterozoic	Leeuwpoort Formation	South Africa	no data	no data	no data	no data	no data	Richards and Eriksson 1988; Eriksson et al. 1993
101	Paleoproterozoic	Paleoproterozoic	Lena Quartzite	Australia (Queensland, Northern Territory)	3	0.1	3	0	0	Eriksson and Simpson 1993
102	Paleoproterozoic	Paleoproterozoic	Lindsey Quartzite	USA (Wyoming)	0	0	0	0	0	Karlstrom et al. 1983
103	Paleoproterozoic	Paleoproterozoic	Lochness Formation	Australia (Queensland, Northern Territory)	<1	<1	<1	0	0	Eriksson et al. 1993c; Driese et al. 1995
104	Paleoproterozoic	Paleoproterozoic	Locker Lake Formation	Canada (Saskatchewan)	<1	<1	0	0	0	Ramaekers, 1979, 1980, 1990; Ramaekers and Catuneanu 2004
105	Paleoproterozoic	Paleoproterozoic	Lorrain Formation	Canada (Ontario, Quebec)	<1	<1	0	0	0	Casshyap 1968; Hadley 1968; Young 1983; Mossman and Harron 1984; Chandler 1986; Young et al. 2001
106	Paleoproterozoic	Paleoproterozoic	Lukkarinvaara Formation	Finland	<1	<1	0	0	0	Härmä 1986; Laajoki et al. 1989
107	Paleoproterozoic	Paleoproterozoic	Magnolia Formation	USA (Wyoming)	<1	<1	0	0	0	Karlstrom et al. 1983

108	Paleoproterozoic	Paleoproterozoic	Main Quartzite Sequence	South Africa	<1	<1	<1	0	0	Clendenin et al. 1991; Eriksson et al. 1993; Kositcin and Krapze 2004; Guy et al. 2010
109	Paleoproterozoic	Paleoproterozoic	Makgabeng Formation	South Africa	0	0	0	0	0	Simpson et al. 2013; Heness et al. 2014
110	Paleoproterozoic	Paleoproterozoic	Malmbäck Formation	Sweden	0	0	0	0	0	Appelquist et al. 2009
111	Paleoproterozoic	Paleoproterozoic	Manitou Falls Formation	Canada (Saskatchewan)	<1	<1	<1	0	0	Ramaekers 1979, 1980; Long et al. 2001; Yeo et al. 2002; 2007; Bernier 2003; Ramaekers and Catuneanu 2004; Long 2006, 2007; Hiatt et al. 2007; Post and Kupsch 2007
112	Paleoproterozoic	Paleoproterozoic	Masterton Sandstone	Australia (Northern Territory)	<1	<1	0	0	0	Jackson 1981b; Southgate et al. 2000
113	Paleoproterozoic	Paleoproterozoic	Matinenda Formation	Canada (Ontario)	0	0	<1	0	0	Young 1983; Fralick and Miall 1989; Fralick 1999; Young et al. 2001
114	Paleoproterozoic	Paleoproterozoic	Mazatzal Peak Quartzite	USA (Arizona)	no data	no data	no data	no data	no data	Trevena 1978; Middleton 1986; Cox 2002
115	Paleoproterozoic	Paleoproterozoic	Mississagi Formation	Canada (Ontario)	<1	<1	<1	0	0	Casshyap 1968; Long 1978; Young 1983; Young et al. 2001; Long et al. 2011; Young et al. 2014
116	Paleoproterozoic	Paleoproterozoic	Mitoba River Group (undivided)	Zambia	0	0	0	0	0	Daly and Unrug 1982
117	Paleoproterozoic	Paleoproterozoic	Mogalakwena Formation	South Africa	0	0	0	0	0	Bumby 2000; Bumby et al. 2001a, b; Eriksson et al. 2008; Long 2011; Simpson et al. 2013
118	Paleoproterozoic	Paleoproterozoic	Mount Guide Quartzite	Australia (Queensland)	0	0	0	0	0	Southgate et al. 2006
119	Paleoproterozoic	Paleoproterozoic	Murky Formation	Canada (NWT)	<1	<1	<1	0	0	Hoffman 1969; Ritts 1994
120	Paleoproterozoic	Paleoproterozoic	Naulaperá Formation	Finland	<1	<1	<1	0	0	Strand 2005
121	Paleoproterozoic	Paleoproterozoic	Noomut Formation	Canada (Nunavut)	0	0	0	0	0	Aspler and Chiarenzelli 1997
122	Paleoproterozoic	Paleoproterozoic	Otherside Formation	Canada (Saskatchewan)	0	0	0	0	0	Ramaekers, 1979, 1980, 1990; Ramaekers and Caatuneanu 2004
123	Paleoproterozoic	Paleoproterozoic	Pajeú Formation	Brazil	no data	no data	no data	no data	no data	Pedreira and de Waele 2008
124	Paleoproterozoic	Paleoproterozoic	Paljakkavaara Formation	Finland	0	0	0	0	0	Strand 1988
125	Paleoproterozoic	Paleoproterozoic	Par Formation	India	no data	no data	no data	no data	no data	Chakraborty and Paul 2014
126	Paleoproterozoic	Paleoproterozoic	Pitz Formation	Canada (Nunavut)	<1	<1	0	0	0	Rainbird and Hadlari 2000; Rainbird and Davis 2007
127	Paleoproterozoic	Paleoproterozoic	Preble Formation	Canada (NWT)	0	0	0	0	0	Hoffnam 1969, 1988a; Ritts 1994
128	Paleoproterozoic	Paleoproterozoic	Rayton Formation	South Africa	no data	no data	no data	no data	no data	Visser 1969; Eriksson et al. 1993
129	Paleoproterozoic	Paleoproterozoic	Read Formation	Canada (Saskatchewan)	<1	<1	0	0	0	Miall 1996; Long 2006, 2007
130	Paleoproterozoic	Paleoproterozoic	Rifle Formation	Canada (Nunavut)	no data	no data	no data	no data	no data	Grotzinger et al. 1989
131	Paleoproterozoic	Paleoproterozoic	Rooihoogte Formation	South Africa	0	0	0	0	0	Eriksson 1988; Catuneanu and Eriksson 2002
132	Paleoproterozoic	Paleoproterozoic	Sandriviersberg Formation	South Africa	0	0	0	0	0	Callaghan et al. 1991
133	Paleoproterozoic	Paleoproterozoic	São João da Chapada Formation	Brazil	<1	<1	<1	0	0	Marins-Neto 1994; Chemale Jr et al. 2012; Santos et al. 2013
134	Paleoproterozoic	Paleoproterozoic	Sekororo Formation	South Africa	0	0	0	0	0	Button 1972; Bosch 1992; Eriksson et al. 1993b
135	Paleoproterozoic	Paleoproterozoic	Serpent Formation	Canada (Ontario)	<1	<1	<1	<1	<1	Casshyap 1968; Fedo et al. 1997a; Young 1983; Young et al. 2001; Long 2004
136	Paleoproterozoic	Paleoproterozoic	Serra du Gameleira Formation	Brazil	0	0	0	0	0	Magalháes et al. 2014; Guadagnin et al. 2015
137	Paleoproterozoic	Paleoproterozoic	Setlaole Formation	South Africa	<1	<1	0	0	0	Callaghan et al. 1991; Bumby 2000; Bumby et al. 2001a; Simpson et al. 2013

138	Paleoproterozoic	Paleoproterozoic	Sioux Quartzite	USA (Minnesota, South Dakota, Iowa)	3	3	0	0	0	Weber 1981; Dott 1983; Morey 1984; Ojakangas and Weber 1984; Southwick and Mossler 1984; Southwick et al. 1986; Anderson 1987
139	Paleoproterozoic	Paleoproterozoic	Skilpadkop Formation	South Africa	no data	no data	no data	no data	no data	Callaghan et al. 1991
140	Paleoproterozoic	Paleoproterozoic	Sly Creek Sandstone	Australia (Queensland, Northern Territory)	0	0	0	0	0	Polito et al. 2006
141	Paleoproterozoic	Paleoproterozoic	Smart Formation	Canada (Alberta, Saskatchewan)	<1	<1	0	0	0	Yeo et al. 2007
142	Paleoproterozoic	Paleoproterozoic	Smelterskop Formation	South Africa	no data	no data	no data	no data	no data	Stear 1977a; Richards and Eriksson 1988; Eriksson et al. 1993
143	Paleoproterozoic	Paleoproterozoic	South Channel Formation	Canada (Nunavut)	<1	<1	0	0	0	Miller 1993; Rainbird et al. 1999; Aspler et al. 2004; Hadlari et al. 2006
144	Paleoproterozoic	Paleoproterozoic	Surprise Creek Formation	Australia (Queensland, Northern Territory)	<1	0	<1	0	0	Derrick et al. 1980; Betts et al. 1999; Neumann 2009
145	Paleoproterozoic	Paleoproterozoic	Taragan Sandstone	Australia (Northern Territory)	7.7	no data	no data	no data	no data	Sweet 1988
146	Paleoproterozoic	Paleoproterozoic	Tavani Formation	Canada (NWT)	0	0	0	0	0	Aspler and Chiarenzelli, 1997; Aspler et al. 2001; Davis et al. 2005
147	Paleoproterozoic	Paleoproterozoic	Thelon Formation	Canada (NWT)	<1	0	0	0	<1	Cecile 1973; Jackson et al. 1984; Miller et al. 1989; Hiatt et al. 2003; Beyer et al. 2011
148	Paleoproterozoic	Paleoproterozoic	Tundavala Formation	Angola	0	0	0	0	0	Kröner and Correia 1980; Jones et al. 1992; Pereira et al. 2011
149	Paleoproterozoic	Paleoproterozoic	Uaimapáe Formation	Venezuela	<1	<1	<1	<1	0	Long 2002
150	Paleoproterozoic	Paleoproterozoic	Uairén Formation	Venezuela	<1	<1	<1	<1	0	Long 2002
151	Paleoproterozoic	Paleoproterozoic	Vallecito Conglomerate	USA (Colorado)	0	0	0	0	0	Ethridge et al. 1984
152	Paleoproterozoic	Paleoproterozoic	Warramana Sandstone	Australia (Northern Territory)	0	0	0	0	0	Haines et al. 1993; Polito et al. 2006
153	Paleoproterozoic	Paleoproterozoic	Westmoreland Conglomerate	Australia (Queensland, Northern Territory)	0	0	0	0	0	Wygralak et al. 1988; Ahmad and Wygralak 1989; Croaker and Lung 1997; Polito et al. 2005, 2006
154	Paleoproterozoic	Paleoproterozoic	Whitworth Formation	Australia (Queensland, Northern Territory)	<1	<1	0	0	0	Simpson and Eriksson 1993
155	Paleoproterozoic	Paleoproterozoic	Wilgerivier Formation	South Africa	<1	<1	<1	0	0	Vos and Eriksson 1977; Eriksson and Vos 1979; Callaghan 1991; Van der Neut et al. 1991; Van der Neit and Eriksson 1999; Eriksson et al. 2008
156	Paleoproterozoic	Paleoproterozoic	Wolverine Point Formation	Canada (Saskatchewan)	<5	no data	no data	no data	no data	Ramaekers and Catuneanu 2004
157	Paleoproterozoic	Paleoproterozoic	Wyllies Poort Formation	South Africa	0	0	0	0	0	Cheney et al. 1990; Bumby 2000; Bumby et al. 2002
158	Paleoproterozoic	Paleoproterozoic	Yinmin Formation	China	<1	no data	no data	no data	no data	Hua 1993; Du and Han 2000; Zhao et al. 2010; Wang et al. 2014
159	Paleoproterozoic	Paleoproterozoic	Yiyintyi Sandstone	Australia (Northern Territory)	0	0	0	0	0	Jackson et al. 2000; Polito et al. 2006; Southgate et al. 2006
160	Paleoproterozoic	Mesoproterozoic	Doomadgee Formation	Australia (Queensland, Northern Territory)	<1	no data	no data	no data	no data	Bradshaw et al., 2000; Krassay et al. 2000; Southgate et al. 2000

161	Paleoproterozoic	Mesoproterozoic	Mbala Formation	Brazil	<1	<1	no data	no data	no data	Daly and Unrug 1982; Unrug 1984; Andrews-Speed 1986a, 1989; Pedreira and de Waele 2008
162	Paleoproterozoic	Mesoproterozoic	Sims Formation	Canada (Labrador, Quebec)	<1	<1	no data	no data	no data	Ware and Hiscott 1985
163	Paleoproterozoic	Mesoproterozoic	Xiaogoubei Formation	China	0	0	0	0	0	Hu et al. 2014
164	Mesoproterozoic	Mesoproterozoic	Adams Sound Formation	Canada (Nunavut)	0	0	0	0	0	Iannelli 1992; Long and Turner 2012
165	Mesoproterozoic	Mesoproterozoic	Agigilik Formation	Canada (Nunavut)	0	0	0	0	0	Knight and Jackson 1994
166	Mesoproterozoic	Mesoproterozoic	Barden Bugt Formation	Greenland	no data	no data	no data	no data	no data	Dawes 1997, 2006
167	Mesoproterozoic	Mesoproterozoic	Bay of Stoer Formation	Scotland	<1	<1	<1	<1	<1	Stewart 1990, 2002
168	Mesoproterozoic	Mesoproterozoic	Beinn na Seamraig Formation	Scotland	<1	<1	<1	<1	<1	Sutton and Watson 1964, Stewart 1988b, 1991, 2002
169	Mesoproterozoic	Mesoproterozoic	Burdur Formation	Russia	<1	<1	<1	0	0	Petrov 2011, 2014
170	Mesoproterozoic	Mesoproterozoic	Chandil Formation	India	7.5	no data	no data	no data	no data	Ray et al. 1996; Mazumder 2005
171	Mesoproterozoic	Mesoproterozoic	Chequamegon Sandstone	USA (Wisconsin, Minnesota)	6	no data	no data	no data	no data	Morey and Ojakangas 1982; Craddock et al. 2013
172	Mesoproterozoic	Mesoproterozoic	Clachtoll Formation	Scotland	5	5	0	0	0	Stewart 1990, 2002
173	Mesoproterozoic	Mesoproterozoic	Copper Harbour Conglomerate	USA (Michigan)	<1	<1	<1	0	0	Wolff and Haber 1973; Elmore 1983, 1984; Sheldon et al. 2012; Wilmeth et al. 2014; Fedonkin et a.l., 2016
174	Mesoproterozoic	Mesoproterozoic	Dala Sandstone	Sweden	no data	no data	no data	no data	no data	Pulvertaft, 1985
175	Mesoproterozoic	Mesoproterozoic	Devdahra Formation	India	0	0	0	0	0	Patra et al. 2013
176	Mesoproterozoic	Mesoproterozoic	Dhandraul Sandstone Formation	India	<1	<1	<1	0	0	Datta 2005; Deb and Chaudhuri 2007; Chakraborty et al. 2009; Dhang and Deb 2011
177	Mesoproterozoic	Mesoproterozoic	Dox Sandstone	USA (Idaho)	1	1	1	0	0	Stevensen 1973; Winston 1990; Timmons et al. 2005
178	Mesoproterozoic	Mesoproterozoic	Dripping Spring Formation	USA (Arizona)	<1	<1	<1	0	0	Winston 1991; Montgomery and Middleton 2000; Beraldi-Campesi et al. 2014
179	Mesoproterozoic	Mesoproterozoic	Eriksfjord Formation	Greenland	7	7	0	0	0	Poulsen 1964; Ladengaard 1988; Tirsgaard 1989; Clemmensen and Tirsgaard 1990; Tirsgaard and Øxnevad 1998
180	Mesoproterozoic	Mesoproterozoic	Fabricius Fiord Formation	Canada (Nunavut)	0	0	0	0	0	Sherman et al. 2012
181	Mesoproterozoic	Mesoproterozoic	Fond du Lac Formation	USA (Minnesota)	7	4	3	0	0	Morey 1967; Morey and Ojakangas 1982; Craddock 2013
182	Mesoproterozoic	Mesoproterozoic	Fort Steel Formation	Canada (British Columbia)	<1	<1	<1	0	0	Höy 1992; Ross and Villeneuve 2004
183	Mesoproterozoic	Mesoproterozoic	Heddersvatnet Formation	Norway	2	1	1	0	0	Köykkä 2011a
184	Mesoproterozoic	Mesoproterozoic	Il'ya Formation	Russia	<1	<1	<1	0	0	Petrov 2011, 2014
185	Mesoproterozoic	Mesoproterozoic	Inuiteq Sø Formation	Greenland	3	3	0	0	0	Collinson 1983; Collinson et al. 2008; Kirkland et al. 2009
186	Mesoproterozoic	Mesoproterozoic	Jacobsville Sandstone	USA (Minnesota)	<1	<1	<1	0	0	Kalliokoski 1982; Ojakangas et al. 2001
187	Mesoproterozoic	Mesoproterozoic	Jakaram Formation	India	0	0	0	0	0	Ramakrishnan and Vaidyanadhan 2008
188	Mesoproterozoic	Mesoproterozoic	Kanuyak Formation	Canada (Nunavut)	10	5	5	0	0	Pelechaty 1990; Pelechaty et al. 1991
189	Mesoproterozoic	Mesoproterozoic	Kasama Formation	Zambia	17	17	0	0	0	Daly and Unrug 1982; Unrug 1982; Andersen and Unrug Fm 1984; de Waele and Fitzsimons 2007
190	Mesoproterozoic	Mesoproterozoic	Kinloch Formation	Scotland	<1	<1	<1	0	0	Stewart 1991, 2002

191	Mesoproterozoic	Mesoproterozoic	Klein Aub Formation	Namibia	0	0	0	0	0	Schalk 1988; Hoffmann 1989; Becker et al. 2005
192	Mesoproterozoic	Mesoproterozoic	Kundargi Formation	India	0	0	0	0	0	Mukhopadhyay et al. 2014; Dey 2015
193	Mesoproterozoic	Mesoproterozoic	Kutovaya Formation	Norway	no data	no data	no data	no data	no data	Siedlecka et al. 1995
194	Mesoproterozoic	Mesoproterozoic	Labaztakh Formation	Russia	<1	<1	<1	0	0	Petrov 2011, 2014
195	Mesoproterozoic	Mesoproterozoic	Loch na Dal Formation	Scotland	<1	<1	<1	0	0	Stewart 1991, 2002
196	Mesoproterozoic	Mesoproterozoic	Mangabeira Formation	Brazil	no data	no data	no data	no data	no data	Guadagnin et al. 2015
197	Mesoproterozoic	Mesoproterozoic	Meall Dearg Formation	Scotland	<1	<1	0	0	0	Stewart 2002, Owen and Santos 2014; Prave, 2002; Brasier et al. 2016; McMahon and Davies, 2017
198	Mesoproterozoic	Mesoproterozoic	Monteso Formation	Mexico	0	0	0	0	0	Stewart et al. 2002; Corsetti et al. 2007
199	Mesoproterozoic	Mesoproterozoic	Nalla Gutta Sandstone	India	0	0	0	0	0	Chaudhuri 2003
200	Mesoproterozoic	Mesoproterozoic	Nelson Head Formation	Canada (Yukon, NWT, Nunavut)	7	4	3	0	0	Rainbird et al. 1994, 1996a, 1997; Long et al. 2008; Rainbird et al. 2012; Ielpi and Rainbird, 2016a
201	Mesoproterozoic	Mesoproterozoic	Nopeming Formation	USA (Minnesota)	<1	<1	<1	0	0	Ojakangas and Morey 1982; Ojakangas et al. 2001
202	Mesoproterozoic	Mesoproterozoic	Nyeboe Formation	Canada (Nunavut)	0	0	0	0	0	Chandler 1988b; Long and Turner 2012
203	Mesoproterozoic	Mesoproterozoic	Orienta Sandstone	USA (Wisconsin, Minnesota)	8	8	0	0	0	Morey and Ojakangas 1982; Craddock et al. 2013
204	Mesoproterozoic	Mesoproterozoic	Osler Group (undivided)	USA (Minnesota)	<1	<1	<1	0	0	Merk and Jirsa 1982; Ojakangas and Morey 1982; Ojakangas et al. 2001
205	Mesoproterozoic	Mesoproterozoic	Outan Island Formation	USA (Minnesota)	14	0	10	4	0	Rogala et al. 2007; Fralick and Zaniewski 2012
206	Mesoproterozoic	Mesoproterozoic	Pandurra Formation	Australia (South Australia)	<1	0	<1	<1	0	Fanning et al. 1983; Preiss 2000; Schmidt and Williams 2011
207	Mesoproterozoic	Mesoproterozoic	Pass Lake Formation	USA (Minnesota, Wisconsin)	0	0	0	0	0	Franklin et al. 1980; Ojakangas and Morey 1982; Cheadle 1986; Chandler 1988; Rogala et al. 2007
208	Mesoproterozoic	Mesoproterozoic	Puckwunge Formation	USA (Minnesota)	<1	<1	<1	<1	<1	Ojakangas and Morey 1982; Ojakangas et al. 2001
209	Mesoproterozoic	Mesoproterozoic	Qaanaag Formation	Greenland	<1	<1	<1	0	0	Dawes 1997, 2006
210	Mesoproterozoic	Mesoproterozoic	Ramdurg Formation	India	<1	<1	<1	0	0	Bose et al. 2008; Mukhopadhyay et al. 2014
211	Mesoproterozoic	Mesoproterozoic	Ravalli Group (undivided)	USA (Idaho)	1	1	0	0	0	Winston 1990
212	Mesoproterozoic	Mesoproterozoic	Revett Formation	USA (Idaho)	<1	<1	<1	0	<1	White et al. 1984; Mauk and White 2004; Winston 2016
213	Mesoproterozoic	Mesoproterozoic	Rubha Guail Formation	Scotland	<1	<1	0	0	0	Stewart 1991, 2002
214	Mesoproterozoic	Mesoproterozoic	Scanlan Conglomerate	USA (Arizona)	<1	0	0	0	0	Middleton and Trujillo, 1984
215	Mesoproterozoic	Mesoproterozoic	Simpson Island Formation	Canada (Ontario)	<1	<1	<1	0	0	Hollings et al. 2007
216	Mesoproterozoic	Mesoproterozoic	Sinasiuvik Formation	Canada (Nunavut)	0	0	0	0	0	Knight and Jackson 1994
217	Mesoproterozoic	Mesoproterozoic	Skottsfjell Formation	Norway	no data	no data	no data	no data	no data	Lamminen and Köykkä 2011
218	Mesoproterozoic	Mesoproterozoic	Solor Church Formation	USA (Wisconsin, Minnesota)	<1	<1	<1	0	0	Morey and Ojakangas 1982; Ojakangas et al. 2001

219	Mesoproterozoic	Mesoproterozoic	Sopa-Brumadinho Formation	Brazil	8	no data	no data	no data	no data	Martins-Neto 1995d, 2000; Cabral et al. 2011; Chemale Jr et al. 2012; Santos et al. 2013
220	Mesoproterozoic	Mesoproterozoic	Svinsaga Formation	Norway	5	no data	no data	no data	no data	Köykkä 2011b
221	Mesoproterozoic	Mesoproterozoic	Tombador Formation	Brazil	<1	<1	<1	0	0	Bállico 2012; Magalhães et al. 2014; Guadagnin et al. 2015; de Almeida et al. 2016
222	Mesoproterozoic	Mesoproterozoic	Troy Quartzite	USA (Arizona)	<1	<1	<1	0	0	Winston 1990
223	Mesoproterozoic	Mesoproterozoic	Urusib Formation	Namibia	0	0	0	0	0	Harrison 1979; Hoal 1985, 1990
224	Mesoproterozoic	Mesoproterozoic	Vemork Formation	Norway	1.5	1.5	0	0	0	Laajoki and Corfu 2007; Lamminen and Köykkä 2011
225	Mesoproterozoic	Mesoproterozoic	Wolstenholme Formation	Greenland	<1	<1	<1	0	0	Dawes 1997, 2006
226	Mesoproterozoic	Mesoproterozoic	Yunmengshan Formation	China	0	0	0	0	0	Hu et al. 2014
227	Mesoproterozoic	Neoproterozoic	El Aguila Formation	Mexico	<1	<1	<1	0	0	Gross et al. 2000; Stewart et al. 2002
228	Mesoproterozoic	Neoproterozoic	El Alamo Formation	Mexico	<1	<1	<1	0	0	Gross et al. 2000; Stewart et al. 2002
229	Mesoproterozoic	Neoproterozoic	Freda Sandstone	USA (Michigan, Wisconsin)	<1	<1	<1	<1	<1	Daniels Jr 1982; Ojakangas et al. 2001; Ojakangas and Dickas 2002
230	Mesoproterozoic	Neoproterozoic	Grassy Bay Formation	Canada (Yukon, NWT, Nunavut)	<1	<1	<1	0	0	Young and Long 1977
231	Mesoproterozoic	Neoproterozoic	Kgwebe Formation	Botswana	0	0	0	0	0	Modie 1996, 2001
232	Mesoproterozoic	Neoproterozoic	Mayamkan Formation	Russia	no data	no data	no data	no data	no data	Rainbird et al. 1998
233	Mesoproterozoic	Neoproterozoic	Moraenesø Formation	Greenland	<1	<1	<1	0	0	Collinson et al. 1989; Kirkland et al. 2009
234	Mesoproterozoic	Neoproterozoic	Morro do Chapéu Formation	Brazil	0	0	0	0	0	Pedreira and de Waele 2008
235	Mesoproterozoic	Neoproterozoic	Rewa Sandstone	India	0	0	0	0	0	Bose and Chakraborty 1994; Chakraborty 2006; Malone et al. 2008; Mukhopadhyay 2012; Mukhopadhyay et al. 2014
236	Neoproterozoic	Neoproterozoic	Applecross Formation	Scotland	<1	<1	<1	0	0	Stewart 1963, 1982, 1988b, 1991, 2002; Selley 1965; Williams 1966, 1969, 2001; Gracie and Stewart 1967; Selley 1969; Stewart and Donnellan 1992; Nicholson 1992, 1993; Owen 1995; Turnbull et al. 1996; McManus and Bajabua 1998; Park et al. 2002; Williams and Foden 2011; Ellis et al. 2012; Owen and Santos 2014;
237	Neoproterozoic	Neoproterozoic	Arroi América Formation	Brazil	0	0	0	0	0	Fragoso-César et al. 2000; Poloshi and Fragoso-César 2003; de Borba 2004
238	Neoproterozoic	Neoproterozoic	Aultbea Formation	Scotland	<1	<1	<1	0	0	Williams 1966; Stewart 1975, 2002; Nicholson 1992, 1993
239	Neoproterozoic	Neoproterozoic	Ayn Formation	Oman	<1	0	<1	0	0	Rieu et al. 2006
240	Neoproterozoic	Neoproterozoic	Barriga Negra Formation	Uruguay	7	7	0	0	0	Fambrini et al. 2005
241	Neoproterozoic	Neoproterozoic	Basnaering Formation	Norway	2	1	1	0	0	Hjellbakk , 1993, 1997
242	Neoproterozoic	Neoproterozoic	Bateau Formation	Canada (Newfoundland)	<1	<1	<1	0	0	Williams and Stevens 1969; Bostock 1983; Cumming 1983
243	Neoproterozoic	Neoproterozoic	Bhander Sandstone	India	<1	<1	0	0	0	Bose et al. 1999
244	Neoproterozoic	Neoproterozoic	Bonney Sandstone	Australia (South Australia)	no data	no data	no data	no data	no data	Von de Borch et al. 1988
245	Neoproterozoic	Neoproterozoic	Browns Hole Formation	USA (Idaho, Utah)	<1	<1	<1	0	0	Crittenden et al. 1971; Link et al. 1993; Link and Christie-Blick 2011
246	Neoproterozoic	Neoproterozoic	Catactin Formation	USA (Virginia)	<1	<1	<1	0	0	Dilliard et al. 1999
247	Neoproterozoic	Neoproterozoic	Chestnut Hill Formation	USA (New Jersey)	1.5	1	0.5	0	0	Gates and Volkert 2004

248	Neoproterozoic	Neoproterozoic	Cochran Formation	USA (Tennesse)	<2	<1	<1	0	0	Mack 1980; Smoot and Southworth 2014
249	Neoproterozoic	Neoproterozoic	Crouse Canyon Formation	USA (Utah)	<1	<1	<1	0	0	Dehler et al. 2005
250	Neoproterozoic	Neoproterozoic	Dead Horse Pass Formation	USA (Utah)	no data	no data	no data	no data	no data	Dehler et al. 2005; Kingsbury-Stewart et al. 2013
251	Neoproterozoic	Neoproterozoic	Diamond Breaks Formation	USA (Utah)	<1	0	0	<1	0	Dehler et al. 2005
252	Neoproterozoic	Neoproterozoic	Doli Sandstone	India	0	0	0	0	0	Ramakrishnan and Vaidyanadhan 2008
253	Neoproterozoic	Neoproterozoic	Dutch Peak Formation	USA (Utah)	0	0	0	0	0	Link et al. 1994; Link and Christie-Blick 2011
254	Neoproterozoic	Neoproterozoic	El Tapiro Formation	Mexico	<1	no data	no data	no data	no data	Stewart et al. 2002
255	Neoproterozoic	Neoproterozoic	Encharani Formation	India	0	0	0	0	0	Chaudhuri 2003
256	Neoproterozoic	Neoproterozoic	Estância Santa Fé Formation	Brazil	0	0	0	0	0	de Borba 2003; Marconato et al. 2014
257	Neoproterozoic	Neoproterozoic	Etusis Formation	Namibia	1	1	0	0	0	Hedberg 1975; Kröner and Correiá 1980; Sawyer 1981; Henry et al. 1988a; Durr and Dingeldey 1996; McDermott et al. 1996; Ashworth 2014
258	Neoproterozoic	Neoproterozoic	Fatira El Zarqa Sequence	Egypt	12	12	0	0	0	Khalaf 2010
259	Neoproterozoic	Neoproterozoic	Flaminkberg Formation	Namibia	0	0	0	0	0	Gresse 1986; Gresse and Germs 1993; Gresse et al. 1996
260	Neoproterozoic	Neoproterozoic	Fugleberget Formation	Norway	<1	<1	<1	0	0	Banks et al. 1974; Hobday 1974; Røe 1987; Røe and Hermansen 1993, 2006; Bylund 1994
261	Neoproterozoic	Neoproterozoic	Golneselv Formation	Norway	<1	<1	<1	0	0	Banks 1973; Banks et al. 1974; Banks and Roe 1974; Johnson et al. 1978; Bylund 1994
262	Neoproterozoic	Neoproterozoic	Hades Pass Formation	USA (Utah)	<1	<1	<1	0	0	Wallace 1972; Link et al. 1993; Dehler et al. 2003; Hayes 2013; Kingsbury-Stewart 2013
263	Neoproterozoic	Neoproterozoic	Hashim Formation	Saudi Arabia	<5	0	<5	0	0	Davis 1985; Genna 2002; Johnson and Woldehaimanot 2003; Johnson et al. 2011; Bezenjani 2014
264	Neoproterozoic	Neoproterozoic	Høyberget Formation	Norway	<1	<1	0	0	0	Nystuen 1980
265	Neoproterozoic	Neoproterozoic	Ifjord Formation	Norway	<1	<1	0	0	0	Laird 1972b
266	Neoproterozoic	Neoproterozoic	Inkom Formation	USA (Utah)	no data	no data	no data	no data	no data	Christie-Blick 1997; Crittenden et al. 1971
267	Neoproterozoic	Neoproterozoic	Jifn Formation	Saudi Arabia	1	<1	<1	0	0	Delfour 1981; Al-Husseini 2011
268	Neoproterozoic	Neoproterozoic	Johnnie Formation	USA (California)	<1	0	<1	0	0	Fedo and Copper 2001; Sharp and Glazner 2006; Miller and Wright 2007; Schoenborn et al. 2012
269	Neoproterozoic	Neoproterozoic	Kampa-Tenpa Formation	India	0	0	0	0	0	Murkute and Joshi 2014
270	Neoproterozoic	Neoproterozoic	Kapra Sandstone	India	0	0	0	0	0	Chaudhuri 2003
271	Neoproterozoic	Neoproterozoic	Keele Formation	Canada (NWT)	<1	0	<1	<1	0	Narbonne and Aitken 1995; Day et al. 2004
272	Neoproterozoic	Neoproterozoic	Kerur Formation (Cave Temple Arenite)	India	0	0	0	0	0	Dey et al. 2009; Mukhopadhyay et al. 2014; Dey 2015
273	Neoproterozoic	Neoproterozoic	Kråkhammaren Formation	Sweden	<1	<1	<1	0	0	Kumpulainen 1980
274	Neoproterozoic	Neoproterozoic	Kuara Formation	Saudi Arabia	0	0	0	0	0	Kemp 1996
275	Neoproterozoic	Neoproterozoic	Kuujjua Formation	Canada (NWT)	<1	<1	0	0	0	Rainbird 1992, 1993; Rainbird et al. 1996a, 1997; Long et al. 2008
276	Neoproterozoic	Neoproterozoic	Landersfjord Formation	Norway	1	<1	<1	0	0	Laird 1972b
277	Neoproterozoic	Neoproterozoic	Liubatang Formation	China	<1	<1	0	0	0	Greentree et al. 2006
278	Neoproterozoic	Neoproterozoic	Lokvikfjell Formation	Norway	2	no data	no data	no data	no data	Levell 1978, 1980; Siedlecki and Levell 1978

279	Neoproterozoic	Neoproterozoic	Lövan Formation	Sweden	<1	<1	<1	0	0	Kumpulainen 1980
280	Neoproterozoic	Neoproterozoic	Lunndörrsfjällen Formation	Sweden	<1	<1	<1	0	0	Kumpulainen 1980
281	Neoproterozoic	Neoproterozoic	Mancheral Quartzite	India	<1	<1	0	0	0	Chakraborty and Chaudhuri 1993; Chakraborty 1994; Chakraborty 1999
282	Neoproterozoic	Neoproterozoic	Maricá Formation	Brazil	0	0	0	0	0	de Borba et al. 2006
283	Neoproterozoic	Neoproterozoic	Marsham Formation	Oman	no data	no data	no data	no data	no data	Rieu and Allen 2008
284	Neoproterozoic	Neoproterozoic	Mindola Clastics Formation	Zambia	<1	<1	0	0	0	Wendorff 2003; Armstrong et al. 2005; Bull et al. 2011
285	Neoproterozoic	Neoproterozoic	Mount Watson Formation	USA (Utah)	no data	no data	no data	no data	no data	Sanderson 1984; Dehler et al. 2005; Kingsbury-Stewart et al. 2013
286	Neoproterozoic	Neoproterozoic	Mutoshi Formation	Zambia	2	1	1	0	0	Wendorff 2003
287	Neoproterozoic	Neoproterozoic	Mutual Formation	USA (Utah, Idaho)	<1	<1	<1	0	0	Crittenden et al. 1971; Link et al. 1993; Christie-Blick, 1982, 1997; Yonkee et al. 2014
288	Neoproterozoic	Neoproterozoic	Nababis Formation	Namibia	2	1	1	0	0	Germs 1983; Geyer 2005
289	Neoproterozoic	Neoproterozoic	Nankoweap Formation	USA (Arizona)	<1	<1	<1	0	0	Weil et al. 2003; Timmons et al. 2005; Dehler et al. 2012; Rainbird et al. 2012
290	Neoproterozoic	Neoproterozoic	Osdalen Formation	Norway	no data	no data	no data	no data	no data	Lamminen et al. 2015
291	Neoproterozoic	Neoproterozoic	Otts Canyon Formation	USA (Utah)	<1	<1	<1	0	0	Link et al. 1994; Link and Christie-Blick 2011
292	Neoproterozoic	Neoproterozoic	Paddeby Formation	Norway	<1	0	<1	0	0	Banks et al. 1974; Johnson et al. 1978; Røe and Hermansen 1993; Bylund 1994
293	Neoproterozoic	Neoproterozoic	Pong Conglomerate	Canada (Newfoundland)	0	0	0	0	0	de Wit 1974
294	Neoproterozoic	Neoproterozoic	Ramgiri Formation	India	<1	<1	<1	0	0	Chakraborty 1991b, 1994
295	Neoproterozoic	Neoproterozoic	Red Castle Formation	USA (Utah)	<1	0	<1	<1	0	Dehler et al. 2005; Kingsbury-Stewart et al. 2013; Winston 2016
296	Neoproterozoic	Neoproterozoic	Rehatikhol Conglomerate	India	no data	no data	no data	no data	no data	Datta 2005; Deb and Chaudhuri 2007; Dhang and Deb 2011
297	Neoproterozoic	Neoproterozoic	Rendalen Formation	Norway	0	0	0	0	0	Kumpulainen and Nystuen 1985; Lamminen et al. 2014
298	Neoproterozoic	Neoproterozoic	Rhynie Sandstone	Australia (South Australia)	<1	<1	0	0	0	Preiss 1997, 2000
299	Neoproterozoic	Neoproterozoic	Ridam Formation	Saudi Arabia	no data	no data	no data	no data	no data	Davis 1985; Genna 2002; Johnson and Woldehaimanot 2003; Johnson et al. 2011; Bezenjani 2014
300	Neoproterozoic	Neoproterozoic	Rivieradal Sandstone	Greenland	5	5	0	0	0	Sønderholm and Tirsgaard 1998; Smith et al. 2004
301	Neoproterozoic	Neoproterozoic	Rubtayn Formation	Saudi Arabia	no data	no data	no data	no data	no data	Davies 1985; Miller et al. 2008; Al-Husseini 2011
302	Neoproterozoic	Neoproterozoic	Shihimiya Formation	Egypt	<1	<1	<1	0	0	Grouthaus 1979; Willis and Stern 1988; Fritz 1999; Wilde and Youssef 2002; Abd El-Wahed 2010; Eliwa et al. 2010; Khalaf 2012, 2013a, 2013b; Fowler 2013; Benzenjani 2014
303	Neoproterozoic	Neoproterozoic	Siemiatycze Formation	Poland	0	0	0	0	0	Pacześna and Poprawa 2005
304	Neoproterozoic	Neoproterozoic	Sixty Mile Formation	USA (Arizona)	<1	<1	0	0	0	Link et al. 1993; Christie-Blick 1997; Yonkee et al. 2014
305	Neoproterozoic	Neoproterozoic	Sonia Sandstone Formation	India	<1	<1	0	0	0	Chaahan 1999; Samanta 2009; Bose et al. 2012; Sarkar et al. 2012
306	Neoproterozoic	Neoproterozoic	Stirling Quartzite	USA (California)	<1	0	<1	0	0	Fedo and Cooper 1999, 2001; Sharp and Glazner 2006; Miller and Wright 2007; Schoenborn et al. 2012
307	Neoproterozoic	Neoproterozoic	Stockdale Formation	Namibia	<1	<1	<1	0	0	Germs 1983; Geyer 2005

308	Neoproterozoic	Neoproterozoic	Styret Formation	Norway	no data	no data	no data	no data	no data	Levell 1978, 1980; Siedlecki and Levell 1978
309	Neoproterozoic	Neoproterozoic	Sugaitebulake Formation	China	0	0	0	0	0	Turner 2010
310	Neoproterozoic	Neoproterozoic	Swift Run Formation	USA (Virginia)	no data	no data	no data	no data	no data	Gattuso et al. 2009
311	Neoproterozoic	Neoproterozoic	Terjit-Aguinob Formation	Morocco	<1	<1	0	0	0	Alvaro 2012
312	Neoproterozoic	Neoproterozoic	Uinta Mountain Group (undivided)	USA (Utah)	<1	0	0	<1	0	Ball and Farmer 1998; Condie et al. 2001; De Grey and Dehler 2005; Dehler et al. 2005, 2010
313	Neoproterozoic	Neoproterozoic	Unicoi Formation	USA (Virginia, Tennesse)	<1	<1	<1	0	0	Cudzil and Driese 1987; Simpson and Eriksson 1989; Smoot and Southworth 2014
314	Neoproterozoic	Neoproterozoic	Urucum Formation	Brazil	0	0	0	0	0	Dorr 1945; Freitas et al. 2011
315	Neoproterozoic	Neoproterozoic	Veidnesbotn Formation	Norway	0	0	0	0	0	Hobday 1974; Banks et al. 1974; Bylund 1994; Rice and Hofmann 2000; Røe 2003
316	Neoproterozoic	Neoproterozoic	Wadi Igla Formation	Egypt	<1	<1	<1	0	0	Grouthaus 1979; Willis and Stern 1988; Fritz 1999; Wilde and Youssef 2002; Abd El-Wahed 2010; Eliwa et al. 2010; Khalaf 2012, 2013a, 2013b; Fowler 2013; Benzenjani 2014
317	Neoproterozoic	Neoproterozoic	Whyte Inlet Formation	Canada (Nunavut)	<1	<1	0	0	0	Long and Turner 2012; Long 2014, 2017
318	Neoproterozoic	Neoproterozoic	Zhafar Formation	Saudi Arabia	no data	no data	no data	no data	no data	Davis 1985; Genna 2002; Johnson and Woldehaimanot 2003; Johnson et al. 2011; Bezenjani 2014
319	Neoproterozoic	Lower Cambrian	Wentnor Group	England	10	10	0	0	0	Toghill and Chell 1984; Pauley 1986, 1990
320	Neoproterozoic	Lower Cambrian	Double Mer Formation	Canada (Labrador)	<1	<1	<1	0	0	Gower et al. 1986; Murthy et al. 1992
321	Neoproterozoic	Lower Cambrian	Estancia Sânta Fé Formation	Brazil	0	0	0	0	0	de Borba 2003; Marconato et al. 2014
322	Neoproterozoic	Lower Cambrian	Hamill Group (undivided)	Canada (British Columbia)	0	0	0	0	0	Høy 1980; Devlin and Bond 1988
323	Neoproterozoic	Lower Cambrian	Pedra do Segredo Formation	Brazil	0	0	0	0	0	de Borba 2003; Marconato et al. 2014
324	Neoproterozoic	Lower Cambrian	Seival Formation	Brazil	11	1	10	0	0	Paim 1994; Fambrini et al. 2014; Marconato et al. 2014
325	Neoproterozoic	Lower Cambrian	Serra dos Lanceiros Formation	Brazil	0	0	0	0	0	Marconato et al. 2014
326	Neoproterozoic	Lower Cambrian	Stretton Group	England	10	10	0	0	0	Toghill and Chell 1984; Pauley 1986, 1990
327	Neoproterozoic	Lower Cambrian	Three Sisters Formation	Canada (British Columbia)	0	0	0	0	0	Devlin and Bond 1988
328	Neoproterozoic	Lower Cambrian	Umbrella Butte Formation	USA (Idaho)	0	0	0	0	0	Lund et al. 2003
329	Neoproterozoic	Lower Cambrian	Umm Ghaddah Formation	Jordan	<1	<1	0	0	0	Konert et al. 2001; Amireh et al. 2008
330	Neoproterozoic	Lower Cambrian	Wood Canyon Formation	USA (California)	<1	<1	0	0	0	Troxel and Wright 1976; Fedo and Cooper 1990; Miller and Wright 2007; Davies et al. 2011; Hogan et al. 2011; Kennedy and Droser 2011
331	Late Ediacaran	Lower Cambrian	Portfjeld Formation	Greenland	<1	<1	0	0	0	Kirkland et al. 2009
332	Latest Ediacaran	Lower Cambrian	Rozel Conglomerate	Jersey	<1	0	0	0	0	Went et al. 1988; Went 2005; Davies et al. 2011
333	Cambrian	Cambrian	Addy Quartzite	USA (Washington)	<1	<1	<1	0	0	Lindsey and Gaylord 1992
334	Cambrian	Cambrian	Amin Formation	Oman	0	0	0	0	0	Mercadier and Livera 1993
335	Cambrian	Cambrian	Araba Formation	Egypt	<1	<1	0	0	0	Said and EL-Kelany 1989; El-Araby and Motelib 1999; Khalifa 2006; Wanas 2011
336	Cambrian	Cambrian	Bolsa Quartzite	Mexico	<1	no data	no data	no data	no data	Stewart et al. 2002
337	Cambrian	Cambrian	Camp Ridge Formation	Antarctica	<1	<1	<1	0	0	Andrews and Laird 1976
338	Cambrian	Cambrian	Haradh Formation	Oman	no data	no data	no data	no data	no data	Mercadier and Livera 1993; Al-bulushi et al. 2009

339	Cambrian	Cambrian	Hato Viejo Formation	Venezuela	no data	no data	no data	no data	no data	Maurrasse 1990
340	Cambrian	Cambrian	Mount Simon Sandstone	USA (Illinois, Minnesota, Wisconsin, Iowa)	2	1	1	0	0	Fischietto 2009; Bowen et al. 2011; Lovell and Bowen 2014
341	Cambrian	Cambrian	Nepean Formation	Canada (Ontario)	0	0	0	0	0	Wolf and Dalrymple 1985; Macnaughton et al. 2002
342	Cambrian	Cambrian	Piekenier Formation	South Africa	<1	<1	<1	0	0	Vos and Tankard 1981
343	Cambrian	Cambrian	Sarabit El-Shillito Formation	Egypt	0	0	0	0	0	Kordi et al. 2011
344	Cambrian	Cambrian	Sebkhet el Mellah Formation	Algeria	0	0	0	0	0	Ghienne et al. 2007
345	Cambrian	Cambrian	Serra do Apertado Formation	Brazil	0	0	0	0	0	Almeida et al. 2009; Marconato et al. 2009; Godinho et al. 2013
346	Cambrian	Cambrian	Siq Sandstone	Saudi Arabia	0	0	0	0	0	Powers 1966; Husseini and Husseini 1990
347	Cambrian	Cambrian	Tapeats Sandstone	USA (Arizona)	<1	0	<1	<1	0	Hereford 1977; Rose 2006
348	Cambrian	Cambrian	Varzinha Formation	Brazil	7	6	1	0	0	Almeida et al. 2009
349	Cambrian	Cambrian	Weverton Formation	USA (Virginia)	no data	no data	no data	no data	no data	Smoot and Southworth 2014
350	Lower Cambrian	Lower Cambrian	Alderney Sandstone Formation	Alderney	0	0	0	0	0	Went 1989, 2013; Todd and Went 1990; Davies et al. 2011
351	Lower Cambrian	Lower Cambrian	Amudei Shelomo Sandstone Formation	Israel	0	0	0	0	0	Kracz et al. 1979; Kolodner et al. 2006
352	Lower Cambrian	Lower Cambrian	Backbone Ranges Formation	Canada (Yukon, BC, NWT)	<1	0	<1	0	0	Macnaughton et al. 1997
353	Lower Cambrian	Lower Cambrian	Bámbola Formation	Spain	0	0	0	0	0	Alvaro et al. 2008
354	Lower Cambrian	Lower Cambrian	Bradore Formation	Canada (Labrador)	<1	<1	<1	0	0	Hiscott et al. 1984; Long and Yip 2009
355	Lower Cambrian	Lower Cambrian	Chapel Island Formation	Canada (Newfoundland)	0	0	0	0	0	Landing and MacGabhann 2010
356	Lower Cambrian	Lower Cambrian	Dahu Formation	Iran	0	0	0	0	0	Huckriede 1962; Forster 1994; Moussavi-Harami 2008; Zand-Moghadam 2013
357	Lower Cambrian	Lower Cambrian	Frehel Formation	France	<1	<1	0	0	0	Doré 1972; Went 1989, 2013; Went and Andrews 1990, 1991; Davies et al. 2011
358	Lower Cambrian	Lower Cambrian	Guarda Velha Formation	Brazil	<1	<1	<1	0	0	Almeida et al. 2009; Santos et al. 2012, 2014
359	Lower Cambrian	Lower Cambrian	Hardyston Formation	USA (New Jersey)	0	0	0	0	0	Aaron 1969; Simpson et al. 2002
360	Lower Cambrian	Lower Cambrian	Herreria Formation	Spain	<1	<1	0	0	0	Van den Bosch 1969; Alvaro et al. 2003; Davies et al. 2011
361	Lower Cambrian	Lower Cambrian	Le Pedrera Formation	Argentina	no data	no data	no data	no data	no data	Moya 1998; Buatois et al. 2000
362	Lower Cambrian	Lower Cambrian	Neksø Formation	Denmark	<1	<1	<1	0	0	Clemmensen and Dam 1993; Davies et al. 2011
363	Lower Cambrian	Lower Cambrian	Ogof Golchfa Cliff Formation	Wales	4	0	0	0	4	Rees et al. 2014
364	Lower Cambrian	Lower Cambrian	Roche Jagu Formation	France	6	0	6	0	0	Went, 2016
365	Lower Cambrian	Lower Cambrian	Salib Formation	Jordan	<1	<1	<1	0	0	Selley 1972; Amireh 1994; Elicki 2007

366	Lower Cambrian	Lower Cambrian	Taba Formation	Egypt	0	0	0	0	0	Said and EL-Kelany 1989; Wanas 2011
367	Lower Cambrian	Lower Cambrian	Tintic Quartzite	USA (Utah)	<1	no data	no data	no data	no data	Yonkee et al. 2014
368	Lower Cambrian	Middle Cambrian	Altona Formation	USA (New York)	no data	no data	no data	no data	no data	Brink 2015
369	Middle Cambrian	Middle Cambrian	Liberty Hills Formation	Antarctica	<1	<1	0	0	0	Webers et al. 1992a, 1992b; Curtish and Lomas 1999
370	Middle Cambrian	Middle Cambrian	Mahwis Formation	Oman	6	0	0	6	0	Heward, 1989; Mercadier and Livera 1993
371	Middle Cambrian	Middle Cambrian	Mount Roosevelt Formation	Canada (British Columbia)	0	0	0	0	0	Post and Long 2008
372	Middle Cambrian	Middle Cambrian	Umm Ishrin Sandstone Formation	Jordan	<1	<1	<1	0	0	Selley 1972; Makhlouf and Abed 1991; Amireh 1994
373	Middle Cambrian	Upper Cambrian	Ausable Formation	USA (New York)	1	<1	<1	0	0	Lowe and Arnott, 2016
374	Middle Cambrian	Upper Cambrian	Covey Hill Formation	Canada (Ontario, Quebec)	0	0	0	0	0	Lewis 1971; Hofmann 1972; Globensky 1986, 1987; Hersi and Lavoie 2000; Sanford 2007
375	Middle Cambrian	Upper Cambrian	Santa Rosita Formation	Argentina	<1	0	<1	0	0	Buatois and Mangano 2003
376	Middle Cambrian	Lower Ordovician	Sticht Range Formation	Australia (Tasmania)	no data	no data	no data	no data	no data	Bailie 1989; Corbett 1992
377	Upper Cambrian	Upper Cambrian	Andam Formation	Oman	<1	<1	0	0	0	Millson et al. 2008
378	Upper Cambrian	Upper Cambrian	Lamotte Sandstone	USA (Missouri)	<1	0	0	<1	0	Ojakangas 1963; Houseknecht and Ethridge 1978
379	Upper Cambrian	Upper Cambrian	Owen Conglomerate	Australia (Tasmania)	<1	<1	<1	0	0	Corbett and Lees 1987; Noll and Hall 2003, 2005, 2010
380	Upper Cambrian	Upper Cambrian	Van Horn Formation	USA (Texas)	0	0	0	0	0	McGowen and Groat 1971; Spencer et al. 2014
381	Upper Cambrian	Upper Cambrian	Wajid Sandstone	Saudi Arabia	7	7	0	0	0	Powers et al. 1966; Dabbagh and Rodgers 1983; Alsharhan 1991
382	Upper Cambrian	Upper Cambrian	Wonewoc Formation	USA (Wisconsin)	<1	no data	no data	no data	no data	Dott et al. 1986
383	Upper Cambrian	Lower Ordovician	Keeseville Formation	USA (New York)	1	<1	<1	0	0	Lowe and Arnott, 2016
384	Ordovician	Ordovician	Table Mountain Group (Natal)	South Africa	<1	0	<1	0	0	Hobday and Von Brunn 1979
385	Ordovician	Ordovician	Tichitt Group	Mauritania	0	0	0	0	0	Ghienne 2003
386	Ordovician	Ordovician	Umm Sahm Formation	Jordan	no data	no data	no data	no data	no data	Amireh et al. 1991
387	Lower Ordovician	Lower Ordovician	Disi Formation	Jordan	<1	<1	<1	0	0	Selley, 1970; Amierh et al. 2001
388	Lower Ordovician	Lower Ordovician	Mahwis Formation	Oman	6	0	0	6	0	Heward, 1989; Mercadier and Livera, 2009
389	Lower Ordovician	Lower Ordovician	Pacoota Sandstone	Australia (Northern Territory, South Australia)	no data	no data	no data	no data	no data	Deckelman 1991
390	Lower Ordovician	Lower Ordovician	Table Mountain Group (Cape)	South Africa	no data	no data	no data	no data	no data	Hobday and Von Brunn 1979
391	Middle Ordovician	Middle Ordovician	Mweelrea Group	Ireland	no data	no data	no data	no data	no data	Pudsey, 1984
392	Middle Ordovician	Middle Ordovician	St Peter Sandstone	USA (Iowa, Minnesota, Wisconsin)	0	0	0	0	0	Mazzullo and Ehrlich 1983; Dott et al. 1986
393	Upper Ordovician	Upper Ordovician	Bald Eagle Formation	USA (Pennsylvania)	5	5	0	0	0	Faill and Wells, 1974; Thompson, 1999; Davies et al. 2011
394	Upper Ordovician	Upper Ordovician	Juniata Formation	USA (Pennsylvania)	10	10	0	0	0	Faill and Wells, 1974; Cotter, 1978
395	Upper Ordovician	Upper Ordovician	Khriem Group	Jordan	12.5	1	11.5	0	0	Powell et al. 1994

396	Upper Ordovician	Upper Ordovician	Misty Point Formation	Canada (Newfoundland)	12.5	no data	no data	no data	no data	Williams et al. 1996; Quinn et al. 1999
397	Upper Ordovician	Upper Ordovician	Were Formation	Benin, Niger	0	0	0	0	0	Konate et al. 2003
398	Upper Ordovician	Late Silurian	Tumblagooda Sandstone	Australia (Western Australia)	<1	<1	0	0	0	Trewin, 1993; Trewin & McNamara, 1995; Evans et al. 2006; Hocking, 1991
399	Silurian	Silurian	Major Mitchell Sandstone	Australia (Victoria)	0	0	0	0	0	Cayley and Taylor, 1997; Gouramanis et al. 2003
400	Silurian	Silurian	Moora Moora Sandstone	Australia (Victoria)	<1	<1	0	0	0	Cayley and Taylor, 1997
401	Silurian	Silurian	Murray Hill Sandstone	Australia (Victoria)	0	0	0	0	0	Cayley and Taylor, 1997
402	Silurian	Silurian	Umm Ras Formation	Egypt, Sudan	<1	<1	0	0	0	Wycisk 1990
403	Llandovery	Llandovery	Coralliferous Group	Wales	17.5	17.5	0	0	0	Hillier 2002
404	Llandovery	Llandovery	Massanutten Sandstone	USA (Virginia)	<1	0	0	<1	0	Tomsecu 2004, Tomescu and Rothwell, 2006; Tomescu et al. 2006
405	Llandovery	Llandovery	Tuscarora Formation	USA (Pennsylvania, Virginia)	<1	<1	0	0	0	Smith, 1970; Faill and Wells, 1974
406	Llandovery	Llandovery	Whirlpool Sandstone	Canada (Ontario), USA (New York)	<1	no data	no data	no data	no data	Rutka et al. 1991; Cheel and Middleton, 1993
407	Llandovery	Wenlock	Shawangunk Formation	USA (New Jersey, Pennsylvania)	<1	<1	0	<1	0	Smith 1970; Epstein and Epistein 1972; Laughrey 1999; Epstein 2006
408	Wenlock	Wenlock	Louisburgh-Clare Island Succession	Ireland	20	20	0	0	0	Maguire & Graham (1996)
409	Wenlock	Emsian	Röde Formation	Sweden	no data	no data	no data	no data	no data	Bassett et al. 1982
410	Ludlow	Ludlow	Stubdal Formation	Norway	<1	<1	<1	0	0	Turner 1973, 194; Turner and Whitaker 1976; Davies 2003; Davies et al. 2005, 2006
411	Ludlow	Pridoli	Bloomsburg Formation	USA (Pennsylvania)	92	69	23	0	0	Faill and Wells 1974; Cotter 1978; Driese et al. 1992; Laughrey 1999; Epstein 2006
412	Pridoli	Pridoli	Holmestrand Formation	Norway	<1	<1	0	0	0	Dam and Andreasen 1990; Davies et al. 2005, 2006
413	Pridoli	Pridoli	Store Arøya Formation	Norway	17	no data	no data	no data	no data	Davies 2003; Davies et al. 2005, 2006
414	Ludlow	Lower Devonian	Swanshaw Sandstone Formation	Scotland	10	10	0	0	0	Smith et al. 2006
415	Pridoli	Pridoli	Downton Castle Sandstone Formation	England	25	0	5	20	0	Allen 1974; Glasspool et al. 2004
416	Pridoli	Pridoli	Eask Formation	Ireland	25	20	5	0	0	Boyd and Sloan 2000
417	Pridoli	Pridoli	Moor Cliffs Formation	Wales	65-95	65-95	no data	no data	no data	Allen and Williams (1982); Love and Williams (2000), Mariott and Wright 2004; Morrisey and Braddy 2004; Williams and Hillier 2004; Wright and Marriott 2007; Mariott et al. 2009
418	Pridoli	Lochkovian	Clam Bank Formation	Canada (Newfoundland)	52	52	0	0	0	Williams et al. 1995; Williams et al. 1996
419	Pridoli	Lochkovian	Peel Sound Formation	Canada (Nunavut)	19	19	0	0	0	Miall et al. 1978; Miall and Gibling 1978; Gibling 1978
420	Pridoli	Praghian	Port Stephens Formation	Falkland Islands	no data	no data	no data	no data	no data	Hunter and Lomas 2003
421	Pridoli	Praghian	Red Marl Group	Wales	<1	<1	<1	0	0	Allen et al. 1981; Owen and Hawley 2000; Morrissey and Braddy 2004; Wright and Marriott 2007
422	Late Silurian	Late Silurian	Siktefjellet Group	Svalbard	45	45	0	0	0	Friend et al. 1997

423	Late Silurian	Late Silurian	Somerset Island Formation	Canada (Nunavut)	10	no data	no data	no data	no data	Miall et al. 1978; Miall and Gibling 1978; Gibling 1978
424	Siluro-Devonian	Siluro-Devonian	Fosen ORS	Norway	25	20	5	0	0	Siedlecka 1975
425	Lower Devonian	Lower Devonian	Ballymastocker ORS	Ireland	1	1	0	0	0	McSherry et al. 2000
426	Lower Devonian	Lower Devonian	Devonian Basal Clastics	Czech Republic	<1	<1	0	0	0	Neyba et al. 2001
427	Lower Devonian	Lower Devonian	Glashabeg Formation	Ireland	1	1	0	0	0	Todd et al. 1988; Todd and Went 1991; Todd 2000
428	Lower Devonian	Lower Devonian	New Mountain Subgroup	Antarctica	no data	no data	no data	no data	no data	Plume 1982
429	Lower Devonian	Lower Devonian	Snowblind Bay Formation	Canada (Nunavut)	51	40	11	0	0	Gibling and Narbonne 1977; Muir and Rust 1982
430	Lower Devonian	Lower Devonian	Xujiachong Formation	China	73	49	24	0	0	Xue et al. 2016
431	Lower Devonian	Middle Devonian	Bulandet-Vaerlandet Formation	Norway	<1	0	<1	0	0	Nilsen 1969
432	Lower Devonian	Middle Devonian	Disappointment Bay Formation	Canada (Nunavut)	no data	no data	no data	no data	no data	Thorsteinsson 1958
433	Lochkovian	Lochkovian	Andréebreen Formation	Svalbard	3	3	0	0	0	Friend et al. 1997
434	Lochkovian	Lochkovian	Cowie Formation	Scotland	4.5	no data	no data	no data	no data	Hartley and Leleu 2015
435	Lochkovian	Lochkovian	Fraenkerlyggen Formation	Svalbard	no data	no data	no data	no data	no data	Friend et al. 1997
436	Lochkovian	Lochkovian	Freshwater West Formation	Wales	40	35	5	0	0	Williams et a. 1982; Williams and Hillier 2004; Morrissey and Braddy 2004; Marriott et al. 2005; Wright and Marriott 2007; Hillier et al. 2007
437	Lochkovian	Lochkovian	Ridgeway Conglomerate Formation	Wales	61	0	61	0	0	Hillier and Williams 2007
438	Lochkovian	Praghian	Dartmouth Group	England	75	72	3	0	0	Smith and Humphreys 1991
439	Lochkovian	Praghian	Ditton Group	England	51-56	51-56	0	0	0	Allen 1974; Edwards and Axe 2004; Glasspool et al. 2006
440	Lochkovian	Praghian	Maccullochs Range beds	Australia (New South Wales)	8	5	3	0	0	Neef 2007
441	Lochkovian	Emsian	Brownstones Formation	Wales, England	21	21	0	0	0	Allen 1964; Allen and Dineley 1976; Tunbridge 1981; Allen 1983; Hillier et al. 2008
442	Lochkovian	Emsian	Lawrenny Cliff Formation	Wales	22	13	9	0	0	Allen et al. 1977, 1982; Thomas et al. 2006
443	Lochkovian	Emsian	Llanstadwell Formation	Wales	23	23	0	0	0	Allen et al. 1977, 1982; Thomas et al. 2006
444	Lochkovian	Emsian	Mill Bay Formation	Wales	22	22	0	0	0	Allen et al. 1977, 1982; Thomas et al. 2006
445	Lochkovian	Emsian	New Shipping Formation	Wales	12	12	0	0	0	Allen et al. 1977, 1982; Thomas et al. 2006
446	Lochkovian	Emsian	Smerwick Group	Ireland	1	1	0	0	0	Richmond and Wililams 2000
447	Lochkovian	Emsian	Strathpeffer Group	Scotland	<1	<1	0	0	0	Clarke and Parnell 1999
448	Praghian	Praghian	Senni Formation	Wales	45	0	45	0	0	Owen 1995; Hillier et al. 2008
449	Praghian	Praghian	Traeth Lligwy Beds	Wales	>75	>50	<25	0	0	Allen 1965
450	Praghian	Emsian	Wood Bay Formation	Svalbard	>51	>50	<1	0	0	Friend and Moody-Stuart 1972; Blomeier et al. 2003 a b
451	Emsian	Emsian	Grey Hoek Formation	Svalbard	>50	no data	no data	no data	no data	Worsley 1970
452	Emsian	Emsian	Red Island Road Formation	Canada (Newfoundland)	<1	<1	<1	0	0	Quinn et al. 2004

453	Emsian	Eifelian	Campbellton Formation	Canada (New Brunswick)	2	2	0	0	0	Wilson et al. 2004
454	Emsian	Eifelian	Coco Range Sandstone	Australia (New South Wales)	0	0	0	0	0	Neef et al. 1996; Neef and Bottrill 2001; Neef 2004
455	Emsian	Eifelian	Trout Valley Formation	USA (Maine)	39	0	39	0	0	Allen and Gastaldo 2006
456	Emsian	Eifelian	Wana Karnu Sandstone	Australia (New South Wales)	no data	no data	no data	no data	no data	Neef and Bottrill 2001; Neef 2004
457	Middle Devonian	Middle Devonian	Battery Point Formation	Canada (Quebec)	2.5	2.5	0	0	0	Cant, 1973, 1987; Cant and Walker 1976; Rust 1981; Lawrence and Williams 1984, 1987; Griffing et al. 2000; Hotton et a., 2001
458	Middle Devonian	Middle Devonian	Bluff Head Formation	China (Hong Kong)	9.5	0	9	0	1	Jones et al. 1997
459	Middle Devonian	Middle Devonian	Hornelen ORS	Norway	17	17	0	0	0	Steel et al. 1977; Bryhni 1978; Garner 1979; Gloppen and Steel 1981; Pollard et al. 1982; Andersen and Cross 2001
460	Middle Devonian	Middle Devonian	Kvamsheten Group	Norway	56	56	0	0	0	Osmundsen et al. 2000
461	Middle Devonian	Middle Devonian	Malbaie Conglomerate	Canada (Quebec)	<1	<1	0	0	0	Rust 1984
462	Middle Devonian	Middle Devonian	Solund Conglomerate	Norway	no data	no data	no data	no data	no data	Nilsen 1968
463	Middle Devonian	Upper Devonian	McAras Brook Formation	Canada (Nova Scotia)	<1	<1	0	0	0	Fralick and Schenk 1981; Murphy, 2001
464	Middle Devonian	Upper Devonian	Pirate Cove Formation	Canada (Quebec)	42	no data	no data	no data	no data	Dineley and Williams 1968
465	Eifelian	Eifelian	Strathcona Fiord Formation	Canada (Nunavut)	no data	no data	no data	no data	no data	Embry and Klovan 1976; Embry 1988, 1991
466	Eifelian	Eifelian	Trentishoe Member	England	8	0	8	0	0	Tunbridge 1984
467	Eifelian	Givetian	Fair Isle Group	Scotland	20	no data	no data	no data	no data	Mykura 1973; Allen 1982
468	Eifelian	Givetian	Hecla Bay Formation	Canada (Nunavut)	2	1	1	0	0	Embry and Klovan 1976; Embry 1988, 1991
469	Givetian	Givetian	Gauja Formation	Estonia, Latvia, Lithuania	12	6	6	0	0	Pontéand Plink-Björklund 2007
470	Givetian	Givetian	Gilwood Member	Canada (Alberta)	5	no data	no data	no data	no data	Williams and Krause 1998
471	Givetian	Givetian	Hamilton Group	USA (New York)	>60	0	>60	<1	0	McCave 1968
472	Givetian	Givetian	Nèvremont Formation	Belgium	0	0	0	0	0	Molenaar 1984, 1986
473	Givetian	Givetian	Tully Clastic Correlatives	USA (New York)	2	0	2	0	0	Johnson and Friedman 1969; Willis and Bridge 1988
474	Givetian	Fammenian	Pertnjara Group	Australia (Northern Territory)	no data	no data	no data	no data	no data	Jones 1991
475	Upper Devonian	Upper Devonian	Agda Dal Formation	Greenland	70	60	10	0	0	Olsen and Larsen 1993
476	Upper Devonian	Upper Devonian	Andersson Land Formation	Greenland	33	33	0	0	0	Olsen and Larsen 1993
477	Upper Devonian	Upper Devonian	Aztec Siltstone	Antarctica	70	0	35	0	35	McPherson 1979, 1980
478	Upper Devonian	Upper Devonian	Catskill Formation	USA (Pennsylvania)	41	11	30	0	0	Ryan, 1965; Allen and Friend 1968; Glaeser 1974; Faill and Wells 1974; Sevon 1985; Bridge 1988, 2000; Cotter and Driese 1998; Harper 1999; Cressler 2001
479	Upper Devonian	Upper Devonian	Cornstone Beds, ORS	Scotland	14	7	7	0	0	Bluck 1967; Read and Johnson 1967; Haughon and Bluck 1988; Bluck 2000
480	Upper Devonian	Upper Devonian	Elsa Dal Formation	Greenland	<1	0	<1	0	0	Olsen and Larsen 1993
481	Upper Devonian	Upper Devonian	Gargunnock Sandstone	Scotland	<1	<1	<1	0	0	Bluck 1967; Read and Johnson 1967; Haughon and Bluck 1988; Bluck 2000
482	Upper Devonian	Upper Devonian	Gupton Formation	Wales	29	29	0	0	0	Williams et al. 1982; Marshall 2000a, b
483	Upper Devonian	Upper Devonian	Idracowra Sandstone	Australia (Northern	no data	no data	no data	no data	no data	Jones 1973

				Territory, South Australia)						
484	Upper Devonian	Upper Devonian	Kaista Formation	Iraq	15	no data	no data	no data	no data	Al-Juboury and Al-Hadidy 2008
485	Upper Devonian	Upper Devonian	Kap Graah Group	Greenland	no data	no data	no data	no data	no data	Olsen, 1990; Olsen & Larsen, 1993
486	Upper Devonian	Upper Devonian	Kiltorcan Formation	Ireland	87	87	0	0	0	Jarvis 2000
487	Upper Devonian	Upper Devonian	Langra Formation	Australia (Northern Territory, South Australia)	5	5	0	0	0	Jones 1973
488	Upper Devonian	Upper Devonian	Lower Taylor Group	Antarctica	20	no data	no data	no data	no data	Sherwood et al. 1988; Woolfe 1990
489	Upper Devonian	Upper Devonian	Perry Formation	Canada (New Brunswick), USA (Maine)	11	10	1	0	0	McIlwaine 1967; Schluger 1973, 1976
490	Upper Devonian	Upper Devonian	Polly Conglomerate	Australia (Northern Territory, South Australia)	0	0	0	0	0	Jones 1973
491	Upper Devonian	Upper Devonian	Rodsten Formation	Greenland	10	10	0	0	0	Olsen and Larsen 1993
492	Upper Devonian	Upper Devonian	Santos Sandstone	Australia (Northern Territory, South Australia)	no data	no data	no data	no data	no data	Jones 1973
493	Upper Devonian	Upper Devonian	West Angle Formation	Wales	50	no data	no data	no data	no data	Williams et al. 1982; Marshall 2000a, b
494	Upper Devonian	Upper Devonian	Yiginli Formation	Turkey	no data	no data	no data	no data	no data	Tunbridge 1988
495	Upper Devonian	Upper Devonian	Zoolodalen Formation	Greenland	53	0	53	0	0	Olsen and Larsen 1993
496	Frasnian	Frasnian	Genesee Group	USA (New York)	65	no data	no data	no data	no data	Buttner 1968; Bridge and Gordon 1985; Gordon and Bridge 1987
497	Frasnian	Frasnian	Plantekløfta Formation	Svalbard	36-55	40	<10	no data	no data	Bergh et al. 2011; Berry and Marshall, 2015;
498	Frasnian	Frasnian	Planteryggen Formation	Svalbard	45	45	0	0	0	Bergh et al. 2011; Pipejohn and Dallman, 2014
499	Frasnian	Fammenian	Beverley Inlet Formation	Canada (Nunavut)	>50	>50	0	0	0	Embry and Klovan 1976; Embry 1988, 1991
500	Frasnian	Fammenian	Bulgeri Formation	Australia (Queensland)	60	60	0	0	0	Lang 1993
501	Frasnian	Fammenian	Caherkeen Formation	Ireland	10	10	0	0	0	James and Graham 1995
502	Frasnian	Fammenian	Eagle Hill Formation	Ireland	no data	no data	no data	no data	no data	James and Graham 1995
503	Frasnian	Fammenian	Fram Formation	Canada (Nunavut)	no data	no data	no data	no data	no data	Embry & Klovan, 1976; Embry, 1987, 1991
504	Frasnian	Fammenian	Hell Gate Formation	Canada (Nunavut)	<1	<1	<1	0	0	Embry and Klovan 1976; Embry 1988, 1991
505	Frasnian	Fammenian	Hervey Group	Australia (New South Wales)	60	0	60	0	0	Conolly, 1965
506	Frasnian	Fammenian	Nordstrand Point Formation	Canada (Nunavut)	10	5	5	0	0	Embry & Klovan, 1976; Embry, 1987, 1991
507	Frasnian	Fammenian	Nundooka Sandstone	Australia (New South Wales)	no data	no data	no data	no data	no data	Neef et al. 1996; Neef & Bottrill, 2001; Neef, 2004
508	Frasnian	Fammenian	Reen Point Formation	Ireland	no data	no data	no data	no data	no data	James and Graham 1995
509	Frasnian	Fammenian	Tholane Formation	Ireland	no data	no data	no data	no data	no data	James and Graham 1995

510	Frasnian	Fammenian	Toe Head Formation	Ireland	no data	no data	no data	no data	no data	Grahan 1975, 1983; Cotter and Graham 1991; James and Graham 1995
511	Famennian	Fammenian	Gun Point Formation	Ireland	24.5	0	24.5	0	0	Sadler and Kelly 1993
512	Fammenian	Fammenian	Parry Islands Formation	Canada (Nunavut)	11	no data	no data	no data	no data	Embry, 1988
513	"Lower Carboniferous"	"Lower Carboniferous"	Buchan Formation	North Sea	9	9	0	0	0	Benzagouta et al. 2001
514	Tournaisian	Tournaisian	Cape Rouge Formation	Canada (Newfoundland)	no data	no data	no data	no data	no data	Hamblin et al. 1995
515	Tournaisian	Tournaisian	Cruise Harbour Formation	Canada (Newfoundland)	no data	no data	no data	no data	no data	Hamblin et al. 1995
516	Tournaisian	Tournaisian	Cuyahoga Formation	USA (Ohio)	1	<1	<1	0	0	Matchen and Kammer 2006
517	Tournaisian	Tournaisian	Horton Group	Canada (Nova Scotia)	2	2	0	0	0	Martel and Gibling 1996; Murphy and Rice 1998; Rygel et al. 2006
518	Tournaisian	Tournaisian	Kanayut Conglomerate	USA (Alaska)	15	15	0	0	0	Nilsen 1981; Moore and Nilsen 1984
519	Tournaisian	Tournaisian	Maam Formation	Ireland	23	23	0	0	0	Graham 1981; Graham and Pollard 1982
520	Tournaisian	Tournaisian	Price Formation	USA (West Virginia)	no data	no data	no data	no data	no data	Bjerstedt 1997; Hohn et al. 1997
521	Tournaisian	Tournaisian	Tindouf Basin	Morocco	2	2	0	0	0	Vos 1976
522	Tournaisian	Visean	Albert Formation	Canada (New Brunswick)	30	30	0	0	0	Chowdhury and Noble 1996; Rygel et al. 2006
523	Tournaisian	Visean	Ballagan Formation	Scotland	36	36	0	0	0	Scott 1986; Scott and Galtier 19888; Stephenson et al. 2006; Bennett et al. 2016
524	Tournaisian	Visean	Capnagower Formation	Ireland	20.5	20	0.5	0	0	Graham 1981; Graham and Pollard 1982
525	Tournaisian	Visean	Kasa Formation	Bolivia	<10	no data	no data	no data	no data	Diaz Martinex 1995
526	Tournaisian	Visean	Mrar Formation	Libya	no data	no data	no data	no data	no data	Whitbread and Kelling 1982
527	Tournaisian	Visean	Nordkapp Formation	Svalbard	21	0	0	0	21	Worsley and Edwards 1976; Worsley et al. 2001
528	Tournaisian	Visean	Pocono Formation	USA (Pennsylvania)	28.5	no data	no data	no data	no data	Robinson and Slingerland 1998
529	Tournaisian	Visean	Saint-Jules Formation	Canada (Quebec)	6	2.5	2.5	0	0	Jutras and Prichonnet 2002
530	Tournaisian	Serpukhovian	Khusayyayn Formation	Saudi Arabia	6	6	0	0	0	Stump and Van Der Eem 1995; Knox et al. 2007
531	Visean	Visean	Bonaventure Formation	Canada (Quebec, New Brunswick)	90	no data	no data	no data	no data	Zaitlan and Rust 1983; Rust et al. 1989
532	Visean	Visean	Cannes de Roche Formation	Canada (Quebec)	1	1	0	0	0	Rust 1979; Rust et al. 1989
533	Visean	Visean	Clifton Down Mudstone Formation	England	59	59	0	0	0	Vanstone 1991
534	Visean	Visean	Cortaderas Formation	Argentina	no data	no data	no data	no data	no data	Limarino et al. 2006
535	Visean	Visean	Downpatrick Formation	Ireland	no data	no data	no data	no data	no data	Graham 1996
536	Visean	Visean	Drzewiany Quartz Sandstone Formation	Poland	43	0	0	0	43	Matyja 2008
537	Visean	Visean	Fell Sandstone Formation	England	<1	<1	<1	0	0	Turner et al. 1997
538	Visean	Visean	Kekiktuk Formation	USA (Alaska)	no data	no data	no data	no data	no data	Melvin 1993; LePain et al. 1994

539	Visean	Visean	La Coulée Formation	Canada (Quebec)	no data	no data	no data	no data	no data	Jutras et al. 1999
540	Visean	Visean	Largysillagh Sandstone Formation	Ireland	5	5	0	0	0	Graham 1996
541	Visean	Visean	Llanelly Formation	Wales	no data	no data	no data	no data	no data	Wright et al. 1991
542	Visean	Visean	Middle Limestone Formation	England	<1	<1	0	0	0	Frank and Tyson 1995
543	Visean	Visean	Middleborough Formation	Canada (Nova Scotia)	68	68	0	0	0	Allen et al. 2013
544	Visean	Visean	Minnaun Formation	Ireland	<1	<1	<1	0	0	Graham 1996
545	Visean	Visean	Mullaghmore Sandstone Formation	Ireland	<1	<1	<1	0	0	Graham 1996; Ketzer et al. 2002
546	Visean	Visean	Pathhead Formation	Scotland	45	no data	no data	no data	no data	Kassi et al. 2004
547	Visean	Visean	Percé Group	Canada (Quebec)	32	no data	no data	no data	no data	Jutras and Prichonnet 2005
548	Visean	Visean	Rerrick Outlier	Scotland	no data	no data	no data	no data	no data	Maguire et al. 1996
549	Visean	Visean	Rocky Brook Formation	Canada (Newfoundland)	no data	no data	no data	no data	no data	Hamblin et al. 1997
550	Visean	Visean	Roelough Conglomerate Formation	Ireland	no data	no data	no data	no data	no data	Graham, 1996
551	Visean	Visean	Siripaca Formation	Bolivia	75	0	<5	0	>70	Diaz Martinez 1995
552	Visean	Visean	Spion Kop Formation	Australia (New South Wales)	1	1	0	0	0	Birgenheier et al. 2009
553	Visean	Visean	Thirlstane Sandstone Member	Scotland	no data	no data	no data	no data	no data	Maguire et al. 1996
554	Visean	Serpukhovian	Alston Formation	England	62	32	30	0	0	Johnson and Nudds 1996
555	Visean	Serpukhovian	Mauch Chunk Formation	USA (Pennsylvania)	58	no data	no data	no data	no data	Tam and Kodama 2002
556	Visean	Serpukhovian	Spanish Room Formation	Canada (Newfoundland)	<10	<5	<5	0	0	Laracy and Hiscott 1982
557	Serpukhovian	Serpukhovian	Bluestone Formation	USA (West Virginia)	42.5	no data	no data	no data	no data	Miller and Eriksson 2000
558	Serpukhovian	Serpukhovian	Buffalo Wallow Formation	USA (Kentucky)	25	no data	no data	no data	no data	Garcia et al. 2006
559	Serpukhovian	Serpukhovian	Claremont Formation	Canada (Nova Scotia)	0	0	36	0	0	Allen et al. 2013
560	Serpukhovian	Serpukhovian	Donets Basin	Russia, Ukraine	86	no data	no data	no data	no data	Sachsenhofer et al. 2003
561	Serpukhovian	Serpukhovian	Great Limestone Member	England	16	16	0	0	0	Elliott 1976
562	Serpukhovian	Serpukhovian	Hinton Formation	USA (West Virginia)	19	19	0	0	0	Turner and Eriksson 1999; Miller and Eriksson 2000
563	Serpukhovian	Serpukhovian	Johnsons Creek Conglomerate	Australia (New South Wales)	1	<1	<1	0	0	Birgenheier et al. 2009
564	Serpukhovian	Serpukhovian	Limestone Coal Formation	Scotland	no data	no data	no data	no data	no data	Read 1994
565	Serpukhovian	Serpukhovian	Passage Formation	Scotland	50	50	0	0	0	Read 1979; Dean et al. 2011
566	Serpukhovian	Serpukhovian	Pomquet Formation	Canada (Nova Scotia)	no data	no data	no data	no data	no data	Boehner and Giles 1993; Hamblin 2001

567	Serpukhovian	Serpukhovian	Princeton Formation	USA (West Virginia)	8	4	4	0	0	Miller and Eriksson 2000
568	Serpukhovian	Serpukhovian	Scar House Beds	England	26	21	5	0	0	Martinsen 1990
569	Serpukhovian	Serpukhovian	Shepody Formation	USA (New Brunswick)	42	0	42	0	0	Allen et al. 2013
570	Serpukhovian	Serpukhovian	Twrch Sandstone Formation	Wales	no data	no data	no data	no data	no data	Hampson, 1998
571	Serpukhovian	Serpukhovian	Upper Limestone Formation	England, Scotland	13	13	0	0	0	Read 1979; Scarboro and Tucker 1993
572	Serpukhovian	Bashkirian	Landnørdingsv-ika Formation	Svalbard	87	no data	no data	no data	no data	Worsley and Edwards 1976; Worsley et al. 2001
573	Serpukhovian	Bashkirian	Millstone Grit Group	England	1	1	0	0	0	Morton and Whitham 2002; Tyrrell et al. 2006; Waters et al. 2008
574	Serpukhovian	Bashkirian	Tupambi Formation	Argentina	49	no data	no data	no data	no data	Di Pasquo and Azuy 1999; Starck and Del Papa 2006
575	Serpukhovian	Moscovian	Seaham Formation	Australia (New South Wales)	21	0	21	0	0	Birgenheier et al. 2009
576	"Mid Carb-Perm"	"Mid-Carb - Perm"	El Imperial Formation	Argentina	7	7	0	0	0	Espejo and Lopez-Gamundi 1994
577	Bashkirian	Bashkirian	Boss Point Formation	Canada (Nova Scotia, New Brunswick)	17	0	17	0	0	Plint 1986; Browne and Plint 1994; Falcon-Lang 2006; Ielpi et al. 2014
578	Bashkirian	Bashkirian	Canyon Fiord Formation	Canada (Nunavut)	6	no data	no data	no data	no data	Theriault and Desrochers 1993
579	Bashkirian	Bashkirian	Crab Orchard Mountains Group	USA (Georgia, Alabama, Tennessee)	47	no data	no data	no data	no data	Churnet 1996
580	Bashkirian	Bashkirian	Crawshaw Sandstone	Scotland	no data	no data	no data	no data	no data	Hampson et al. 1997, 1999a
581	Bashkirian	Bashkirian	Doonlicky Sandstone	Ireland	no data	no data	no data	no data	no data	Hampson et al. 1997, 1999a
582	Bashkirian	Bashkirian	Farewell Rock	Wales	0	0	0	0	0	Hampson 1998
583	Bashkirian	Bashkirian	Gizzard Group	USA (Georgia, Alabama, Tennessee)	57	no data	no data	no data	no data	Churnet 1996
584	Bashkirian	Bashkirian	Hebden Formation	England	1	<1	<1	0	0	McCabe 1977; Jones and McCabe 1980; Hmapson 1997
585	Bashkirian	Bashkirian	Joggins Formation	Canada (Nova Scotia)	89	83	6	0	0	Way (1968); Archer et al. (1995); Falcon-Lang et al. (2004); Davies et al. (2005); Falcon-Lang (2003a, 2003b, 2006); Calder et al. (2006); Rygel and Gibling (2006); Davies and Gibling (2013)
586	Bashkirian	Bashkirian	Kanawha Formation	USA (West Virginia)	26	0	26	0	0	Greb and Martino 2005
587	Bashkirian	Bashkirian	Kilkee Sandstone	Ireland	5	no data	no data	no data	no data	Hampson et al., 1997, 1999a
588	Bashkirian	Bashkirian	Lee Formation	USA (Virginia, W Virginia, Tennessee, Kentucky)	<1	<1	<1	0	0	Rice 1885; Chesnut et al., 1992; Wizevich 1992, 1993; Greb and Chesnut 1996
589	Bashkirian	Bashkirian	Little River Formation	Canada (Nova Scotia)	47	0	47	0	0	Calder et al. 2005
590	Bashkirian	Bashkirian	Lower Coal Measures	Germany	18	18	0	0	0	Hampson et al. 199b
591	Bashkirian	Bashkirian	Marsden Formation	England	2	1	1	0	0	McCabe 1977; Jones 1979; Jones and McCabe 1980; Okolo 1983; Brettle et al., 2002
592	Bashkirian	Bashkirian	Morrow Formation	USA (Kansas, Colorado, Oklahoma)	31	31	0	0	0	Blackeney et al. 1990; Krystink and Blackeney 1990; Sonnenberg et al. 1990; Breyer 1995; Montgomery 1996; Buatois et al. 2002; Bowen and Weimer 2003, 2004
593	Bashkirian	Bashkirian	New Glasgow Formation	Canada (Nova Scotia)	50	no data	no data	no data	no data	Chandler 1998
594	Bashkirian	Bashkirian	New River Formation	USA (West Virginia)	7	4	3	0	0	Korus et al. 2008

595	Bashkirian	Bashkirian	Pine Creek Sandstone	USA (Kentucky)	no data	no data	no data	no data	no data	Greb & Martino, 1995
596	Bashkirian	Bashkirian	Port Hood Formation	Canada (Nova Scotia)	50	22	28	0	0	Gersib & McCabe, 1981; Keighley & Pickerill, 1994, 1996, 1998
597	Bashkirian	Bashkirian	Pottsville Formation	USA (Alabama, Ohio)	no data	no data	no data	no data	no data	Gastaldo et al. 1991; Greb & Martino, 1995; Gastaldo & Degges, 2007
598	Bashkirian	Bashkirian	Productive Coal Formation	Wales	no data	no data	no data	no data	no data	Evans et al. 2003
599	Bashkirian	Bashkirian	Raccoon Mountain Formation	USA (Tennessee)	no data	no data	no data	no data	no data	Shaver et al. 2005
600	Bashkirian	Bashkirian	Ragged Reef Formation	Canada (Nova Scotia)	27	0	27	0	0	Allen et al. 2013
601	Bashkirian	Bashkirian	Rockcastle Sandstone	USA (Kentucky)	51	no data	no data	no data	no data	Greb and Martino 2005
602	Bashkirian	Bashkirian	Rocky Creek Conglomerate	Australia (New South Wales)	1.5	1.5	0	0	0	Birgenheier et al. 2009
603	Bashkirian	Bashkirian	Rough Rock Group	England, Scotland	1	1	0	0	0	Bristow, 1988, 1993; Hampson, 1995; Hampson et al. 1997, 1999
604	Bashkirian	Bashkirian	Scottish Lower Coal Measures Formation	Scotland	no data	no data	no data	no data	no data	Kirk, 1983
605	Bashkirian	Bashkirian	Sharon Formation	USA (Ohio)	no data	no data	no data	no data	no data	Wells et al. 1992; Ninke & Evans, 2002
606	Bashkirian	Bashkirian	Silesian Mudstone Series	Poland	no data	no data	no data	no data	no data	Gradzinski et al. 1982
607	Bashkirian	Bashkirian	Springhill Mines Formation	Canada (Nova Scotia)	80	0	80	0	0	Allen et al. 2013
608	Bashkirian	Bashkirian	Tynemouth Creek Formation	Canada (New Brunswick)	40	0	40	0	0	Plint & Van de Poll, 1982; Plint, 1985; Falcon-Lang, 2006
609	Bashkirian	Bashkirian	Upper Sandstone Group	Wales	no data	no data	no data	no data	no data	George, 2001
610	Bashkirian	Moscovian	Breathitt Group	USA (Virginia, W Virginia, Tennessee, Kentucky)	no data	no data	no data	no data	no data	Gardner, 1983; Chesnut et al. 1992; Aitken & Flint, 1994, 1995, 1996; Andrews et al. 1994; Greb & Chesnut, 1996
611	Bashkirian	Moscovian	Caister Sandstone	North Sea	no data	no data	no data	no data	no data	Ritchie et al. (1998); O'Mara and Turner (1999); Kosters and Donselaar (2003)
612	Bashkirian	Moscovian	Charleroi Formation	Belgium	no data	no data	no data	no data	no data	Dreesen et al. 1995
613	Bashkirian	Moscovian	Coal Measures Group	England	no data	no data	no data	no data	no data	Fielding (1984, 1986); Besly and Fielding (1989); O'Mara and Turner (1999)
614	Bashkirian	Moscovian	Currabubula Formation	Australia (New South Wales)	no data	no data	no data	no data	no data	Birgenheier et al. 2009
615	Bashkirian	Moscovian	Etruria Formation	England	no data	no data	no data	no data	no data	Besly 1988
616	Bashkirian	Moscovian	Fountain Formation	USA (Colorado)	0	0	0	0	0	Maples and Suttner 1990
617	Bashkirian	Moscovian	Jericho Formation	Australia (Queensland)	43	0	43	0	0	Jones and Fielding 2008
618	Bashkirian	Moscovian	Malanzán Formation	Argentina	no data	no data	no data	no data	no data	Andreis et al. 1986; Buatois and Mangano 1995; Gutierrez and Limarino 2001
619	Bashkirian	Moscovian	Mansfield Formation	USA (Indiana)	10	10	0	0	0	Huff 1985; Archer et al. 1994; Kvale and Barnhill 1994; Evans and Reed 2007
620	Bashkirian	Moscovian	Molas Formation	USA (Colorado)	70	6	64	0	0	Evans and Reed 2007
621	Bashkirian	Moscovian	Radnice Member	Czech Republic	57.5	no data	no data	no data	no data	Pešek, 1994; Oplustil and Vizdal 1995; Oplustil et al. 2009

622	Bashkirian	Moscovian	Tarija Formation	Argentina	90	90	0	0	0	Di Pasquo and Azcuy 1999; Starck and Del Papa 2006
623	Moscovian	Moscovian	Allegheny Formation	USA (Pennsylvania, Maryland, West Virginia)	48.5	no data	no data	no data	no data	Wise et al. 1991; Staub and Richards 1993
624	Moscovian	Moscovian	Baker Coal	USA (Illinois)	>90	no data	no data	no data	no data	Falcon-Lang et al. 2009a, 2009b
625	Moscovian	Moscovian	Barachois Group	Canada (Newfoundland)	29	no data	no data	no data	no data	Falcon-Lang and Bashforth 2005a, 2005b
626	Moscovian	Moscovian	Barren Red Beds	North Sea	53	no data	no data	no data	no data	Besly et al. 1993
627	Moscovian	Moscovian	Bartlesville Sandstone	USA (Oklahoma)	3	3	0	0	0	Ye and Kerr 2000
628	Moscovian	Moscovian	Basal Conglomerate (Garfield Field)	USA (Kansas)	no data	no data	no data	no data	no data	Rogers 2007
629	Moscovian	Moscovian	Battle Formation	USA (Nevada)	no data	no data	no data	no data	no data	Saller and Dickinson 1982
630	Moscovian	Moscovian	Clifton Formation	Canada (New Brunswick)	75	65	10	0	0	Legun and Rust 1982; Rust and Legun 1982
631	Moscovian	Moscovian	Donets Basin	Russia, Ukraine	no data	no data	no data	no data	no data	Izart et al. 1998; Sachsenhofer et al. 2003
632	Moscovian	Moscovian	Kittanning Formation	USA (Pennsylvania)	5	5	0	0	0	Ferm 1962; Beutner et al. 1967
633	Moscovian	Moscovian	Lorraine Coal Basin	France	51	0	12	no data	39	Fleck et al. 2001; Izart et al. 2005
634	Moscovian	Moscovian	Malagash Formation	Canada (Nova Scotia)	72	0	72	0	0	Allen et al. 2013
635	Moscovian	Moscovian	Minturn Formation	USA (Colorado)	15	15	0	0	0	Houck 1997; Hoy and Ridgway 2002
636	Moscovian	Moscovian	Flénu Formation	Belgium	no data	no data	no data	no data	no data	Dreesen et al. 1995
637	Moscovian	Moscovian	Neeroeteren Formation	Belgium	60	no data	no data	no data	no data	Dreesen et al. 1995; Delmer et al. 2001
638	Moscovian	Moscovian	Pennant Sandstone Formation	England, Wales	5	5	0	0	0	Bluck and Kelling 1963; Kelling 1969; Foster et al. 1989
639	Moscovian	Moscovian	Petersburg Formation	Indiana	no data	no data	no data	no data	no data	Eggert 1984
640	Moscovian	Moscovian	Sidi-Kassem Basin	Morocco	no data	no data	no data	no data	no data	Hoepffner et al. 2000
641	Moscovian	Moscovian	South Bar Formation	Nova Scotia	26	no data	no data	no data	no data	Gibling and Rust 1984, 1987, 1993; Rust and Gibling 1990a, 1990b; Tibert and Gibing 1999; Gibling et al. 2004, 2010
642	Moscovian	Moscovian	Sydney Mines Formation	Nova Scotia	74	74	0	0	0	Masson and Rust 1983, 1984, 1990; Gibling and Rust 1987, 1993; Gibling and Bird 1994; Gibling and Wightman 1994; Marchioni et al. 1996; Tandon and Gibling 1997; Batson and Gibling 2002
643	Moscovian	Moscovian	Trenchard Formation	England	2	1	1	0	0	Jones 1972
644	Moscovian	Moscovian	Tubbergen Formation	Netherlands	39	no data	29	10	no data	Kombrink et al. 2007
645	Moscovian	Moscovian	Unayzah C Member	Saudi Arabia	10	no data	no data	no data	no data	Alsharhan 1994; Melvin and Srague 2006
646	Moscovian	Moscovian	Upper Freeport Formation	Pennsylvania	>80	no data	no data	no data	no data	Ruppert et al. 1991; Garces et al. 1997
647	Moscovian	Moscovian	Waddens Cove Formation	Nova Scotia	35	35	0	0	0	Gibling and Rust 1990; Rust and Gibling 1990a
648	Moscovian	Kasimovian	Dobrudzha Coalfield	Bulgaria	56	0	0	0	56	Tenchov 2007
649	Moscovian	Kasimovian	Lower Paganzo Group	Argentina	3	0	3	0	0	Andreis et al. 1986; Net et al. 2001; Buatois and Mangano 2002; Limarino et al. 2006; Desjardins et al. 2009
650	Moscovian	Kasimovian	Nýřany Member	Czech Republic	43	no data	no data	no data	no data	Pešek 1994; Oplustil et al. 2005, 2009; Falcon-Lang and Bashforth 2005a, 2005b
651	Moscovian	Gzhelian	Asker Group	Norway	10	no data	no data	no data	no data	Dahlgren and Corfu 2001

652	Moscovian	Gzhelian	Balfron Formation	Canada (Nova Scotia)	50	0	50	0	0	Allen et al. 2013
653	Moscovian	Gzhelian	Bechtsrieth Formation	Germany	48	no data	no data	no data	no data	Dill 1992
654	Moscovian	Gzhelian	Halesowen Formation	England	5	no data	no data	no data	no data	Besly 1988; Glover and Powell 1996
655	Moscovian	Gzhelian	San Lorenzo Shales	Italy	77	no data	no data	no data	no data	Cassinis 1997; Degl'Innocenti et al. 2008
656	Moscovian	Gzhelian	Tatamagouche Formation	Canada (Nova Scotia)	43	0	43	0	0	Allen et al. 2013
657	Moscovian	Permian	Cutler Group	USA (Colorado, New Mexico)	17	0	0	0	17	Mack and Rasmussen 1984; Eberth and Miall 1991; Soreghan et al. 2009
658	Moscovian	Permian	Peine Group (Middle Member)	Chile	39	no data	no data	no data	no data	Breitkreuz 1991
659	Moscovian	Permian	Sangre de Cristo Formation	USA (New Mexico, Colorado)	0	0	0	0	0	McBryde and Casey 1979; Hoy and Ridgway 2002
660	Kasimovian	Kasimovian	Cleveland Formation	Texas	no data	no data	no data	no data	no data	Hentz 1994
661	Kasimovian	Kasimovian	Escarpment Formation	Argentina	1	1	0	0	0	Di Pasquo and Azcuy 1999; Starck and Del Papa 2006
662	Kasimovian	Kasimovian	Glenshaw Formation	USA (Ohio, Kentucky, W Virginia)	52	no data	no data	no data	no data	Martino 2004; Nadon and Kelly 2004
663	Kasimovian	Kasimovian	Guadaloupe Box Formation	USA (New Mexico)	61	no data	no data	no data	no data	Krainer et al. 2005
664	Kasimovian	Kasimovian	La Magdalena Coalfield	Spain	42	no data	no data	no data	no data	Heward 1978a, 1978b; Bashforth et al. 201a, 2010b
665	Kasimovian	Kasimovian	Ocejo Formation	Spain	5	no data	no data	no data	no data	Iwaniw 1984
666	Kasimovian	Kasimovian	Salvan Dorénaz Unit I	Switzerland, France	33	no data	no data	no data	no data	Niklaus and Wetzel 1996; Capuzzo and Wetzel 2004
667	Kasimovian	Kasimovian	Solca Formation	Argentina	no data	no data	no data	no data	no data	Andreis et al. 1986
668	Kasimovian	Kasimovian	Týnec Formation	Czech Republic	1	0	1	0	0	Pešek 1994; Oplustil et al. 2005, 2009
669	Kasimovian	Kasimovian	Warrensburg Sandstone	USA (Missouri)	<1	<1	<1	0	0	Emerson and Nold 2001
670	Kasimovian	Kasimovian	Žaltman Arkoses	Czech Republic	no data	no data	no data	no data	no data	Mencl et al. 2009
671	Kasimovian	Gzhelian	Cape John Formation	Canada (Nova Scotia)	36	36	0	0	0	Farrell 1983; Calder 1998; Allen et al. 2013
672	Kasimovian	Gzhelian	Conemaugh Group	USA (Pennsylvania, W Virginia, Ohio, Maryland, Kentucky)	73	no data	no data	no data	no data	Joeckel 1995; Martino 2004; Nadon and Kelly 2004
673	Kasimovian	Gzhelian	Dunkard Group	USA (West Virginia)	50	no data	no data	no data	no data	Beerbower 1969; Dominic 1991
674	Kasimovian	Gzhelian	Juwayl Formation	Saudi Arabia	no data	no data	no data	no data	no data	Stump and Van Der Eem 1995; Knox et al. 2007
675	Kasimovian	Gzhelian	Kapp Hanna Formation	Svalbard	26	no data	no data	no data	no data	Worsley and Edwards 1976; Worsley et al. 2001
676	Kasimovian	Gzhelian	Monongahela Group	USA (West Virginia)	65	35	0	30	0	Beerbower 1969; Dominic 1991
677	Kasimovian	Gzhelian	Stranger Formation	USA (Kansas, Iowa)	87	87	0	0	0	Goebel et al. 1989; Lanier et al. 1993; Archer et al. 1994; Feldman et al. 1995; Buatois et al. 1997
678	Kasimovian	Gzhelian	Tindouf Basin	Morocco	58	no data	no data	no data	no data	Padgett and Ehrlich 1976
679	Kasimovian	Permian	Malpas Formation	Spain	54	41	13	0	0	Besly and Collinson 1991

680	Kasimovian	Permian	Prince Edward Island Group	Canada (PEI)	15	no data	no data	no data	no data	Van De Poll and Forbes 1979; Van De Poll 1989; Tanner et al. 2005
681	Kasimovian	Permian	Salop Formation	England	49	no data	no data	no data	no data	Besly 1988; Glover and Powell 1996; Tucker and Smith 2004
682	Gzhelian	Gzhelian	Autiniano Sardo	Italy	<1	<1	<1	0	0	Pittau et al. 2008; Ronchi et al. 2008
683	Gzhelian	Gzhelian	Corona Formation	Italy	no data	no data	no data	no data	no data	Massari et al. 1991
684	Gzhelian	Gzhelian	Graissessac Basin	France	52	0	52	0	0	Martin-Closas and Galtier 2005
685	Gzhelian	Gzhelian	Ida Ou Zal Basin	Morocco	10	no data	no data	no data	no data	Saber et al. 2001
686	Gzhelian	Gzhelian	Ifeld Basin Stephanian C	Germany	no data	no data	no data	no data	no data	Paul 1999
687	Gzhelian	Gzhelian	Indian Cave Sandstone	USA (Nebraska)	67.5	67.5	0	0	0	Fischbein et al. 2009
688	Gzhelian	Gzhelian	Karoo Basal Unit (Tuli Basin)	South Africa	47	no data	no data	no data	no data	Bordy and Catuneanu 2002
689	Gzhelian	Gzhelian	Líně Formation	Czech Republic	no data	no data	no data	no data	no data	Pešek 1994
690	Gzhelian	Gzhelian	Markley Formation	USA (Texas)	72	0	37	0	35	Tabor and Montanez 2004
691	Gzhelian	Gzhelian	Northern Swiss Trough	Switzerland	32	0	32	0	0	Matter 1987
692	Gzhelian	Gzhelian	Sakoa Group	Madagascar	20	0	20	0	0	Wescott and Diggens 1997
693	Gzhelian	Gzhelian	Salvan Dorénaz Unit II	Switzerland, France	60	no data	no data	no data	no data	Capuzzo and Wetzel 2004
694	Gzhelian	Gzhelian	Salvan Dorénaz Unit III	Switzerland, France	70	no data	no data	no data	no data	Capuzzo and Wetzel 2004
695	Gzhelian	Gzhelian	Salvan Dorénaz Unit IV	Switzerland, France	1	no data	no data	no data	no data	Capuzzo and Wetzel 2004
696	Gzhelian	Gzhelian	Slaný Formation	Czech Republic	10	10	0	0	0	Pešek 1994
697	Gzhelian	Gzhelian	Vamoosa Formation	USA (Oklahoma)	5	5	0	0	0	Doyle et al. 1991; Doyle and Sweet 1995
698	Gzhelian	Permian	Gwembe Coal Formation	Zambia	70	no data	no data	no data	no data	Nyambe 1999b
699	Gzhelian	Permian	Tirrawarra Sandstone	Australia (South Australia)	no data	no data	no data	no data	no data	Hamlin et al. 1996
700	Gzhelian	Permian	Treskelodden Formation	Svalbard	10	10	0	0	0	Birkenmejer 1984
701	Late Carboniferous	Late Carboniferous	Siankondobo Sandstone Formation	Zambia	21	21	0	0	0	Nyambe 1999a
702	Late Carboniferous	Late Carboniferous	Tuppa Niedda Conglomerates	Italy	<1	<1	0	0	0	Costamagna and Barca 2008
703	Late Carboniferous	Late Carboniferous	Zongwe Sandstone Formation	Zambia	0	0	0	0	0	Nyambe 1999a
704	Carboniferous	Permian	Bani Khatmah Formation	Yemen, Saudi Arabia	2	1	1	0	0	Alsharhan et al. 1991

Table A3. Database of pre-vegetation alluvium characteristics (Archean-Cambrian). See Table A2 for unit locations, oldest and youngest possible ages, mudrock contents and references

	Unit	Age (Myr)	Thickness (m)	Conglomerate?	Sandstone Petrology	Sedimentary structures	Cross-stratification thickness (cm)	Architectural elements	Dominant transport regime	Associated aeolian strata?	Soft-sediment deformation	Fluvial style	Paleolatitude	Basin type/Tectonic setting	Climate	Additional information
1	Baviaanskop Formation				Quartz arenite							Braided				
2	Clatha Formation	3300	100-130	Yes	Quartz arenite	St, Sh, Sl	20 cm	CH	Lower-flow regime			Braided		Fold and thrust belt		
3	Hooggenoeg Formation	3470-3458	70		Quartz arenite			CH			Yes					
4	Joe's Luck Formation				Quartz arenite							Braided				
5	Serra do Córrego Formation	3600-3250	1000	Yes	Quartzite	Sp			Lower-flow regime			Braided				
6	Bababudan Group (undivided)	3200-3000		Yes	Quartz arenite	St, Sh			Upper-flow regime		Yes (local)	Braided		stable platform		
7	Blyvooruitzicht Formation											Braided				
8	Maraisburg Formation	<2902		Yes	Quartz arenite							Braided				
9	Sinqeni Formation	2980-2870			Quartz arenite	St			Lower-flow regime			Braided				Mud clasts
10	Woodburn Lake Formation	2980-3004		Yes	Quartzite	Sp, St	up to 200 cm (mostly 20 - 100 cm)		Lower-flow regime							
11	Bell Lake Group (undivided)	2800	1000	Yes		Sp, St	5 - 30 cm		Lower-flow regime			Sheetflood				Mud clasts
12	Elsburg Formation	2890-2760			Arkose	Sp, St			Lower-flow regime			Braided				
13	Kimberley Formation	2890-2760			Arkose	St, Sp	Sp up to 90 cm					Braided				
14	Manjeri Formation			Yes								Braided				
15	Mondeor Formation	2890-2760			Arkose							Braided				
16	Pote Formation	2700-3200		Yes	Quartzite	St, Sh					Yes (local)	Braided/ Sheetflood				
17	Águas Claras Formation	2650														
18	Black Reef Formation	2658-2550	200	Yes	Quartz arenite	St, Sp, Sh						Braided		Intracratonic sag/Stable		
19	Buffelsfontein Group (undivided)	>2557			Arkose											
20	Casa Forte Formation			Yes		St, Sp, Sh, Sm										"Scour and fill"
21	Crowduck Lake Group (undivided)	<2699	30 - 50	Yes												
22	English Subprovince	2701-2691		Yes												
23	Godwan Group (undivided)	>2557			Arenite											
24	Hardey Formation	2770-2700	>440	Yes	Arenite							Braided				MISS

25	Jackson Lake Formation	2599-2611	300	Yes	Quartz arenite	St, Sp, Sl										Mud clasts
26	Jones Creek Supersequence	2665	60	Yes		Sm, Sh		CH	Upper-flow regime			Braided		Fault bound		
27	Keskarrah Formation	<2605	700	Yes (89%)	Arenite/Quartz arenite	St, Sp, Sh	4 - 100 cm		Upper-flow regime		Yes	Braided				
28	Lalla Rookh Formation	<2770			Arenite							Braided		Strike slip		
29	Merougil Formation	2658-2668	>1630		Arenite	St, Sm, Sh		CH				Braided		Overfilled molasse		
30	Midway Sequence	2685-2695		Yes										Pull-apart		Mud clasts
31	Moeda Formation	>2500	350		Quartzite	St, Sm		CH				Braided plain				
32	Ogishkemuncie Sequence	2720-2680		Yes (dominant)				CH						Syndepositional		
33	Ongers River Formation	2700-2778	500	Yes (60%)	Arkose	Sp, Sh								Active		
34	Raquette Lake Formation	2680-2690	200	Yes (68%)		Sh, Sm, Sl, Sp		CH				Hyperconcentrated flood		Fringing continental arc		
35	Renosterspruit Sandstone Formation	<2800	120	Y	Arkosic arenite							Braided				
36	Shivakala Formation	>2504		Yes	Arkose							Braided				
37	Timiskaming Group (undivided)	2680-2690	>100	Yes		St (45%), Sh (55%)			Upper-flow regime		Yes	Braided		Strike slip		
38	Harmony Formation				Quartz arenite/Quartz wacke	St, Sh, Sp, Sr		CH	Lower-flow regime			Braided				
39	Beaulieu Rapids Formation		1000	Yes	Arenite	St, Sp, Sh, Sl		CH, LA				Braided				
40	Bothaville Formation		>19		Quartzite/Subarkose							Braided				Stromatolites in abandoned pools
41	Duparquet Formation		735	Yes (75%)	Argillite sandstone	Gm, Gp,St, Sp, Sh	5 - 100 cm (St)		Upper-flow regime			Braided		Strike slip		
42	Hauy Formation			Yes		St, Sp, Sh, Sl	<20 cm					Braided				
43	Leadbetter Conglomerate			Yes		St, Sp, Sh		CH	Lower-flow regime			Braided				Mud clasts
44	Mount Roe Formation			Yes (dominant)	Arenite							Braided				
45	North Spirit Lake Group (undivided)				Arenite/Arkose	St, Sh						Braided				
46	Rainy Lake Group (undivided)				Arenite/Arkose	St, Sl, Sh						Braided				
47	Rajkharsawan Conglomerate			Yes	Quartzite							Meandering				
48	Randfontein Formation				Quartzite	St										
49	Schelem Formation											Braided				
50	Scotty Creek Formation				Arkose	St, Sm, Sh						Braided		Fault bound		
51	Stella Formation			Yes		St, Sp, Sh	2-180					Braided		Fault bound		
52	Yandal Sandstone		>800	Yes		St, Sp, Sh						Braided				
53	Aasvoëlkop Formation				Arkose	St, Sp	<12 cm					Braided				

54	Ahven-Kivilampi Formation		500-150	Yes	Arkose	Sh, Sl			Upper-flow regime			Braided				
55	Amarook Formation	>1758		Yes	Subarkose	Sh			Upper-flow regime	Yes		Ephemeral		Rift		
56	Arkosite Formation				Arkose	Gt						Meandering				
57	Bandeirinha Formation	1715-1710		Yes	Quartzite							Braided		Intracontinental rift		
58	Banganapalli Formation			Yes		St, Sh					Yes	Sheetflood				
59	Baraboo Quartzite	1712-1782			Quartz arenite	St, Sr, Sh			Lower-flow regime			Braided		Stable	Warm/humid	
60	Barron Quartzite	1712-1782		Yes	Quartz arenite	Sp						Braided				
61	Beasley River Quartzite	2200-2400			Quartzite	St, Sp, Sh, Sm		CH			Yes					
62	Bigie Formation	1708		Yes	Arkose			CH								
63	Billstein Formation	1700-1800	1500		Arkose									Fault bound		
64	Bisrampur Formation			Yes	Arkose	St						Braided/Sheetflood		Rift		
65	Blouberg Formation	1900-2000	1400	Yes (38%)	Arkose	St, Sp	15-50	CH			Yes	Braided/ Ephemeral		Pull apart		
66	Bonner Formation	1640	300-500		Arkose											
67	Boshoek Formation			Yes				CH				Braided		Synrift	Periglacial	
68	Bottletree Formation	1790-1810		Yes		St, Sm, Sh						Braided				
69	Bruco Formation	1718		Yes	Arenite			CH				Braided		Epicratonic		
70	Burnside River Formation	1900	3500	Yes (10%)	Arkose (80%)/Quartz arenite (5%)	St, tangential	<20	CH	Lower-flow regime		Yes	Braided				
71	Cangalongue Formation	<1718			Arkose							Braided				
72	Changzhougou Formation	1744-1800		Yes	Arkose									Rift graben		
73	Cromwell Member		100									Braided				
74	Daspoort Formation	2175			Quartz arenite/ Arkose	Sp, St, Sh			Upper-flow regime		Yes	Braided		Intracratonic sag		
75	Deadman Quartzite	1700-1650	334	Yes	Quartzite	St, Sh, Sp	8 to 20					Braided				
76	Deighton Quartzite			Yes	Quartzite											
77	Dhalbhum Formation	2000	2000-4000		Subarkose/ Arkose	Sh, Sp, St					Yes	Braided				
78	Dhanjori Formation	2100			Arkosic arenite	St, Sp, Sh	10 to 15					Mixed		Intracontinental rift	Semi-arid	
79	Dodmanberget Formation			Yes	Arkose	St			Lower-flow regime			Braided				
80	Droogedal Formation	2224		Yes	Quartzite	Sp, St, Sh			Upper-flow regime			Streamflow			Arid	
81	Dwaalheawel Formation	2175			Quartz arenite/Arkosic	Sp, St, Sh	10 tp 100		Upper-flow regime		Yes	Braided		Synrift, extensional		
82	Echo Sandstone		70	Yes								Braided				

83	Ellice Formation			Yes (10%)	Quartz arenite/Sublitharenite	St, Sp, Sl, Sh						Braided				
84	FA Formation	2100														
85	Fair Point Formation	1830-1780						CH				Hyperconcentrated/ Braided				
86	Fish River Formation	1800		Yes												
87	Flambeau Quartzite	1714-1880	800		Quartzite											
88	Gulcheru Quartzite	2000		Yes	Quartzite	St, Sp, Sh	2 - 6.5					Ephemeral/ Hyperconcentrated		Intracratonic	Warm/Semi-arid	
89	Hutte Sauvage Group (Undivided)	1840		Yes	Arkose/Quartzite/Wacke											
90	Kazan Formation	1850			Arkose	St, Sh	10-100			Yes		Braided				
91	Kazput Formation (middle)				Arenite											
92	Kiskonkoski Formation	2250-2100	50-150	Yes	Arkose											
93	Kiyuk Group (Undivided)			Yes	Arkose	St, Sp, Sl, Sh			Upper-flow regime			Sheetflood				
94	Kolhan Sandstone	2000	5 to 20		Quartz arenite	St, Sp, Sh	10 to 40		Upper-flow regime			Braided		Passive margin	Warm/Humid	
95	Koolbye Formation	2200-2400				St, Sm, Sh						Braided				
96	Kunwak Formation	1785			Arkose							Braided				Mud clasts
97	Kurinelli Sandstone		3000		Litharenite/Sublithic arenite	St, Sh			Lower-flow regime		Yes	Braided				
98	Laanhongikko Formation		300-400	Yes	Arkose	St, Sp, Sh, Sl						Braided				
99	Lazenby Lake Formation	1830		Yes								Ephemeral/ Braided			Arid	
100	Leeuwpoort Formation	<2089	1500	Yes	Arkosic arenite	Sp, St, Sh	<30				Yes	Mixed				
101	Lena Quartzite			Yes	Quartzite	St, Sp, Sh, Sr					Yes	Braided				
102	Lindsey Quartzite	>2092	410		Quartz arenite/Subarkose	St										
103	Lochness Formation	1800			Arkose	St, Sp, Sh						Braided			Cool/Temperate	
104	Locker Lake Formation	1830														
105	Lorrain Formation				Subarkose/Lithic arkose/Arenite	Sm									Warm/Hot	
106	Lukkarinvaara Formation		600-800	Yes	Quartz arenite	St			Lower-flow regime			Braided		Reactivated rift faults		
107	Magnolia Formation			Yes	Arkose/Subarkose/Quartz arenite	St			Lower-flow regime			Braided				
108	Main Quartzite Sequence	<2460			Quartzite											

109	Makgabeng Formation	2000			Arenite	St			Lower-flow regime	Yes		Ephemeral/ Braided				MISS
110	Malmbäck Formation	1800		Yes (dominant)												
111	Manitou Falls Formation	1830	900	Yes		Sp, St, Sm		CH, GB, SB, DA, LA				Braided			Humid	MISS
112	Masterton Sandstone	1665-1650			Arkose	St			Lower-flow regime							
113	Matinenda Formation		<600		Arkose	St, Sp, Sm, Sh, Antidune, Sr	3-150					Braided		Passive continental margin		
114	Mazatzal Peak Quartzite	1700-1650			Litharenite/Lithic arkose	St, Sp, Sh, Sl	>50					Braided				
115	Mississagi Formation	2450		Yes	Subarkose/Lithic arkose/Arenite	Sp			Lower-flow regime			Braided				
116	Mitoba River Group (undivided)	2580			Quartzite	Sp, St			Lower-flow regime			Braided				
117	Mogalakwena Formation	1900-1700	<1500	Yes	Arkose	St, Antidunes	<60		Lower-flow regime			Braided		Fault-bound	Humid	
118	Mount Guide Quartzite				Quartzite											
119	Murky Formation		>1000	Yes		St, Sh, Sm, Sl						Sheetflood		Intercratonic		
120	Naulaperá Formation		200-500	Yes	Arkose	St	<50		Lower-flow regime			Braided				
121	Noomut Formation	2450-2100		Yes	Subarkose/Quartz arenite	St, Sm, Sh			Upper-flow regime			Sheetflood				
122	Otherside Formation	1830												Impact crater		
123	Pajeú Formation			Yes	Arkose											
124	Paljakkavaara Formation		800-1200			Gt			Lower-flow regime			Braided				
125	Par Formation	1700-2000		Yes	Arenite	St (58%), Sh (40%)		LA, UA	Lower-flow regime		Yes	Braided			Dry	Mud clasts
126	Pitz Formation	1753		Yes	Subarkose							Braided				
127	Preble Formation			Yes		St, Sh, Sl, Gm					Yes	Braided/ Ephemeral		Intercratonic		Mud clasts
128	Rayton Formation	2089-2224														
129	Read Formation	1740-1690	600	Yes		Sm, Sh		CH, DA, LA, LS	Upper-flow regime		Yes	Ephemeral	50-54˚N		Arid	
130	Rifle Formation				Subarkose	St		CH	Lower-flow regime		Yes	Braided				Mud clasts
131	Rooihoogte Formation	2300	400	Yes	Quartz arenite	Sp, St	10 to 70	CH	Lower-flow regime			Braided		Synrift		
132	Sandriviersberg Formation	1900-1700			Arenite	St, Sp						Braided				
133	São João da Chapada Formation	1715-1710	200			St (43-58%), Sh (28%), Sp, Sl	5 - 120				Yes	Braided/ Ephemeral		Intracontinental rift		

134	Sekororo Formation	2460		Yes								Braided		Rifting		
135	Serpent Formation				Subarkose/Lithic arkose							Braided		fault bound, ensialic trough or aulacogen	Arid	Mud clasts
136	Serra du Gameleira Formation		>2000			Sh						Braided				Mud clasts
137	Setlaole Formation	1900-1700	450	Yes	Arkose	Sp, St			Lower-flow regime			Braided				
138	Sioux Quartzite	1760-1630		Yes	Quartz arenite	St, Sp			Lower-flow regime			Braided		Fault bound		
139	Skilpadkop Formation	1900-1700			Litharenite	St					Yes	Braided				
140	Sly Creek Sandstone		770	Yes	Quartz arenite											
141	Smart Formation	1740-1690		Yes		Sr, Sh						Braided				MISS
142	Smelterskop Formation	<2089		Yes	Arkose	St, Sp	100					Mixed				
143	South Channel Formation	1850-1760		Yes	Arkose	St	5 to 20		Lower-flow regime					Rift		
144	Surprise Creek Formation	1688	3000	Yes	Arkose	Sp, St					Yes	Braided				
145	Taragan Sandstone		1000		Sublitharenite/Subarkose	St		LA	Lower-flow regime		Yes	Mixed				Mud clasts
146	Tavani Formation	1911		Yes (dominant)												
147	Thelon Formation	1720-1750		Yes	Subarkose/Quartz arenite	Gt, Sp, Sl				Yes		Braided		Intracratonic		Mud clasts
148	Tundavala Formation	1947-1810	20-80	Yes	Litharenite/ Quartz arenite									Epicratonic		
149	Uaimapáe Formation	1730-1800												Foreland basin	Arid	
150	Uairén Formation	1730-1800	850	Yes		St, Sp, Sh					Yes	Braided/ Sheetflood		Foreland basin	Arid	
151	Vallecito Conglomerate	>1700		Yes		Sp, St, Sh			Lower-flow regime			Braided/ Sheetflood				
152	Warramana Sandstone	1753-1713			Arkose							Braidplain				
153	Westmoreland Conglomerate	1800		Yes (20%)	Arkose	Gt, St (62%), Gp, Sp (11%), Sh (10%)	St >100, Sp <100					Braided/ Sheetflood				
154	Whitworth Formation	1808-1740			Arenite	St, Sh						Ephemeral			Arid/Semi-arid	Mud clasts
155	Wilgerivier Formation	1800	2000	Yes	Arkose	Sp, Sh		CH			Yes	Braided		Fault-bound		
156	Wolverine Point Formation	1830										Braided				
157	Wyllies Poort Formation	1800-1970	700			St, Sh	5 to 40				Yes	Braided		Aulacogen		
158	Yinmin Formation	>1742	150-360		Arkose	St			Lower-flow regime			Braided		Fault-bound	Tropical/ Subtropical	Mud clasts
159	Yiyintyi Sandstone	1851-1726	>3500	Yes	Arkose/Quartz arenite							Braided				

160	Doomadgee Formation	<1585	25		Arkose/Litharenite											
161	Mbala Formation	1130-1839	1500	Yes	Arkose	St, Sp, Gm, Gt, Sr, Sh	<70		Lower-flow regime			Braided				Mud clasts
162	Sims Formation	1370-1700	700	Yes	Arkose	St, Sp, Sh						Braided				Mud clasts
163	Xiaogoubei Formation		200	Yes										Passive continental margin		
164	Adams Sound Formation	<1270		Yes			<100	DA, LA, UA								
165	Agigilik Formation	1210-1190				Sp, St			Lower-flow regime			Ephemeral			Arid	
166	Barden Bugt Formation				Quartz arenite	Sl, Sr						Braided				
167	Bay of Stoer Formation				Arkose	St			Lower-flow regime			Braided	15˚N	Fault bound		Mud clasts
168	Beinn na Seamraig Formation				Arkose	St, Sr					Yes	Braided				Mud clasts
169	Burdur Formation	1580	230-240		Quartz arenite	Sr						Braided				MISS
170	Chandil Formation	1500-1600				St			Lower-flow regime					Back arc marginal basin		
171	Chequamegon Sandstone	1035		Yes	Arkose	St										
172	Clachtoll Formation				Greywacke/Arkose											
173	Copper Harbour Conglomerate	1087.2	200-2000	Yes		St, Sp, Sh	30-50		Lower-flow regime		Yes	Braided/Sheetflood	Low latitude		Arid	Stromatolites
174	Dala Sandstone				Subarkose	Sp, St			Lower-flow regime							
175	Devdahra Formation	1455		Yes	Arkose											
176	Dhandraul Sandstone Formation		400			Sp, Sh, Sl, St, Sr	10 to 15				Yes	Braided/Ephemeral				Mud clasts
177	Dox Sandstone	1100			Arkose											
178	Dripping Spring Formation	1200	200	Yes	Arkose	St, Sp, Sh						Braided				MISS, Mud clasts
179	Eriksfjord Formation	<1300	1500		Arkose/Quartz arenite	St, Sp, Sl, Sh				Yes		Braided		Rift	Humid	Mud clasts
180	Fabricius Fiord Formation			Yes	Arkose									Rift		
181	Fond du Lac Formation	1010	650	Yes	Arkose							Meandering				
182	Fort Steel Formation		>2000		Quartz arenite/Arkose							Braided				
183	Heddersvatnet Formation			Yes	Arkose	St, Sl, Sh	<150					Braided		Rift	Semi-arid	
184	Il'ya Formation	1580	180-210			Sh, St, Sp, Sr, Sl		CH								
185	Inuiteq Sø Formation	1380			Quartz arenite/Arkose	Sp, St, Sh	10									
186	Jacobsville Sandstone			Yes	Subarkose/Quartz arenite			DA				Braided	Equatorward	Fault-bound, Convergent	Tropical	

187	Jakaram Formation		90-230		Arkose											
188	Kanuyak Formation		60	Yes		St, Sp	5 to 50		Lower-flow regime			Braided				
189	Kasama Formation	1434	80-300		Quartz arenite	St, Sp, Sh			Lower-flow regime			Braided				
190	Kinloch Formation				Arkose						Yes	Braided				Mud clasts
191	Klein Aub Formation				Arkose											
192	Kundargi Formation		189	Yes	Quartzite											
193	Kutovaya Formation	1040-1050	25													
194	Labaztakh Formation		110-200									Braided				MISS
195	Loch na Dal Formation	1187														
196	Mangabeira Formation	1514								Yes						
197	Meall Dearg Formation				Arkose	Chute and Pool, Antidune, Sh, Sl, Humpback, Sp, Sr				Yes		Ephemeral	10-20˚N			MISS
198	Monteso Formation	1100			Quartzite							Braided				
199	Nalla Gutta Sandstone	<1400		Yes	Arkose							Braided		Fault-controlled		
200	Nelson Head Formation	1077			Quartz arenite							Mixed		Epicratonic		
201	Nopeming Formation	>1108			Quartz arenite						Yes					
202	Nyeboe Formation			Yes	Quartz arenite	St	60					Braided				
203	Orienta Sandstone	1059	<1000	Yes	Arkose	St						Meandering				
204	Osler Group (undivided)		210	Yes												
205	Outan Island Formation	1400				St, Sr			Lower-flow regime	Yes	Yes				Humid/Semi-humid	
206	Pandurra Formation	1424		Yes	Arkose											
207	Pass Lake Formation	1340		Yes	Quartz arenite/Subarkose/Sublitharenite	Sh, St				Yes		Braided		Failed-rift	Arid	Mud clasts
208	Puckwunge Formation		60	Yes	Quartz arenite							Braided				
209	Qaanaag Formation				Quartz arenite	Sp, St	Usually 15-50 (some >100)		Lower-flow regime			Braided				
210	Ramdurg Formation	1260-1000	71		Litharenite/ Arkose	Sl, St, Sh	80	DA, CH		Yes	Yes	Braided		Intracontinental rift	Semi-arid	
211	Ravalli Group (undivided)	1400			Arenite	St, Sp, Sh						Braided/ Ephemeral				
212	Revett Formation	1468-1454			Quartzite	Sp, St, Sh, Antidune, Chute and Pool	30-180		Upper-flow regime			Ephemeral				

213	Rubha Guail Formation		200		Arkose	St			Lower-flow regime			Braided				Mud clasts
214	Scanlan Conglomerate		53	Yes		Gp, St, Gm, Gt, Sp, Sh	15-100 (most <50)		Lower-flow regime			Braided				
215	Simpson Island Formation	1100		Yes	Arkose	St, Sh		CH	Lower-flow regime			Braided		Continental rift	Semi-arid	Mud clasts
216	Sinasiuvik Formation	1210-1190			Arkose/Subarkose/Litharenite	Sh			Upper-flow regime			Sheetflood		Subsiding	Arid	
217	Skottsfjell Formation		1000	Yes	Arkose	St			Lower-flow regime			Braided				
218	Solor Church Formation			Yes	Subarkose (31%)/Lithic arkose (20%)/Arkose(14%)/Feldspathic lithic(14%)							Meandering				
219	Sopa-Brumadinho Formation	<1180	>200	Yes	Quartzite	Sh, Sp, St		CH				Braided/ Ephemeral				
220	Svinsaga Formation	1170	200	Yes	Arkose/Subarkose	Sl, Sh, St	15-110					Ephemeral		Strike-slip	Periglacial	
221	Tombador Formation	1416	350-600			St, Sp, Sm, Sh, Sl				Yes		Braided				Mud clasts
222	Troy Quartzite	1150	400	Yes	Arkose							Braided				
223	Urusib Formation		2400			St, Sp, Sh, Sr						Braided /Ephemeral		Fault-bound		Mud clasts
224	Vemork Formation	1495-1347	430	Yes	Arkose	St			Lower-flow regime			Braided				Mud clasts
225	Wolstenholme Formation			Yes (70%)		St, Sp			Lower-flow regime			Braided				
226	Yunmengshan Formation		700		Arenite									Passive continental margin		
227	Eduni Formation	1005-779	300-600			Sp (77%), Sl, Sr, Sh		CH	Lower-flow regime							
228	El Aguila Formation		385		Quartzite											
229	El Alamo Formation		770		Arkose	St, Sh			Lower-flow regime			Braided				
230	Freda Sandstone	1042-982		Yes	Arkose	Sp, St					Yes	Braided				
231	Grafe River Formation	1005-779	<454	Yes		Sp (85%), St (<2%), Sl and Sinusoidal cross strat (c. 14%)	64	CH	Lower-flow regime							
232	Grassy Bay Formation	<1077														
233	Kgwebe Formation	820-1020			Arenite										Semi-arid	
234	Mayamkan Formation		1000	Yes	Arenite	St			Lower-flow regime							

235	Moraenesø Formation	1230-570		Yes	Arkose	St, Sp	10 to 50		Lower-flow regime							
236	Morro do Chapéu Formation	1000		Yes	Arkose											
237	Rewa Sandstone	700-1100				St	15cm	DA	Lower-Flow regime		Yes	Braided	44°N, 214°E	Intracratonic	Humid	
238	Shattered Range Formation	1005-779	<376		Quartz arenite	Sm (10%), Sp (86%), Sr, Sh	51		Lower-Flow regime		Yes					
239	Applecross Formation	977	>3000	Yes	Arkose/Lithic arkose	St, Sp, Sh, Sl	27		Lower-flow regime		Yes	Braided	30-50^{0}S	Foreland	Temperate	Mud clasts
240	Arroi América Formation		600	Yes	Arkose	St			Lower-flow regime			Braided				
241	Aultbea Formation	<977			Arkose	St, Sp, Sl, Sh	5 to 70		Lower-flow regime		Yes	Braided				
242	Ayn Formation	<722				St, Sp, Sh, Sr						Glacial outwash				
243	Barriga Negra Formation			Yes								Braided			Arid	
244	Basnaering Formation		130-350		Arkose	St, Sp, Sh, Sm						Braided				
245	Bateau Formation		240		Quartzite	Sm										
246	Bhander Sandstone					St, Sp, Sh						Ephemeral				
247	Bonney Sandstone				Arkose											
248	Browns Hole Formation	580			Quartz arenite							Braided				
249	Catactin Formation	564		Yes	Arkose/Arenite	Sm, St, Sh		CH	Upper-flow regime			Braided		Rift		
250	Chestnut Hill Formation				Arkose						Yes	Ephemeral		Intracratonic		Mud clasts
251	Cochran Formation			Yes	Arkose	St			Lower-flow regime			Braided				
252	Crouse Canyon Formation		1170-3200									Braided	Equatorial	Intracratonic		Mud clasts
253	Dead Horse Pass Formation		900		Quartz arenite	Sp, St			Lower-flow regime		Yes	Braided	Equatorial	Intracratonic		Mud clasts
254	Diamond Breaks Formation		500-1000		Quartz arenite/Subarkose/Subarkosic arenite							Braided	Equatorial	Intracratonic		
255	Doli Sandstone	800-900		Yes								Braided				
256	Dutch Peak Formation				Quartzite	Sh, St, Sp			Upper-flow regime						Possibly glacial	
257	El Tapiro Formation		100	Yes	Quartzite											
258	Encharani Formation	<1000	90	Yes	Arkose/Arenite/Quartz arenite	St			Lower-flow regime			Braidplain				
259	Estância Santa Fé Formation		400	Yes	Arkose	St, Sp, Sh, Antidunes			Lower-flow regime			Braided				Mud clasts

260	Etusis Formation	1000-900	1200-3000		Arenite/Arkose	Sp			Lower-flow regime			Braided				
261	Fatira El Zarqa Sequence	600-585				Sm, Sh			Upper-flow regime		Yes	Floodsheets				
262	Flaminkberg Formation	<590		Yes	Quartzite							Braided		Foreland basin		
263	Fugleberget Formation			Yes	Arkose/Subarkose	Sl, Sh, Sigmoidal, Tangential	<200				Yes	Braided				
264	Golneselv Formation		50-150	Yes	Subarkosic		<100				Yes	Braided				
265	Hades Pass Formation		1825-3600		Quartz arenite/Subarkosic arenite/Arkosic arenite/Arkose	Sp, St			Lower-flow regime		Yes	Braided	Equatorial	Intracratonic		Mud clasts
266	Hashim Formation	635	5000	Yes	Litharenite		10 to 50									
267	Høyberget Formation				Arkose	Sp, St, Sh						Braided				Mud clasts
268	Husky Creek Formation		4000													
269	Ifjord Formation		>2700	Yes		St, Sp, Sh	5 to 50				Yes	Braided/ Sheetflood				
270	Inkom Formation	635-650	100-200	Yes								Braided				
271	Jifn Formation	585-560														
272	Johnnie Formation	640	35-40		Quartz arenite/Subarkose/Arkose							Braided		Passive margin		
273	Kampa-Tenpa Formation				Arenite	St, Sh, Sp, Antidunes	50-200					Braided		Cratonic	Semi-arid to hot-humid	
274	Kapra Sandstone			Yes	Arkose/Quartz arenite	St	5.5		Lower-flow regime		Yes	Braided				
275	Keele Formation	635-850			Quartz arenite/Subarkose	St			Lower-flow regime		Yes	Braided			Humid to semi-arid	
276	Kerur Formation (Cave Temple Arenite)		89	Yes	Arenite							Braided				
277	Kråkhammaren Formation		>700		Arenite	St, Sp, Sh					Yes	Mixed				
278	Kuara Formation	620-630	>600	Yes								Braided /Sheetflood		Fault bound		
279	Kuujjua Formation	1000-723	120		Quartz arenite	Sp, St, Sh	30-100		Lower-flow regime			Braided		Epicratonic	Arid	Mud clasts
280	Landersfjord Formation		2600	Yes	Quartz arenite	Sh, St, Sp		CH				Braided				
281	Liubatang Formation	968		Yes	Quartz arenite											
282	Lokvikfjell Formation		2300	Yes	Arenite	St			Lower-flow regime			Braided				
283	Lövan Formation		1500	Yes	Arkose	St, Sh										

284	Lunndörrsfjällen Formation				Arkose	Sl, St, Sr, Sp					Yes	Braided				Mud clasts
285	Mancheral Quartzite		76	Yes	Quartzite	Sp, St	5-120		Lower-flow regime	Yes	Yes	Braided			Arid	Mud clasts
286	Maricá Formation	>592	2500	Yes	Subarkose	St, Sl						Braided				
287	Marsham Formation			Yes		Sm, Sh, St										
288	Mindola Clastics Formation		300	Yes	Arkose							Braided		Rift		
289	Mount Watson Formation		550-1000		Quartz arenite/Subarkosic arenite							Braided	Equatorial	Intracratonic		
290	Mutoshi Formation	<575		Yes	Arkose/Quartz arenite							Braided				
291	Mutual Formation	580	300-800	Yes	Sublitharenite	St			Lower-flow regime			Braided				
292	Nababis Formation				Arkose/Quartz arenite							Braided				Mud clasts
293	Nankoweap Formation	900										Braided	10°S, 163°E			
294	Osdalen Formation		400	Yes	Arkose							Braided		Rift		
295	Otts Canyon Formation				Quartzite	Sh						Braided				
296	Paddeby Formation		117	Yes	Subarkose/Arkose	St, Sp, Sh					Yes	Braided				
297	Pong Conglomerate			Yes												
298	Ramgiri Formation			Yes	Arkose	St, Sp			Lower-flow regime		Yes					
299	Red Castle Formation				Arkose/Arenite							Mixed	Equatorial	Intracratonic		Mud clasts
300	Rehatikhol Conglomerate	>700	20		Arenite/Arkose	Sh(80%), St (18%), scour fills (2%)			Upper-flow regime			Braidplain/Sheetflood		Intracratonic	Arid/Temperate	
301	Rendalen Formation		2000	Yes	Arkose							Braided		Rift		
302	Rhynie Sandstone				Arkose	St, Sp	30-100		Lower-flow regime		Yes					
303	Ridam Formation	660-635		Yes	Litharenite											
304	Rivieradal Sandstone		370		Quartz arenite	Sp, Sh, St, Tangential		CH			Yes	Braided			Humid	
305	Rubtayn Formation	585-560		Yes										Pull apart		
306	Shihimiya Formation	650-593		Yes		Sh, Sp			Upper-flow regime		Yes	Braided				
307	Siemiatycze Formation	551-542			Arkose							Braided/ Ephemeral				
308	Sixty Mile Formation		60		Arkose											
309	Sonia Sandstone Formation	635-541	85		Arenite	St, Sh, Sp		CH, DA, LA	Lower-flow regime	Yes	Yes	Braided		Intracratonic/ Sag		
310	Stirling Quartzite		700-1600		Quartz arenite	Sh, St			Upper-flow regime			Braided				

311	Stockdale Formation				Arkose	St, Sp, Sh					Yes	Braided				
312	Styret Formation	665-545														
313	Sugaitebulake Formation	<610	400-450	Yes	Subarkose	St, Sp			Lower-flow regime		Yes	Braided				
314	Swift Run Formation				Arkose									Rift		
315	Terjit-Aguinob Formation	<610	80-100	Yes	Litharenite	St, Sp			Lower-flow regime			Braided				
316	Uinta Mountain Group (undivided)	770-740	60		Quartz arenite/Arenite							Braided	Equatorial	Intracratonic		
317	Unicoi Formation			Yes	Subarkose	St, Sp, Sl, Sh						Braided		Rift/Passive		
318	Urucum Formation	550-889	15-20	Yes	Arkose	St, Sh, Sl	40-60					Sheetflood				
319	Veidnesbotn Formation		300		Arenite/Subarkose	St	50		Lower-flow regime							
320	Wadi Igla Formation	650-593	4000	Yes		Sh, St, Sp			Upper-flow regime		Yes	Braidplain				
321	Whyte Inlet Formation			Yes	Arenite			LA, DA				Braided/ Ephemeral				
322	Zhafar Formation	660-635			Litharenite											
323	Wentnor Group	<552.9	1690-2172	Yes		St			Lower-flow regime			Braided				
324	Double Mer Formation			Yes	Arkose	Sp, St, Sh			Lower-flow regime			Braided	21-31°S			
325	Estância Santa Fé Fm	566-535.2	400	Yes		St, Sp, Sh			Lower-flow regime			Braided				
326	Hamill Group (undivided)			Yes	Arenite	St, Sp, Sl						Braided				
327	Pedra do Segredo Formation	566-535.2	>1000	Yes	Arkose	St, Sh, Sl			Lower-flow regime			Braided				
328	Seival Formation	566-535.2	800			Sh, Sr, St										
329	Serra dos Lanceiros Formation	566-535.2	400		Arkose	St, Sp, Sl			Lower-flow regime			Braided				
330	Stretton Group															
331	Three Sisters Formation		45	Yes												
332	Umbrella Butte Formation		100	Yes	Quartzite											
333	Umm Ghaddah Formation		60	Yes	Arkose	Sp, St, Sh			Lower-flow regime		Yes	Braided	15°S	Intracratonic	Humid	
334	Wood Canyon Formation		90-130	Yes	Subarkose/Arkose	St, Sh, Sp	10 to 50		Lower-flow regime			Braided	Low		Warm/Arid	
335	Portfjeld Formation		100													
336	Rozel Conglomerate		500	Yes								Sheetflood	High	Extensional/Transtensional	Humid/Cool	

337	Addy Quartzite			Yes	Quartzite/Subarkose	Gt, Gp, Gm, St, Sp, Sm			Lower-flow regime			Braidplain	Low	Actively subsiding		
338	Amin Formation			Yes						Yes						
339	Araba Formation		25	Yes	Quartz arenite/Arkosic arenite	Sh, Sl, Sp, St	<15		Lower-flow regime			Braided/ Ephemeral				
340	Bolsa Quartzite		70-140		Quartz arenite											
341	Camp Ridge Formation		>1000		Arenite	Sh, St	10 to 50					Braided				
342	Haradh Formation		<1360	Yes		St						Braided/ Sheetflood				Mud clasts
343	Hato Viejo Formation															
344	Mount Simon Sandstone			Yes		Sm, Sp						Braided		Intracratonic		
345	Nepean Formation		1	Yes						Yes		Ephemeral				
346	Piekenier Formation			Yes		Sh, St						Braided				
347	Sarabit El-Shillito Formation		15-27	Yes	Arkose/Subarkose	St			Lower-flow regime			Braided				
348	Sebkhet el Mellah Formation		<200		Arkose	St, Sp	30-100		Lower-flow regime		Yes	Braided				
349	Serra do Apertado Formation		200	Yes	Arkose	St, Sp, Sh			Lower-flow regime			Ephemeral				Mud clasts
350	Siq Sandstone			Yes	Arkose											
351	Tapeats Sandstone				Arkose/Subarkose							Braided		Epicratonic		
352	Varzinha Formation				Arkose	Sh, Sr, St, Sp	20					Ephemeral				Mud clasts
353	Weverton Formation			Yes								Braided				
354	Alderney Sandstone Formation		500	Yes	Subarkose/Lithic arkose	St, Sp, Sh	15-45		Lower-flow regime			Braided	70°S	Extensional/Transtensional	Humid/Cool	Mud clasts
355	Amudei Shelomo Sandstone Formation			Yes	Arkose							Braided	Low		Warm/Humid	
356	Backbone Ranges Formation				Quartz arenite	Sp, St			Lower-flow regime	Yes	Yes	Braided				Mud clasts
357	Bámbola Formation		200-400	Yes	Quartz arenite									Intracratonic		
358	Bradore Formation		40-50		Subarkose/Arkose	St, Sp	20-150		Lower-flow regime			Braided				
359	Chapel Island Formation	531		Yes								Braided				
360	Dahu Formation		400													
361	Frehel Formation				Arkose	St, Sh	10 to 50	DA, LA, CH, UFR	Lower-flow regime			Braided	70°S	Extensional/Transtensional	Humid/Cool	Mud clasts
362	Guarda Velha Formation	542-535	518	Yes	Arenite/Arkose	St (49.3%), Sp(17.5%), Sd(12.59%), Sh(9.2%), Ss(5.3%)	40-57	SB, UFR, FF, FF(CH), GB, DA, HO, LA				Braided		Synrift	Semi-humid/Humid	Mud clasts
363	Hardyston Formation					Sp(5%), St(8%),										

						Gm(69%), Sm (16%)										
364	Herreria Formation		500-1700		Quartz arenite/Quartz litharenite	St, Sl, Sh					Yes	Braided	Mid-High			Mud clasts
365	Le Pedrera Formation															
366	Neksø Formation		100		Arkose	St, Sp, Sr, Sh				Yes		Braided/ Ephemeral	45°S	Stable craton	Arid	
367	Ogof Golchfa Cliff Formation															
368	Roche Jagu Formation					St, Sp, Sh, Sl	15-50					Braided				
369	Salib Formation		>200	Yes	Arkose	Sp, St, Sh					Yes	Braided				
370	Taba Formation			Yes												
371	Tintic Quartzite	520-550			Arkose	St		CH	Lower-flow regime							
372	Altona Formation		84		Arkose/Subarkose									Aulacogen		
373	Liberty Hills Formation				Quartzite	St			Lower-flow regime			Braided				
374	Mahwis Formation	510-499										Sheetflood			Semi-arid	
375	Mount Roosevelt Formation			Yes		Sm, Sp								Rift		
376	Umm Ishrin Sandstone Formation		100-320		Quartz arenite	Sp (3%), St (52%), Ss(25%)	20-50				Yes	Braided				
377	Ausable Formation				Arkose	Sr, Antidunes, St, Sp, Sr, Chute and Pool						Braided				
378	Covey Hill Formation				Quartz arenite/Arkose							Braided		Rift		
379	Santa Rosita Formation		35	Yes								Braided				
380	Sticht Range Formation															
381	Andam Formation					Sh, Sm, Sr, St, Sp	<60					Braided				
382	Lamotte Sandstone				Arkose	St, Sh, Tangential	15					Braided				
383	Owen Conglomerate	502.6-494.4		Yes	Quartz arenite	Sm, St, Sp, Sh						Braided		Fault controlled		
384	Van Horn Formation	519-522	>500		Lithic arkose							Braided				
385	Wajid Sandstone					St, Sh, Sp						Braided				
386	Wonewoc Formation		30-50			St	10 to 30		Lower-flow regime			Braided				Mud clasts
387	Keeseville Formation					Sr, Antidunes, St, Sp, Sr, Chute and Pool						Braided/ Ephemeral				